

Transport of environmental contaminants in saturated porous media

DISSERTATION

zur Erlangung des akademischen Grades eines Doktors

der Naturwissenschaften (Dr. rer. nat.)

in der Bayreuther Graduiertenschule für Mathematik und Naturwissenschaften (BayNAT)
der Universität Bayreuth

Vorgelegt von

Taotao Lu

aus Wuhan, China

Bayreuth, 2021

Die vorliegende Arbeit wurde in der Zeit von Oktober 2017 bis Mai 2021 in Bayreuth am Lehrstuhl für Hydrologie unter Betreuung von Herrn PD Dr. Sven Frei und Herrn Prof. Dr. Stefan Peiffer angefertigt.

Dissertation eingereicht am: 09.06.2021

Zulassung durch das Leitungsgremium: 30.06.2021

Wissenschaftliches Kolloquium: 10.12.2021

Amtierender Direktor: Prof. Dr. Markus Lippitz

Prüfungsausschuss:

PD Dr. Sven Frei	(Gutachter)
Prof. Dr. Andrea Carminati	(Gutachter)
Prof. Dr. Eva Lehndorff	(Vorsitz)
Prof. Dr. Stefan Peiffer	

Acknowledgements

When I started to write the doctoral dissertation, it meant that the day of departure would come soon. From October 2017, when I arrived in Germany, to now, there are so many people who have helped me a lot. I am very grateful for that.

Firstly, I would like to thank my main supervisor, PD Dr. Sven Frei, and co-supervisors, Prof. Dr. Stefan Peiffer and Dr. Benjamin S. Gilfedder. During these years, my supervisors have taken great care of me in my study and life; they have given me patient guidance in research, which has helped me become a qualified researcher and be able to conduct research independently. I would like to express my highest respect for them.

I am particularly grateful for the support and encouragement from my research partners, Dr. Hao Peng and Dr. Zhichong Qi. With their help, I was able to carry out my doctoral research and obtain some scientific achievements.

I would like to acknowledge the China Scholarship Council for sponsoring my study abroad for 4 years, which allowed me to receive advanced education at the University of Bayreuth in Germany. In addition, I am thankful for SFB 1357 project B03 for funding my research.

Thanks to all my colleagues in the Hydrology department, Stefan Durejka, Aira Sacha Nadine Ferrer, Barbara Jakob, Luisa Hopp, Bouchra Marouane, Karel As, Katharina Blaurock, Jan-Pascal Boos, Hassan Elagami, Lisa Kaule, Robin Kaule, Xingyu Liu, Usman Munir, Joscha Opitz, Johanna Schmidtman, Isolde Baumann, Jutta Eckert, Silke Hammer, Martina Rohr, and my friends, Yixin Qiu, Sihan Lin, Jiajia Wang, Qiong Liu, Nanfeng Liu, Biaodian Chen, Xiaochen Liu, Xuan Wei. Because of you, my life in a foreign country became warm and interesting.

Finally, I would like to sincerely thank my family for their selfless support and dedication over the years. My parents and brother accompanied me through those darkest and most helpless days. I owe a lot to my wife, Huan Yan, and my newborn son, Yeran Lu. I am very sorry that I have not returned to China to take care of you since birth. In the future, we will pull through trials and hardship together, as well as accompany you to grow up happily.

I would like to dedicate this dissertation to every person who has offered me help and concern.

Contents

0 Abstract	1
0 Zusammenfassung	3
1 Introduction	5
1.1 Mechanisms controlling contaminants transport in porous media	5
1.1.1 Derjaguin–Landau–Verwey–Overbeek (DLVO) theory.....	5
1.1.2 Physical straining	6
1.1.3 Steric hindrance.....	7
1.1.4 Cation bridging effect.....	8
1.1.5 Competition for deposition sites	8
1.2 Current research progress in contaminants transport in porous media	8
1.2.1 Effects of pH.....	8
1.2.2 Effects of ionic strength.....	9
1.2.3 Effects of divalent cations.....	9
1.2.4 Effects of organic matters	9
1.2.5 Effects of different porous media.....	10
1.3 Objectives and structure of the studies	10
1.3.1 Objectives	10
1.3.2 Structure of each study	11
2 Materials and methods	13
2.1 Materials.....	13
2.1.1 Contaminants	13
2.1.2 Porous media.....	13
2.2 Column experiment.....	13
2.3 DLVO calculation	15
2.4 Numerical simulation.....	15
3 Results and discussion	17
3.1 How does the solution chemistry affect the transport of contaminants?	17
3.1.1 Effects of LMWOAs on the transport of Cd ²⁺ (study 1).....	17
3.1.2 Effects of pH on the transport of Cd ²⁺ , petroleum colloids, and PS-NPs (study 1–4).....	18
3.1.3 Effects of ionic strength (IS) on the transport of petroleum colloids and PS-NPs (study 2–4).....	19
3.1.4 Effects of cations on the transport of Cd ²⁺ , petroleum colloids, and PS-NPs (study 1–3)	20
3.1.5 Effects of surfactant on the transport of petroleum colloids (study 2).....	21
3.2 How does the porous media affect the transport of contaminants?	21
3.2.1 Effects of quartz sand on Cd ²⁺ and petroleum colloids transport (study 1–2)...	21
3.2.2 Effects of sandy soil on petroleum colloids transport (study 2)	22
3.2.3 Effects of iron oxyhydroxide coated sand on PS-NPs transport (study 3)	22
3.2.4 Effects of clay minerals on PS-NPs transport (study 4).....	22

3.3 How does the contaminant property affect the transport of contaminants?	23
4 Conclusions and outlook.....	25
4.1 Conclusions	25
4.2 Research outlook.....	26
5 References	29
6 Contribution statement	35
Study 1: Transport of Cd²⁺ through saturated porous media: Insight into the effects of low-molecular-weight organic acids.....	37
Study 2: Factors affecting the transport of petroleum colloids in saturated porous media	75
Study 3: Relevance of iron oxyhydroxide and pore water chemistry on the mobility of nanoplastic particles in water-saturated porous media environments	107
Study 4: Effects of clay minerals on the transport of nanoplastic particles in water-saturated porous media	135

0 Abstract

With the development of industrial and agricultural activities, groundwater pollution is becoming a more serious concern. The presence of contaminants in groundwater is known to significantly increase the occurrence of diseases, which constitutes a significant threat to physical health. Water is a substance necessary to the human body, as well as a natural carrier of contaminants. Thus, contaminants can transport in porous media with groundwater flow. Understanding the migration patterns of contaminants in groundwater aquifers can provide valuable information for solving groundwater pollution problems. In addition, although contaminants can dissolve or suspend in water and migrate with the water flow, they are more likely to bind strongly to porous media, allowing most contaminants to be retained in the porous media. Therefore, it is crucial to elucidate the interactions between environmental contaminants and porous media in order to reduce the potential risks of these contaminants to physical health.

In this dissertation, typical and new emerging environmental contaminants, namely heavy metals, petroleum colloids, and nanoplastics, were chosen as study subjects. Column experiments were conducted to investigate the migration patterns of these contaminants in saturated porous media (quartz sand, sandy soil, iron oxyhydroxide coated sand, clay minerals) under different hydrochemical conditions (low-molecular-weight organic acids, pH, ionic strength, etc.). Meanwhile, batch experiments and numerical simulations were also carried out to comprehensively understand the interaction mechanisms between the pollutants and porous media. In total, 4 studies were addressed in the present dissertation.

In study 1, the effects of low-molecular-weight organic acids (LMWOAs) and competing cations (Pb^{2+}) on the transport of heavy metal (Cd^{2+}) in saturated pure quartz sand under different pHs were discussed. At pH 5, LMWOAs inhibited the transport of Cd^{2+} , and inhibition capacity decreased in the following sequence citric acid > tartaric acid > acetic acid, which depends on their molecular structures (i.e., amount and type of functional groups) and complexing strength with Cd^{2+} . Contrastingly, at pH 7, LMWOAs promoted the transport of Cd^{2+} due to the formation of stable aqueous non-adsorbing Cd-organic acid complexes. Pb^{2+} promoted Cd^{2+} transport due to its stronger complex affinity to citric acid. Therefore, the effects of solution chemistry play an important role in the transport of heavy metal ions.

In study 2, the transport of petroleum colloids in quartz sand and sandy soil was studied. More petroleum colloids were retained with increasing ionic strength (IS) as well as decreasing pH. This observation can be explained by the increase in hydrodynamic diameter of petroleum colloids under these conditions, resulting in apparent physical straining. On the other hand, the electrostatic repulsion between colloids and grain surfaces reduces. In addition, greater mobility of petroleum colloids was found in the sand rather than in soil. This can be ascribed to the unique physicochemical properties of soil, like containing a lot of metal oxides and clay minerals. Hence, the solution chemistry and the porous media characteristics greatly influence the migration of petroleum colloids.

In study 3, the migration of polystyrene nanoplastics (PS-NPs) in iron oxyhydroxide coated

quartz sand under different water chemistry conditions was investigated. The effect of iron oxyhydroxide coated sand on PS-NPs transport was greater than that in pure quartz sand under the same conditions. For most cases ($\text{pH} < 9$), the iron coating was positively charged, while PS-NPs were negatively charged. Thus, electrostatic attraction is the main reason for the weakened PS-NPs transport. In addition, solution chemistry changed the surface charge of PS-NPs and uncoated quartz sand, resulting in changes in the interaction energy between them. Charge heterogeneity of porous media is crucial for PS-NPs transport.

In study 4, the effects of porous media properties on PS-NPs transport were further investigated based on the findings of study 3. Different clay minerals were used to understand their influence. Compared with quartz sand, clay minerals have a relatively high surface charge, which results in PS-NPs being more easily deposited onto clay minerals. Thus, both kaolinite and illite inhibited the transport of PS-NPs. Except for the permanent negative charges, some variable charges on the edge of the clay mineral are sensitive to the water chemistry. The positive edge sites of kaolinite and negative edge sites of illite under experimental conditions ($\text{pH} 5.9$) led to a stronger inhibition on PS-NPs transport in kaolinite than illite.

It can be seen that the transport of environmental contaminants is closely related to the properties of contaminant and porous media, as well as water chemistry conditions. In order to obtain a more precise understanding, all these factors need to be taken into account when evaluating contaminant transport in groundwater aquifers.

0 Zusammenfassung

Die Zunahme der industriellen und landwirtschaftlichen Aktivität führte in der Vergangenheit zu einer ansteigenden Verschmutzung des Grundwassers. Grundwasser wird weltweit als primäre Trinkwasserquelle genutzt wird, weshalb sich die ansteigende Belastung des Grundwassers mit Schadstoffen direkt negativ auf die menschliche Gesundheit auswirkt. Im Grundwasser kontrollieren advective und dispersive Prozesse den Transport bzw. die Mobilisierung von Schadstoffen. Interaktionen mit dem porösen Medien können zu einer langfristigen oder temporären Immobilisierung von Schadstoffen in Grundwasserleitern führen. Für die Entwicklung effektiver Maßnahmen, die dem zunehmenden Verschmutzungsgrad von Grundwasser entgegenwirken, ist deshalb ein prozessbasiertes Verständnis hinsichtlich der Wechselwirkung zwischen Schadstoffen und dem porösen Medium von Grundwasserleitern notwendig.

Als Teil dieser Dissertation wurden typische und in der Vergangenheit verstärkt auftretende Schadstoffe in der Umwelt, wie Schwermetalle, Erdölkolloide und Nanoplastik, auf ihre Transportverhalten in porösen Medien hin untersucht. Das Mobilitäts- und Retartationsverhalten dieser Stoffe wurde als Teil von Säulenexperimenten mit unterschiedlichen, umweltrelevanten porösen Medien (Quarzsand, Sandböden, mit Eisenoxid beschichteter Sand, Tonminerale) unter verschiedenen hydrochemischen Bedingungen (niedermolekulare organische Säuren, pH-Wert, Ionenstärke), untersucht. Ergänzt wurden die Säulenexperimente durch Batch-Versuche sowie modellgestützte Simulationen, um so die Mechanismen der Wechselwirkung zwischen Schadstoff und porösem Medien umfassend und mechanistisch zu erforschen. Die vorliegende Dissertation umfasst insgesamt 4 Studien.

In Studie 1 wurde die Auswirkung von niedermolekularen organischen Säuren (LMWOAs) sowie konkurrierender Kationen (Pb^{2+}) auf den Transport von Schwermetall (Cd^{2+}), in wasser-gesättigtem Quarzsand bei unterschiedlichen pH-Werten, untersucht. Bei niedrigen pH-Werten (pH 5) hemmten LMWOAs den Transport von Cd^{2+} deutlich, wobei die Hemmungskapazität entsprechend der Reihenfolge Zitronensäure > Weinsäure > Essigsäure abnahm. Die Abnahme der Hemmungskapazität konnte auf die molekulare Struktur der Säuren (d.h. Menge und Art der funktionellen Gruppen) und der damit verbundeneren Komplexierungsstärke mit Cd^{2+} zurückgeführt werden. Im Gegensatz dazu wird bei pH 7 die Mobilität von Cd^{2+} , durch die Bildung stabiler wassergelöster und nicht-adsorbierender Cd-Säurekomplexe, gefördert. Pb^{2+} förderte die Mobilität von Cd^{2+} aufgrund seiner stärkeren Komplexaffinität zu Zitronensäure. Ergebnisse dieser Studie zeigen wie sehr die Zusammensetzung des Porenwassers sowie die darin ablaufenden lösungsschemischen Effekte den Transport von Schwermetallionen im porösen Medium kontrollieren.

In Studie 2 wurde das Transportverhalten von Erdölkolloiden in Quarzsand sowie sandigen Böden untersucht. Die Retention von Erdölkolloiden nahm mit zunehmender Ionenstärke (IS) sowie mit abnehmendem pH-Werten zu. Die abnehmende Mobilität ließ sich 1) durch die Zunahme der Größe der Erdölkolloiden bei niedrigeren pH-Werten bzw. höheren IS und der damit verbundenen Zunahme des „physical straining“ Effekts bei dem Porenräume blockiert

werden, sowie 2) durch die Verringerung der elektrostatischen Abstoßung zwischen Kolloiden und Kornoberflächen des porösen Mediums erklären. Darüber hinaus wurde eine generelle erhöhte Mobilität von Erdölkolloiden im Sand im Vergleich zu sandigen Böden festgestellt. Dies kann auf die besonderen physikochemischen Eigenschaften des benutzten Bodens zurückgeführt werden. Ebenso wie bereits in Studie 1 für Schwermetallionen gezeigt werden konnte, spielt die geochemische Zusammensetzung des Porenwassers sowie die Oberflächeneigenschaften des Porösen Mediums eine zentrale Rolle bei der Mobilität von Erdölkolloiden.

In Studie 3 wurde das Migrationsverhalten von Polystyrol-Nanokunststoff-Partikeln (PS-NPs) in mit Eisenoxid beschichtetem Quarzsand, unter Berücksichtigung verschiedener wasserchemischer Bedingungen, untersucht. Das Vorhandensein von Eisenoxiden hatte dabei einen großen Einfluss auf die Mobilität von PS-NP-Partikeln. Bei niedrigen pH-Werten war die Oberfläche der Eisenbeschichtung positiv geladen, während die PS-NPs negative Oberflächenladung aufwies. Die sich daraus ergebenden elektrostatischen Anziehungskräfte, zwischen PS-NPs und dem beschichteten porösen Medium, wurde als Hauptursache für die beobachtete hohe Retention bei niedrigen pH-Werten identifiziert. Die Oberflächenladung der PS-NP Partikel sowie des Quarzsandes wurde dabei maßgeblich von der chemischen Beschaffenheit der Porenwassers bestimmt, was sich direkt auf die Partikel-Matrix Wechselwirkungen auswirkte.

In Studie 4 wurden die Auswirkungen der Eigenschaften poröser Medien auf den PS-NPs-Transport, basierend auf den Ergebnissen von Studie 3 untersucht. Hier lag der Fokus auf dem Verhalten von PS-NPs in porösen Medien mit unterschiedlichen Tongehalten und Tonmineralien (Kaolinit und Illit). Im Vergleich zu Quarzsand haben Tonminerale eine hohe Oberflächenladung mit einer höheren Bindungsaffinität zu PS-NPs. Da die verwendeten Tonminerale unterschiedlich Ladungseigenschaften aufweisen, die stark von der chemischen Zusammensetzung des Porenwassers abhängen, verhalten sich PS-NPs unterschiedlich bei Anwesenheit von Kaolinit und Illit. Die positiv geladenen Randstellen von Kaolinit führten unter den experimentellen Bedingungen (pH 5.9) zu einer verstärkten Retention von PS-NPs im Vergleich zu Illit.

Zusammenfassend lässt sich sagen, dass das Transportverhalten der untersuchten Schadstoffe 1) von der oberflächenladung des Schadstoffes, 2) den chemischen Bedingungen im Porenwasser und 3) der ladungsspezifischen Eigenschaften des porösen Mediums kotolliert wird. Diese Aspekte müssen berücksichtigt werden, um den Transport dieser Schadstoffe in Grundwasserleitern besser bewerten zu können.

1 Introduction

Since the twentieth century, the remarkable progress in science and technology as well as the development of productive forces enabled human beings to vastly increase fortune, accelerate the growth of civilization, and make brilliant achievements in the transformation of nature. At the same time, the mismanagement in the industrialization process, especially the irrational exploitation of natural resources, has caused global environmental pollution and ecological damage, which poses a severe threat to the survival and the development of human beings (Rao and Yan, 2020; Victor, 2017). At present, groundwater contamination has caused great harm to physical health (Baba and Tayfur, 2011). This is due to the fact that groundwater is an important drinking water source for people (Ross and Martinez-Santos, 2010). Long-term consumption of contaminated groundwater leads to various diseases; for example, fluoride and chloride in the groundwater do harm to human organs and induce cancer diseases (Mukherjee and Singh, 2020). Heavy metals, such as arsenic, chromium, lead, and mercury, exceeding the limits in drinking water standards cause neurological disorders and digestive system diseases (Durube et al., 2007; Raikwar et al., 2008). Therefore, the urgent need to solve these problems has motivated more and more researchers to focus on groundwater pollution.

To solve the groundwater pollution problem, the first thing is to figure out the migration patterns of contaminants in groundwater aquifers. The porous media in the groundwater aquifers, which can effectively adsorb and retain the pollutants, can be recognized as a natural and effective purification device (Stevik et al., 2004). As a result, studying the transport of environmental contaminants in the porous media provides the foundation for solving groundwater contamination issues.

1.1 Mechanisms controlling contaminants transport in porous media

The mechanisms introduced below are based on the transport of particles under the unfavorable condition, which means the surface charge of both particles and porous media are the same (e.g., the petroleum colloids and quartz sand are negatively charged, and there is an electrostatic repulsion between them).

1.1.1 Derjaguin–Landau–Verwey–Overbeek (DLVO) theory

DLVO theory is widely used to calculate the interaction energy between particles (e.g., colloids and nanoparticles) and porous media (Elimelech and O'Melia, 1990b; Tian et al., 2010). According to DLVO theory, the total interaction potential energy between particles and porous media depends on the Van der Waals attraction and electrostatic repulsion (Buschow et al., 2001). As shown in Figure 1, when the particles are far away from the surface of the porous media, Van der Waals attractive force between them is dominant; thus, the total interaction potential energy is negative, and there exists the secondary minimum. Some particles will deposit at this location (Ryan and Elimelech, 1996). As the particles gradually approach the surface of the porous media, the electrostatic repulsion force begins to work. The total

interaction potential energy gradually becomes positive and reaches its maximum at a distance, constituting an energy barrier. When the particles are able to leap over the energy barrier, the total interaction potential energy decreases rapidly since Van der Waals attraction becomes dominant again. The total interaction potential energy will get negative again, resulting in the primary minimum (Shen et al., 2007). The particles that get across the energy barrier will deposit at this location. In addition, the deposition of particles resulting from the second minimum is called “rapid deposition”, while the deposition caused by the primary minimum is called “slow deposition”(Tufenkji and Elimelech, 2005). In general, the lower the secondary minimum, the easier particle deposition; conversely, the higher the energy barrier, the harder particle deposition.

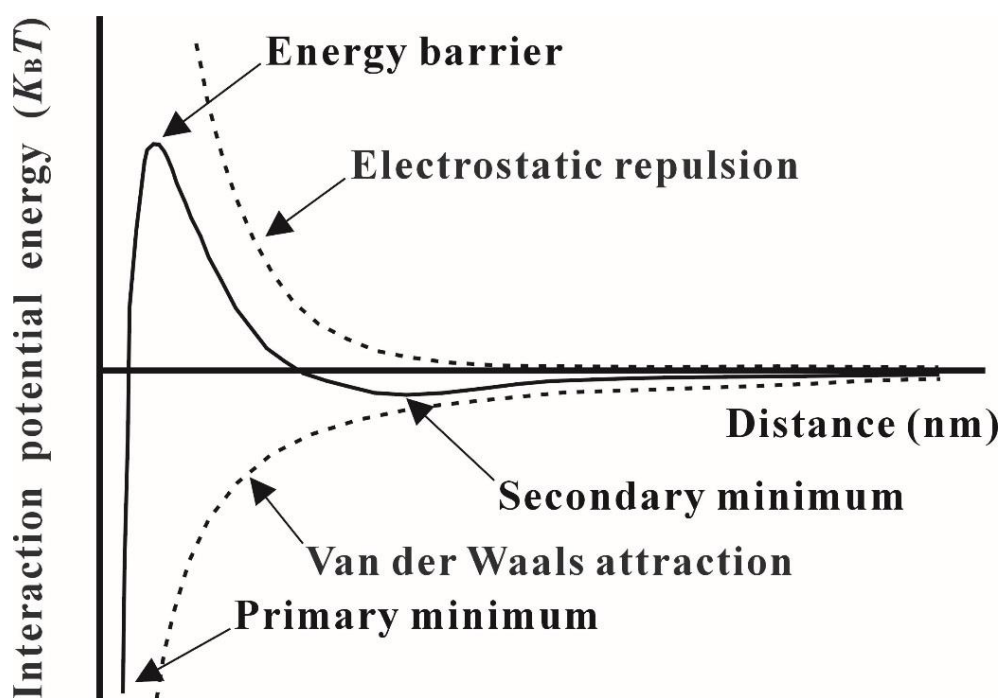


Figure 1. Schematic diagram of interaction potential energy versus distance described by the DLVO theory.

1.1.2 Physical straining

As presented in Figure 2, the term “physical straining” refers to the fact that the particles are intercepted by the narrow pores in porous media consisting of small grains, resulting in partially clogged pores. Thus, particles are only able to transport through the larger continuous pores in the porous media (Bradford et al., 2006; Jaisi et al., 2008). Currently, a series of studies have proposed that when the ratio of d_p/d_c is above 0.002 (d_p and d_c represent the average diameter of particle and porous media, respectively). If the particles aggregate obviously, the d_p refers to the hydrodynamic diameter of aggregated particles), physical straining has a noticeable influence (Liang et al., 2016). Conversely, if the ratio is below the critical value, the effect of physical straining can be ignored (Lu et al., 2021). Some research shows that physical straining plays a vital role in the transport of particles in porous media (Bradford et al., 2006; Qi et al., 2014b). As a result, physical straining should be considered when analyzing the transport of

contaminants in porous media.

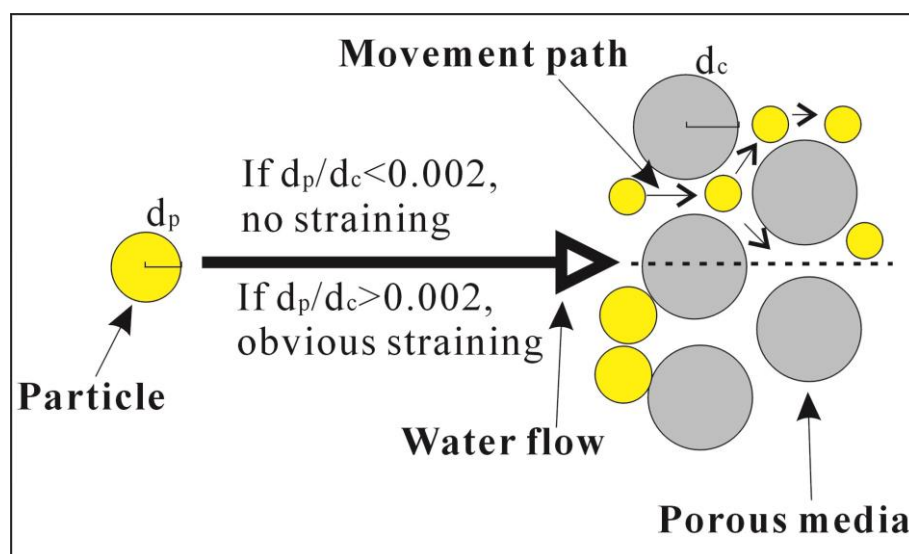


Figure 2. Schematic diagram of physical straining.

1.1.3 Steric hindrance

In Figure 3, the steric hindrance refers to the phenomenon wherein particle A is inhibited from depositing to the porous media by the previously deposited particle B during its transportation (Zhu et al., 2014). Because of the interactions between particle A and particle B, particle B exerts strong repulsive forces on particle A, or particle B has a weak complexation ability to particle A, resulting in the reduction of deposition of particle A onto the porous media. When particle A is the same as particle B, the breakthrough curve of particle A usually presents a blocking phenomenon (Nascimento et al., 2006). In addition, particle B can be colloid, protein, organic acid, surfactant, ion, and so on (Dong et al., 2020; Wang et al., 2020a; Wang et al., 2020b).

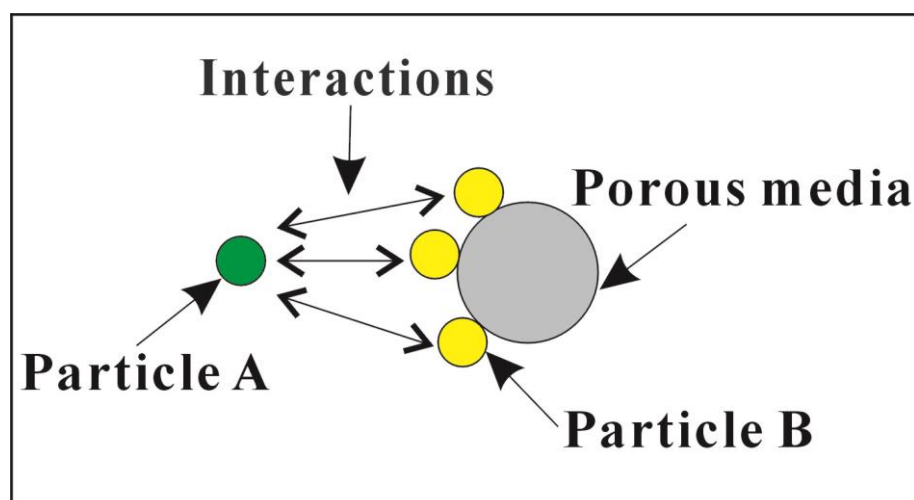


Figure 3. Schematic diagram of steric hindrance.

1.1.4 Cation bridging effect

The cation bridging effect usually takes place between cations and negatively charged oxygen-containing functional groups on both particles and porous media (Wang et al., 2020a; Zhang et al., 2020). As described in Figure 4, the bridging agent (e.g., Ca^{2+} , Ba^{2+}) interacts with functionalities on the particle and porous media surface to form complexes, which enhances the deposition of contaminant particles onto porous media (Lu et al., 2021).

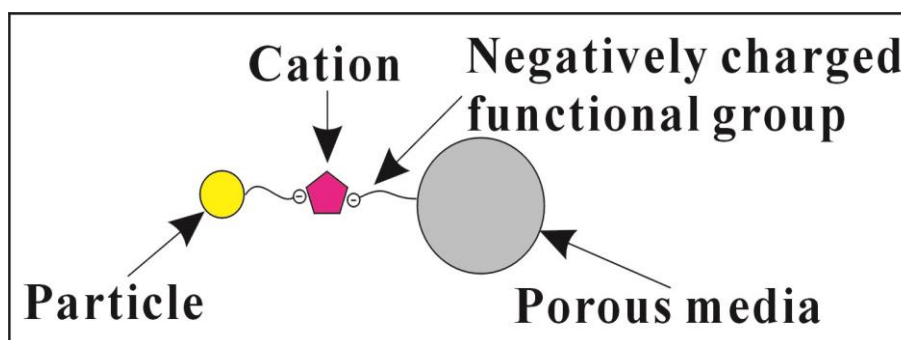


Figure 4. Schematic diagram of cation bridging effect.

1.1.5 Competition for deposition sites

When the competing particles B coexist with particles A in the solutions (these particles can be ions, organic matters, colloids, etc.), particles A and particles B will compete against each other for the limited deposition sites on porous media. If particle B wins the competition, the limited deposition sites will be occupied by particle B, and the transport of particle A will be promoted (Cai et al., 2016; He et al., 2019).

1.2 Current research progress in contaminants transport in porous media

Up to now, a lot of studies have been conducted to investigate the transport of contaminants in porous media under various hydrochemical conditions (Dong et al., 2016; Kretzschmar and Sticher, 1998; Marino, 1974; Sen, 2011). In general, the fate of contaminants depends on their own properties (e.g., surface charge, particle size) (Shaniv et al., 2021), solution chemistry (e.g., pH, ionic strength) (Fang et al., 2013), and porous media types (e.g., pure sand, sandy soil) (Qi et al., 2014a). In addition, the solution chemistry can also affect the properties of contaminants and porous media (Lu et al., 2021). In the following part, the effects of different factors on the transport of contaminants are discussed separately. Note that in this section, we mainly consider the transport of negatively charged particles under unfavorable conditions.

1.2.1 Effects of pH

The pH of the solution plays an important role in the surface charge (zeta potential) of both contaminants and porous media due to the protonation/deprotonation of functional groups on their surface (Saka and Guler, 2006). Thus, according to the interaction energy calculated by DLVO theory, the energy barrier between particles and porous media is relatively low at a low

pH, which means the particles can overcome the energy barrier to deposit by the primary minimum; furthermore, the secondary minimum is also deeper at a lower pH; therefore the particles also deposit via the secondary minimum (Kamrani et al., 2018). Apart from the above-mentioned aspect, the interaction energy between particles also depends on the pH (Illés and Tombácz, 2006). For instance, at low pH, the particles preferably form aggregates due to the weak electrostatic repulsion. When the hydrodynamic diameter of aggregated particles reaches $d_p/d_c > 0.002$, the physical straining works during the particle transport (Lin et al., 2010).

1.2.2 Effects of ionic strength

The effects of ionic strength (IS) on particle transport in porous media are mainly caused by two aspects. On the one hand, increasing IS compresses the electrical double layer, leading to an increase in the zeta potential (less negative) of particles and porous media (Hu et al., 2013). Thus, the electrostatic repulsion between particles and grain surfaces reduces. According to the DLVO theory, the energy barrier and secondary minimum between particles and collector decrease with increasing IS (Kuznar and Elimelech, 2007; Shen et al., 2011). As a consequence, more particles will deposit on the surface of the collector at higher IS. On the other hand, the aggregation of particles is promoted due to a reduction in the repulsive force between particles at high ionic strength (Liu et al., 2013). When the hydrodynamic diameter of aggregated particles exceeds the critical value, physical straining will be triggered to retain more particles in the porous media.

1.2.3 Effects of divalent cations

At present, a lot of studies have discussed the effects of divalent cations on particle transport (Fan et al., 2015; Grolimund and Borkovec, 2006). Compared with monovalent cations, divalent cations have a higher charge density due to the charge screening. As a result, the particles aggregate at a low concentration of divalent cations (Vermöhlen et al., 2000). For instance, the average hydrodynamic diameter of graphene oxide particles was 235 nm at 1.5 mM NaCl, while at 0.3 mM CaCl₂, it was 303 nm (Qi et al., 2014b). The first possible consequence caused by divalent cations is the physical straining due to the particles' aggregation. In addition, apart from the interaction between particles, the presence of divalent cations also affects the surface charge of porous media (Cheng et al., 2016). The interaction potential energy between particles and porous media is strongly influenced by divalent cations. It has been reported that the strong and irreversible deposition of particles on the porous media has been found in the presence of divalent salt (Shen et al., 2012). In addition, divalent cations usually act as the bridge agents between particles and porous media via negatively charged functional groups (Li et al., 2019b).

1.2.4 Effects of organic matters

Organic matters like humic acid, fulvic acid, low-molecular-weight organic acids, etc., are widely used to study their influence on contaminant transport (Li et al., 2019a; Weng et al., 2002; Yang et al., 2012). When these organic matters are adsorbed onto the contaminants, they lead to steric hindrance/electrostatic repulsion, promoting the contaminant dispersion and preventing aggregation (Yang et al., 2019). In these cases, the physical straining is usually

negligible. In addition, the organic acids will be adsorbed onto the surfaces of porous media (e.g., soil grains). The increased steric hindrance between particles and collectors enhances the contaminant transport in porous media (Franchi and O'Melia, 2003). Lastly, some organic matter can compete with the contaminants for deposition sites on porous media (Wu et al., 2016). For example, Suwannee River humic acid in suspension might compete with bacteria for deposition sites on quartz sand, contributing to the enhanced transport of bacteria in quartz sand (Yang et al., 2016).

1.2.5 Effects of different porous media

Currently, most research on contaminant transport has focused on the influence of the solution chemistry on contaminant transport. In order to simplify the conditions, pure quartz sand is frequently chosen as the porous media (Akbour et al., 2002; Foppen et al., 2010). However, the characteristics of porous media also play an essential role in the transport of contaminants (Wang et al., 2014). Various porous media, like clay minerals, iron oxides, and rock sediments, can be ubiquitously found in the environment. Several studies have shown that different porous media affects pollutant transport to different extents. For example, in the studies of Wang et al. (2012), the positively charged iron oxyhydroxide attracted the negatively charged particles via electrostatic attraction. According to the research of Lu et al. (2017), clay minerals (kaolinite, montmorillonite, and illite) had positively charged edge sites on their crystalline structures, which provided favorable deposition sites for negatively charged colloids. Qi et al. (2014a) used Lula soil instead of pure quartz sand in their experiment and found that more graphene oxides were retained in the soil column because there were high contents of clay minerals and iron oxides in the soil, which provided more favorable deposition sites (positively charged) for negatively charged graphene oxide. Finally, the small size of soil components, such as clay minerals, results in narrow pore space and complex flow pathways, which dramatically enhances the importance of the physical straining effect on contaminant transport (Cornelis et al., 2014).

1.3 Objectives and structure of the studies

1.3.1 Objectives

This dissertation aims to investigate the migration patterns of environmental contaminants in saturated porous media via a series of column experiments. In order to make the results more representative, we chose (i) three different contaminants (Cd^{2+} as a representative of heavy metals, petroleum colloids, and polystyrene nanoplastics (PS-NPs)) to study their transport in (ii) different porous media (quartz sand, sandy soil, iron oxyhydroxide coated sand, clay minerals) under (iii) various solution chemistries (e.g., different pH, different ionic strength, organic matters, different cation species). This dissertation will help us to analyze and predict the transport and fate of pollutants in saturated aquifers.

The specific objectives of each study presented in this dissertation are the following:

Study 1 focuses on the effect of solution chemistry on the transport of Cd^{2+} under favorable conditions. This study aims to investigate (i) the effect of different low-molecular-weight

organic acids (LMWOAs) on Cd^{2+} transport behaviors under acidic and neutral conditions and (ii) the effects of a competing ion (Pb^{2+}) on Cd^{2+} transport in the presence of LMWOAs.

Study 2 aims to investigate the effects of solution chemistry and porous media. In order to achieve the goals, the transport of petroleum colloids is studied by varying (i) solution chemistry conditions (different IS, divalent cations (Ca^{2+}), different pH, and surfactants) and (ii) the porous medium (quartz sand and sandy soil).

Studies 3 and 4 concentrate on the effect of porous media on the transport of polystyrene nanoplastic (PS-NPs) under unfavorable conditions. Study 3 aims to better understand the role of iron oxyhydroxide on PS-NPs transport under normal solution chemistry conditions (different ionic strength, different cation species, different pH). Study 4 aims to gain a more fundamental understanding of how the transport of PS-NPs is affected by clay minerals (kaolinite and illite) under regular solution chemistry (different IS and pH). Furthermore, the differences between kaolinite and illite are discussed to illustrate the influence of the structures of clay minerals.

1.3.2 Structure of each study

In order to help the readers better understand the structure of each study, the experimental ideas and settings are presented in Figures 5 to 8.

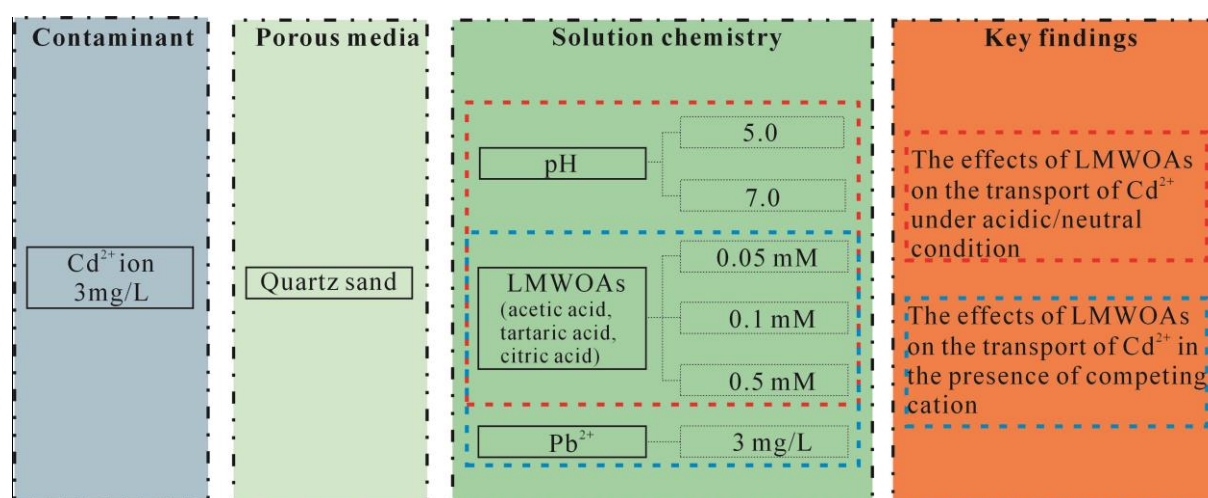


Figure 5. The structure and key findings of study 1.

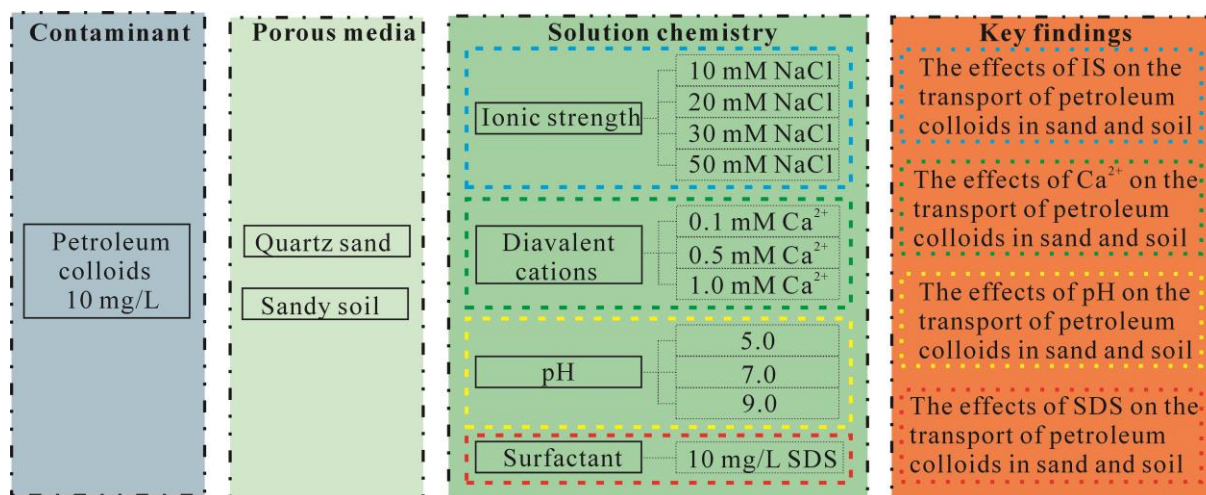


Figure 6. The structure and key findings of study 2.

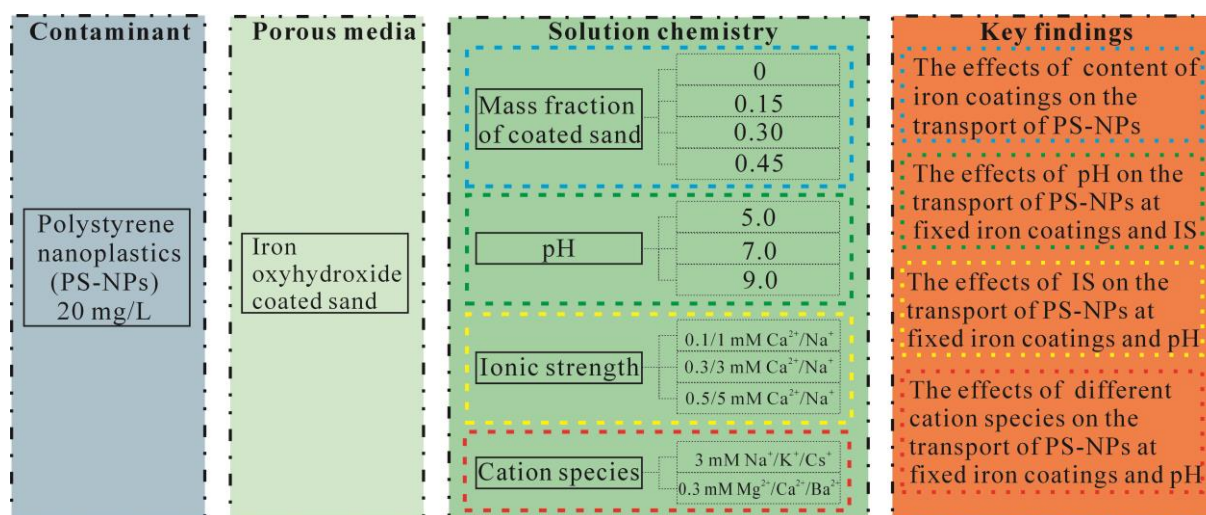


Figure 7. The structure and key findings of study 3.

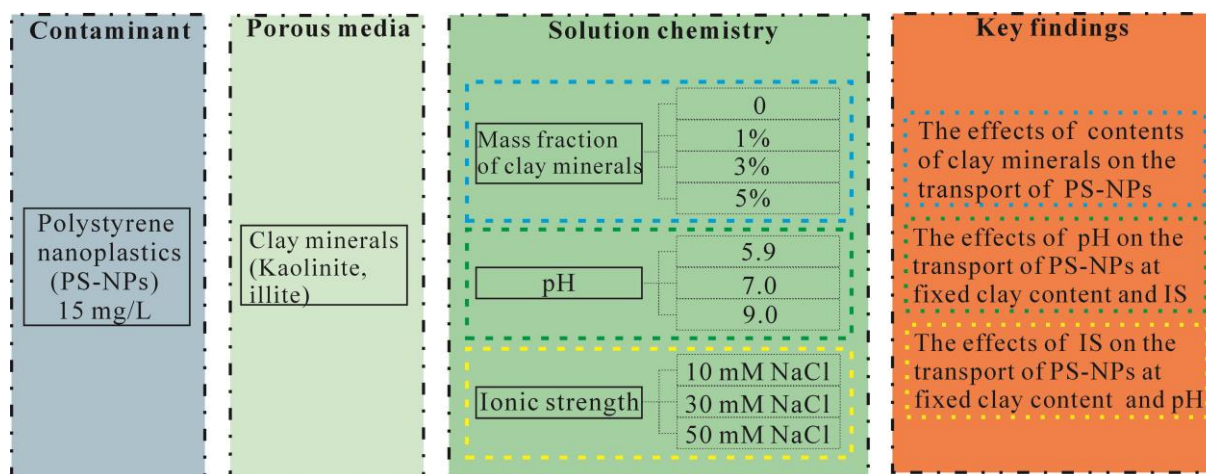


Figure 8. The structure and key findings of study 4.

2 Materials and methods

2.1 Materials

2.1.1 Contaminants

Study 1: 100 mg/L Cd(NO₃)₂ stock solution was diluted to 3 mg/L for the column experiments. Three low-molecular-weight organic acids (LMWOAs; acetic acid, tartaric acid, and citric acid) were added to obtain the Cd²⁺ solutions with 0.05 mM, 0.1 mM, and 0.5 mM LMWOAs. In addition, 0.1 M HCl and NaOH were used to adjust the pH of the solutions.

Study 2: 30 mg/L petroleum colloid stock solution (the specific method for preparing stock solution could be found in study 2) was diluted to 10 mg/L for the column experiments. 0.1 M NaCl, 0.1 M CaCl₂, and 50 mg/L sodium dodecyl sulfate (SDS) were added to prepare petroleum colloid suspension under different solution chemistry conditions. In addition, 0.1 M HCl and NaOH were used to adjust the pH of the solutions.

Study 3 and 4: The desired concentrations of polystyrene nanoplastic (20 mg/L PS-NPs in study 3 and 15 mg/L PS-NPs in study 4) were obtained by diluting the PS-NPs stock solution. Similarly, 0.1 M NaCl, 0.1 M KCl, 0.1 M CsCl, 0.1 M MgCl₂, 0.1 M CaCl₂, and 0.1 M BaCl₂ were used to change the suspension's chemical properties. In addition, 0.1 M HCl and NaOH were used to adjust the pH of the solutions.

2.1.2 Porous media

Study 1: Only quartz sand was used to fill the columns.

Study 2: In addition to quartz sand, the sandy soil from the Yellow River Basin was utilized to fill the columns.

Study 3: Iron oxyhydroxide coated sand was prepared to fill the columns.

Study 4: Typical clay minerals (kaolinite and illite) were used to fill the columns.

2.2 Column experiment

As shown in Figure 9, the experimental setup comprised of a solution container, a peristaltic pump, a glass column, and an auto-sampler (in some studies, a syringe and a syringe pump were used, but the function was the same). Each part was connected by polytetrafluoro-ethylene tubes.

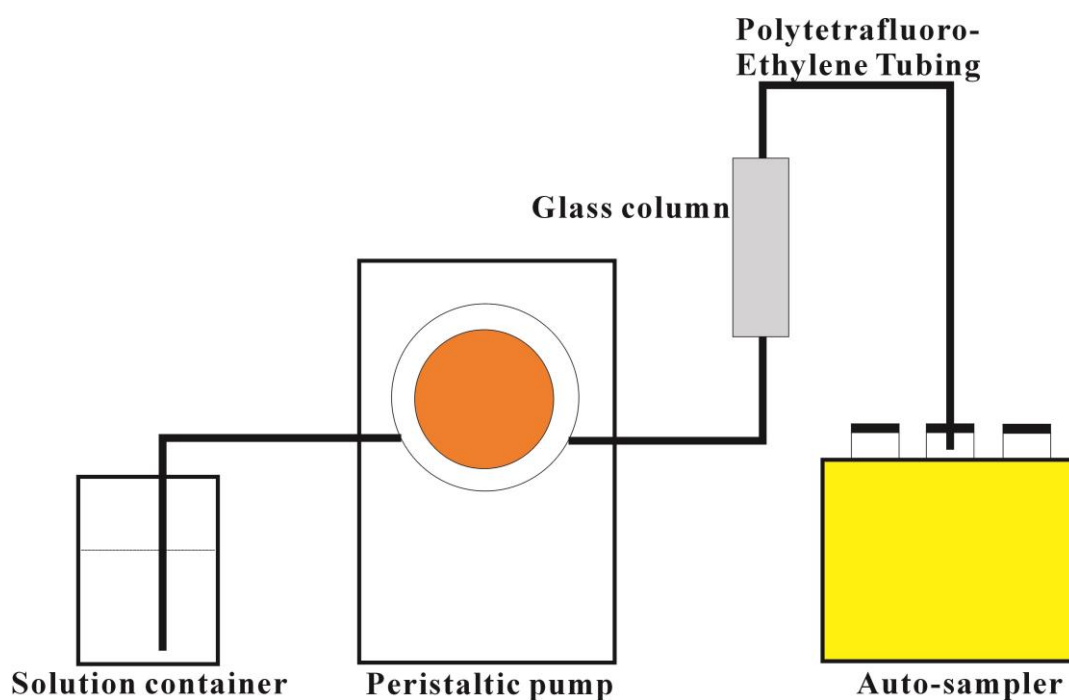


Figure 9. Schematic illustration of experimental apparatus of column tests.

Solution container was used to preserve the prepared solutions for the four studies (the specific hydrochemical characteristics of solution refer to section 1.3.2). A peristaltic pump was utilized to control the flow speed to simulate the groundwater flow. The glass column was packed with different porous media according to the research purpose. Before starting the experiment, the packed column was flushed with CO₂ gas to remove residual air in the sand column. Then, the column was rinsed with deionized water at a rate of 3 mL/h. Since CO₂ gas can dissolve in water, it was easy to saturate the column using this method. Next, the column was flushed with background electrolyte solution (without contaminants) to achieve equilibrium of porous media in the column. Then the experiment was started by injecting the solution containing the contaminant into the column. During the experiment, the solution was upwardly pumped into the column. When the solution flowed out from the outlet of the column, the vials in the auto-sampler collected the solution at a fixed time interval.

After the column experiment, the collected water samples were measured to get the contaminant concentration via pre-established calibration lines (the measurements of different contaminants were different, so the specific method to obtain the calibration line can be found in the corresponding study). Then the breakthrough curve could be obtained. According to the different shapes of the breakthrough curves, the contaminant migration patterns in porous media were revealed. In addition, in some studies, the retention profile was obtained by dissecting the sand column, and the mass balance was within 90–110% (the specific procedures can be found in study 2).

Apart from the column experiment, in studies 1 and 2, a batch sorption experiment was also conducted to reveal the binding affinities of pollutants from another aspect. Since it is not the main content of this study, the specific methods are not introduced in detail here, which can be found in studies 1 and 2.

2.3 DLVO calculation

The total interaction potential energy between particle and porous media (V_{TOT}) can be calculated as the sum of the attractive van der Waals interaction (V_{VDW} , Van der Waals attraction) and the repulsive electrostatic double layer interaction (V_{EDL} , Electrostatic repulsion) (Hogg et al., 1966):

$$V_{TOT} = V_{VDW} + V_{EDL} \quad (1)$$

The van der Waals interaction is calculated using the Hamaker approach and Gregory's formulation (Gregory, 1981):

$$V_{VDW}(h) = \frac{Ar_{NP}}{6h(1 + \frac{14h}{\lambda})} \quad (2)$$

The electrical double layer interaction is calculated as below (Elimelech and O'Melia, 1990a; Hogg et al., 1966):

$$V_{EDL}(h) = \pi r_{NP} \varepsilon_0 \varepsilon_r \left\{ 2\varphi_1 \varphi_2 \ln \left[\frac{1 + \exp(-\kappa h)}{1 - \exp(-\kappa h)} \right] + (\varphi_1^2 + \varphi_2^2) \ln [1 - \exp(-2\kappa h)] \right\} \quad (3)$$

Where A is the Hamaker constant; r_{NP} is the radius of the particle; h is the separation distance between the particle and porous media; λ is the characteristic wavelength; ε_0 is the vacuum permittivity; ε_r is the relative dielectric permittivity of water; φ_1 denotes the measured zeta potential of the particle; φ_2 corresponds to the zeta potential of porous media; κ is the Debye reciprocal length.

2.4 Numerical simulation

Numerical simulation can help to analyze the breakthrough curves (BTCs) of contaminants. In this dissertation, the two-site model considering attachment and straining was used to fit the BTCs in studies 1 and 2. The data could be perfectly matched by the model, which means that the adsorption of contaminants onto the collector and physical straining affect the transport of contaminants. Due to the fact that the numerical simulation is not a necessary part, the detailed descriptions are not introduced here.

3 Results and discussion

3.1 How does the solution chemistry affect the transport of contaminants?

3.1.1 Effects of LMWOAs on the transport of Cd^{2+} (study 1)

We found that the LMWOAs inhibited the transport of Cd^{2+} under acidic conditions (see Fig. 1 in study 1). There are two main reasons to explain it. On the one hand, the LMWOAs adsorbed onto the sand via hydrogen bonds can bring more negative charges to the sand (Huang et al., 2003); thus, more positively charged Cd^{2+} ions were adsorbed. On the other hand, the adsorbed LMWOAs interact with Cd^{2+} to form LMWOAs-Cd complexes (Huang et al., 2010); therefore, the retention of Cd^{2+} increased in the sand column. In addition, different LMWOAs inhibited the Cd^{2+} transport to different extents, which followed the sequence of citric acid > tartaric acid > acetic acid. This is caused by the molecular structures (molecular weight and functional groups) of LMWOAs and the strength of LMWOAs-Cd complexes. Wu et al. (2011) proposed that the adsorbed LMWOAs with larger molecular weight had larger surface coverage on grains; thus, citric acid has the largest surface coverage on sand which can bind with more Cd^{2+} ions. In addition, the numbers of carboxylic and hydroxyl groups of LMWOAs play essential roles in the stability of LMWOAs-Cd complexes (Najafi and Jalali, 2015). The more carboxylic and hydroxyl groups, the more stable complexes. As a result, the citric acid-Cd complex is the most stable, and the acetic acid-Cd complex is the least stable. This could explain the strongest inhibition on Cd^{2+} transport in the presence of citric acid. Furthermore, the concentration of LMWOAs affected their inhibition effects. When the concentration of LMWOAs increased from 0.05 mM to 0.1 mM, the inhibition effects increased (see Fig. 1 (a, b) in study 1). However, when the concentration continued to increase to 0.5 mM, the inhibition effects decreased (see Fig. 1 (b, c) in study 1). The following reasons contribute to this phenomenon. With an increase in LMWOAs concentrations, the relatively limited amount of deposition sites on the sand surface will be occupied, resulting in more and more free LMWOAs in the solution. Before being fully occupied, the Cd^{2+} can be adsorbed to the sand surface or interact with adsorbed LMWOAs leading to the increased deposition. After full occupation, the free LMWOAs-Cd complexes which are unlikely to deposit on the sand surface are formed. Besides, the excessive LMWOAs and free LMWOAs-Cd complexes compete with Cd^{2+} for deposition sites (Hu et al., 2007); therefore, less Cd^{2+} ions were retained in the sand column at the high concentration of LMWOAs.

Interestingly, the LMWOAs enhanced the transport of Cd^{2+} under neutral conditions (see Fig. 4 in study 1). The promoting effects of LMWOAs are attributed to the formation of stable non-adsorbing LMWOAs-Cd complexes (Kong et al., 2018; Malandrino et al., 2006). These complexes reduce the free Cd^{2+} in the solution, which could deposit onto the sand. Additionally, the adsorption of LMWOAs-Cd complexes onto the sand would be inhibited because of the stronger repulsive force between them at pH 7, thus promoting the Cd^{2+} transport (Hizal et al., 2009). In addition, Cd^{2+} transport enhancements by different LMWOAs were in the following order: citric acid > tartaric acid > acetic acid. Similar to the reasons mentioned above, this trend

is also dependent on the molecular structures and the complexing ability of LMWOAs. Among the three chosen LMWOAs, citric acid has the largest molecular weight, most negative surface charge and largest surface area and therefore exhibits the strongest ability to attract/chelate more Cd^{2+} ions; thus, a greater number of Cd^{2+} ions were present in the aqueous phase in the form of citric acid-Cd complexes, which facilitated the transport of Cd^{2+} .

3.1.2 Effects of pH on the transport of Cd^{2+} , petroleum colloids, and PS-NPs (study 1–4)

The effects of pH on the transport of contaminants are achieved by changing the surface charge of both contaminants and porous media by ionization/deionization processes under different pH. Then the interaction potential energy between them will be modified, which will lead to the deposition of contaminants onto the porous media or the aggregation of contaminants resulting in physical straining.

In study 1, the transport of Cd^{2+} was inhibited more significantly at pH 7 than at pH 5. With the increase in pH, the zeta-potential of sand is more negative due to the deionization of surface hydroxyl groups. Therefore, more positively charged Cd^{2+} ions could be adsorbed onto the sand through the stronger electrostatic attraction, inhibiting the Cd^{2+} mobility.

In study 2, the transport of petroleum colloids in both sand and sandy soil was strongly promoted with increasing pH (5.0–9.0) (see Fig. 5(a, b) in study 2). The mechanisms are as follows: on the one hand, due to the deprotonation of the acidic groups on petroleum colloids (Nenningsland et al., 2011), the surface charge of petroleum colloids is more negative at higher pH, resulting in stronger electrostatic repulsion. Therefore, the aggregation of petroleum colloids is significantly inhibited at higher pH, which could be proven by the decrease of hydrodynamic diameter of petroleum colloids (1.23 μm at pH 5.0, 1.05 μm at pH 7.0 and 0.92 μm at pH 9.0). Thus the effect of physical straining becomes weak. On the other hand, the pH variation has an influence on the electrostatic interaction between petroleum colloids and porous media., the zeta potential values of sand and sandy soil were also more negative at a higher pH (see Fig. S10 in study 2). Thus, the electrostatic repulsion force between petroleum colloids and sand/ sandy soil plays a more dominant role in enhancing the transport of petroleum colloids at different pH.

In study 3, the pH significantly influenced the transport of polystyrene nanoplastics (PS-NPs). PS-NPs showed high mobility at pH 9 and low mobility at pH 5 (see Fig. 3(a) in study 3). These retentions of PS-NPs can be explained from the following aspects: Firstly, the increase in pH affects the surface charge of iron oxyhydroxide coating. For example, at pH 9, iron oxyhydroxide coating was negatively charged; in contrast, at pH 7 and 5, the coating was positively charged (Wang et al., 2012). The PS-NPs were negatively charged over the analyzed pH range and their zeta potential decreased with increasing pH (-24.6 mV at pH 5, -32.7 mV at pH 7 and -42.6 mV at pH 9). Therefore, at pH 5 and 7, more negatively charged PS-NPs can be adsorbed onto the positively charged iron oxyhydroxide coatings via electrostatic attraction, while at pH 9, fewer PS-NPs deposit on the coatings due to the electrostatic repulsion. Secondly, similar to the above-mentioned reason, the zeta-potential value of uncoated sand is more negative with the increase in pH. The interaction energy between PS-NPs and uncoated sand was calculated by DLVO theory (see Fig. 3(b) in study 3). Both energy barrier and secondary

minimum are higher at higher pH, meaning that PS-NPs are more difficult to deposit onto the sand at higher pH.

In study 4, pH exerted a significant impact on the transport behavior of PS-NPs in clay minerals (see Fig. 2 in study 4). For kaolinite, significant retention was observed at pH 5.9. With the increase of pH, retention of PS-NPs was gradually reducing. Similarly, for illite, the strongest retention of PS-NPs was found at pH 5.9. Interestingly, at pH 7.0 and 9.0, the breakthrough curves of PS-NPs were almost identical. This can be attributed to the surface charge (variable charge and permanent charge) of clay minerals affected by different pH. For example, the variable charge at the edge sites of kaolinite was positive at pH 5.9 but negative at pH 7.0 and 9.0. In contrast, under all test conditions, the variable charge of illite was negative. Besides, the total surface charge of both kaolinite and illite became more negative at higher pH. Thus, the absolute values of the zeta potential of PS-NPs and clay minerals increased with increasing pH (see Table 2 in study 4), indicating that the deposition of PS-NPs becomes more difficult at higher pH. Results from the DLVO calculation also support this conclusion.

3.1.3 Effects of ionic strength (IS) on the transport of petroleum colloids and PS-NPs (study 2–4)

The effects of IS on the transport of contaminants mainly depend on its influence on the surface potential of both contaminants and porous media resulting from the compression of the electrical double layer at high IS. Accordingly, the changed interaction potential energy will contribute to the deposition of contaminants onto the porous media or the aggregation of contaminants which leads to physical straining.

In study 2, the IS strongly inhibited the transport of petroleum colloids, especially at high IS (see Fig. 1 in study 2). Under the experimental conditions, the petroleum colloids and porous media are negatively charged. With increasing IS, the surface potential of petroleum colloids and porous media is less negative due to the compression of the electrical double layer (Ryan and Elimelech, 1996); for example, when IS increased from 10 mM to 50 mM NaCl, the zeta potential values of petroleum colloids and sand changed from -23.3 mV to -7.5 mV and from -19.5 mV to -8.6 mV, respectively. The electrostatic repulsion between colloids and sand declines with increasing IS, enhancing petroleum colloid deposition onto the porous media as expected by DLVO theory. In addition, due to the decrease of the surface potential of petroleum colloids, significant aggregation occurs at high IS (from 0.76 μm at 10 mM NaCl to 1.56 μm at 50 mM NaCl) (Gong et al., 2014). Physical straining gradually plays a vital role in the transport of petroleum colloids at high IS (Bradford et al., 2007).

In study 3, the transport of PS-NPs was also inhibited at high IS. Like in study 2, IS affects PS-NPs mobility by changing the surface charge of PS-NPs and porous media. For example, the zeta potential of PS-NPs and uncoated sand increased from -28.4 mV to -27.4 mV and from -48.1 mV to -46.4 mV, respectively, when IS increased from 1 mM NaCl to 5 mM NaCl. As a result, based on DLVO theory, the energy barrier and secondary minimum are lower at the higher IS, indicating that the PS-NPs can easily deposit onto the uncoated sand by secondary minimum or primary minimum. Therefore, PS-NPs retention increases with increasing ionic strength. Note that the effect of IS on PS-NPs aggregation can be ignored because the

hydrodynamic diameter of PS-NPs was stable and close to the single PS-NP size. Physical straining could be overlooked in this research.

In study 4, IS also played an important role in the transport of PS-NPs in clay minerals. The PS-NPs mobility decreased with increasing IS. For example, In the kaolinite group, increasing IS from 10 mM NaCl to 50 mM NaCl caused a drop in maximum breakthrough from 51.3% to ~0%. The influence of IS on the surface charge of both PS-NPs and porous media is the dominant factor for the mobility of PS-NPs. For instance, as presented in Table 1 of study 4, changing IS from 10 mM over 30 mM to 50 mM NaCl caused an increase in zeta potential values: for PS-NPs from -78.9 mV over -69.4 mV to -61.7 mV and for kaolinite from -38.1 mV over -33.7 mV to -31.7 mV. The surface charge of both particles and porous media becomes less negative due to the compression of the electrical double layer with increasing IS (Ryan and Elimelech, 1996); thus, the electrostatic repulsion between PS-NPs and collector decreases at high IS, favoring the PS-NPs deposition. This mechanism also can be applied for the PS-NPs transport in illite. Moreover, even though the electrostatic repulsion between PS-NPs also decreased at high IS, no obvious aggregation happened among PS-NPs, indicating that physical straining did not work during their transport.

3.1.4 Effects of cations on the transport of Cd^{2+} , petroleum colloids, and PS-NPs (study 1–3)

In general, the effects of cations are mainly demonstrated in the following aspects: (1) cations can be competing ions to promote the contaminant transport; (2) the surface potentials of both contaminant and porous media will be modified to different extents by different cations; the interaction potential energy between contaminants and porous media may be in favor of contaminants deposition or the interaction between contaminants can be conducive to the aggregation of contaminants leading to physical straining; (3) the cations can interact with contaminants to form complexes, which may increase the retention of contaminants; (4) some cations, especially divalent cations, are bridging agents which can act as a bridge connecting the porous media and contaminant.

In study 1, we investigated the effects of Pb^{2+} on the transport of Cd^{2+} in the presence /absence of citric acid (see Fig. 5 in study 1). The addition of Pb^{2+} could significantly promote the transport of Cd^{2+} irrespective of citric acid presence. This phenomenon is attributed to the intense competition between Cd^{2+} and Pb^{2+} for the deposition sites. The affinity of Pb^{2+} toward sand is stronger than that of Cd^{2+} (Fonseca et al., 2011); additionally, citric acid has a more remarkable complex ability with Pb^{2+} rather than Cd^{2+} (Kalmykova et al., 2008). Therefore, Pb^{2+} acting as a competing ion will do good to the Cd^{2+} transport.

In study 2, the effects of Ca^{2+} on the transport of petroleum colloids were studied. In general, the retention of petroleum colloids in the porous media increased with the increase of Ca^{2+} concentration (see Fig. 4 in study 2). This behavior is caused by three main reasons: Firstly, due to the compression of the electrical double layer caused by increasing Ca^{2+} concentration, the surface charges of petroleum colloids and porous media are less negative (Ryan and Elimelech, 1996). The decrease in electrostatic repulsion between colloids and porous media leads to more deposition of petroleum colloids. Secondly, the electrostatic repulsion between petroleum colloids is also reduced; their aggregation becomes obvious (from 0.81 μm at 0.1 mM CaCl_2 to

1.18 μm at 1.0 mM CaCl_2); thus, the physical straining exerts a significant influence on their mobility. Thirdly, Ca^{2+} is a typical bridging agent, which means Ca^{2+} can serve as a bridge between the colloids and porous media via connecting the carboxylic, hydroxyl functional groups on colloid and porous media surfaces (Yi and Chen, 2011). Therefore, with the increase in Ca^{2+} concentration, more petroleum colloids can be fixed in the porous media by the cation bridging effect.

In study 3, the effects of monovalent cations and divalent cations on the transport of PS-NPs were analyzed. Overall, the mobility of PS-NPs decreased with increasing atomic number: $\text{Na}^+ > \text{K}^+ > \text{Cs}^+$; $\text{Mg}^{2+} \geq \text{Ca}^{2+} > \text{Ba}^{2+}$ (see Fig. 5 in study 3). Even though the concentrations of monovalent and divalent cations were maintained constant, different cations affected the surface potential of both PS-NPs and porous media to different extents (see Table 1 in study 3). DLVO theory provides the first explanation of this sequence. In addition, for the analyzed group of monovalent cations, unlike Na^+ and K^+ , Cs^+ can work as a bridging agent (Xia et al., 2017), more PS-NPs connect to the collector via Cs bridge. Furthermore, the positively charged cations are adsorbed onto the negatively charged uncoated sand; thereby, inhibiting the deposition of PS-NPs by steric hindrance which depends on the hydrated radius of the cation (Xia et al., 2015). Usually, the hydrated radius of monovalent cation is in the order of $\text{Na}^+ > \text{K}^+ > \text{Cs}^+$ (Nightingale Jr, 1959); thus, Cs^+ has the weakest steric hindrance resulting in the strongest deposition of PS-NPs. For divalent cations, the mechanisms are similar; DLVO theory and cation bridging are responsible for the deposition of PS-NPs; and Ba^{2+} is a stronger bridging agent than Ca^{2+} and Mg^{2+} (Xia et al., 2017). Note that these cations seemed to have no significant effect on the hydrodynamic diameter of PS-NPs. Physical straining can be ignored.

3.1.5 Effects of surfactant on the transport of petroleum colloids (study 2)

The existence of sodium dodecyl sulfate (SDS), a model surfactant, could promote the transport of petroleum colloids (see Fig. 6 in study 2) via the following mechanisms. First, SDS has an amphiphilic nature which could facilitate the dispersion of petroleum colloids (Atta et al., 2014), avoiding physical straining during transport. Second, SDS can also be adsorbed onto porous media via hydrophobic bonding, ion exchange, ion pairing, etc. (Paria and Khilar, 2004), which can enhance the steric hindrance with petroleum colloids.

3.2 How does the porous media affect the transport of contaminants?

3.2.1 Effects of quartz sand on Cd^{2+} and petroleum colloids transport (study 1–2)

Quartz sand is the ideal porous media to study the transport of contaminants, especially for the studies focusing on effects of solution chemistry; because the size and surface properties of quartz sand are uniform and stable. Usually, the impact of quartz sand on the transport of contaminants is mainly dependent on its surface charge. Some studies also suggest the presence of metal oxides on the sand surface, which may provide additional deposition sites for contaminants (Lu et al., 2017; Qi et al., 2014b).

In study 1, the positively charged Cd^{2+} ions were adsorbed by the negatively charged quartz

sand via electrostatic attraction. In addition, with the addition of LMWOAs, the surface charge of quartz sand was more negative resulting from the LMWOAs adsorption onto the sand (Huang et al., 2003). Thus, more Cd^{2+} deposited on quartz sand.

In study 2, the surface charge of quartz sand became more negative with increasing pH due to the pH-dependent functional groups on quartz sand surface which can gain or lose protons at different pH (Jada et al., 2006). Furthermore, the surface charge of quartz sand was less negative with the increase in IS because of the compression of the electrical double layer (Ryan and Elimelech, 1996). Therefore, the transport of petroleum colloids was inhibited at low pH or high IS.

3.2.2 Effects of sandy soil on petroleum colloids transport (study 2)

Like quartz sand, the effects of sandy soil on petroleum colloid transport are also dependent on its surface charge. Certainly, sandy soil exhibits its own unique properties. For instance, there are many impurities, such as metal oxides, organic matter, and clays, in sandy soil, which could provide favorable deposition sites for petroleum colloids (Cornelis et al., 2013). In addition, the wide ranges of particle size distributions, the non-uniform and irregular shapes of the soil ingredients, as well as rough surfaces of grains can result in narrow pore throats and complex flow pathways in the sandy soil (Qi et al., 2014a), which caused enhanced physical straining. Therefore, the retention of petroleum colloids was stronger in sandy soil than in quartz sand under the same experimental condition.

3.2.3 Effects of iron oxyhydroxide coated sand on PS-NPs transport (study 3)

Iron oxyhydroxide coated sand also affected the transport of PS-NPs through its surface charges. We can divide iron oxyhydroxide coated sand into a coated part (iron oxyhydroxide) and an uncoated part (quartz sand) to analyze its effects. Because the point of zero charge (pH_{pzc}) of iron oxyhydroxide is relatively high (Cornell and Schwertmann, 2003), the iron oxyhydroxide is positively charged for most cases; and the uncoated quartz sand is negatively charged. In addition, the surface charges of both iron oxide coatings and uncoated quartz sand are controlled by solution chemistry. For example, the surface charge of uncoated quartz sand was more negative at increasing pH; the surface charge of iron oxyhydroxide changed from positive at pH 5 and 7 to negative at pH 9 (pH_{pzc} of iron oxyhydroxide is 8.5–8.8). As a result, at low pH, not only is the electrostatic repulsion between PS-NPs and uncoated sand weak, but the positively charged iron oxyhydroxide also provides additional deposition sites via electrostatic attraction. Thus, the negatively charged PS-NPs had the strongest mobility at pH 9 and the weakest mobility at pH 5.

3.2.4 Effects of clay minerals on PS-NPs transport (study 4)

Kaolinite and illite showed significant effects on the transport of PS-NPs via their physical and chemical properties. For instance, compared with quartz sand, the zeta potentials of clay minerals were less negative under the experimental conditions; Besides, illite was more negative than kaolinite (see Table 2 in study 4). Thus, more PS-NPs deposited onto clay minerals rather than quartz sand, which was explained by DLVO theory. In addition, even though the net charges of these clay minerals are negative, there are some positive charges

resulting from protonation/deprotonation of some amphoteric sites, such as octahedral Al–OH sites, at broken edges, when the pH is higher than the pH_{pzc} of clay minerals (Singh et al., 2014). For example, under the experimental condition (pH 5.9), the edge sites of kaolinite were positively charged (pH_{PZC} of kaolinite is ~ 6.5); in contrast, the edge sites of illite were negatively charged (pH_{PZC} of illite is ~ 2.5). Therefore, the negatively charged PS-NPs were adsorbed onto kaolinite via electrostatic attraction. Except for the influence of the surface charge of clay minerals, physical straining caused by the small size of clay minerals cannot be ignored. In this study, the average sizes of the clay minerals were much smaller compared to the quartz sand ($d_{0.5} = 8.6 \mu\text{m}$ for kaolinite; $4.5 \mu\text{m}$ for illite and $292 \mu\text{m}$ for quartz sand) (see Fig. S1 in study 4). Thus, the clay minerals can alter the flow pathways by creating narrower pore throats and dead-end pores (Lu et al., 2017). Physical straining enhanced the retention of PS-NPs. At last, clay minerals usually contain some metal oxide impurities due to different degrees of weathering (Singer, 1984). It has been reported that even small amounts of metal oxides could significantly affect the transport behavior of negatively charged particles (Wu et al., 2020).

3.3 How does the contaminant property affect the transport of contaminants?

In this thesis, we chose three different contaminants. Overall, the surface charge of contaminants is the most crucial aspect affecting their mobility. Cd^{2+} is positively charged, whereas petroleum colloids and polystyrene nanoplastics are negatively charged. Because quartz sand, sandy soil, and clay minerals are negatively charged, the transport of Cd^{2+} is under favorable conditions; in contrast, the transport of petroleum colloid and the transport of polystyrene nanoplastics are under unfavorable conditions. Besides, the surface charge of petroleum colloids and polystyrene nanoplastics are under the control of solution chemistry; for instance, the zeta potential of these particles decreased (more negative) with the increase in pH, which facilitated their transport. Apart from chemical properties, these particles can form aggregation under some favorable conditions (like high IS and low pH), which will induce physical straining. As an illustration, in study 2, the petroleum colloids aggregated obviously at low pH (particle size: $1.23 \mu\text{m}$ at pH 5.0, $1.05 \mu\text{m}$ at pH 7.0, and $0.92 \mu\text{m}$ at pH 9.0). Thus, dp/dc (~ 0.003) was above the critical value of physical straining (0.002).

4 Conclusions and outlook

4.1 Conclusions

In order to comprehensively and systematically evaluate migration patterns of environmental contaminants in groundwater aquifers, the studies of contaminant transport in porous media were carried out from three fundamental aspects: the contaminant properties, the types of porous media, and the water chemistry conditions. For example, we set different clay mineral contents to model environmentally relevant soil conditions as well as different pH, IS, and organic matters to reveal groundwater hydrochemistry in the real environment. These factors are considered to gain insights into the interaction mechanisms between environmental contaminants, porous media, and solution chemistry. Combining the research contents and results from studies 1–4, the following conclusions were drawn.

- (1) Cd^{2+} , a positively charged ion, could be adsorbed onto the negatively charged quartz sand by electrostatic attraction. However, the transport of Cd^{2+} was significantly affected after the addition of LMWOAs, because Cd^{2+} can form complexes with these organic acids. At the same time, the organic acids are adsorbed onto the quartz sand through hydrogen bonds, which could change the surface charge of the quartz sand. Under acidic conditions, the addition of organic acids inhibited the transport of Cd^{2+} : Firstly, the quartz sand adsorbed by organic acids becomes more negative, causing stronger electrostatic attraction between Cd^{2+} and sand. Secondly, the adsorbed organic acids form complexes with Cd^{2+} . In addition, the inhibitory effects of different LMWOAs were in the following order: citric acid > tartaric acid > acetic acid, resulting from the structure of the organic acid and its affinity towards Cd^{2+} . Interestingly, under neutral conditions, organic acids promoted the transport of Cd^{2+} . Because high pH inhibits the adsorption of LMWOAs on quartz sand, and Cd^{2+} is more likely to form non-absorbing Cd-organic acid complexes with LMWOAs. When competing ions (Pb^{2+}) were added, Pb^{2+} significantly facilitated the migration of Cd^{2+} due to its more pronounced ability to form complexes with organic acid than Cd^{2+} .
- (2) The migration of petroleum colloids was enhanced with increasing pH, weakened by increasing ionic strength, and strengthened by the addition of SDS in both sand and sandy soil. The variation in the migration capacity of these colloids is mainly caused by the surface potentials of the porous media and colloids which vary with the water chemistry conditions. For instance, as the pH increased, the zeta potential of the porous media and colloid became more and more negative, leading to an increase in the electrostatic repulsion between them. Besides, the electrostatic repulsion between petroleum colloids also increased, which inhibited the aggregation of colloids. Physical straining is inhibited, which facilitates the transport of petroleum colloids. In addition, Ca^{2+} has a cation bridging effect and SDS has an amphiphilic nature, which also affected petroleum colloid migration. There were some differences in the transport of petroleum colloids in the sand and sandy soil due to the different physicochemical components in these two different porous media. Sandy soil usually contains metal oxides, clay minerals, and organic matter, which provide more

deposition sites for petroleum colloids. In addition, soil particles are smaller, finer, and more inhomogeneous than the sand, leading to thinner pore throats and more complicated flow pathways in the soil column. Therefore, physical straining was more significant in sandy soil during petroleum colloid transport.

- (3) The PS-NPs transport in iron oxyhydroxide coated sand was also influenced by the solution chemistry. The main reason is that the solution chemistry affects the surface charge of PS-NPs and iron oxyhydroxide coated quartz sand. For example, under most experimental conditions ($\text{pH} < 9$), the iron oxyhydroxide coating was positively charged, which attracted the negatively charged PS-NPs and inhibited the migration of PS-NPs. However, when the solution pH increased to 9, the iron coatings became negatively charged, which weakened the adsorption of PS-NPs and enhanced the transport of PS-NPs. In addition, PS-NPs migration was more greatly influenced by divalent cations than monovalent cations. The effect of cations having the same valence on PS-NPs migration is dependent on their cation radius. The smaller the radius of the cation, the larger its hydration radius (hydration radius $\text{Na}^+ > \text{K}^+ > \text{Cs}^+$, $\text{Mg}^{2+} > \text{Ca}^{2+} > \text{Ba}^{2+}$). The cation with a larger hydration radius has a weaker ability to bind PS-NPs, which favored the lowest retention of PS-NPs in the presence of Na^+ . In addition, the bridging effect of divalent cations led to a stronger inhibition on PS-NPs transport than monovalent cations.
- (4) Under different water chemistry conditions, clay minerals had a strong influence on PS-NPs transport due to the impacts of water chemistry on the surface charge of the clay minerals. For example, increasing IS and decreasing pH resulted in the less negative zeta potential of clay minerals, which enhanced PS-NPs deposition. In addition, the small size of the clay minerals led to significant physical straining which promoted PS-NPs retention in illite. Different clay minerals have different effects on PS-NPs migration. The inhibition on PS-NPs transport was stronger in kaolinite than in illite. Clay minerals have a portion of variable charge on their surface which varies with the pH of the solution. pH_{pzc} of kaolinite and illite are ~ 6.5 and ~ 2.5 , respectively. Under experimental conditions ($\text{pH} 5.9$), more negatively charged PS-NPs were adsorbed onto kaolinite (with positive variable charges) than onto illite (with negative variable charges).

4.2 Research outlook

This dissertation has presented a preliminary study on the transport of environmental contaminants in saturated porous media. The relationships between contaminant properties, the types of porous media, and the water chemistry conditions were discussed. Although we have tried to consider a variety of factors in this work, there remain some shortcomings. Therefore, subsequent studies should be carried out in the following aspects.

Firstly, the research scope of contaminants should be expanded. In this thesis, only three typical contaminants were selected. However, in nature, pollutants with different surface charges, binding capacities, particle sizes, shapes, etc., can be found in abundance. As this thesis has shown, different contaminant properties will significantly influence its migration capacity. In addition, the interaction mechanisms between two or more pollutants and the laws of co-

transport of these pollutants need to be studied in detail.

Secondly, more diversification in the choice of investigated porous media is needed. Different types of soils and rock sediments can be collected. For example, soil containing metallic minerals such as iron ore, aluminum ore, and manganese ore can be chosen as the porous media to fill the columns. Experiments with porous media that have been extracted from nature will enhance the applicability of the research findings to realistic environmental conditions.

Finally, more efforts should be put into the development of mathematical models. The two-site model used in this thesis only considers the attachment and straining processes, which restricts its application in more complex conditions, like the co-transport of two contaminants in natural soil. The establishment of mathematical models suitable for describing different pollutants, different types of porous media, and various water chemistry conditions is essential for accurately predicting the migration of contaminants.

5 References

- Akbour, R.A., Douch, J., Hamdani, M., Schmitz, P., 2002. Transport of kaolinite colloids through quartz sand: influence of humic acid, Ca²⁺, and trace metals. *Journal of Colloid and Interface Science* 253, 1–8.
- Atta, A.M., Allohedan, H.A., El-Mahdy, G.A., 2014. Dewatering of petroleum crude oil emulsions using modified Schiff base polymeric surfactants. *Journal of Petroleum Science and Engineering* 122, 719–728.
- Baba, A., Tayfur, G., 2011. Groundwater contamination and its effect on health in Turkey. *Environmental Monitoring and Assessment* 183, 77–94.
- Bradford, S.A., Simunek, J., Bettahar, M., Van Genuchten, M.T., Yates, S., 2006. Significance of straining in colloid deposition: Evidence and implications. *Water Resources Research* 42, W12S15.
- Bradford, S.A., Torkzaban, S., Walker, S.L., 2007. Coupling of physical and chemical mechanisms of colloid straining in saturated porous media. *Water research* 41, 3012–3024.
- Buschow, K.J., Cahn, R.W., Flemings, M.C., Ilshner, B., Kramer, E.J., Mahajan, S., 2001. *Encyclopedia of materials: Science and technology*. Elsevier.
- Cai, L., Peng, S., Wu, D., Tong, M., 2016. Effect of different-sized colloids on the transport and deposition of titanium dioxide nanoparticles in quartz sand. *Environmental Pollution* 208, 637–644.
- Cheng, D., Liao, P., Yuan, S., 2016. Effects of ionic strength and cationic type on humic acid facilitated transport of tetracycline in porous media. *Chemical Engineering Journal* 284, 389–394.
- Cornelis, G., Hund-Rinke, K., Kuhlbusch, T., Van den Brink, N., Nickel, C., 2014. Fate and bioavailability of engineered nanoparticles in soils: a review. *Critical Reviews in Environmental Science & Technology* 44, 2720–2764.
- Cornelis, G., Pang, L., Doolette, C., Kirby, J.K., McLaughlin, M.J., 2013. Transport of silver nanoparticles in saturated columns of natural soils. *Science of the Total Environment* 463, 120–130.
- Cornell, R.M., Schwertmann, U., 2003. *The iron oxides: structure, properties, reactions, occurrences and uses*. John Wiley & Sons.
- Dong, S., Gao, B., Sun, Y., Shi, X., Xu, H., Wu, J., Wu, J., 2016. Transport of sulfacetamide and levofloxacin in granular porous media under various conditions: Experimental observations and model simulations. *Science of the Total Environment* 573, 1630–1637.
- Dong, Z., Hou, Y., Han, W., Liu, M., Wang, J., Qiu, Y., 2020. Protein corona-mediated transport of nanoplastics in seawater-saturated porous media. *Water Research* 182, 115978.
- Duruibe, J.O., Ogwuegbu, M., Egwurugwu, J., 2007. Heavy metal pollution and human biotoxic effects. *International Journal of Physical Sciences* 2, 112–118.
- Elimelech, M., O'Melia, C.R., 1990a. Effect of particle size on collision efficiency in the deposition of Brownian particles with electrostatic energy barriers. *Langmuir* 6, 1153–1163.
- Elimelech, M., O'Melia, C.R., 1990b. Kinetics of deposition of colloidal particles in porous media. *Environmental Science & Technology* 24, 1528–1536.

- Fan, W., Jiang, X., Yang, W., Geng, Z., Huo, M., Liu, Z., Zhou, H., 2015. Transport of graphene oxide in saturated porous media: Effect of cation composition in mixed Na–Ca electrolyte systems. *Science of the Total Environment* 511, 509–515.
- Fang, J., Xu, M.J., Wang, D.J., Wen, B., Han, J.Y., 2013. Modeling the transport of TiO₂ nanoparticle aggregates in saturated and unsaturated granular media: effects of ionic strength and pH. *Water Research* 47, 1399–1408.
- Fonseca, B., Figueiredo, H., Rodrigues, J., Queiroz, A., Tavares, T., 2011. Mobility of Cr, Pb, Cd, Cu and Zn in a loamy sand soil: A comparative study. *Geoderma* 164, 232–237.
- Foppen, J.W., Lutterodt, G., Röling, W.F., Uhlenbrook, S., 2010. Towards understanding inter-strain attachment variations of *Escherichia coli* during transport in saturated quartz sand. *Water Research* 44, 1202–1212.
- Franchi, A., O'Melia, C.R., 2003. Effects of natural organic matter and solution chemistry on the deposition and reentrainment of colloids in porous media. *Environmental Science & Technology* 37, 1122–1129.
- Gong, Y., Zhao, X., Cai, Z., O'reilly, S., Hao, X., Zhao, D., 2014. A review of oil, dispersed oil and sediment interactions in the aquatic environment: influence on the fate, transport and remediation of oil spills. *Marine Pollution Bulletin* 79, 16–33.
- Gregory, J., 1981. Approximate expressions for retarded van der Waals interaction. *Journal of Colloid and Interface Science* 83, 138–145.
- Grolimund, D., Borkovec, M., 2006. Release of colloidal particles in natural porous media by monovalent and divalent cations. *Journal of Contaminant Hydrology* 87, 155–175.
- He, L., Wu, D., Tong, M., 2019. The influence of different charged poly (amido amine) dendrimer on the transport and deposition of bacteria in porous media. *Water Research* 161, 364–371.
- Hizal, J., Apak, R., Hoell, W., 2009. Modeling competitive adsorption of copper (II), lead (II), and cadmium (II) by kaolinite–based clay mineral/humic acid system. *Environmental Progress & Sustainable Energy* 28, 493–506.
- Hogg, R., Healy, T.W., Fuerstenau, D.W., 1966. Mutual coagulation of colloidal dispersions. *Transactions of the Faraday Society* 62, 1638–1651.
- Hu, H.-Q., Liu, H.-L., He, J.-Z., Huang, Q.-Y., 2007. Effect of selected organic acids on cadmium sorption by variable- and permanent-charge soils. *Pedosphere* 17, 117–123.
- Hu, Y., Guo, T., Ye, X., Li, Q., Guo, M., Liu, H., Wu, Z., 2013. Dye adsorption by resins: effect of ionic strength on hydrophobic and electrostatic interactions. *Chemical Engineering Journal* 228, 392–397.
- Huang, L., Hu, H., Li, X., Li, L.Y., 2010. Influences of low molar mass organic acids on the adsorption of Cd²⁺ and Pb²⁺ by goethite and montmorillonite. *Applied Clay Science* 49, 281–287.
- Huang, Q., Zhao, Z., Chen, W., 2003. Effects of several low-molecular weight organic acids and phosphate on the adsorption of acid phosphatase by soil colloids and minerals. *Chemosphere* 52, 571–579.
- Illés, E., Tombácz, E., 2006. The effect of humic acid adsorption on pH-dependent surface charging and aggregation of magnetite nanoparticles. *Journal of Colloid and Interface Science* 295, 115–123.
- Jada, A., Akbourn, R.A., Douch, J., 2006. Surface charge and adsorption from water onto quartz

- sand of humic acid. *Chemosphere* 64, 1287–1295.
- Jaisi, D.P., Saleh, N.B., Blake, R.E., Elimelech, M., 2008. Transport of single-walled carbon nanotubes in porous media: filtration mechanisms and reversibility. *Environmental Science & Technology* 42, 8317–8323.
- Kalmykova, Y., Strömvall, A.-M., Steenari, B.-M., 2008. Adsorption of Cd, Cu, Ni, Pb and Zn on Sphagnum peat from solutions with low metal concentrations. *Journal of Hazardous Materials* 152, 885–891.
- Kamrani, S., Rezaei, M., Kord, M., Baalousha, M., 2018. Transport and retention of carbon dots (CDs) in saturated and unsaturated porous media: Role of ionic strength, pH, and collector grain size. *Water Research* 133, 338–347.
- Kong, Q., Xie, B., Preis, S., Hu, Y., Wu, H., Wei, C., 2018. Adsorption of Cd²⁺ by an ion-imprinted thiol-functionalized polymer in competition with heavy metal ions and organic acids. *RSC advances* 8, 8950–8960.
- Kretzschmar, R., Sticher, H., 1998. Colloid transport in natural porous media: influence of surface chemistry and flow velocity. *Physics and Chemistry of the Earth* 23, 133–139.
- Kuznar, Z.A., Elimelech, M., 2007. Direct microscopic observation of particle deposition in porous media: Role of the secondary energy minimum. *Colloids and Surfaces A: Physicochemical and Engineering Aspects* 294, 156–162.
- Li, J., Chen, J., Lu, T., Wang, Y., Zhang, H., Shang, Z., Li, D., Zhou, Y., Qi, Z., 2019a. Effects of low-molecular weight organic acids on the transport of graphene oxide nanoparticles in saturated sand columns. *Science of the Total Environment* 666, 94–102.
- Li, W., Zhang, H., Lu, T., Li, Y., Song, Y., Shang, Z., Liu, S., Li, D., Qi, Z., 2019b. Effects of divalent metal cations and inorganic anions on the transport of tetracycline in saturated porous media: column experiments and numerical simulations. *Environmental Science: Processes & Impacts* 21, 1153–1163.
- Liang, L., Ju, L., Hu, J., Zhang, W., Wang, X., 2016. Transport of sodium dodecylbenzene sulfonate (SDBS)-dispersed carbon nanotubes and enhanced mobility of tetrabromobisphenol A (TBBPA) in saturated porous media. *Colloids and Surfaces A: Physicochemical and Engineering Aspects* 497, 205–213.
- Lin, D., Tian, X., Wu, F., Xing, B., 2010. Fate and transport of engineered nanomaterials in the environment. *Journal of Environmental Quality* 39, 1896–1908.
- Liu, W., Sun, W., Borthwick, A.G., Ni, J., 2013. Comparison on aggregation and sedimentation of titanium dioxide, titanate nanotubes and titanate nanotubes-TiO₂: Influence of pH, ionic strength and natural organic matter. *Colloids and Surfaces A: Physicochemical and Engineering Aspects* 434, 319–328.
- Lu, T., Gilfedder, B.S., Peng, H., Peiffer, S., Papastavrou, G., Ottermann, K., Frei, S., 2021. Relevance of Iron Oxyhydroxide and Pore Water Chemistry on the Mobility of Nanoplastic Particles in Water-Saturated Porous Media Environments. *Water, Air, & Soil Pollution* 232, 1–13.
- Lu, T., Xia, T., Qi, Y., Zhang, C., Chen, W., 2017. Effects of clay minerals on transport of graphene oxide in saturated porous media. *Environmental Toxicology and Chemistry* 36, 655–660.
- Malandrino, M., Abollino, O., Giacomino, A., Aceto, M., Mentasti, E., 2006. Adsorption of heavy metals on vermiculite: influence of pH and organic ligands. *Journal of Colloid and*

- Interface Science 299, 537–546.
- Marino, M.A., 1974. Distribution of contaminants in porous media flow. *Water Resources Research* 10, 1013–1018.
- Mukherjee, I., Singh, U.K., 2020. Fluoride abundance and their release mechanisms in groundwater along with associated human health risks in a geologically heterogeneous semi-arid region of east India. *Microchemical Journal* 152, 104304.
- Najafi, S., Jalali, M., 2015. Effects of organic acids on cadmium and copper sorption and desorption by two calcareous soils. *Environmental Monitoring and Assessment* 187, 1–10.
- Nascimento, A., Totola, M., Souza, C., Borges, M., Borges, A., 2006. Temporal and spatial dynamics of blocking and ripening effects on bacterial transport through a porous system: A possible explanation for CFT deviation. *Colloids and Surfaces B: Biointerfaces* 53, 241–244.
- Nenningsland, A.L., Gao, B., Simon, S., Sjöblom, J., 2011. Comparative study of stabilizing agents for water-in-oil emulsions. *Energy & Fuels* 25, 5746–5754.
- Nightingale Jr, E., 1959. Phenomenological theory of ion solvation. Effective radii of hydrated ions. *The Journal of Physical Chemistry* 63, 1381–1387.
- Paria, S., Khilar, K.C., 2004. A review on experimental studies of surfactant adsorption at the hydrophilic solid–water interface. *Advances in Colloid and Interface Science* 110, 75–95.
- Qi, Z., Zhang, L., Chen, W., 2014a. Transport of graphene oxide nanoparticles in saturated sandy soil. *Environmental Science: Processes & Impacts* 16, 2268–2277.
- Qi, Z., Zhang, L., Wang, F., Hou, L., Chen, W., 2014b. Factors controlling transport of graphene oxide nanoparticles in saturated sand columns. *Environmental Toxicology and Chemistry* 33, 998–1004.
- Raikwar, M.K., Kumar, P., Singh, M., Singh, A., 2008. Toxic effect of heavy metals in livestock health. *Veterinary World* 1, 28.
- Rao, C., Yan, B., 2020. Study on the interactive influence between economic growth and environmental pollution. *Environmental Science and Pollution Research* 27, 39442–39465.
- Ross, A., Martinez-Santos, P., 2010. The challenge of groundwater governance: case studies from Spain and Australia. *Regional Environmental Change* 10, 299–310.
- Ryan, J.N., Elimelech, M., 1996. Colloid mobilization and transport in groundwater. *Colloids and Surfaces A: Physicochemical and Engineering Aspects* 107, 1–56.
- Saka, E., Guler, C., 2006. The effects of electrolyte concentration, ion species and pH on the zeta potential and electrokinetic charge density of montmorillonite. *Clay Minerals* 41, 853–861.
- Sen, T.K., 2011. Processes in pathogenic biocolloidal contaminants transport in saturated and unsaturated porous media: a review. *Water, Air, & Soil Pollution* 216, 239–256.
- Shaniv, D., Dror, I., Berkowitz, B., 2021. Effects of particle size and surface chemistry on plastic nanoparticle transport in saturated natural porous media. *Chemosphere* 262, 127854.
- Shen, C., Lazouskaya, V., Jin, Y., Li, B., Ma, Z., Zheng, W., Huang, Y., 2012. Coupled factors influencing detachment of nano- and micro-sized particles from primary minima. *Journal of Contaminant Hydrology* 134, 1–11.
- Shen, C., Li, B., Huang, Y., Jin, Y., 2007. Kinetics of coupled primary- and secondary-minimum deposition of colloids under unfavorable chemical conditions. *Environmental Science &*

- Technology 41, 6976–6982.
- Shen, C., Li, B., Wang, C., Huang, Y., Jin, Y., 2011. Surface roughness effect on deposition of nano - and micro - sized colloids in saturated columns at different solution ionic strengths. *Vadose Zone Journal* 10, 1071–1081.
- Singer, A., 1984. The paleoclimatic interpretation of clay minerals in sediments—a review. *Earth-Science Reviews* 21, 251–293.
- Singh, B., Cattle, S., Field, D., 2014. Edaphic Soil Science, Introduction to. *Encyclopedia of Agriculture and Food Systems* 3, 35–58.
- Stevik, T.K., Aa, K., Ausland, G., Hanssen, J.F., 2004. Retention and removal of pathogenic bacteria in wastewater percolating through porous media: a review. *Water Research* 38, 1355–1367.
- Tian, Y., Gao, B., Silvera-Batista, C., Ziegler, K.J., 2010. Transport of engineered nanoparticles in saturated porous media. *Journal of Nanoparticle Research* 12, 2371–2380.
- Tufenkji, N., Elimelech, M., 2005. Breakdown of colloid filtration theory: Role of the secondary energy minimum and surface charge heterogeneities. *Langmuir* 21, 841–852.
- Vermöhlen, K., Lewandowski, H., Narres, H.-D., Schwuger, M., 2000. Adsorption of polyelectrolytes onto oxides—the influence of ionic strength, molar mass, and Ca²⁺ ions. *Colloids and Surfaces A: Physicochemical and Engineering Aspects* 163, 45–53.
- Victor, P.A., 2017. *Pollution: Economy and environment*. Routledge.
- Wang, D., Bradford, S.A., Harvey, R.W., Gao, B., Cang, L., Zhou, D., 2012. Humic acid facilitates the transport of ARS-labeled hydroxyapatite nanoparticles in iron oxyhydroxide-coated sand. *Environmental Science & Technology* 46, 2738–2745.
- Wang, M., Lu, T., Chen, W., Zhang, H., Qi, W., Song, Y., Qi, Z., 2020a. Enhanced role of humic acid on the transport of iron oxide colloids in saturated porous media under various solution chemistry conditions. *Colloids and Surfaces A: Physicochemical and Engineering Aspects* 607, 125486.
- Wang, Q., Cheng, T., Wu, Y., 2014. Influence of mineral colloids and humic substances on uranium (VI) transport in water-saturated geologic porous media. *Journal of Contaminant Hydrology* 170, 76–85.
- Wang, Y., Lu, T., Zhang, H., Li, Y., Song, Y., Chen, J., Fu, X., Qi, Z., 2020b. Factors affecting the transport of petroleum colloids in saturated porous media. *Colloids and Surfaces A: Physicochemical and Engineering Aspects* 585, 124134.
- Weng, L., Fest, E.P., Fillius, J., Temminghoff, E.J., Van Riemsdijk, W.H., 2002. Transport of humic and fulvic acids in relation to metal mobility in a copper-contaminated acid sandy soil. *Environmental Science & Technology* 36, 1699–1704.
- Wu, D., Tong, M., Kim, H., 2016. Influence of perfluorooctanoic acid on the transport and deposition behaviors of bacteria in quartz sand. *Environmental Science & Technology* 50, 2381–2388.
- Wu, H., Jiang, D., Cai, P., Rong, X., Huang, Q., 2011. Effects of low-molecular-weight organic ligands and phosphate on adsorption of *Pseudomonas putida* by clay minerals and iron oxide. *Colloids and Surfaces B: Biointerfaces* 82, 147–151.
- Wu, X., Lyu, X., Li, Z., Gao, B., Zeng, X., Wu, J., Sun, Y., 2020. Transport of polystyrene nanoplastics in natural soils: Effect of soil properties, ionic strength and cation type. *Science of the Total Environment* 707, 136065.

- Xia, T., Fortner, J.D., Zhu, D., Qi, Z., Chen, W., 2015. Transport of sulfide-reduced graphene oxide in saturated quartz sand: Cation-dependent retention mechanisms. *Environmental Science & Technology* 49, 11468–11475.
- Xia, T., Qi, Y., Liu, J., Qi, Z., Chen, W., Wiesner, M.R., 2017. Cation-inhibited transport of graphene oxide nanomaterials in saturated porous media: the Hofmeister effects. *Environmental Science & Technology* 51, 828–837.
- Yang, H., Ge, Z., Wu, D., Tong, M., Ni, J., 2016. Cotransport of bacteria with hematite in porous media: Effects of ion valence and humic acid. *Water Research* 88, 586–594.
- Yang, H., Kim, H., Tong, M., 2012. Influence of humic acid on the transport behavior of bacteria in quartz sand. *Colloids and Surfaces B: Biointerfaces* 91, 122–129.
- Yang, Q., Li, X., Zhang, L., Wang, G., Chen, G., Lin, D., Xing, B., 2019. Dispersion and stability of multi-walled carbon nanotubes in water as affected by humic acids. *Journal of Molecular Liquids* 279, 361–369.
- Yi, P., Chen, K.L., 2011. Influence of surface oxidation on the aggregation and deposition kinetics of multiwalled carbon nanotubes in monovalent and divalent electrolytes. *Langmuir* 27, 3588–3599.
- Zhang, H., Lu, T., Wang, M., Jin, R., Song, Y., Zhou, Y., Qi, Z., Chen, W., 2020. Inhibitory role of citric acid in the adsorption of tetracycline onto biochars: Effects of solution pH and Cu^{2+} . *Colloids and Surfaces A: Physicochemical and Engineering Aspects* 595, 124731.
- Zhu, M., Wang, H., Keller, A.A., Wang, T., Li, F., 2014. The effect of humic acid on the aggregation of titanium dioxide nanoparticles under different pH and ionic strengths. *Science of the Total Environment* 487, 375–380.

6 Contribution statement

Study 1: Transport of Cd²⁺ through saturated porous media: Insight into the effects of low-molecular-weight organic acids

Authors: Haojing Zhang, Taotao Lu (Co-first author), Zhongbo Shang, Yanxiang Li, Jianying He, Shanhu Liu, Deliang Li, Yanmei Zhou, and Zhichong Qi

Status: Published in *Water Research*, Vol. 168, 2020

Own contribution: concept and study design 60%, data acquisition 5%, analyses of samples 5%, data analyses and figures 80%, discussion of results 70%, manuscript writing 80%

TL and ZQ designed and directed the study. HZ ZS and YL conducted the experiment. JH, SL, and DL performed the simulation. TL, YZ, and ZQ discussed and interpreted the results. TL and HZ prepared the figures and tables. TL and ZQ prepared the manuscript with input from all co-authors. ZQ is the corresponding author.

Study 2: Factors affecting the transport of petroleum colloids in saturated porous media

Authors: Ying Wang, Taotao Lu (Co-first author), Haojing Zhang, Yanxiang Li, Yumeng Song, Jiuyan Chen, Xiaowen Fua, Zhichong Qi, Qiang zhang

Status: Published in *Colloids and Surfaces A: Physicochemical and Engineering Aspects*, Vol. 585, 2020

Own contribution: concept and study design 50%, data acquisition 5%, analyses of samples 5%, data analyses and figures 70%, discussion of results 80%, manuscript writing 70%

TL and ZQ designed and directed the study. YW, HZ and YL conducted the experiment. YS, JC and XF performed the simulation. TL, YW, and ZQ discussed and interpreted the results. TL and YW prepared the figures and tables. TL, ZQ, and QZ prepared the manuscript with input from all co-authors. ZQ and QZ are the corresponding authors.

Study 3: Relevance of iron oxyhydroxide and pore water chemistry on the mobility of nanoplastic particles in water-saturated porous media environments

Authors: Taotao Lu, Benjamin S. Gilfedder, Hao Peng, Stefan Peiffer, Georg Papastavrou, Katharina Ottermann, Sven Frei

Status: Published in *Water, Air, & Soil Pollution*, Vol. 232, 2021

Own contribution: concept and study design 80%, data acquisition 80%, analyses of samples 80%, data analyses and figures 80%, discussion of results 70%, manuscript writing 80%

Contribution statement

TL designed and directed the study. TL and KO conducted the experiment. TL, BG, SP, and SF discussed and interpreted the results. TL and HP prepared the figures and tables. TL, SF, and GP prepared the manuscript with input from all co-authors. TL is the corresponding author.

Study 4: Effects of clay minerals on the transport of nanoplastic particles in water-saturated porous media

Authors: Taotao Lu, Benjamin S. Gilfedder, Hao Peng, Geng Niu, Sven Frei

Status: Under reivew in *Science of the Total Environment*

Own contribution: concept and study design 90%, data acquisition 30%, analyses of samples 50%, data analyses and figures 90%, discussion of results 80%, manuscript writing 80%

TL designed and directed the study. GN and HP conducted the experiment. TL, BG, and SF discussed and interpreted the results. TL and HP prepared the figures and tables. TL and HP prepared the manuscript with input from all co-authors. HP is the corresponding author.

**Study 1: Transport of Cd²⁺ through saturated porous media:
Insight into the effects of low-molecular-weight organic acids**

Haojing Zhang, Taotao Lu, Zhongbo Shang, Yanxiang Li, Jianying He, Shanhu Liu, Deliang Li, Yanmei Zhou, and Zhichong Qi

Published in *Water Research* (Vol. 168, 2020)



Transport of Cd²⁺ through saturated porous media: Insight into the effects of low-molecular-weight organic acids

Haojing Zhang^{a,1}, Taotao Lu^{b,c,1}, Zhongbo Shang^a, Yanxiang Li^d, Jianying He^a, Shanhu Liu^a, Deliang Li^a, Yanmei Zhou^a, Zhichong Qi^{a,b,*}

^a Henan Joint International Research Laboratory of Environmental Pollution Control Materials, College of Chemistry and Chemical Engineering, Henan University, Kaifeng, 475004, China

^b Ministry of Education Key Laboratory of Pollution Processes and Environmental Criteria, Nankai University, Tianjin, 300350, China

^c Department of Hydrology, University of Bayreuth, Bayreuth, D-95440, Germany

^d The Testing Center of Shandong Bureau of China Metallurgical Geology Bureau, Jinan, 250014, China



ARTICLE INFO

Article history:

Received 4 May 2019

Received in revised form

1 October 2019

Accepted 11 October 2019

Available online 14 October 2019

Keywords:

Cd²⁺

LMWOAs

Transport model

Porous media

ABSTRACT

Low-molecular-weight organic acids (LMWOAs) are ubiquitous in the aquatic environment and consequently may affect the heavy metal transport in aquifer systems. In this study, the influences of LMWOAs on the transport of Cd²⁺ under different pH conditions in saturated porous media were evaluated. For this, three LMWOAs such as acetic acid, tartaric acid, and citric acid were employed. A two-site nonequilibrium transport model was applied to simulate the transport data. Under acidic conditions (pH 5.0), the results indicated that LMWOAs inhibited the transport of Cd²⁺ even at the low concentrations of organic acids (i.e., 0.05 and 0.1 mM). The inhibition effects might be attributed to the complexation role of the sand surface-bound organic acids and also electrostatic interaction. Meanwhile, the inhibition effects of LMWOAs on Cd²⁺ transport in the following order of citric acid > tartaric acid > acetic acid, which was also in agreement with the decreasing complex stability constants between Cd²⁺ and LMWOAs. This order may be dependent on their molecular structures (i.e., amount and type of functional groups) and complexing strength. Interestingly, when the LMWOWA concentrations 0.5 mM, tartaric acid and citric acid still inhibited Cd²⁺ transport, while acetic acid slightly enhanced the Cd²⁺ mobility due to its weaker complexing strength. However, under neutral conditions (pH 7.0), LMWOAs generally enhanced the transport of Cd²⁺. The transport-enhancement of LMWOAs was ascribed to the formation of stable aqueous non-adsorbing Cd-organic acid complexes. In addition, citric acid could obviously inhibit the transport of Cd²⁺ under competitive transport conditions (i.e., with competing cations), which is mainly due to different complex affinities of citric acid to Pb²⁺ and Cd²⁺. These findings demonstrate that LMWOAs may inhibit or facilitate Cd²⁺ transport under different environmental conditions. Thus, environmental assessment concerning the transport of heavy metals should consider the roles of organic acids.

© 2019 Elsevier Ltd. All rights reserved.

1. Introduction

Cadmium (Cd) is one of the most toxic heavy-metal pollutants and it exhibits adverse effects on living organisms (Kabatapendias and Mukherjee, 2007; Butter et al., 1998; Singh et al., 2018). The

anthropogenic processes and human activities can result in a significant release of cadmium ion (Cd²⁺) into the groundwater environment. The permissible limit for Cd²⁺ concentration in groundwater as per the World Health Organization (WHO) guidelines is 3 µg/L (WHO, 2004). However, many studies have demonstrated that the concentrations of Cd²⁺ from different places exceeded its standard value. For example, in the Shibganj area (Bangladesh), the mining area of Lavrio (Greece) and the residential wells of Central Anne Arundel (Maryland), the maximum Cd²⁺ concentrations were found to be 13 µg/L, 43 µg/L and 66 µg/L, respectively (Saha and Zaman, 2011; Stamatis et al., 2001; Bolton,

* Corresponding author. Henan Joint International Research Laboratory of Environmental Pollution Control Materials, College of Chemistry and Chemical Engineering, Henan University, Kaifeng, 475004, China.

E-mail address: qizhichong1984@163.com (Z. Qi).

¹ Haojing Zhang and Taotao Lu contributed equally.

2006). In addition, it has been found that Cd^{2+} concentration was 90 $\mu\text{g/L}$ near the Alara landfill, Nigeria (Adeyemi et al., 2007). Buragohain et al. (2010) found that the concentration of Cd^{2+} was 120 $\mu\text{g/L}$ in the Dhemaji District, India. Moreover, higher Cd^{2+} concentration was also reported on the surface of the river water. For example, Ambedkar and Muniyan (2012) demonstrated that the maximum concentration was as high as 1.46 mg/L in Gadilam River, Tamilnadu, India. Consequently, the highly toxic Cd^{2+} in the environment has attracted many researchers' wide concern due to its harmful effects on the living organism (Xiao and Wu, 2014). Thus, the study about the transport properties of Cd^{2+} in the aquifers becomes highly desirable.

As on date, a number of studies have been investigated about the transport properties of Cd^{2+} which is affected by aging, ionic strength, cation species, initial concentrations, and colloids in saturated porous media (Seuntjens et al., 2001; Zuo et al., 2015; Elbana and Selim, 2010; Tsang et al., 2007; Kookana and Naidu, 1998; Wikiniyadhane et al., 2015; Xie et al., 2018). For example, Kookana and Naidu (1998) found that the transport of Cd^{2+} at a constant ionic strength was in an order of magnitude faster in the presence of Ca^{2+} than that in the presence of Na^+ ions. Tsang et al. (2007) demonstrated that Cd^{2+} transport behavior was predominantly affected by rate-limited sorption at low concentration (i.e., 10^{-5} M). Similarly, Elbana and Selim (2010) reported that Cd^{2+} retention exhibited strong nonlinear and kinetic behavior in alkaline and acidic soils. Wikiniyadhane et al. (2015) claimed that the presence of kaolinite colloids probably retarded the transport of Cd^{2+} in porous media under higher ionic strength conditions. Moreover, it has been reported that porous media's pH is an important factor in determining the retention of heavy metals (Herreweghe et al., 2002; Najafi and Jalali, 2015). However, the low-molecular-weight organic acids (LMWOAs) based studies on transport of Cd^{2+} have been paid limited interest.

Low-molecular-weight organic acids (LMWOAs) are ubiquitous water-soluble organic compounds that have been detected in a variety of environmental conditions (Xiao and Wu, 2014; Brinkmann et al., 2003; Tedetti et al., 2006), particularly in natural soil solutions (Jones, 1998; Strobel, 2001; Wang et al., 2009). Generally, the concentration of LMWOAs has a wide range of 1 μM to 1 mM in soil solutions (Jones, 1998; Strobel, 2001; Hu et al., 2005). LMWOAs regulates the heavy metals in terms of their environmental migration and ecological toxicology, through chelation, complexation, and adsorption reactions (Xiao and Wu, 2014; Elkhatib et al., 2007). The complexation with Cd^{2+} could reduce the respiration rate of soil (Renella et al., 2004). Lu et al. (2007) indicated that when the soil was spiked by Cd^{2+} , monocarboxylic acids, di- and tri-carboxylic acids were found in the root exudates. Krishnamurti et al. (1997) reported that Cd^{2+} may form complexes with various organic acids. Many researchers have reported that LMWOAs affected the adsorption/desorption of heavy metals on soils and minerals (McBride, 1989; Huang et al., 2010; Li et al., 2015). McBride (1989) found that citrate and amino acids exhibited the obvious inhibition of Cu^{2+} , Cd^{2+} , Zn^{2+} , Pb^{2+} adsorption on oxides and clay minerals. However, Huang et al. (2010) reported that LMWOAs (such as acetic acid, tartaric acid, and citric acid) enhanced Cd^{2+} adsorption on goethite and montmorillonite at low concentrations. Meanwhile, Li et al. (2015) demonstrated that the amounts of three metals (Cu^{2+} , Cd^{2+} , and Pb^{2+}) desorbed from a field soil by LMWOAs (i.e., malonic acid and *DL*-hydroxybutanedioic acid) strongly decreased with an increase in pH, the results indicated that pH was the dominant factor affecting the release of metal ions in the extraction procedure using LMWOAs. In addition, organic acids also play an important role in controlling the transport of heavy metals (Jiang et al., 2012; Zhang and Zhang, 2010; Paradelo et al., 2012; Kantar, 2007). Zhang and Zhang (2010)

reported that the concentrations of metal ions (e.g., Cu^{2+} , Cd^{2+} , and Zn^{2+}) in the leachates were positively correlated with dissolved organic matters. Paradelo et al. (2012) found that the coupled transport of humic acids (HA) and Cu^{2+} was controlled by the pH and the binding capacity of Cu–HA. Furthermore, Kantar (2007) simulated metal ion transport through the saturated systems in the presence of organic ligands.

Based on the above knowledge, the presence of LMWOAs may enhance, inhibit or have no effect on the transport of Cd^{2+} in aquifer system, which is dependent on the pH of the solution and the characteristics of organic acids. However, up to now, there has been limited reports are only available about the effects of LMWOAs on Cd^{2+} transport. Thus, it is necessary to study the influence of LMWOAs on the transport of Cd^{2+} under different pH conditions. In this study, three LMWOAs (acetic acid, tartaric acid, and citric acid) with different chemical structures were employed to study the influence of LMWOAs on the transport of Cd^{2+} . The main objectives of this study are as follows: (1) to assess the effect of LMWOAs on Cd^{2+} transport behaviors under acidic and neutral conditions, (2) to examine the transport of Cd^{2+} in saturated quartz sand as affected by various LMWOAs, (3) to investigate the effects of competitive ions (using Pb^{2+} as the model metal ions) on Cd^{2+} transport in the presence of LMWOAs. Meanwhile, the specific goals are to explore the primary mechanisms controlling the transport of Cd^{2+} in saturated quartz sand. Moreover, a two-site nonequilibrium transport model was used to analyze the transport data under the experimental conditions. Our findings from experiments are reliable for understanding the underlying retention mechanisms and predicting the Cd^{2+} migration in similar systems.

2. Materials and methods

2.1. Materials

The quartz sand used for the column experiments was purchased from Sigma–Aldrich. The sand sieved to a size range of 0.21–0.30 mm was used as the porous medium and the average grain size was about 0.26 mm. Before use, the sand was cleaned thoroughly according to the procedure described by Mattison et al. (2011) to remove impurities (e.g., metal oxides) on the grain surface. The measured Brunauer–Emmett–Teller (BET) surface area (Micromeritics, Norcross, GA) of the sand is 0.06 m^2/g , the pH of zero charge (pH_{zpc}) is 3.3, and the cation exchange capacity (CEC) is 1.8 meq/100 g (detailed procedures are provided in Supplementary Material). An electro-kinetic analyzer (Anton Paar, Graz, Austria) was used to determine the streaming potential of quartz sand to obtain its ζ -potential using the Helmholtz–Smoluchowski equation (Kim et al., 2009; Wang et al., 2010) (relevant information is given in Supplementary Material).

Acetic acid ($\geq 99.5\%$), tartaric acid ($\geq 99\%$), and citric acid ($\geq 99\%$) were purchased from Sinopharm Chemical Reagent Co. Ltd. (Shanghai, China). Selected physicochemical parameters of the three LMWOAs are presented in Table 1. The compounds $\text{Cd}(\text{NO}_3)_2$ and NaCl were all analytical reagent and were obtained by Sinopharm Chemical Reagent Co. Ltd. (Shanghai, China). Deionized (DI) water was used for all the solution preparations.

2.2. Preparations of Cd^{2+} solutions

The Cd^{2+} solution (~ 3 mg/L) used for the column experiments was prepared by the dilution of a 100 mg/L stock solution of cadmium nitrate ($\text{Cd}(\text{NO}_3)_2$) in an electrolyte solution (0.5 mM NaCl). In order to conduct the experiments in the presence of LMWOAs, firstly, it was necessary to prepare the 0.5 mM NaCl background solution was amended with 0.1 mM organic acid. Then, a certain

Table 1
Structures and acidity coefficient (pK_a) of various organic acids.

Organic acid	Structure	Molecular weight	pK_{a1}	pK_{a2}	pK_{a3}
Acetic acid	CH_3-COOH	60.05	4.74		
Tartaric acid	$HOOC-CHOH-CHOH-COOH$	150.09	3.04	4.37	
Citric acid	$HOOCOC-(CH_2COOH)_2$	192.14	3.13	4.76	6.4

amount of $Cd(NO_3)_2$ stock solution was added into the prepared background solution to obtain the desired solution. In addition, each desired pH value of the Cd^{2+} solutions (with or without LMWOAs) was achieved by 0.1 M HCl or NaOH. The changes of pH values are negligibly small in the influent solutions during the experimental operation period (Fig. S1a and S1c in Supplementary Material).

2.3. Column experiments

The procedures were followed as described in the previous studies (Chung et al., 2016; Miralles et al., 2010). About 15.2 g of the sands were packed into a 10.3 cm length and 11 mm diameter borosilicate glass columns, yielding the bulk density of 1.55 ± 0.02 g/cm³ and the porosity of 0.41 ± 0.01 . The columns were employed in an up-flow mode using syringe pumps (KD Scientific). For each experiment, the column was first flushed with up to 30 pore volumes (PV) of DI water to ensure a saturated steady-state flow condition at a constant pore velocity of 0.31 cm/min (0.292 mL/min); following 21 PV of background solution (0.5 mM NaCl) was injected. Then, 15 PV of the Cd^{2+} solution was injected into the column at the same pore velocity. About 3.5 mL (~0.8 PV) of the effluent was collected for the analysis of Cd^{2+} concentrations at around 30-min of intervals. The concentrations of Cd^{2+} in effluents were measured by the inductively coupled plasma optical emission spectrometer (ICP-OES) (IRIS Intrepid II XSP, Thermo Electron Corporation, USA). Column transport studies were conducted at least in duplicate. For every column experiment, a new column filled with sand was used. Column properties are shown in Table S1.

2.4. Batch sorption experiments

Based on our previous research, a batch sorption method (Li et al., 2019) was adopted to investigate the binding affinities of Cd^{2+} to quartz sand in the presence of different LMWOAs. Briefly, approximately 5 g of quartz sand and 20 mL of Cd^{2+} solution (3 mg/L) with or without LMWOAs were placed into 20-ml amber glass vials. These vials were equilibrated for 10 h by horizontally shaking (the duration equals column experiment). The vials were then centrifuged at 5000 rpm for 20 min and the supernatants were withdrawn to obtain the concentrations of Cd^{2+} in the aqueous solution, using an ICP-OES instrument as mentioned above. The concentrations of Cd^{2+} adsorbed to sand were calculated based on a mass balance approach. All experiments were run in triplicate. The distribution coefficients of Cd^{2+} , K_d (L/kg), between sand and water were calculated by using the equation: $K_d = q/C_e$, where q (mg/kg) was the concentration of Cd^{2+} adsorbed on the sand. In addition, C_e (mg/L) was the concentration of Cd^{2+} in the solution. The values of K_d were listed in Table S2. Additionally, the amount of LMWOAs adsorbed onto the sand was determined by adsorption experiments at different pH conditions. Detailed experimental procedures are given in the Supplementary Material.

2.5. Modeling Cd^{2+} transport in saturated porous media

The simulation models have been commonly used to predict the

transport behavior of metal ions. The transport of metal ions in a steady-state can be described by one-dimensional convection dispersion equation (CDE) which can be expressed as follow (Kasten et al., 1952):

$$R \frac{\partial C}{\partial t} = D \frac{\partial^2 C}{\partial x^2} - v \frac{\partial C}{\partial x} \quad (1)$$

where R is the retardation factor; C (mg/L) is the solute concentration; t is the time; v (m/d) is the average pore water velocity; x (m) is distance, and D (m²/d) is the longitudinal dispersion coefficient.

However, the transport of reactive solutes in porous media may also be influenced by physicochemical nonequilibrium processes (Nielsen et al., 1986; Worch, 2004). Chemical nonequilibrium behavior may arise from adsorption kinetics (Uyusur et al., 2014); physical nonequilibrium caused by immobile water region during transport (Leij and Bradford, 2009). Several nonequilibrium transport models based on physical, chemical or combined physical and chemical nonequilibrium processes were applied widely to describe the nonequilibrium mass transfer during transport (Worch, 2004; Leij and Bradford, 2009; Field and Leij, 2014; Chung et al., 2016). In this work, the two-site nonequilibrium transport model was used to describe Cd^{2+} transport in the sand column.

The two-site nonequilibrium transport model assumes that sorption sites in porous media can be classified into two sites, i.e., an equilibrium site and a kinetic site (Nkedi-Kizza et al., 1984). The dimensionless form of the CDE for two-site nonequilibrium transport model can be written as (Nkedi-Kizza et al., 1984):

$$\beta R \frac{\partial C_1}{\partial T} = \frac{1}{P} \frac{\partial^2 C_1}{\partial X^2} - \frac{\partial C_1}{\partial X} - \omega(C_1 - C_2) \quad (2)$$

$$(1 - \beta)R \frac{\partial C_2}{\partial T} = \omega(C_1 - C_2) \quad (3)$$

where the dimensionless parameters are defined as follows:

$$X = \frac{x}{L} \quad (4)$$

$$P = \frac{vL}{D} \quad (5)$$

$$R = 1 + \frac{\rho_b}{\theta} \cdot K_d \quad (6)$$

$$\beta = \frac{\theta + f\rho_b K_d}{\theta + \rho_b K_d} \quad (7)$$

$$\omega = \frac{\alpha(1 - \beta)RL}{v} \quad (8)$$

In the above the subscripts 1 and 2 represent equilibrium and kinetic sites, respectively; C_1 and C_2 (mg/L) are the relative concentration of solutes in equilibrium and kinetic sites, respectively; T is the dimensionless time and L (m) is the column length; X is

dimensionless versions of the axial distance; P is the Peclet number; ρ_b (g/cm^3) and θ ($-$) are the sorbent bulk density and porosity of the sand column, K_d (L/kg) is the partition coefficient. β is the fraction of instantaneous retardation to the total retardation (Wikiniyadhane et al., 2015); f is the fraction of Type 1 sites; ω is the dimensionless mass transfer coefficient (Kuntz and Grathwohl, 2009) and α (h^{-1}) is the first-order rate for kinetics at Type 2 sites.

To obtain the value of dispersion coefficient (D), the breakthrough curves (BTCs) of the conservative tracer (KBr) were fitted with the one-dimensional steady-state advection–dispersion equation (Fig. S2) using CXTFIT 2.1 code (a published computer program for estimating the solute transport parameters in the subsurface) (Toride et al., 1999). Bromide concentrations were measured using an ICS-2100 ion chromatograph (Dionex Corporation, Sunnyvale, CA, USA). As expected, the fitted retardation factors (R) for the tracer were equal to 1.0. The CDE model showed a good agreement with the tracer BTCs (Fig. S2) that meant that the immobile water region in the pore structure seemed to be small. Thus, the physical nonequilibrium caused by immobile water region during transport could be negligible in this study (Chung et al., 2016). We assumed that the dispersion coefficient of Cd^{2+} was as same as that of the tracer ($0.498 \text{ m}^2/\text{d}$) in the column (Chen et al., 2011). The parameters R , β , and ω were obtained by fitting the breakthrough curve of Cd^{2+} . The values of K_d , f , and α were calculated using Equations (6)–(8).

3. Results and discussion

3.1. Effects of LMWOAs on the transport of Cd^{2+} under acidic conditions

The Cd^{2+} mobility affected by LMWOAs is shown in Fig. 1. In general, LMWOAs could inhibit the transport of Cd^{2+} at lower concentrations of organic acids (i.e., 0.05 and 0.1 mM) under acidic conditions (i.e., pH 5.0). In the absence of LMWOAs, the breakthrough of Cd^{2+} ions reached 92% after 10 PV (Fig. 1a). On the basis of previous studies, the surface hydroxyl groups ($\equiv\text{Si}-\text{OH}$, approximately $4.5\text{--}5.0$ hydroxyls/ nm^{-2} on silicon dioxide surfaces (Morrow and Mcfarlan, 1991)) can be ionized and provide the net negative charge ($\equiv\text{Si}-\text{O}^-$) on the sand surface at pH 5.0 (Jada et al., 2006). Thus, the positively charged Cd^{2+} without organic acids could bind to the negatively charged hydroxyl groups of sand grains (Uyusur et al., 2014). With the addition of organic acids, acetic acid had a slightly inhibitory effect on the transport of Cd^{2+} . In comparison, the maximum C/C_0 values increased to essentially 84% with 11 PV in the presence of 0.1 mM citric acid (Fig. 1b). These observations that LMWOAs inhibited the transport of Cd^{2+} can be understood via the following mechanisms. On one hand, at pH 5.0, acetic acid (denoted as HL, L represents ligand), tartaric acid (denoted as H_2L) and citric acid (denoted as H_3L) present HL, HL^- or HL^{2-} , hence, they also may be adsorbed on sand surface by hydrogen bond formation (Malandrino et al., 2006; Christy, 2010; Kong et al., 2018). Additionally, although the porous media was cleaned before column experiments, there were still some traces of metal oxides (e.g., Fe/Al oxides) on the sand surface which may provide favorable sites for the adsorption of LMWOAs (Dong et al., 2016). As shown in Table S3, in the presence of organic acids, a part of LMWOAs were adsorbed onto grain surfaces, resulting in more negative charges on the sand surfaces (Table S4) (Huang et al., 2003; Yuan et al., 2007). Thus, more positively charged Cd^{2+} deposited on the porous media. In addition, the slightly higher pH values in effluents (i.e., pH = 5.2–5.5), in comparison with the corresponding pH values in influents (i.e., pH = 5.0). Thus, it may also be an indication of organic acid adsorption onto sand surfaces under the test conditions due to the decrease of LMWOAs in

effluents (Fig. S1b). Note that the deposition of LMWOAs on porous media could also be influenced by aquifer properties (e.g., the pore-scale heterogeneity in flow; the surface roughness of sand particles; the blocking effect) during the transport process (Liu et al., 2015; Morales et al., 2009; Akbourn et al., 2013). On the other hand, the adsorbed LMWOAs may offer new deposition sites for Cd^{2+} (Hu et al., 2007). It might be due to electrostatic repulsion between the negatively charged dissociated acid anions and the porous media (Huang et al., 2010), and then the amounts of LMWOAs adsorbed onto sand were small ($0.19\text{--}0.32 \text{ mmol}/\text{kg}$, Table S3). As mentioned above, $\sim 15.2 \text{ g}$ of the sands were packed into the columns; thus approximately $2.89\text{--}4.86 \text{ }\mu\text{mol}$ LMWOAs were adsorbed onto sand during the transport process. It is noteworthy that the injected concentration of Cd^{2+} was $3 \text{ mg}/\text{L}$ (the influent volume was $\sim 55 \text{ mL}$; thus the influent solution contained about $1.35 \text{ }\mu\text{mol}$ Cd ions). Hence, the amounts of adsorbed LMWOAs onto sand were greater than those of Cd^{2+} in the aqueous phase. In this case, Cd^{2+} could bind to LMWOAs in the form of sand–LMWAO–Cd (instead of $\equiv\text{SiO}-\text{Cd}$) because LMWOAs are rich in oxygen-containing functional groups (Table 1) and are able to form a complex with Cd^{2+} (especially for citric acid, which has three $-\text{COOH}$ and one $-\text{OH}$) (Tsang et al., 2007; Najafi and Jalali, 2015; Huang et al., 2010; Collins et al., 1999; Parfitt et al., 1977; Lee et al., 1996; Holm et al., 2003; Wang et al., 2012). Consequently, LMWOAs inhibited the transport of Cd^{2+} in the sand columns. Moreover, considering the fact that carbon dioxide present in the air can be dissolved in water, it is always in equilibrium with H_2CO_3 , HCO_3^- , and CO_3^{2-} (Sadhukhan et al., 2014). Some previous studies have demonstrated that Cd^{2+} could form complexes with bicarbonate and carbonate (Chada et al., 2005; Pivovarov, 2005; Foti et al., 2011). However, Cd^{2+} –carbonate complexes had negligible effect on transport of Cd^{2+} under the test conditions possibly due to the low concentrations of bicarbonate and carbonate in the prepared background solution (the concentrations of bicarbonate (the predominant species of dissolved CO_2 in the aqueous phase) were $0.013 \pm 0.002 \text{ mM}$ and $0.025 \pm 0.001 \text{ mM}$ at pH 5.0 and pH 7.0, respectively). The concentration of bicarbonate was determined by the titration method with hydrochloric acid methyl orange as indicators (Fletcher and Staden, 2003) (Fig. S3).

To further prove the importance of organic acids adsorption on porous media, we conducted an additional experiment by saturating the porous media with the citric acid solution before injecting Cd^{2+} solution through the column (Yang et al., 2012). In this case, all the sands were coated with citric acid. The transport of Cd^{2+} in the citric acid-saturated columns was significantly more inhibited in comparison with the transport of Cd^{2+} in the presence of citric acid (Fig. 2). Judging from the relative positions of points in the breakthrough curves, it was possible to verify that organic acids adsorption on sand grains contributed to the transport inhibition effects of organic acids under acidic conditions.

Note that the transport inhibition effects of LMWOAs on Cd^{2+} transport were dependent on organic acid species at lower concentrations of organic acids. The inhibition effects followed the order of citric acid > tartaric acid > acetic acid. These obvious different effects on the transport of Cd^{2+} among the three organic acids may be due to their different molecular structures (i.e., amount and type of functional groups) and their strengths of complex formation. Wu et al. (2011) reported that surface coverage on the grain surface usually depended on the molecular weights of organic acid. For example, organic acids with higher molecular weight, such as citric acid, usually have broader and larger surface coverage than those with lower molecular weight (Huang et al., 2003; Jing et al., 2007). Thereby more number of Cd^{2+} ions could bind with the citric acid which adsorbed on the sand surface. In addition, the amount of heavy metals complexation by LMWOAs

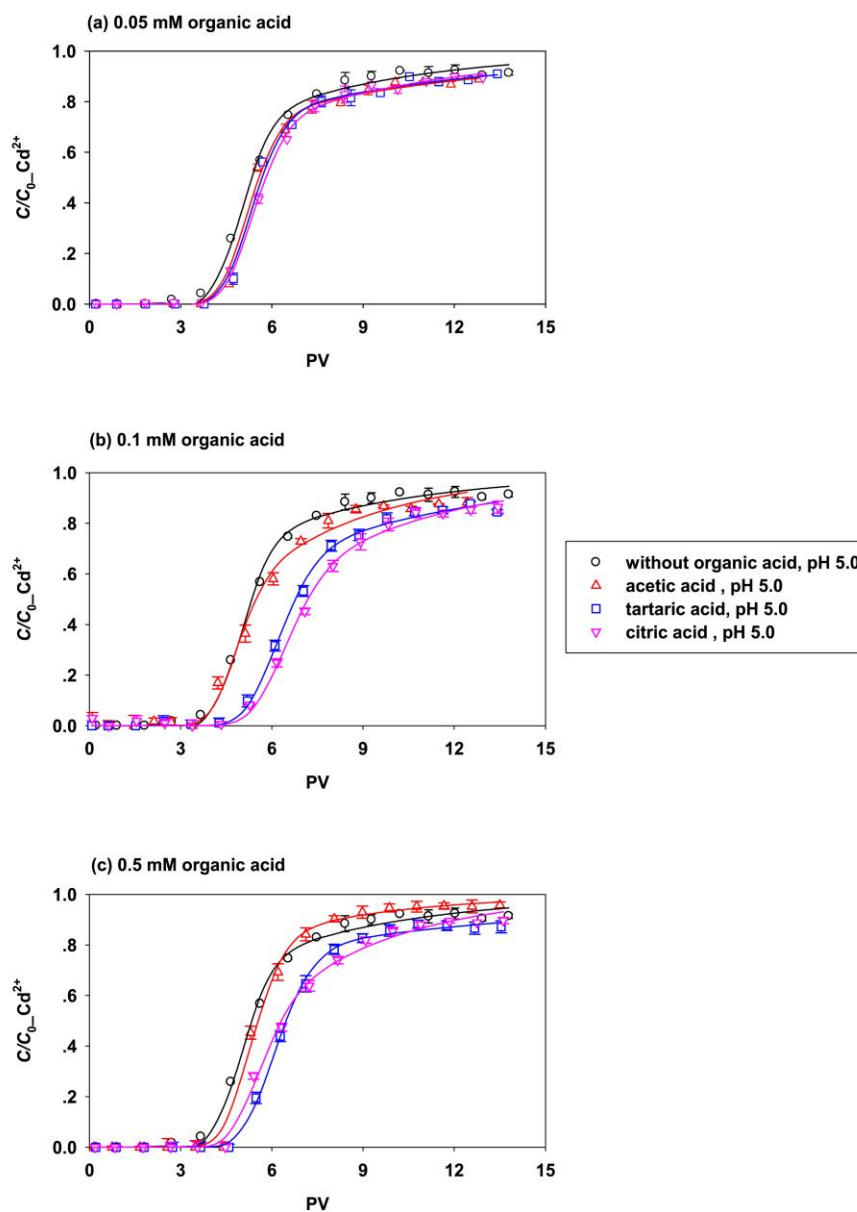


Fig. 1. Effects of low-molecular-weight organic acids on the transport of Cd^{2+} under acidic conditions: (a) 0.05 mM organic acid (columns 1–4); (b) 0.1 mM organic acid (columns 1, 5–7); and (c) 0.5 mM organic acids (columns 1, 8–10). Symbols are experimental data and lines are plotted by curve-fitting experimental data with the two-site nonequilibrium transport model.

depends on the type of organic acid (number of functional groups) (Najafi and Jalali, 2015). Compared with acetic acid and tartaric acid, citric acid has more carboxylic and hydroxyl groups (Table 1). In general, increasing the number of carboxylic acid groups in the LMWOAs will result in the formation of more stable complexes between LMWOAs and metal ions (Liu et al., 2017). According to the $\text{p}K_{\text{a}}$ of organic acids (Table 1), the predominant species of citric acid, tartaric acid, and acetic acid were HL^{2-} , L^{2-} , and L^{-} at pH 5.0, respectively. In this case, the logarithms of complex stability constants ($\log K$) between citric acid, tartaric acid, and acetic acid, with

Cd^{2+} were found to be 3.32, 2.15 and 1.30, respectively (Bunting and Thong, 1970; Janoš, 1993). The larger the complex stability constants, results in the more stable metal–organic acid complexes. Consequently, the transport of Cd^{2+} could be more strongly inhibited by citric acid as compared with others. This result previously demonstrates that the stability of metal–organic acid complexes affects the mobility of Cd^{2+} . The distribution coefficients (K_{d}) also indicated that the strongest adsorption of Cd^{2+} on the sand was observed in the presence of citric acid (Table S2). Furthermore, we also investigated the transport of Cd^{2+} at lower

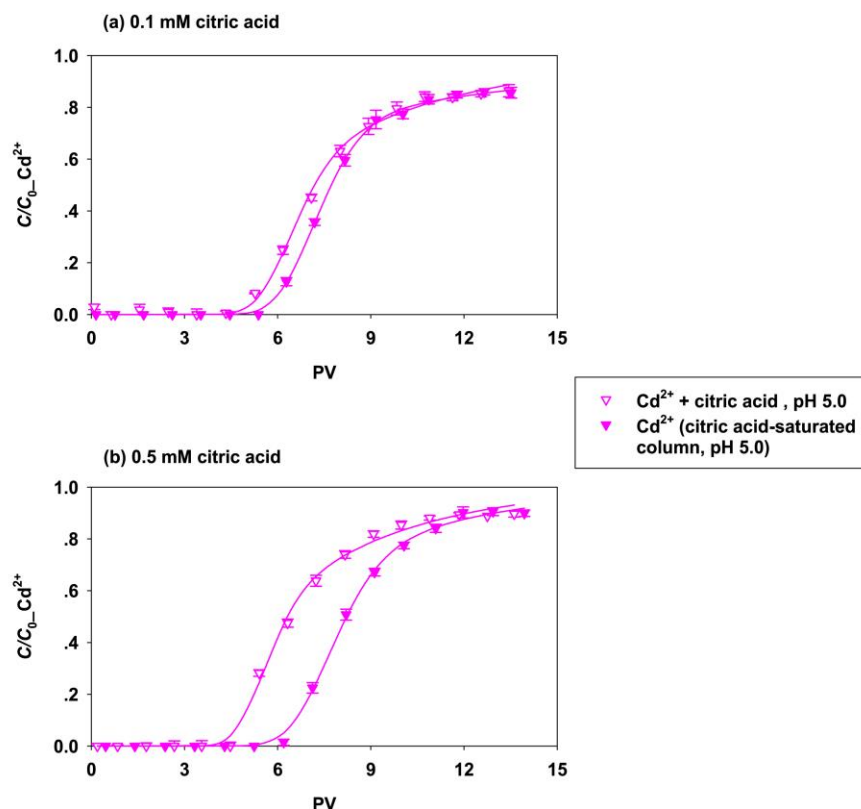


Fig. 2. Effects of citric acid on the transport of Cd^{2+} : (a) 0.1 mM citric acid (columns 7 and 11); and (b) 0.5 mM citric acid (columns 10 and 12). The open symbol indicates that Cd^{2+} transport through saturated porous media in the presence of citric acid. The solid symbol indicates that the column was saturated the sand with the citric acid solution before injecting Cd^{2+} solution. Lines are plotted by curve-fitting experimental data with the two-site nonequilibrium transport model.

concentration (1 mg/L) through saturated sand columns in the presence of LMWOAs. Similar patterns were observed at lower concentration of Cd^{2+} (Fig. S4).

It is already known that nonequilibrium transport behavior results from rate-limited sorption exhibits early breakthrough and long tailing (Tsang et al., 2007). Some previous studies found that the corresponding chemical characteristics of porous media (e.g., phenolic and carboxylate content) could influence the rate-limited Cd^{2+} sorption (Christl et al., 2001; Tsang et al., 2007). It is not surprising that the simulation of the transport data was also well fitted with the two-site nonequilibrium transport model in this study ($r^2 = 0.982\text{--}0.998$, Table 2). The optimized parameters are given in Table 2. As expected from the breakthrough curves, the R values of Cd^{2+} followed the order of citric acid (8.53) > tartaric acid (8.37) > acetic acid (6.90) in the presence of 0.1 mM organic acid (Fig. 3). The result was well in agreement with the increasing complex stability constants between Cd^{2+} and LMWOAs. Furthermore, the f parameter of Cd^{2+} followed the order of citric acid > tartaric acid > acetic acid at lower concentration of organic acid, which was consistent with the transport results as mentioned above. The higher values of f (>0.5) indicate that the mechanism of Cd^{2+} sorption onto quartz sand appears to be changed from the nonequilibrium sorption to the equilibrium sorption (Wikiniyadhane et al., 2015). This phenomenon was also observed for the parameter β which represents the fraction of instantaneous retardation to the total retardation (Fig. S5b) (Florido et al., 2010).

The value of β revealed that a larger amount of Cd^{2+} ions were adsorbed at equilibrium sites rather than at nonequilibrium sites (Candela et al., 2007). The first-order rate coefficient (α) of Cd^{2+} followed the sequence: citric acid > tartaric acid > acetic acid (Fig. S5c). The α value reflects the rate of sorption reaction to reach the equilibrium condition. Here, the higher α value means the lower transport at the lower concentration of Cd^{2+} in the aqueous phase (Wikiniyadhane et al., 2015).

Furthermore, for a given organic acid, the inhibition effects of tartaric acid or citric acid depended on the concentrations of organic acids (Fig. S6). Interestingly, the inhibition effects increased with the increasing concentration of organic acids from 0.05 mM to 0.1 mM, but then the effects decreased with the further increase in organic acid concentration (0.5 mM). This observation may be explained via the following mechanisms. On one hand, when the organic acid concentrations increased, the deposition sites for organic acids on the sand are saturated at higher organic acid concentrations. More free organic acids remained in the aqueous phase, and the remaining organic acids in solutions can then form a complex with Cd^{2+} (Liao, 2006). The water-soluble Cd^{2+} -complexes were not more likely to deposit on the sand surfaces (Kong et al., 2018). On the other hand, the remaining organic acids and the Cd^{2+} -complexed organic acids (e.g., CdL^+ , CdHL^+ , and CdH_2L^+) in the system may directly compete with Cd^{2+} for new deposition sites as mentioned above (Hu et al., 2007). Hence, less Cd^{2+} could be deposited on sand surface at high concentrations of organic

Table 2
Fitted parameters of two-site nonequilibrium transport model from breakthrough results of column experiments.

Column No.	Background solution	Competing cation	pH	Parameters of two-site nonequilibrium transport model					
				$R(-)$	$\beta(-)$	$\omega(-)$	$f(-)$	$\alpha(1/d)$	r^2
1	0.5 mM NaCl	/	5.0	6.51	0.745	0.288	0.746	7.16	0.994
2	0.5 mM NaCl + 0.05 mM acetic acid	/	5.0	6.56	0.746	0.294	0.702	7.33	0.995
3	0.5 mM NaCl + 0.05 mM tartaric acid	/	5.0	7.28	0.752	0.312	0.712	7.52	0.999
4	0.5 mM NaCl + 0.05 mM citric acid	/	5.0	7.44	0.759	0.327	0.721	7.69	0.998
5	0.5 mM NaCl + 0.1 mM acetic acid	/	5.0	6.90	0.747	0.312	0.704	7.34	0.997
6	0.5 mM NaCl + 0.1 mM tartaric acid	/	5.0	8.37	0.748	0.392	0.715	7.59	0.996
7	0.5 mM NaCl + 0.1 mM citric acid	/	5.0	8.53	0.763	0.508	0.732	10.1	0.998
8	0.5 mM NaCl + 0.5 mM acetic acid	/	5.0	6.22	0.876	0.184	0.852	9.82	0.992
9	0.5 mM NaCl + 0.5 mM tartaric acid	/	5.0	7.60	0.729	0.239	0.688	4.82	0.994
10	0.5 mM NaCl + 0.5 mM citric acid	/	5.0	7.69	0.758	0.595	0.721	13.2	0.989
11 ^a	0.5 mM NaCl, 0.1 mM citric acid saturated column	/	5.0	8.79	0.761	0.284	0.730	5.60	0.999
12 ^a	0.5 mM NaCl, 0.5 mM citric acid saturated column	/	5.0	9.19	0.860	0.324	0.842	10.8	0.999
13	0.5 mM NaCl	/	7.0	14.7	0.735	0.478	0.715	5.17	0.996
14	0.5 mM NaCl + 0.1 mM acetic acid	/	7.0	13.3	0.732	0.458	0.710	5.36	0.996
15	0.5 mM NaCl + 0.1 mM tartaric acid	/	7.0	11.2	0.741	0.375	0.715	5.62	0.995
16	0.5 mM NaCl + 0.1 mM citric acid	/	7.0	8.96	0.754	0.325	0.723	6.05	0.992
17	0.5 mM NaCl + 0.5 mM acetic acid	/	7.0	8.91	0.789	0.332	0.740	7.39	0.998
18	0.5 mM NaCl + 0.5 mM tartaric acid	/	7.0	6.22	0.795	0.317	0.756	10.7	0.991
19	0.5 mM NaCl + 0.5 mM citric acid	/	7.0	5.64	0.812	0.305	0.771	12.0	0.982
20	0.5 mM NaCl	3 mg/L Pb ²⁺	5.0	5.29	0.656	0.251	0.576	5.75	0.995
21	0.5 mM NaCl + 0.1 mM citric acid	3 mg/L Pb ²⁺	5.0	7.95	0.782	0.298	0.751	7.16	0.995
22	0.5 mM NaCl + 0.5 mM citric acid	3 mg/L Pb ²⁺	5.0	7.57	0.836	0.269	0.811	9.14	0.996

^a Column was presaturated with citric acid before injecting Cd²⁺ solution.

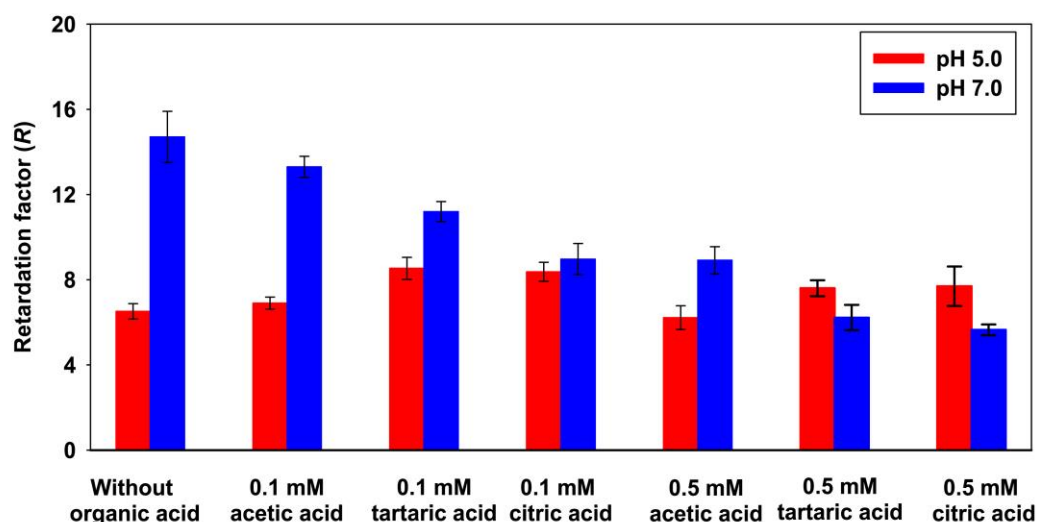


Fig. 3. Retardation factor (R) of Cd²⁺ in sand columns under different solution chemical conditions.

acids. This is evidenced by the transport of Cd²⁺ at higher acetic acid concentration. As shown in Fig. 1c, Cd²⁺ mobility in the sand column increased slightly in the presence of 0.5 mM acetic acid. On the basis of the discussion above, we propose that the slightly transport-enhancement of acetic acid was likely attributable to the weaker complexing strength of acetic acid (the log K value was only 1.30 for Cd–acetic acid complexes) and deposition site competition.

3.2. Effects of LMWOAs on the transport of Cd²⁺ under neutral conditions

Marked effects of LMWOAs on the Cd²⁺ BTCs were observed

under neutral conditions (Fig. 4). In the absence of LMWOAs, Cd²⁺ was detected after 9 PV (Fig. 4a). The maximum C/C_0 in the effluent was less than 65%, indicating that transport of Cd²⁺ decreased with pH (Fig. S7). The effect of pH on Cd²⁺ mobility is consistent with the results of published research (Chotpanarat and Kiatvarangkul, 2018). The ζ -potential values of sand at pH 7.0 were more negative than that at pH 5.0 (Table S4). Therefore, more Cd²⁺ could be adsorbed via the electrostatic adsorption reactions (Liao, 2006), and Cd²⁺ may be irreversibly adsorbed to grains at pH 7.0 (Dijkstra et al., 2004). Thus, the potential mobility of Cd²⁺ is lower under neutral conditions.

Interestingly, unlike pH 5.0, LMWOAs could enhance the

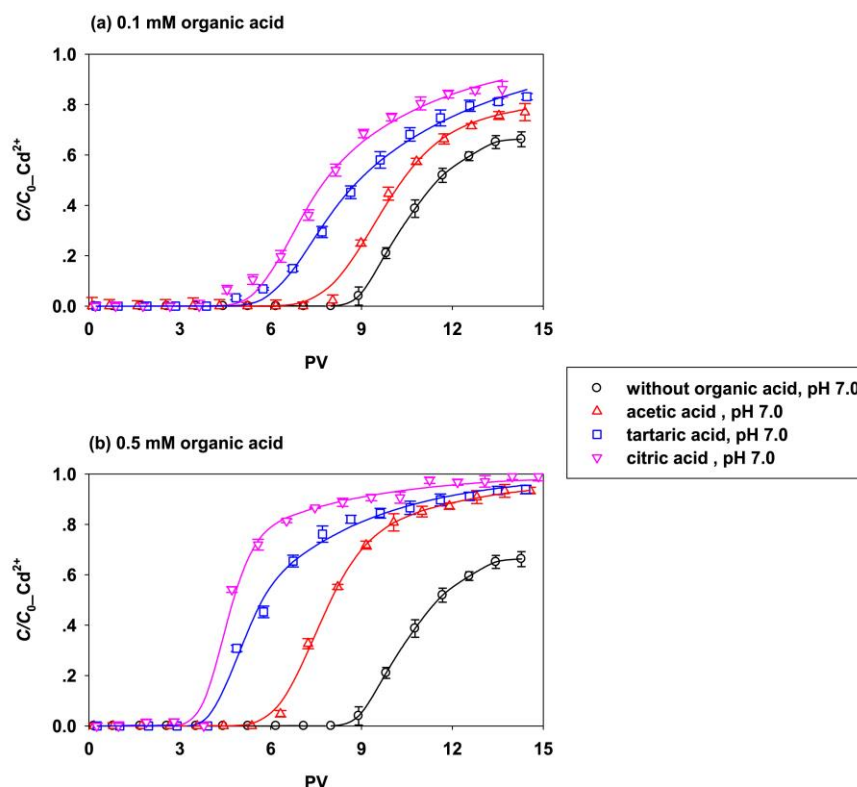


Fig. 4. Effects of low-molecular-weight organic acids on the transport of Cd²⁺ under neutral conditions: (a) 0.1 mM organic acid (columns 13–16); and (b) 0.5 mM organic acids (columns 13, 17–19). Symbols are experimental data and lines are plotted by curve-fitting experimental data with the two-site nonequilibrium transport model.

transport of Cd²⁺ under neutral conditions (i.e., pH 7.0) (Fig. 4). Similarly, this phenomenon was also observed for the lower concentration of Cd²⁺ (1 mg/L) (Fig. S8). Moreover, for a given organic acid, the transport-enhancement effects increased with increasing organic acid concentrations (Fig. S9). These observations are evident from the decrease of *R* values in Fig. 3. We propose that the transport-enhancement effects were likely attributable to the formation of stable aqueous non-adsorbing Cd–organic acid complexes (Huang et al., 2010; Hizal et al., 2009; Malandrino et al., 2006; Shirvani et al., 2015; Kong et al., 2018). Organic acids were deprotonated at pH 7.0 (see the pK_a of organic acids in Table 1) (Wei et al., 2011). For example, the main form of citric acid (denoted as H₃L) changed from H₃L to H₂L⁻ then to HL²⁻ and finally to L³⁻ with increasing solution pH. It has already known that L³⁻ (the predominant species of acetic acid at pH 7.0) had higher chelating ability to heavy metals and efficiently inhibited the hydrolysis of heavy metals than H₂L⁻ and HL²⁻ (Ding et al., 2014). In this case, the formation of stable aqueous non-adsorbing complexes reduced the concentration of free Cd²⁺, and thus the transport of metal ions increased. Similarly, Hizal et al. (2009) found that the possibility of metal ions (e.g., Cd²⁺ and Pb²⁺) to form soluble (i.e., non-adsorbable) metal ion–humic acid complexes increased at higher pH. Moreover, with the addition of organic acid, Cd²⁺ could form CdL⁺, CdL, and CdL⁻ complexes with acetic acid, tartaric acid, and citric acid at pH 7.0, respectively. Therefore, the electrostatic attraction between complexes and sands becomes weaker as compared with that between Cd²⁺ and grains. In addition, it has been reported that the adsorption of organic acids on aquifer media

(e.g., soil, sand and clay minerals) decreased with increasing pH due to the repulsive effects (Hizal et al., 2009; Ward and Brady, 1998; Xu et al., 2007). For example, when 0.5 mM citric acid presented in the background solution, the adsorbed mass of citric acid onto sand grains decreased from 0.24 mmol/kg to 0.17 mmol/kg with increasing pH from 5.0 to 7.0 (Table S3). In other words, compared with acidic conditions, most organic acids remained in the aqueous phase at pH 7.0. Consequently, more stable aqueous complexes formed under these test conditions. Hence, organic acids would facilitate Cd²⁺ transport more readily under neutral conditions.

Regardless of high or low LMWOA concentrations in the background solutions, transport-enhancement effects followed the order of citric acid > tartaric acid > acetic acid. For example, from the breakthrough curve of Cd²⁺, only approximate 8 PV were needed with 0.1 mM acetic acid comparing with about 6 PV in the presence of 0.1 mM citric acid (Fig. 4a). In addition, the maximum value of C/C₀ reached 76% in the presence of acetic acid, lower than the 93% in the presence of citric acid. When the concentration of organic acid was 0.5 mM (Fig. 4b), the maximum breakthrough reached 83% and 97% in the presence of acetic acid and citric acid, respectively. As mentioned above, such a trend may be ascribed to the differences in structure, complexing capability, and molecular weight of the two organic acids. Organic acid that has a higher molecular weight (i.e. citric acid) can attract and/or chelate more Cd²⁺ because it carries more negative charges and has a larger surface area than a lower molecular weight organic acid (i.e., acetic acid) (Wang et al., 2012; Jing et al., 2007; Liao, 2006), resulting in a larger number of Cd²⁺ being retained in the aqueous phase. Accordingly, complexes

formed by Cd^{2+} with citric acid have higher stability constants (the log K values were 3.77 (Capone et al., 1986)) than those formed by Cd^{2+} with acetic acid (the log K values were 1.30 (Bunting and Thong, 1970)) under neutral conditions. Consequently, citric acid is more effective in enhancing the transport of Cd^{2+} under neutral conditions. Similarly, Huang et al. (2010) investigated the influence of LMWOAs on Cd^{2+} adsorption on montmorillonite; the results showed that the concentration of Cd^{2+} in the liquid phase in the presence of citric acid was higher than that in the presence of acetic acid.

The experimental data under neutral conditions was also fitted with the two-site nonequilibrium transport model. Data in Table 2 and Fig. 3 show that the retardation factors (the R values) for Cd^{2+} decreased when concentrations of organic acids increased, indicating that LMWOAs can retard Cd^{2+} deposition. In contrast, f tended to increase from 0.715 in the absence of organic acid to 0.771 in the presence of citric acid (Fig. S5a); likewise, β of Cd^{2+} increased from 0.735 to 0.812, implying that the degree of nonequilibrium decreased (Chung et al., 2016). The results of $\beta > 0.5$ suggested that the transport of Cd^{2+} was dominated by equilibrium conditions because the majority of Cd^{2+} adsorption sites were equilibrium at pH 7.0 (Fig. S5b) (Pang et al., 2004). This was in agreement with the results of previous studies (Fonseca et al., 2011). In addition, the value of the first-order rate coefficient (α) obtained from Cd^{2+} was the highest in the presence of citric acid (Fig. S5c), indicating that Cd^{2+} was the most likely to enter into Type-2 nonequilibrium sites during transport due to the strongest complexing capacity among the three organic acids (Liu et al., 2013). K_d (distribution coefficients) also decreased with increasing organic acid concentrations (Table S2). The trends implied that higher organic acid concentrations had a stronger effect on the adsorption of Cd^{2+} . In addition, the K_d values of Cd^{2+} calculated from the fitted R value using Equation (6) were compared with the values obtained from the batch sorption experiments. The results showed that the fitted values agreed reasonably with the experimentally observed values in this study which are consistent with other published studies (Kookana and Naidu, 1998).

3.3. Effects of citric acid on the transport of Cd^{2+} in the presence of competing cation

Cd^{2+} mobility affected by citric acid in the presence of competitive ion (i.e., Pb^{2+}) is shown in Fig. 5. Interestingly, citric acid could markedly inhibit the transport of Cd^{2+} in the presence of 3 mg/L Pb^{2+} . In the absence of citric acid, the maximum C/C_0 reached 98% within 5 PV. Note that the transport of Cd^{2+} in column experiments tend to increase in the presence of 3 mg/L Pb^{2+} compared with that of Cd^{2+} without competing cations (Fig. S10). This observation might be attributed to the strong competition of Pb^{2+} with Cd^{2+} for the deposition sites (Fonseca et al., 2011; Naidu et al., 1994; Jiang et al., 2010). In the presence of citric acid, the BTCs of Cd^{2+} nearly overlapped at two different concentrations, and Cd^{2+} was detected after 5 PV. The value of the retardation factor (R) with organic acids was smaller than that without organic acids (Table 2). The phenomena can be ascribed to different complex affinities of citric acid to Pb^{2+} and Cd^{2+} (as evident from the comparison between the transport of Pb^{2+} and Cd^{2+} (Fig. S11)). It has been reported that organic acids had greater complexing strength for Pb^{2+} comparing with Cd^{2+} (Fonseca et al., 2011; Kalmykova et al., 2008; Wang et al., 2013; Appel and Ma, 2002). For example, the stability constant of citric acid–Cd complex (Log $K = 3.32$) is lower than that of the citric acid–Pb complex (Log $K = 4.10$) (Janoš, 1993). The different complexing strengths could lead to the redistribution of metals between citric acid and aqueous system (He et al., 2018). In

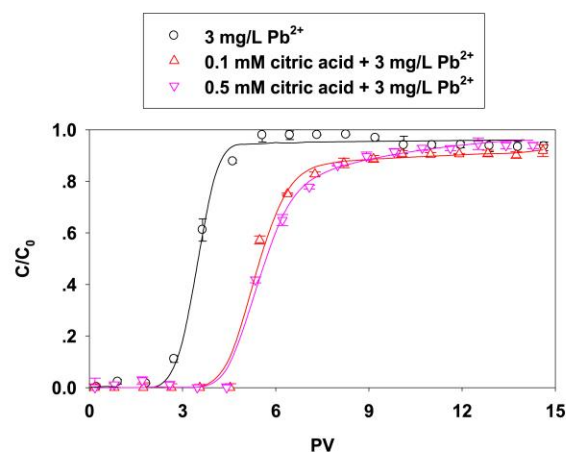


Fig. 5. Effects of citric acid on the transport of Cd^{2+} in the presence of competing cation (i.e., Pb^{2+}) (columns 20–22). Symbols are experimental data and lines are plotted by curve-fitting experimental data with the two-site nonequilibrium transport model.

aqueous system, the preferential binding of Pb^{2+} by dissolved citric acid (i.e., not adsorbed by sand) can keep more Pb^{2+} in the solution, accordingly, less Cd^{2+} complex with citric acid. Consequently, as one might expect, citric acid could markedly enhance the transport of Pb^{2+} and inhibit the transport of Cd^{2+} (Fig. 5 and Fig. S12). In addition, a certain amount of Pb^{2+} complex with citric acid in the influent, resulting in binding of more Cd^{2+} to $-\text{OH}$ groups and the adsorbed LMWOAs on the sand surfaces (Yuan et al., 2007). Meanwhile, the negatively charged organic acids adsorbed to sand will facilitate the Cd^{2+} deposition to sand due to the electrostatic interaction (He et al., 2018). Finally, the formation of sand–organic acid–Cd ternary complex may also contribute to the inhibition of Cd^{2+} in the presence of citric acid (Heidmann et al., 2005). The results imply that cadmium may pose a lesser threat to groundwater in the presence of LMWOAs than that in the absence of LMWOAs under the competitive transport conditions.

4. Conclusions

Laboratory column experiments were conducted to study the effects of LMWOAs on the transport of Cd^{2+} under acidic and neutral conditions. This study has demonstrated that LMWOAs such as acetic acid, tartaric acid, and citric acid played an important role in Cd^{2+} transport in saturated porous media. In general, LMWOAs inhibited the transport of Cd^{2+} at lower concentrations of organic acids (i.e., 0.05 and 0.1 mM) under acidic conditions. This observation was attributed to the development of new deposition sites and the increase in electrostatic interaction. Interestingly, Cd^{2+} mobility in the sand column increased slightly in the presence of 0.5 mM acetic acid. We proposed that the result was likely attributable to the weaker complexing strength of acetic acid and deposition site competition. Notably, at lower concentrations of organic acids under acidic conditions, the transport inhibition effects of LMWOAs on Cd^{2+} transport followed the order of citric acid > tartaric acid > acetic acid, which was in agreement with the decreasing complex stability constants between LMWOAs and Cd^{2+} . This statement may be related to their different molecular structures and their complex forming ability. Conversely, LMWOAs could enhance the transport of Cd^{2+} under neutral conditions (i.e., pH 7.0). The transport-enhancement of LMWOAs was probably due

to the formation of stable aqueous non-adsorbing Cd–organic acid complexes. Furthermore, citric acid could markedly inhibit the transport of Cd^{2+} in the presence of competing cation (i.e., Pb^{2+}). This phenomenon was due to the different complex affinities of citric acid to Pb^{2+} and Cd^{2+} . From this perspective, whether inhibition or enhancement, the transport behaviors were mainly dependent on the concentration of organic acids, pH, organic acid species, and also surrounding conditions (such as competitive transport conditions). Finally, this study is expected to provide critical knowledge to evaluate the fate and transport of Cd^{2+} in subsurface environments and to provide the evidence-based strategies for the remediation of cadmium-contaminated soil. Obviously, natural aquatic environments contain many different heavy-metal ions. These ions may have a significant difference in complex forming ability, hydrated radii, and charge density. It is probably reasonable to expect that the different effects of LMWOAs on the transport behaviors of metal ions may also possibly vary with different species of metal ions. Therefore, more studies are required to get a better understanding of the transport of various metal ions (e.g., Pb^{2+} , Cu^{2+} , and Zn^{2+}) as a function of different LMWOAs.

Declaration of competing interest

The authors declare that they have no known competing financial interests or personal relationships that could have appeared to influence the work reported in this paper.

Acknowledgments

This project was supported by the National Natural Science Foundation of China (Grants 21707081), the Natural Science Foundation of Shandong Province (ZR2017BB083), the Opening Foundation of Ministry of Education Key Laboratory of Pollution Processes and Environmental Criteria (2018–06), the program for Science & Technology Innovation Team in Universities of Henan Province (19IRTSTHN029), and Chinese Scholarship Council (201708420145).

Appendix A. Supplementary data

Supplementary data to this article can be found online at <https://doi.org/10.1016/j.watres.2019.115182>.

References

- Adeyemi, O., Oloyede, O., Oladiji, A., 2007. Physicochemical and microbial characteristics of leachate-contaminated groundwater. *Asian J. Biochem.* 3 (5), 343–348.
- Akbour, R.A., Amal, H., Ait-Addi, A., Douch, J., Jada, A., Hamdani, M., 2013. Transport and retention of humic acid through natural quartz sand: influence of the ionic strength and the nature of divalent cation. *Colloids Surf., A* 436, 589–598.
- Ambedkar, G., Muniyan, M., 2012. Analysis of heavy metals in water, sediments and selected freshwater fish collected from Gadilam river, Tamilnadu, India. *Toxicol. Appl. Pharmacol.* 2, 25–30.
- Appel, C., Ma, L., 2002. Concentration, pH, and surface charge effects on cadmium and lead sorption in three tropical soils. *J. Environ. Qual.* 31 (2), 581–589.
- Bolton, D.W., 2006. Analysis of Cadmium in Ground Water and Sediment Samples in the Aquia Aquifer in Central Anne Arundel Country (Maryland).
- Brinkmann, T., Horsch, P., Sartorius, D., Frimmel, F.H., 2003. Photoformation of low-molecular-weight organic acids from brown water dissolved organic matter. *Environ. Sci. Technol.* 37 (18), 4190–4198.
- Bunting, J.W., Thong, K.M., 1970. Stability constants for some 1:1 metal–carboxylate complexes. *Can. J. Chem.* 48 (11), 1654–1656.
- Buragohain, M., Bhuyan, B., Sarma, H.P., 2010. Seasonal variations of lead, arsenic, cadmium and aluminium contamination of groundwater in Dhemaji district, Assam, India. *Environ. Monit. Assess.* 170, 345–351.
- Butter, T.J., Evison, L.M., Hancock, I.C., Holland, F.S., Matis, K.A., Philipson, A.M., 1998. The removal of cadmium from dilute aqueous solutions by biosorption and electrolysis at laboratory scale. *Water Res.* 32 (2), 400–406.
- Candela, L., Alvarez-Benedí, J., Condeso de Melo, M.T., Rao, P.S.C., 2007. Laboratory studies on glyphosate transport in soils of the Maresme area near Barcelona, Spain: transport model parameter estimation. *Geoderma* 140 (1–2), 8–16.
- Capone, S., Robertis, A.D., Stefano, C.D., Sammartano, S., 1986. Formation and stability of zinc (II) and cadmium(II) citrate complexes in aqueous solution at various temperatures. *Talanta* 33 (9), 763–767.
- Chada, V.G.R., Hausner, D.B., Strongin, D.R., Rouff, A.A., Reeder, R.J., 2005. Divalent Cd and Pb uptake on calcite cleavage faces: an XPS and AFM study. *J. Colloid Interface Sci.* 288 (2), 350–360.
- Chen, H., Gao, B., Li, H., Ma, L.Q., 2011. Effects of pH and ionic strength on sulfamethoxazole and ciprofloxacin transport in saturated porous media. *J. Contam. Hydrol.* 126 (1–2), 29–36.
- Chotpanarat, S., Kiatvarangkul, N., 2018. Facilitated transport of cadmium with montmorillonite KSF colloids under different pH conditions in water-saturated sand columns: experiment and transport modeling. *Water Res.* 146, 216–231.
- Christl, I., Milne, C.J., Kinniburgh, D., Kretzschmar, R., 2001. Relating ion binding by fulvic and humic acids to chemical composition and molecular size: 2. Metal binding. *Environ. Sci. Technol.* 35, 2512–2517.
- Christy, A.A., 2010. New insights into the surface functionalities and adsorption evolution of water molecules on silica gel surface: a study by second derivative near infrared spectroscopy. *Vib. Spectrosc.* 54 (1), 42–49.
- Chung, J., Kim, Y.J., Lee, G., Nam, K., 2016. Experimental determination of nonequilibrium transport parameters reflecting the competitive sorption between Cu and Pb in slag-sand column. *Chemosphere* 154, 335–342.
- Collins, C.R., Ragnarsdóttir, K.V., Sherman, D.M., 1999. Effect of inorganic and organic ligands on the mechanism of cadmium sorption to goethite. *Geochem. Cosmochim. Acta* 63 (19), 2989–3002.
- Dijkstra, J.J., Meeussen, J.C.L., Comans, R.N.J., 2004. Leaching of heavy metals from contaminated soils: an experimental and modeling study. *Environ. Sci. Technol.* 38 (16), 4390–4395.
- Ding, Y.Z., Song, Z.G., Feng, R.W., Guo, J.K., 2014. Interaction of organic acids and pH on multi-heavy metal extraction from alkaline and acid mine soils. *Int. J. Environ. Sci. Technol.* 11 (1), 33–42.
- Dong, S.N., Gao, B., Sun, Y.Y., Shi, X.Q., Xu, H.X., Wu, J.F., Wu, J.C., 2016. Transport of sulfacetamide and levofloxacin in granular porous media under various conditions: experimental observations and model simulations. *Sci. Total Environ.* 573, 1630–1637.
- Elbana, T.A., Selim, H.M., 2010. Cadmium transport in alkaline and acidic soils: miscible displacement experiments. *Soil Sci. Soc. Am. J.* 74 (6), 1956–1966.
- Elkhatib, E.A., Mahdy, A.M., Saleh, M.E., Barakat, N.H., 2007. Kinetics of copper desorption from soils as affected by different organic ligands. *Int. J. Environ. Sci. Technol.* 4 (3), 331–338.
- Field, M.S., Leij, F.J., 2014. Combined physical and chemical nonequilibrium transport model for solution conduits. *J. Contam. Hydrol.* 157, 37–46.
- Fletcher, P.J., Staden, J.F.V., 2003. Determination of carbonate and hydrogencarbonate by titration using sequential injection analysis. *Anal. Chim. Acta* 485 (2), 187–194.
- Florido, A., Valderrama, C., Arévalo, J.A., Casas, I., Martínez, M., Miralles, N., 2010. Application of two sites non-equilibrium sorption model for the removal of Cu(II) onto grape stalk wastes in a fixed-bed column. *Chem. Eng. J.* 156 (2), 298–304.
- Fonseca, B., Figueiredo, H., Rodrigues, J., Queiroz, A., Tavares, T.M., 2011. Mobility of Cr, Pb, Cd, Cu and Zn in a loamy sand soil: a comparative study. *Geoderma* 164 (3–4), 232–237.
- Foti, C., Lando, G., Millero, F.J., Sammartano, S., 2011. Experimental study and modelling of inorganic Cd^{2+} speciation in natural waters. *Environ. Chem.* 8 (3), 320.
- He, S., Li, Y., Weng, L., Wang, J., He, J., Liu, Y., Zhang, K., Wu, Q., Zhang, Y., Zhang, Z., 2018. Competitive adsorption of Cd^{2+} , Pb^{2+} and Ni^{2+} onto Fe^{3+} -modified argillaceous limestone: influence of pH, ionic strength and natural organic matters. *Sci. Total Environ.* 637–638, 69–78.
- Heidmann, I., Christl, I., Kretzschmar, R., 2005. Sorption of Cu and Pb to kaolinite-fulvic acid colloids: assessment of sorbent interactions. *Geochem. Cosmochim. Acta* 69 (7), 1675–1686.
- Herreweghe, S.V., Swennen, R., Cappuyns, V., Vandecasteele, C., 2002. Chemical associations of heavy metals and metalloids in contaminated soils near former ore treatment plants—a differentiated approach with emphasis on pH state-leaching. *J. Geochem. Explor.* 76 (2), 113–138.
- Hizal, J., Apak, R., Hoell, W.H., 2009. Modeling competitive adsorption of copper(II), lead(II), and cadmium(II) by kaolinite-based clay mineral/humic acid system. *Environ. Prog. Sustain.* 28 (4), 493–506.
- Holm, P.E., Rootzén, H., Borggaard, O.K., Moberg, J.P., Christensen, T.H., 2003. Correlation of cadmium distribution coefficient to soil characteristics. *J. Environ. Qual.* 32 (1), 138–145.
- Hu, H., Tang, C., Rengel, Z., 2005. Influence of phenolic acids on phosphorus mobilisation in acidic and calcareous soils. *Plant Soil* 268 (1), 173–180.
- Hu, H.G., Liu, H.L., He, J.Z., Huang, Q.Y., 2007. Effect of selected organic acids on cadmium sorption by variable- and permanent-charge soils. *Pedosphere* 17 (1), 117–123.
- Huang, Q., Zhao, Z., Chen, W., 2003. Effects of several low-molecular weight organic acids and phosphate on the adsorption of acid phosphatase by soil colloids and minerals. *Chemosphere* 52 (3), 571–579.
- Huang, L., Hu, H., Li, X., Li, L.Y., 2010. Influences of low molar mass organic acids on the adsorption of Cd^{2+} and Pb^{2+} by goethite and montmorillonite. *Appl. Clay Sci.* 49 (3), 281–287.
- Jada, A., Ait Akbour, R., Douch, J., 2006. Surface charge and adsorption from water onto quartz sand of humic acid. *Chemosphere* 64 (8), 1287–1295.

- Janoš, P., 1993. Determination of stability constants of metal complexes from ion chromatographic measurements. *J. Chromatogr. A* 641 (2), 229–234.
- Jiang, M.Q., Jin, X.Y., Lu, X.Q., Chen, Z., 2010. Adsorption of Pb(II), Cd(II), Ni(II) and Cu(II) onto natural kaolinite clay. *Desalination* 252 (1–3), 33–39.
- Jiang, H., Li, T., Han, X., Yang, X., He, Z., 2012. Effects of pH and low molecular weight organic acids on competitive adsorption and desorption of cadmium and lead in paddy soils. *Environ. Monit. Assess.* 184 (10), 6325–6335.
- Jing, Y.D., He, Z.L., Yang, X.E., 2007. Effects of pH, organic acids, and competitive cations on mercury desorption in soils. *Chemosphere* 69 (10), 1662–1669.
- Jones, D.L., 1998. Organic acids in the rhizosphere—a critical review. *Plant Soil* 205 (1), 25–44.
- Kabatapendias, A., Mukherjee, A.B., 2007. Trace Elements from Soil to Human. Springer Berlin Heidelberg.
- Kalmykova, Y., Stromvall, A.M., Steenari, B.M., 2008. Adsorption of Cd, Cu, Ni, Pb and Zn on Sphagnum peat from solutions with low metal concentrations. *J. Hazard Mater.* 152 (2), 885–891.
- Kantar, C., 2007. Heterogeneous processes affecting metal ion transport in the presence of organic ligands: reactive transport modeling. *Earth Sci. Rev.* 81 (3–4), 175–198.
- Kasten, P.R., Lapidus, L., Amundson, N.R., 1952. Mathematics of adsorption in beds. V. effect of intra-particle diffusion in flow systems in fixed beds. *J. Phys. Chem.* 56 (6), 683–688.
- Kim, H.N., Bradford, S.A., Walker, S.L., 2009. Escherichia coli O157:H7 transport in saturated porous media: role of solution chemistry and surface macromolecules. *Environ. Sci. Technol.* 43 (12), 4340–4347.
- Kong, Q., Xie, B., Preis, S., Hu, Y., Wu, H., Wei, C., 2018. Adsorption of Cd²⁺ by an ion-imprinted thiol-functionalized polymer in competition with heavy metal ions and organic acids. *RSC Adv.* 8 (16), 8950–8960.
- Kookana, R.S., Naidu, R., 1998. Effect of soil solution composition on cadmium transport through variable charge soils. *Geoderma* 84 (1–3), 235–248.
- Krishnamurti, G.S.R., Huang, P.M., van Rees, K.C.J., 1997. Kinetics of cadmium release from soils as influenced by organic acids: Implication in cadmium availability. *J. Environ. Qual.* 26 (1), 271–277.
- Kuntz, D., Grathwohl, P., 2009. Comparison of steady-state and transient flow conditions on reactive transport of contaminants in the vadose soil zone. *J. Hydrol.* 369 (3–4), 225–233.
- Lee, S.Z., Allen, H.E., Huang, C.P., Sparks, D.L., Sanders, P.F., Peijnenburg, W.J.G.M., 1996. Predicting soil-water partition coefficients for cadmium. *Environ. Sci. Technol.* 30 (12), 3418–3424.
- Leij, F.J., Bradford, S.A., 2009. Combined physical and chemical non-equilibrium transport model: analytical solution, moments, and application to colloids. *J. Contam. Hydrol.* 110 (3–4), 87–99.
- Li, Y.S., Hou, Y.X., Song, X.Y., Sun, L.Q., Li, S., Guo, Q., Hu, X.J., 2015. Effect of pH on the desorption of trace metals by different LMWOAs from a field soil. *Adv. Mater. Res.* 1073–1076, 193–196.
- Li, J., Chen, J., Lu, T., Wang, Y., Zhang, H., Shang, Z., Li, D., Zhou, Y., Qi, Z., 2019. Effects of low-molecular weight organic acids on the transport of graphene oxide nanoparticles in saturated sand columns. *Sci. Total Environ.* 666, 94–102.
- Liao, M., 2006. Effects of organic acids on adsorption of cadmium onto kaolinite, goethite, and bayerite. *Pedosphere* 16 (2), 185–191.
- Liu, H., Zhang, D., Li, M., Tong, L., Feng, L., 2013. Competitive adsorption and transport of phthalate esters in the clay layer of Jiangnan plain, China. *Chemosphere* 92 (11), 1542–1549.
- Liu, Y.Y., Liu, C.X., Zhang, C.Y., Yang, X.F., Zachara, J.M., 2015. Pore and continuum scale study of the effect of subgrid transport heterogeneity on redox reaction rates. *Geochem. Cosmochim. Acta* 163, 140–155.
- Liu, H.L., Wang, Y.J., Xuan, L., Dang, F., Zhou, D.M., 2017. Effects of low-molecular-weight organic acids on the acute lethality, accumulation, and enzyme activity of cadmium in Eisenia fetida in a simulated soil solution. *Environ. Toxicol. Chem.* 36 (4), 1005–1011.
- Lu, H.L., Yan, C.L., Liu, J.C., 2007. Low-molecular-weight organic acids exuded by Mangrove (Kandelia candel (L.) Druce) roots and their effect on cadmium species change in the rhizosphere. *Environ. Exp. Bot.* 61 (2), 159–166.
- Malandrino, M., Abollino, O., Giacomino, A., Aceto, M., Mentasti, E., 2006. Adsorption of heavy metals on vermiculite: influence of pH and organic ligands. *J. Colloid Interface Sci.* 299 (2), 537–546.
- Mattison, N.T., O'Carroll, D.M., Kerry Rowe, R., Petersen, E.J., 2011. Impact of porous media grain size on the transport of multi-walled carbon nanotubes. *Environ. Sci. Technol.* 45 (22), 9765–9775.
- McBride, M.B., 1989. Reactions controlling heavy metal solubility in soils. *Adv. Soil Sci.* 10, 1–56.
- Miralles, N., Valderrama, C., Casas, I., Martínez, M., Florido, A., 2010. Cadmium and lead removal from aqueous solution by grape stalk wastes—modeling of a fixed-bed column. *J. Chem. Eng. Data* 55 (9), 3548–3554.
- Morales, V.L., Gao, B., Steenhuis, T.S., 2009. Grain surface-roughness effects on colloidal retention in the vadose zone. *Vadose Zone J.* 8 (1), 11–20.
- Morrow, B.A., McFarlan, A.J., 1991. Infrared and gravimetric study of an aerosol and a precipitated silica using chemical and hydrogen/deuterium exchange probes. *Langmuir* 7 (8), 1695–1701.
- Naidu, R., Bolan, N.S., Kookana, R.S., Tiller, K.G., 1994. Ionic strength and pH effects on the sorption of Cd and the surface charge of soils. *Eur. J. Soil Sci.* 45 (4), 419–429.
- Najafi, S., Jalali, M., 2015. Effects of organic acids on cadmium and copper sorption and desorption by two calcareous soils. *Environ. Monit. Assess.* 187 (9), 585.
- Nielsen, D.R., Genuchten, M.T.V., Biggar, J.W., 1986. Water flow and solute transport processes in the unsaturated zone. *Water Resour. Res.* 22 (9), 895–1088.
- Nkedi-Kizza, P., Bigga, J.W., Selim, H.M., Genuchten, M.T.V., Wierenga, P.J., Davidson, J.M., 1984. On the equivalence of two conceptual models for describing ion exchange during transport through an aggregated oxisol. *Water Resour. Res.* 20 (8), 1123–1130.
- Pang, L., Close, M., Greenfield, H., Stanton, G., 2004. Adsorption and transport of cadmium and rhodamine WT in pumice sand columns. *New Zeal. J. Journal of Mar. Fresh.* 38 (2), 367–378.
- Paradelo, M., Pérez-Rodríguez, P., Fernández-Calviño, D., Arias-Estévez, M., López-Periago, J.E., 2012. Coupled transport of humic acids and copper through saturated porous media. *Eur. J. Soil Sci.* 63 (5), 708–716.
- Parfitt, R.L., Farmer, V.C., Russell, J.D., 1977. Adsorption on hydrous oxides Oxalate and benzoate on goethite. *Eur. J. Soil Sci.* 28 (1), 29–39.
- Pivovarov, S., 2005. Modeling of ionic equilibria of trace metals (Cu²⁺, Zn²⁺, Cd²⁺) in concentrated aqueous electrolyte solutions at 25 °C. *J. Colloid Interface Sci.* 291 (2), 421–432.
- Renella, G., Landi, L., Nannipieri, P., 2004. Degradation of low molecular weight organic acids complexed with heavy metals in soil. *Geoderma* 122 (2–4), 311–315.
- Sadhukhan, T., Latif, I.A., Datta, S.N., 2014. Solvation of CO₂ in water: effect of RuBP on CO₂ concentration in bundle sheath of C4 plants. *J. Phys. Chem. B* 118 (29), 8782–8791.
- Saha, N., Zaman, M., 2011. Concentration of selected toxic metals in groundwater and some cereals grown in Shibganj area of Chapai Nawabganj, Rajshahi, Bangladesh. *Curr. Sci.* 101, 427–431.
- Seuntjens, P., Tirez, K., Simunek, J., van Genuchten, M.T., Cornelis, C., Geuzens, P., 2001. Aging effects on cadmium transport in undisturbed contaminated sandy soil columns. *J. Environ. Qual.* 30 (3), 1040–1050.
- Shirvani, M., Sherkat, Z., Khalili, B., Bakhtiary, S., 2015. Sorption of Pb(II) on palygorskite and sepiolite in the presence of amino acids: equilibria and kinetics. *Geoderma* 249–250, 21–27.
- Singh, P.K., Wenjing, W., Shrivastava, A.K., 2018. Cadmium-mediated morphological, biochemical and physiological tuning in three different, anabaena, species. *Aquat. Toxicol.* 202, 36–45.
- Stamatis, G., Voudouris, K., Kareflakis, F., 2001. Groundwater pollution by heavy metals in historical mining area of Lavrio, Attica, Greece. *Water Air Soil Pollut.* 128 (1–2), 61–83.
- Strobel, B.W., 2001. Influence of vegetation on low-molecular-weight carboxylic acids in soil solution—a review. *Geoderma* 99 (3–4), 169–198.
- Tedetti, M., Kawamura, K., Charrière, B., Chevalier, N., Sempéré, R., 2006. Determination of low molecular weight carboxylic acids and ketocarboxylic acids in seawater samples. *Anal. Chem.* 78 (17), 6012–6018.
- Toride, N., Leij, F.J., van Genuchten, M.T., 1999. The CXTFIT Code for Estimating Transport Parameters from Laboratory or Field Tracer Experiments. U.S. Salinity Laboratory, Riverside, CA, USA.
- Tsang, D.C.W., Zhang, W., Lo, I.M.C., 2007. Modeling cadmium transport in soils using sequential extraction, batch, and miscible displacement experiments. *Soil Sci. Soc. Am. J.* 71 (3), 674–681.
- Uyusur, B., Li, C., Baveye, P.C., Darnault, C.J.G., 2014. pH-dependent reactive transport of uranium(VI) in unsaturated sand. *J. Soils Sediments* 15 (3), 634–647.
- Wang, Y.J., Chen, J.H., Cui, Y.X., Wang, S.Q., Zhou, D.M., 2009. Effects of low-molecular-weight organic acids on Cu(II) adsorption onto hydroxyapatite nanoparticles. *J. Hazard Mater.* 162 (2–3), 1135–1140.
- Wang, Y.G., Li, Y.S., Kim, H.N., Walker, S.L., Abriola, L.M., Pennell, K.D., 2010. Transport and retention of fullerene nanoparticles in natural soils. *J. Environ. Qual.* 39 (6), 1925–1933.
- Wang, J., Lv, J., Fu, Y., 2012. Effects of organic acids on Cd adsorption and desorption by two anthropic soils. *Front. Environ. Sci. Eng.* 7 (1), 19–30.
- Wang, T., Liu, W., Xiong, L., Xu, N., Ni, J., 2013. Influence of pH, ionic strength and humic acid on competitive adsorption of Pb(II), Cd(II) and Cr(III) onto titanate nanotubes. *Chem. Eng. J.* 215–216, 366–374.
- Ward, D.B., Brady, P.V., 1998. Effect of Al and organic acids on the surface chemistry of kaolinite. *Clay Clay Miner.* 46 (4), 453–465.
- Wei, W., Zhang, X., Cui, J., Wei, Z., 2011. Interaction between low molecular weight organic acids and hydroxyapatite with different degrees of crystallinity. *Colloids Surf., A* 392 (1), 67–75.
- WHO, 2004. Cadmium in Drinking-Water: Background Document for Development of WHO Guidelines for Drinking-Water Quality. World Health Organization, Geneva.
- Wikiniyadhane, R., Chotpanarat, S., Ong, S.K., 2015. Effects of kaolinite colloids on Cd²⁺ transport through saturated sand under varying ionic strength conditions: column experiments and modeling approaches. *J. Contam. Hydrol.* 182, 146–156.
- Worch, E., 2004. Modelling the solute transport under nonequilibrium conditions on the basis of mass transfer equations. *J. Contam. Hydrol.* 68 (1–2), 97–120.
- Wu, H., Jiang, D., Cai, P., Rong, X., Huang, Q., 2011. Effects of low-molecular-weight organic ligands and phosphate on adsorption of Pseudomonas putida by clay minerals and iron oxide. *Colloids Surf., B* 82 (1), 147–151.
- Xiao, M., Wu, F.C., 2014. A review of environmental characteristics and effects of low-molecular weight organic acids in the surface ecosystem. *J. Environ. Sci.* 26 (5), 935–954.
- Xie, B., Jiang, Y., Zhang, Z., Cao, G., Sun, H., Wang, N., Wang, S., 2018. Co-transport of Pb (II) and Cd (II) in saturated porous media: effects of colloids, flow rate and grain size. *Chem. Speciat. Bioavailab.* 30 (1), 55–63.
- Xu, R.K., Xiao, S.C., Zhang, H., Jiang, J., Ji, G.L., 2007. Adsorption of phthalic acid and

- salicylic acid by two variable charge soils as influenced by sulphate and phosphate. *Eur. J. Soil Sci.* 58 (1), 335–342.
- Yang, H., Kim, H., Tong, M., 2012. Influence of humic acid on the transport behavior of bacteria in quartz sand. *Colloids Surf., B* 91, 122–129.
- Yuan, S., Xi, Z., Jiang, Y., Wan, J., Wu, C., Zheng, Z., Lu, X., 2007. Desorption of copper and cadmium from soils enhanced by organic acids. *Chemosphere* 68 (7), 1289–1297.
- Zhang, M., Zhang, H., 2010. Co-transport of dissolved organic matter and heavy metals in soils induced by excessive phosphorus applications. *J. Environ. Sci.* 22 (4), 598–606.
- Zuo, Y., Chen, G., Zeng, G., Li, Z., Yan, M., Chen, A., Guo, Z., Huang, Z., Tan, Q., 2015. Transport, fate, and stimulating impact of silver nanoparticles on the removal of Cd(II) by *Phanerochaete chrysosporium* in aqueous solutions. *J. Hazard Mater.* 285, 236–244.

Supplementary Material Cover Sheet

Transport of Cd²⁺ through saturated porous media: Insight into the effects of low-molecular-weight organic acids

Haojing Zhang ^{1, a}, Taotao Lu ^{2, 3, a}, Zhongbo Shang ¹, Yanxiang Li ⁴, Jianying He ¹,
Shanhu Liu ¹, Deliang Li ¹, Yanmei Zhou¹, and Zhichong Qi ^{1, 2, *}

¹ Henan Joint International Research Laboratory of Environmental Pollution Control Materials, College of Chemistry and Chemical Engineering, Henan University, Kaifeng 475004, China

² Ministry of Education Key Laboratory of Pollution Processes and Environmental Criteria, Nankai University, Tianjin 300350, China

³ Department of Hydrology, University of Bayreuth, Bayreuth D-95440, Germany

⁴ The Testing Center of Shandong Bureau of China Metallurgical Geology Bureau, Jinan 250014, China

^a Haojing Zhang and Taotao Lu contributed equally.

*Corresponding author: Zhichong Qi (qizhichong1984@163.com);

Manuscript prepared for *Water Research*

S1. Determination of the pH_{pzc} of quartz sand

The pH of zero charge (pH_{pzc}) was measured by the salt addition method (Benjamin et al., 1996; Abdelwaheb et al., 2019). In 6 different beakers, known amounts of sand were mixed with 100 mL of sodium chloride (0.1 M). A pH value was adjusted for each beaker (from 2 to 12) by adding the necessary amounts of nitric acid or potassium hydroxide. After 24 h of stirring at room temperature, the pH was measured again and plotted as a function of the initial pH. The intersection of this curve with the straight-line $\text{pH}_i = \text{pH}$ corresponds to pH_{pzc} (Kavitha and Thambavani, 2014).

S2. Determination of the CEC of quartz sand

The cation exchange capacity (CEC) of sand was measured by the following the previously reported method (Ollat and Combeau, 1960; Abdelwaheb et al., 2019). In brief, 500 mL of CaCl_2 (1eq/L) are injected from bottom to top through a column filled with 10 g of sand. Then, 150 mL of CaCl_2 (0.05 eq/L) is injected followed by 500 mL of KNO_3 (1eq/L). The percolate is collected in 500 mL flask and the total calcium was titrated with EDTA (0.02eq/L) at pH 12 using the Eriochrome Black T as indicator. At the same time, the chloride is titrated with AgNO_3 (0.05eq/L) using the K_2CrO_4 as indicator. The CEC is given by:

$$\text{CEC (meq /100g)} = 2v-5V$$

where v is the volume (mL) of EDTA required for calcium titration and V the volume (mL) of AgNO_3 required for chlorides titration.

S3. Determination of the ζ -potential of quartz sand

In order to characterize the electro-kinetic properties of the porous medium, the streaming potential of quartz sand was determined using an electro-kinetic analyzer (Anton Paar, Graz, Austria) (Kim et al., 2009; Wang et al., 2010). The sand was packed into a cylindrical cell (1.5 cm inside diameter \times 3 cm length) and flushed with the background electrolyte solution for approximately 20 min. For each packed cell, four streaming potential readings were obtained after the system reached steady-state conditions. Three cell experiments were performed for sand to obtain an average streaming potential, which was converted to a zeta potential using the Helmholtz-Smoluchowski equation (Childress and Elimelech, 1996):

$$\zeta = \frac{\Delta V}{\Delta P} \frac{\mu}{\varepsilon \varepsilon_0} \frac{L}{A} \frac{1}{R}$$

Where ζ is the zeta potential (V), V is the streaming potential (V), P is the pressure (Pa), μ is the solution dynamic viscosity ($\text{M L}^{-1} \text{t}^{-1}$), ε is the relative dielectric constant of the solution (–), ε_0 is the permittivity of a vacuum, L is the cell length (L), A is the cross-sectional area of the cell (L^2), and R is the channel resistance (Ω). The results are listed in Table S4.

S4. Adsorption studies of LMWOAs onto sand

Adsorption studies were conducted to determine the adsorption capacity of LMWOAs onto sand under different pH conditions. First, approximately 5 g quartz sand and 20 mL of organic acid solutions (0.1 mM) were added to each of a series of 20-ml amber glass vials. Then, the vials were equilibrated for 10h by horizontally shaking (the duration equal to the transport experiment). Then, the vials were centrifuged at 5000 rpm for 20 min and the supernatants were withdrawn. The concentration of LMWOAs was analyzed by a total organic carbon analyzer from Shimadzu Scientific (Columbia, MD, USA). The adsorbed LMWOAs were then determined by the difference between the initial and final LMWOA concentrations in the aqueous phase. All experiments were run in triplicate. The test results are presented in Table S3.

Table S1. Experimental protocols of column tests

Column No.	Background solution	Competing Cation	pH	porosity (-)	density Bulk (g/cm ³)
1	0.5 mM NaCl	/	5.0	0.41	1.55
2	0.5 mM NaCl + 0.05 mM acetic acid	/	5.0	0.42	1.53
3	0.5 mM NaCl + 0.05 mM tartaric acid	/	5.0	0.40	1.55
4	0.5 mM NaCl + 0.05 mM citric acid	/	5.0	0.41	1.57
5	0.5 mM NaCl + 0.1 mM acetic acid	/	5.0	0.42	1.54
6	0.5 mM NaCl + 0.1 mM tartaric acid	/	5.0	0.41	1.53
7	0.5 mM NaCl + 0.1 mM citric acid	/	5.0	0.40	1.57
8	0.5 mM NaCl + 0.5 mM acetic acid	/	5.0	0.41	1.53
9	0.5 mM NaCl + 0.5 mM tartaric acid	/	5.0	0.41	1.56
10	0.5 mM NaCl + 0.5 mM citric acid	/	5.0	0.4	1.56
11 ^a	0.5 mM NaCl, 0.1 mM citric acid saturated column	/	5.0	0.41	1.57
12 ^a	0.5 mM NaCl, 0.5 mM citric acid saturated column	/	5.0	0.42	1.55
13	0.5 mM NaCl	/	7.0	0.41	1.53
14	0.5 mM NaCl + 0.1 mM acetic acid	/	7.0	0.4	1.54
15	0.5 mM NaCl + 0.1 mM tartaric acid	/	7.0	0.41	1.53
16	0.5 mM NaCl + 0.1 mM citric acid	/	7.0	0.42	1.57
17	0.5 mM NaCl + 0.5 mM acetic acid	/	7.0	0.41	1.55
18	0.5 mM NaCl + 0.5 mM tartaric acid	/	7.0	0.41	1.56
19	0.5 mM NaCl + 0.5 mM citric acid	/	7.0	0.40	1.54
20	0.5 mM NaCl	3 mg/L Pb ²⁺	5.0	0.41	1.53
21	0.5 mM NaCl + 0.1 mM citric acid	3 mg/L Pb ²⁺	5.0	0.41	1.55
22	0.5 mM NaCl + 0.5 mM citric acid	3 mg/L Pb ²⁺	5.0	0.41	1.53

^a Column was pre-saturated with citric acid before injecting Cd²⁺ solution.

Table S2. Comparison of experimentally obtained and fitted K_d values of Cd^{2+} to sand

No.	Background solution	Competing cation	pH	K_d (L/kg)	
				Column ^a	Batch ^b
1	0.5 mM NaCl	/	5.0	1.48	1.42 ± 0.08
2	0.5 mM NaCl + 0.05 mM acetic acid	/	5.0	1.47	1.45 ± 0.03
3	0.5 mM NaCl + 0.05 mM tartaric acid	/	5.0	1.54	1.62 ± 0.09
4	0.5 mM NaCl + 0.05 mM citric acid	/	5.0	1.67	1.71 ± 0.15
5	0.5 mM NaCl + 0.1 mM acetic acid	/	5.0	1.60	1.50 ± 0.20
6	0.5 mM NaCl + 0.1 mM tartaric acid	/	5.0	1.99	1.77 ± 0.24
7	0.5 mM NaCl + 0.1 mM citric acid	/	5.0	2.11	2.30 ± 0.24
8	0.5 mM NaCl + 0.5 mM acetic acid	/	5.0	1.41	1.39 ± 0.03
9	0.5 mM NaCl + 0.5 mM tartaric acid	/	5.0	1.75	1.78 ± 0.03
10	0.5 mM NaCl + 0.5 mM citric acid	/	5.0	1.80	1.86 ± 0.06
11	0.5 mM NaCl	/	7.0	3.56	3.85 ± 0.18
12	0.5 mM NaCl + 0.1 mM acetic acid	/	7.0	3.23	3.09 ± 0.04
13	0.5 mM NaCl + 0.1 mM tartaric acid	/	7.0	2.52	3.83 ± 0.13
14	0.5 mM NaCl + 0.1 mM citric acid	/	7.0	2.15	2.04 ± 0.14
15	0.5 mM NaCl + 0.5 mM acetic acid	/	7.0	2.07	2.02 ± 0.23
16	0.5 mM NaCl + 0.5 mM tartaric acid	/	7.0	1.30	1.42 ± 0.06
17	0.5 mM NaCl + 0.5 mM citric acid	/	7.0	1.21	1.18 ± 0.23
18	0.5 mM NaCl	3 mg/L Pb^{2+}	5.0	1.13	1.05 ± 0.03
19	0.5 mM NaCl + 0.1 mM citric acid	3 mg/L Pb^{2+}	5.0	1.84	1.91 ± 0.05
20	0.5 mM NaCl + 0.5 mM citric acid	3 mg/L Pb^{2+}	5.0	1.70	1.87 ± 0.03

^a Calculated from the fitted R value using Equation 6; R was obtained by fitting the transport data with two-site nonequilibrium transport model.

^b Measured in batch sorption experiments.

Table S3. Adsorption amount of LMWOAs onto sand under different pH conditions. Error bars represent standard deviations from replicate experiments (n=3)

LMWOAs	Electrolyte solution	pH	<i>q</i> (mmol-LMWOAs/kg-sand)
0.1 mM acetic acid	0.5 mM NaCl	5.0	0.19 ± 0.02
0.1 mM tartaric acid	0.5 mM NaCl	5.0	0.21 ± 0.01
0.1 mM citric acid	0.5 mM NaCl	5.0	0.27 ± 0.03
0.5 mM acetic acid	0.5 mM NaCl	5.0	0.24 ± 0.03
0.5 mM tartaric acid	0.5 mM NaCl	5.0	0.27 ± 0.01
0.5 mM citric acid	0.5 mM NaCl	5.0	0.32 ± 0.03
0.1 mM acetic acid	0.5 mM NaCl	7.0	0.07 ± 0.05
0.1 mM tartaric acid	0.5 mM NaCl	7.0	0.09 ± 0.02
0.1 mM citric acid	0.5 mM NaCl	7.0	0.13 ± 0.03
0.5 mM acetic acid	0.5 mM NaCl	7.0	0.09 ± 0.01
0.5 mM tartaric acid	0.5 mM NaCl	7.0	0.14 ± 0.02
0.5 mM citric acid	0.5 mM NaCl	7.0	0.17 ± 0.02

Table S4. ζ -potential of sand under different solution chemistry conditions

No.	Background solution	pH	ζ -potential of sand ^a (mV)
1	0.5 mM NaCl	5.0	-35.6 ± 1.1
2	0.5 mM NaCl + 0.05 mM acetic acid	5.0	-36.3 ± 0.9
3	0.5 mM NaCl + 0.05 mM tartaric acid	5.0	-38.1 ± 0.5
4	0.5 mM NaCl + 0.05 mM citric acid	5.0	-40.2 ± 0.8
5	0.5 mM NaCl + 0.1 mM acetic acid	5.0	-36.9 ± 1.5
6	0.5 mM NaCl + 0.1 mM tartaric acid	5.0	-37.9 ± 0.6
7	0.5 mM NaCl + 0.1 mM citric acid	5.0	-39.2 ± 1.4
8	0.5 mM NaCl + 0.5 mM acetic acid	5.0	-37.5 ± 0.3
9	0.5 mM NaCl + 0.5 mM tartaric acid	5.0	-38.7 ± 0.2
10	0.5 mM NaCl + 0.5 mM citric acid	5.0	-41.5 ± 1.3
11	0.5 mM NaCl	7.0	-40.2 ± 0.8
12	0.5 mM NaCl + 0.1 mM acetic acid	7.0	-42.3 ± 0.7
13	0.5 mM NaCl + 0.1 mM tartaric acid	7.0	-43.5 ± 1.6
14	0.5 mM NaCl + 0.1 mM citric acid	7.0	-45.9 ± 1.8
15	0.5 mM NaCl + 0.5 mM acetic acid	7.0	-43.7 ± 2.5
16	0.5 mM NaCl + 0.5 mM tartaric acid	7.0	-46.1 ± 2.1
17	0.5 mM NaCl + 0.5 mM citric acid	7.0	-49.6 ± 0.7

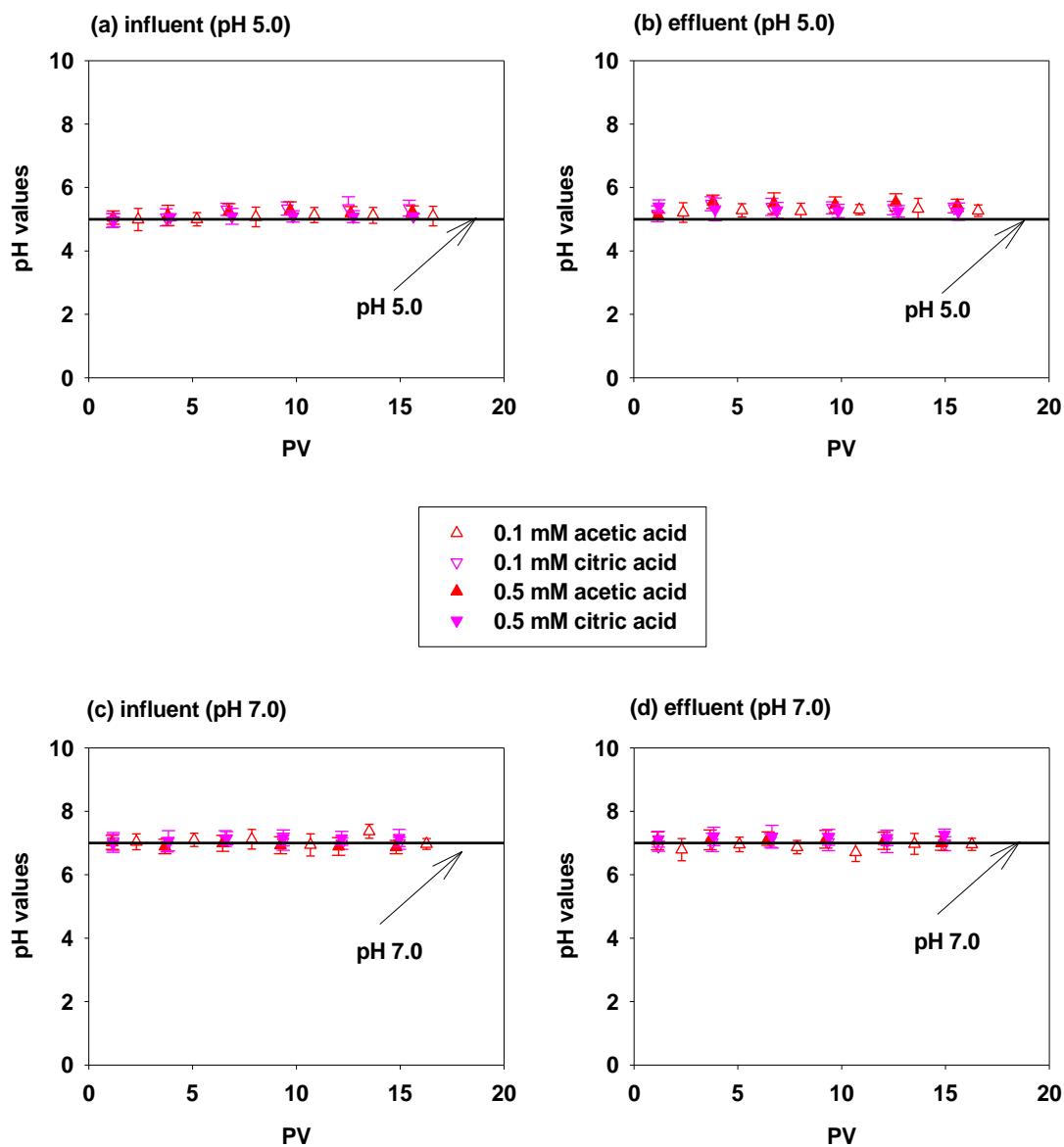


Fig. S1. The change of pH values in effluents in comparison to the respective pH in influents under different pH conditions: pH 5.0 (a and b, Columns 5, 7, 8, and 10) and pH 7.0 (c and d, Columns 14, 16, 17 and 19).

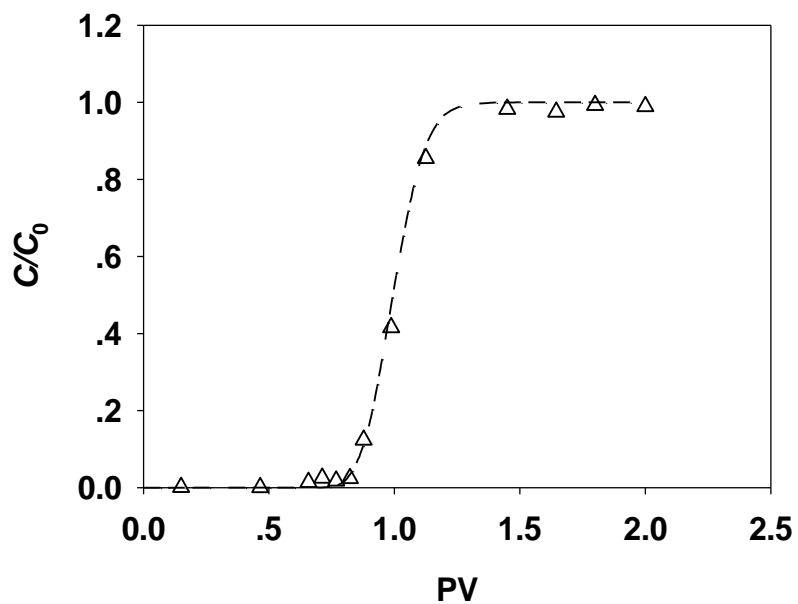


Fig. S2. The representative breakthrough curve of conservative tracer (Br^-). The line was plotted by fitting the breakthrough data with the one-dimensional steady-state advection–dispersion equation.

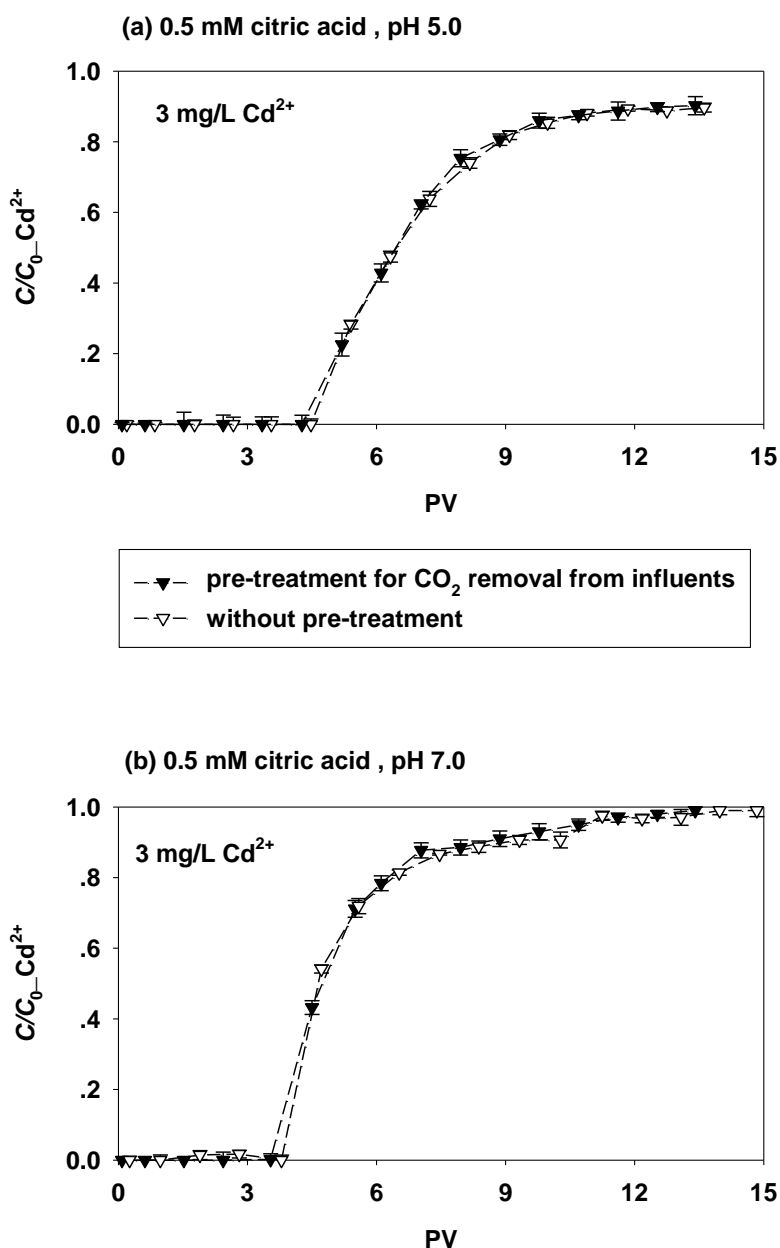


Fig. S3. The effects of dissolved CO₂ on the transport of Cd²⁺ (3 mg/L) in the presence of LMWOAs (using citric acid as the model organic acid) under different pH conditions: (a) pH 5.0 and (b) pH 7.0. Filled triangle (▼): the injection solution was carried out under magnetic stirring and pre-saturated N₂ was bubbled through the solution in order to exclude CO₂ inside (Derikvand et al., 2013; De Stefano et al., 2014). Hollow triangle (▽): the injection solution was not treated with N₂ before injection.

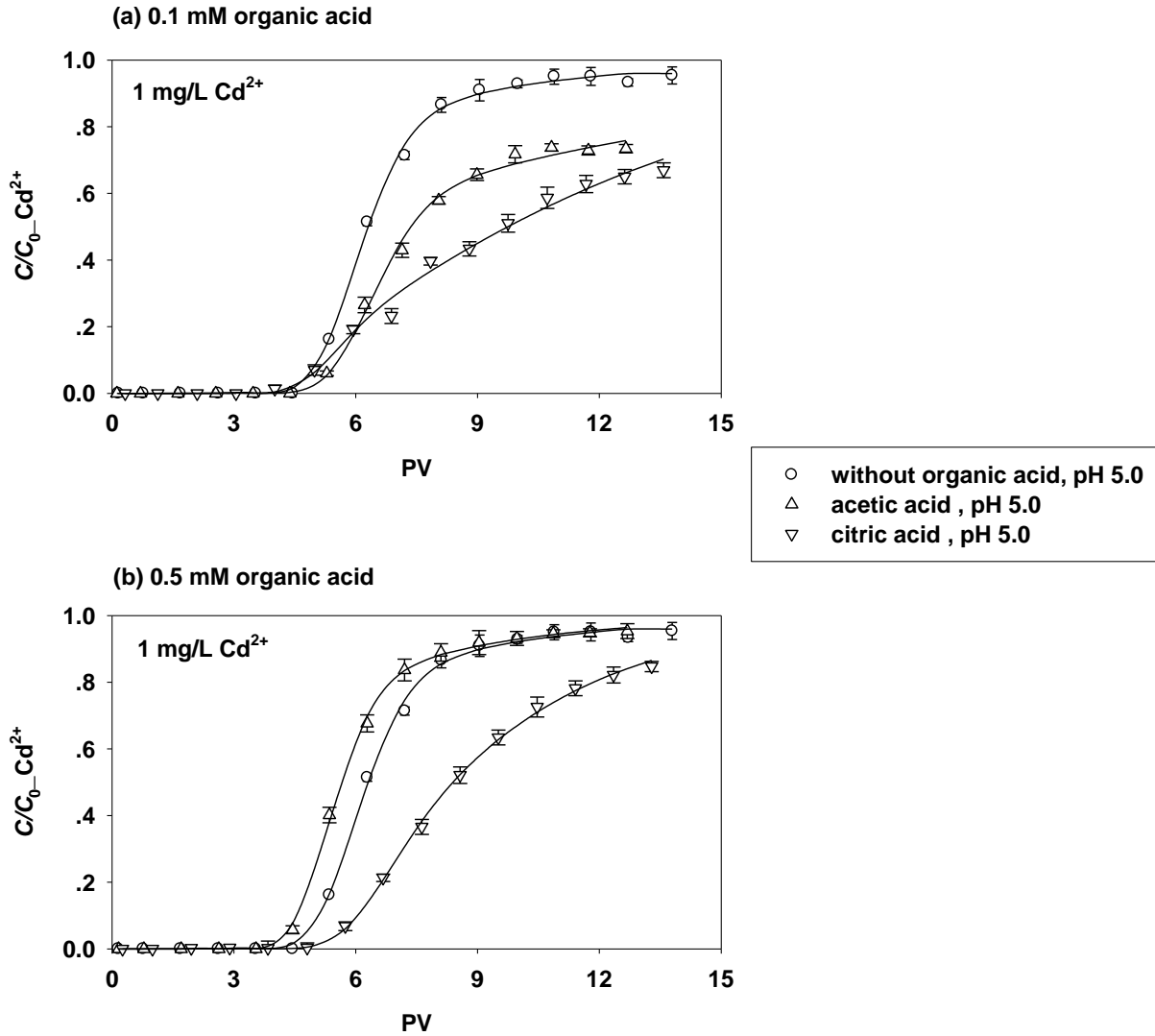


Fig. S4. Effects of low-molecular-weight organic acids on the transport of Cd²⁺ (1 mg/L) under acidic conditions: (a) 0.1 mM organic acid; and (b) 0.5 mM organic acids. Symbols are experimental data and lines are plotted by curve-fitting experimental data with the two-site nonequilibrium transport model.

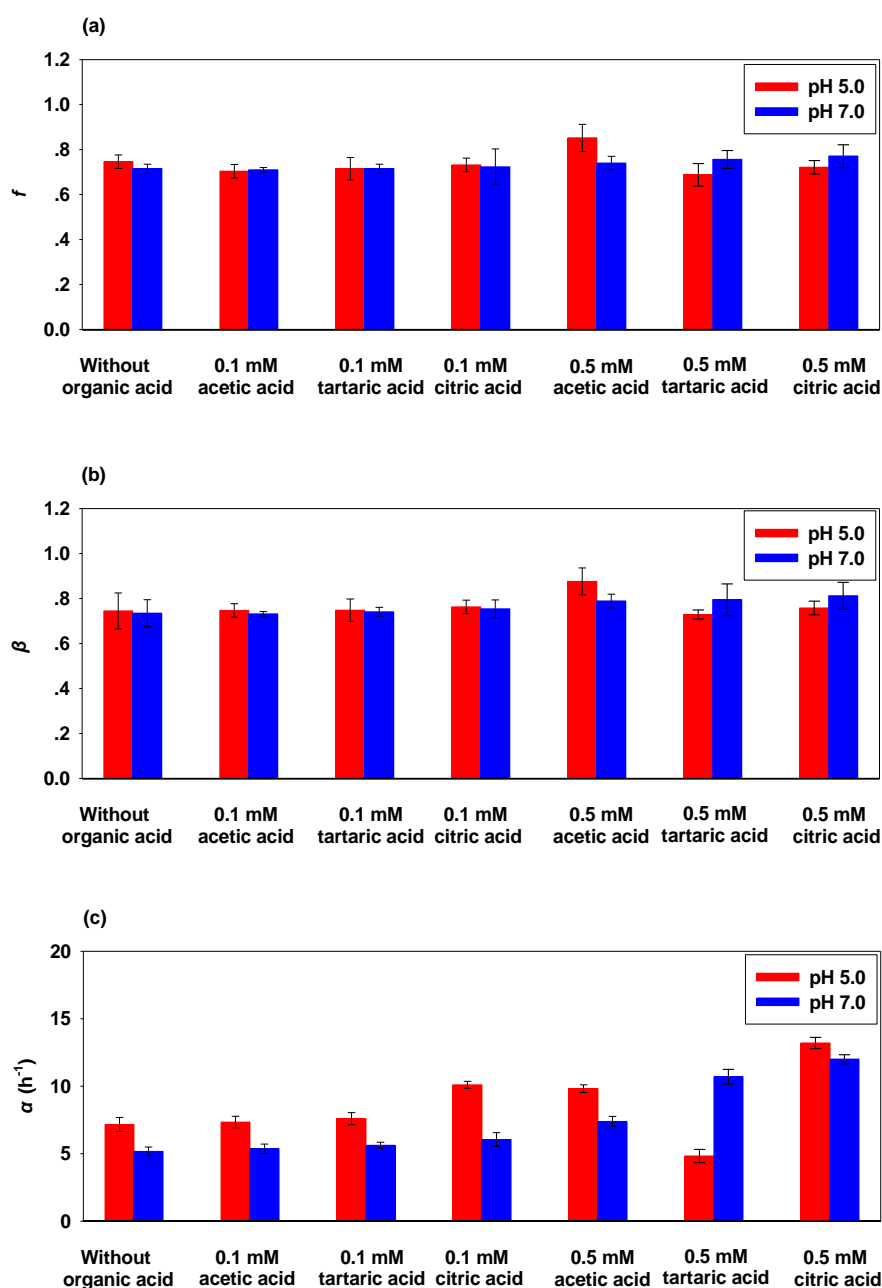


Fig. S5. Fitted parameters of two-site nonequilibrium transport model from breakthrough results of column experiments under different solution chemical conditions: (a) the fraction of Type 1 sites; (b) the fraction of instantaneous retardation to the total retardation; and (c) the first-order rate for kinetics at Type 2 sites.

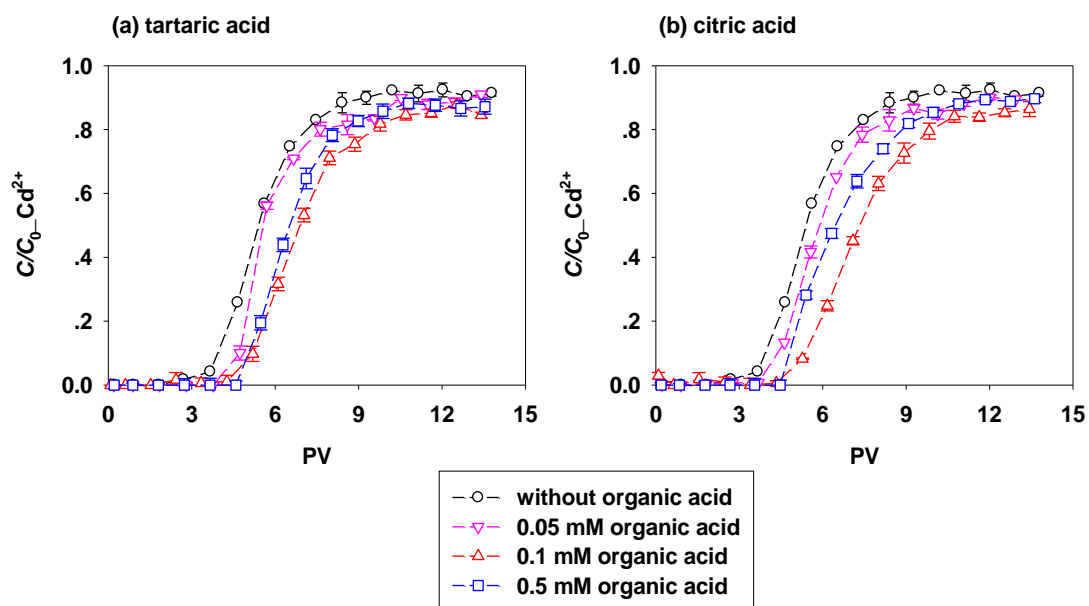


Fig. S6. Effects of low-molecular weight organic acids on the transport of Cd^{2+} (3 mg/L) at pH 5.0: (a) tartaric acid (columns 3, 6, and 9); and (b) citric acid (columns 4, 7, and 10).

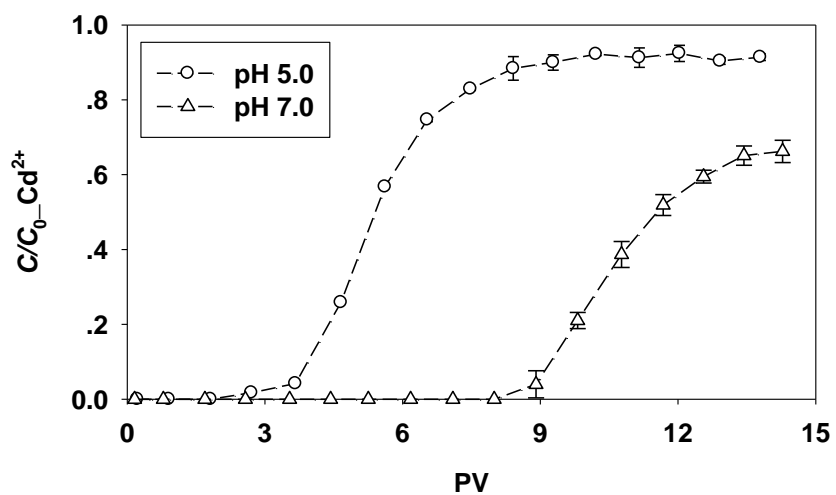


Fig. S7. Transport of Cd²⁺ (3 mg/L) in saturated porous media at different pH (columns 1 and 13).

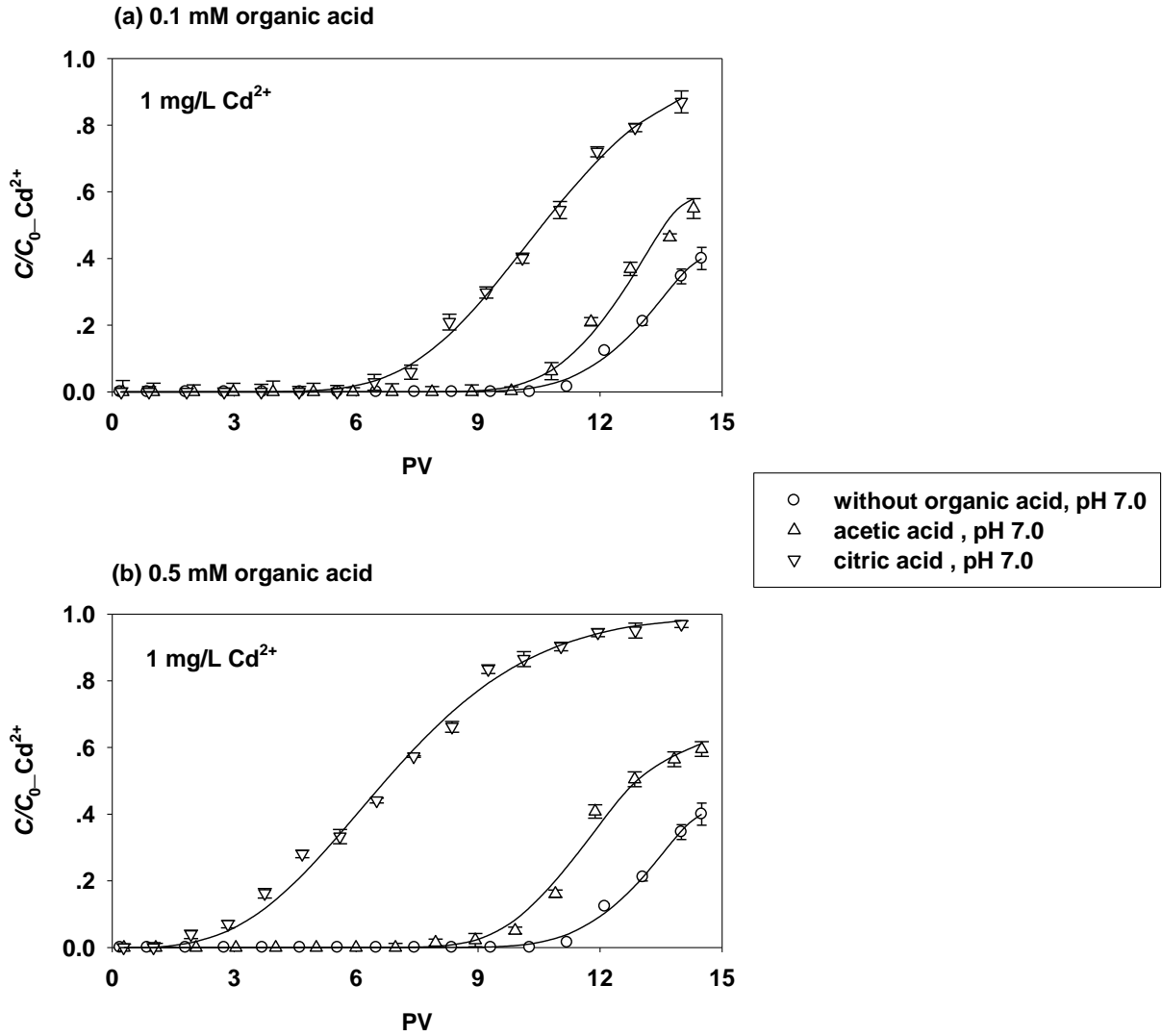


Fig. S8. Effects of low-molecular-weight organic acids on the transport of Cd²⁺ (1 mg/L) under neutral conditions: (a) 0.1 mM organic acid; and (b) 0.5 mM organic acids. Symbols are experimental data and lines are plotted by curve-fitting experimental data with the two-site nonequilibrium transport model.

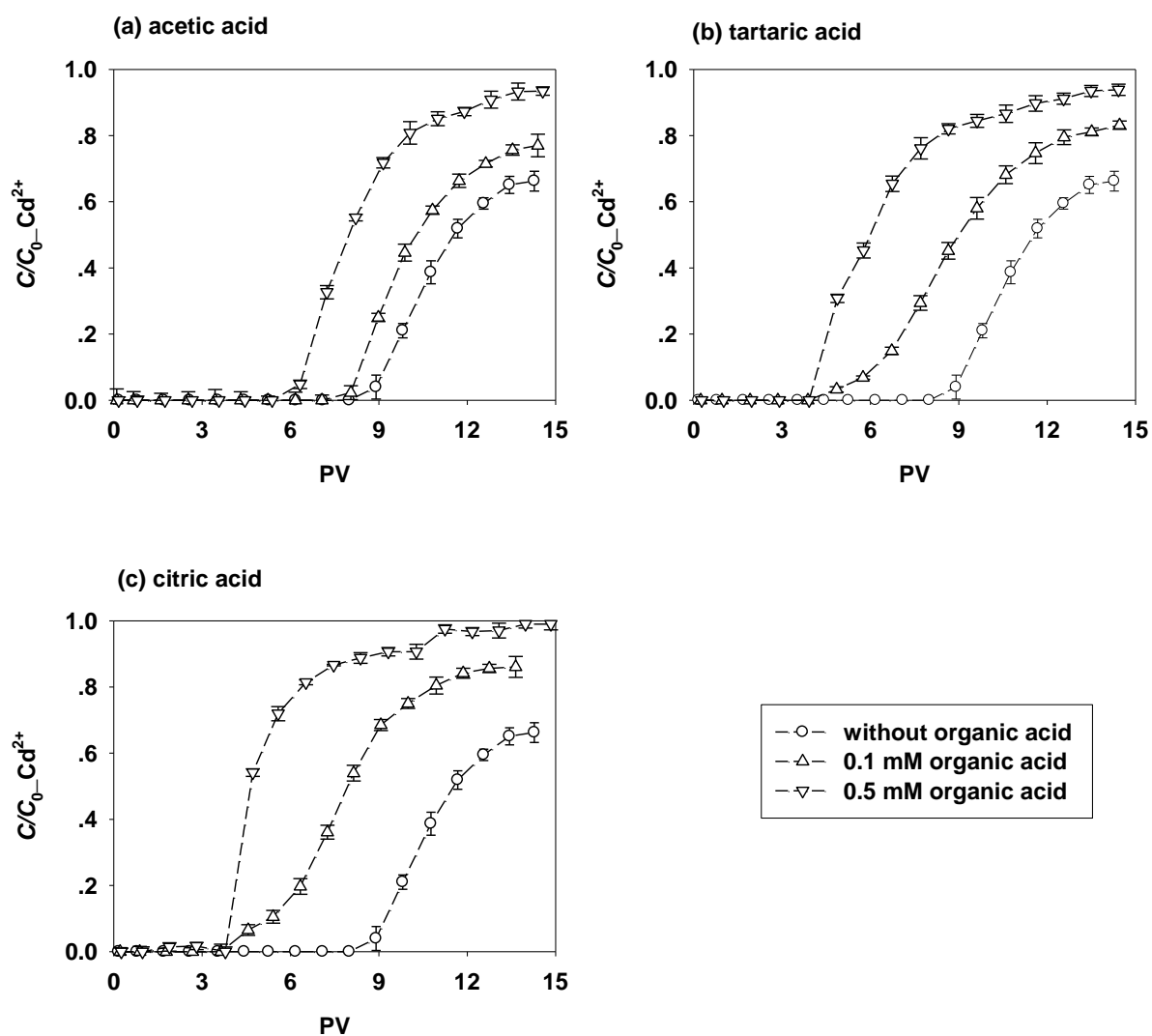


Fig. S9. Effects of low-molecular weight organic acids on the transport of Cd^{2+} (3 mg/L) at pH 7.0: (a) acetic acid (columns 13, 14, and 17); (b) tartaric acid (columns 13, 15, and 18); and (c) citric acid (columns 13, 16, and 19).

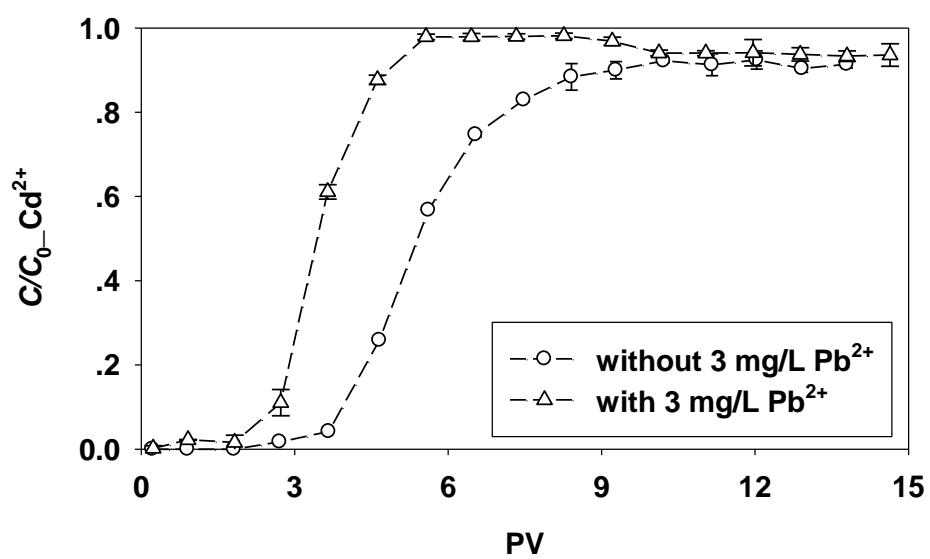


Fig. S10. Transport of Cd²⁺ with or without 3 mg/L Pb²⁺ at pH 5.0 (columns 1 and 20).

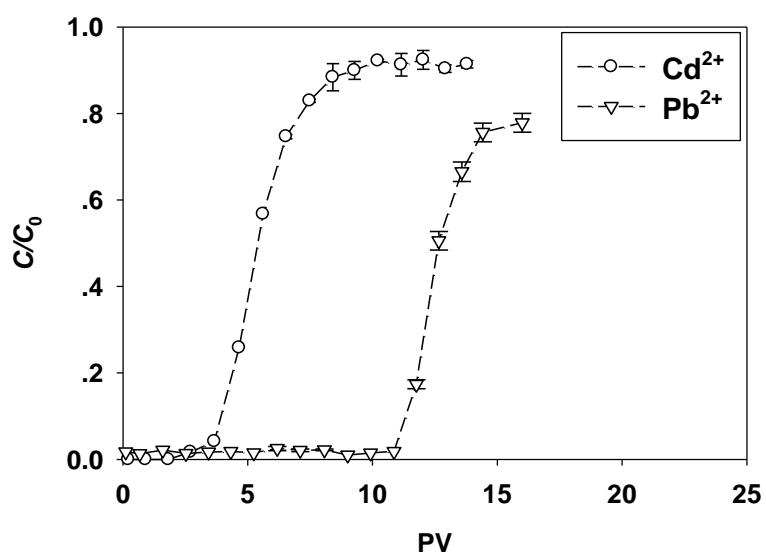


Fig. S11. Transport of Cd^{2+} and Pb^{2+} in sand columns in the absence of low-molecular weight organic acids at pH 5.0.

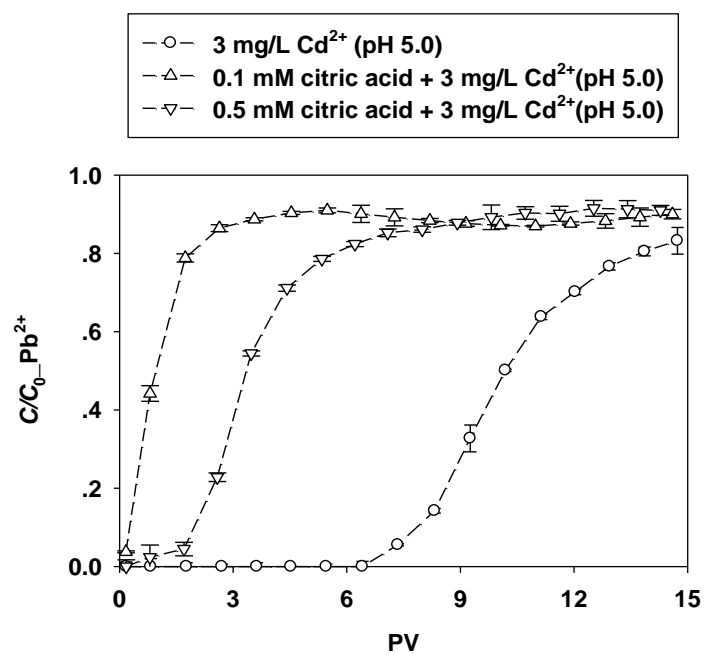


Fig. S12. Effects of citric acid on the transport of Pb^{2+} in the presence of 3 mg/L Cd^{2+} at pH 5.0 (columns 20–22).

References:

- Abdelwaheb, M., Jebali, K., Dhaouadi, H., Dridi-Dhaouadi, S., 2019. Adsorption of nitrate, phosphate, nickel and lead on soils: risk of groundwater contamination. *Ecotox. Environ. Safe.* 179, 182–187.
- Benjamin, M.M., Sletten, R.S., Bailey, R.P., Bennett, T., 1996. Sorption and filtration of metals using iron oxide coated sand. *Water Res.* 30, 2609–2620.
- Childress, A.E., Elimelech, M., 1996. Effect of solution chemistry on the surface charge of polymeric reverse osmosis and nanofiltration membranes. *J. Membr. Sci.* 119, 253–268.
- Derikvand, Z., Olmstead, M.M., Mercado, B.Q., Shokrollahi, A., Shahryari, M., 2013. Solution and solid state studies of three new supramolecular compounds of zinc(II), nickel(II) and uranium(VI) with chelidamic acid and 9-aminoacridine. *Inorg. Chim. Acta* 406, 256–265.
- De Stefano, C., Lando, G., Pettignano, A., Sammartano, S., Sequestering ability of aminopolycarboxylic (APCs) and aminopolyphosphonic (APPs) ligands towards palladium (II) in aqueous solution. *J. Chem. Eng. Data* 59, 1970–1983.
- Kavitha, B., Thambavani, D.S., 2014. Characterization of riverbed sand from mullai periyar, tamilnadu by FT-IT, XRD and SEM/EDAX. *Asian J. Chem.* 27, 54–56.
- Kim, H.N., Bradford, S.A., Walker, S.L., 2009. Escherichia coli O157:H7 transport in saturated porous media: Role of solution chemistry and surface macromolecules. *Environ. Sci. Technol.* 43 (12), 4340–4347.
- Ollat, C., Combeau, A., 1960. Méthode de détermination de la capacité d'échange et du pH d'un sol; relations entre le complexe absorbant et le pH. *Sols Afr.* 5, 343–372.

Wang, Y.G., Li, Y.S., Kim, H.N., Walker, S.L., Abriola, L.M., Pennell, K.D., 2010. Transport and retention of fullerene nanoparticles in natural soils. *J. Environ. Qual.* 39 (6), 1925–1933.

Study 2: Factors affecting the transport of petroleum colloids in saturated porous media

Ying Wang, Taotao Lu, Haojing Zhang, Yanxiang Li, Yumeng Song, Jiuyan Chen, Xiaowen Fua, Zhichong Qi, Qiang zhang

Published in *Colloids and Surfaces A: Physicochemical and Engineering Aspects* (Vol. 585, 2020)



Factors affecting the transport of petroleum colloids in saturated porous media



Ying Wang^{a,b,1}, Taotao Lu^{c,1}, Haojing Zhang^b, Yanxiang Li^d, Yumeng Song^b, Jiuyan Chen^b, Xiaowen Fu^a, Zhichong Qi^{a,b,*}, Qiang zhang^{a,*}

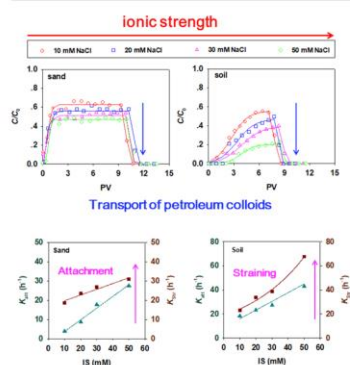
^a Ecology Institute of the Shandong Academy of Sciences, Qilu University of Technology (Shandong Academy of Sciences), Jinan 250353, China

^b Henan Joint International Research Laboratory of Environmental Pollution Control Materials, College of Chemistry and Chemical Engineering, Henan University, Kaifeng 475004, China

^c Department of Hydrology, University of Bayreuth, Bayreuth 95440, Germany

^d The Testing Center of Shandong Bureau of China Metallurgical Geology Bureau, Jinan 250014, China

GRAPHICAL ABSTRACT



ARTICLE INFO

Keywords:

Petroleum colloids
Transport
Porous media
Model
Solution chemistry

ABSTRACT

Batch and column experiments were performed to evaluate the responses of attachment and transport of petroleum colloids to the changes in solution chemistry conditions. We found that transport of petroleum colloids was inhibited with increasing the ionic strength or decreasing the pH. This observation can be explained by the increase in particle size of petroleum colloids and the reduction in electrostatic repulsion between colloids and grain surfaces. Meanwhile, the extent of transport inhibition by ionic strength depended on the type of porous media, that is, greater mobility of petroleum colloids could be found in sand rather than in soil at the same ionic strength. This can probably be ascribed to surface chemistry of soil minerals. In the case of divalent ion (e.g., Ca^{2+}), the retention of petroleum colloids was more obvious in soil than in sand resulting from the complexing between the oxygen functional groups from both petroleum colloids and grains, i.e., petroleum colloids could bind to the sand/soil grains through Ca^{2+} bridging. Additionally, the presence of sodium dodecyl sulfate (SDS, selected as a model surfactant) significantly enhanced the mobility of petroleum colloids as a result of enhanced

* Corresponding authors at: Ecology Institute of the Shandong Academy of Sciences, Qilu University of Technology (Shandong Academy of Sciences), Jinan 250353, China.

E-mail addresses: qizhichong1984@163.com (Z. Qi), zhbuaiji@sina.com (Q. zhang).

¹ These authors contributed equally.

<https://doi.org/10.1016/j.colsurfa.2019.124134>

Received 31 May 2019; Received in revised form 14 September 2019; Accepted 16 October 2019

Available online 20 October 2019

0927-7757/ © 2019 Elsevier B.V. All rights reserved.

steric hindrance that remarkably inhibited aggregation of petroleum colloids. Also, a two-site transport model was used to fit the transport data to gain further insights on deposition mechanisms. These findings from this research are helpful to understand the transport and fate of petroleum colloids in subsurface systems.

1. Introduction

Subsurface contamination due to uncontrolled spillage of petroleum is a widespread environmental problem all over the world. Particularly, it can cause irreversible economic and ecological impacts in aquatic systems. Petroleum contains persistent organic pollutants that induced adverse effects in human and environmental health [1,2]. Also, petroleum may change the characteristics of the aquifer media (e.g., wettability, water permeability, dispersivity) [3,4].

With the increase in wide application of petroleum, colloidal petroleum particles are inevitably released into the subsurface aquifer in various ways, including manufacturing storing, drilling, and transporting [5–7]. It has been reported that petroleum could be released from the well into the subsurface plume in the form of oil droplets [5,8]. Compared with insoluble crude oil in water, its colloidal droplets from nanometers to several micrometers in diameter could disperse well in water [6,9,10]. The environmental fate and impacts of petroleum colloids will strongly depend on its mobility within the aquifer materials. Therefore, it is necessary to have a thorough understanding of the transport of petroleum colloids in the subsurface environments.

To our knowledge, some work focused on the crude oil or petroleum hydrocarbons mobility in porous media [11–14]. Nevertheless, only few studies investigated the transport and fate of petroleum colloids in the porous media. For example, Lin et al. studied the dynamics of asphaltene deposition in porous media using microfluidic devices [15]. The results showed that the deposition dynamics varied significantly with different concentrations of heptane. Sun et al. investigated the migration of petroleum in nanopores (used the silica as a micro model) and found that oil molecules in the central part of oil phase migrated firstly under external force [16]. Xue et al. explored the mechanism of oil droplets transportation in a nano-sized shale channel by molecular dynamic simulations. They found that the competition between the oil adsorption strength to the shale surface played an important role in the oil translocation process in the shale channel [17]. Moreover, Taborda et al. also reported that the addition of nanoparticles modified the flow behavior of the oil phase and increased its mobility in the porous medium [18]. It is noted that petroleum could be strongly adsorbed to soil particles [19,20]. However, transport of petroleum colloids may still occur in the sandy aquifer (e.g., sand or sandy soil).

In order to evaluate the potential environmental risks of petroleum colloids, knowledge of the transport mechanism is urgently required. Solution chemistry (such as ionic strength, pH, divalent cations, surfactant, and dissolved organic matter) is expected to play an important role in the transport properties of colloids [21]. For example, increasing ionic strength compresses electrical double layer thickness and reduces electrostatic repulsion between colloids and grain surfaces [21]. The presence of surfactants or natural organic matter can enhance the transport of colloids by increasing steric repulsion between colloids and collectors [22,23]. Furthermore, in earlier studies, several mathematical models (e.g., the clean-bed filtration theory (CFT), the computational fluid dynamics (CFD) simulation, the one-dimensional discrete random-walk particle-tracking model, and two-site transport model) were applied to interpret the retention of colloids in saturated porous media [24–27].

In this study, we investigated the transport of petroleum colloids in saturated porous media under different environmental conditions. Batch sorption and column experiments were conducted to examine the interaction between colloids and aquifer media. Various solution chemistry conditions, such as ionic strength, divalent cations, pH and surfactant, were taken into consideration to investigate the transport of

petroleum colloids. The specific goals were to link the observed transport properties to solution chemistry parameters. Meanwhile, the differences between sand (a homogeneous aquifer medium) and soil (a representative heterogeneous aquifer medium) were analyzed. Finally, a two-site transport model representing both attachment and straining was used to fit the breakthrough curves (BTCs) and retention profiles.

2. Materials and methods

2.1. Materials

The petroleum product provided by Shengli oil field, China, was used in the experiments. The density, viscosity, and surface tension of petroleum (at 20 °C) were 0.901 g/cm³, 78 m Pa·s, and 35.8 mN/m, respectively.

Sand and soil were chosen as the porous media for the transport experiments. Quartz sand with a particle size from 0.21 mm to 0.33 mm was employed as received from Sigma-Aldrich (St. Louis, MO). The average grain size was 0.26 mm. Prior to use, the sand was cleaned to remove impurities on the grain surface using the method of Mattison et al. [28]. Sandy soil, containing 52% sand, 32% silt, and 16% clay, was collected from the yellow river basin in Henan province, China. The soil sample had the following grain size distribution: ~1.8% of the particulate mass ranged from 0.25–0.5 mm, ~16.2% ranged from 0.25–0.5 mm, ~16.2% ranged from 0.21–0.25 mm, ~15.3% ranged from 0.18–0.21 mm, ~40% ranged from 0.11–0.18 mm, ~14% ranged from 0.075–0.11 mm, ~5.8% ranged from 0.063–0.075 mm, ~6.9% smaller than 0.075 mm. The average grain size of the soil was 0.15 mm. The organic carbon content was 0.29%. Organic matter content was measured with the wet digestion technique [3]. The zeta potential of porous media was measured by electrophoretic mobility, using a ZetaPALS (Brookhaven Instruments) [29,30].

Sodium dodecyl sulfate (SDS) was purchased from Sinopharm Chemical Reagent Co. Ltd., Shanghai, China.

2.2. Preparation of petroleum colloids

Prior to performing the experiment, the original crude oil was cleaned to remove impurities (see Supplementary Material for detailed procedures). Approximately 2 g petroleum was added into 1000 mL Deionized water (DI water). Then, the mixtures were rotated vigorously for 48 h, allowed to settle undisturbed for up to 7 days. After that, the unsettled petroleum colloid suspension in DI water was collected as stock solution, which was then diluted for sorption and column experiments. The concentration of stock petroleum suspensions was about 30 mg/L, which was determined by a solvent (i.e. tetrachloromethane) exchange method [31]. Technology using infrared spectrophotometry method was applied to determine the concentration of petroleum colloids in tetrachloromethane [31–33]. The detailed procedures are described in the Supplementary Material. The average particle size of petroleum colloids in stock petroleum suspensions was about $0.71 \pm 0.05 \mu\text{m}$ (see the particle size distribution of petroleum colloids in Fig. S1). The obtained stock suspension was kept in dark at 4 °C and was stable during the period of the study.

2.3. Column transport experiments

The experiments setup is found in Supplemental Data, Fig. S2. Glass column with length of 10.3 cm and inner diameter of 1.1 cm was employed. Porous media, Quartz sand or soil, was dry-packed into

columns. The column properties are summarized in Table S1. A syringe pump (KD Scientific, Holliston, MA) was used to inject suspension in the upward direction and keep a stable pore velocity (0.18 cm/min). The packed columns were flushed with 50 ml deionized (DI) water to reach equilibrate, and then followed by 70 ml background electrolyte solution (see Table 1).

For all experiments, the influents were prepared by diluting the stock petroleum colloid suspension with a certain electrolyte, and then stirring for 2 h [34]. The inflow concentration of petroleum colloids was ~10 mg/L. The pH for the experimental solutions was adjusted with 0.1 M HCl or NaOH. Hydrodynamic diameter of petroleum colloids was measured at a concentration of 10 mg/L by dynamic light scattering (DLS), the ζ -potential values of the petroleum colloid suspensions were obtained through the Zeta Potential Analyzer mentioned above.

In a typical column experiment, the influents were pumped into the column for approximately 9 pore volumes (PV), and then the columns were flushed by a petroleum colloid-free background electrolyte solution. Solution samples collected from outlet of column were preserved in 4 mL glass vials every 0.8 PV during sample injection and column flushing processes to analyze the concentration of petroleum colloids. The retention profiles of petroleum colloids were achieved by separating the sand columns into 10 layers after the transport experiments (the detailed procedures provided in Supplementary Material). In general, the mass balance of the transport experiments fell in the range from 90.6% to 99.3% (Supplementary Material, Table S2).

2.4. Batch experiments

The attachment isotherms of petroleum colloids onto sand or soil were conducted in 20 mL amber glass vials under different solution chemistry conditions. The process was shown in Fig. S3. First, 5 g of sand or 1 g of soil was added to each of a series of vials. Then, 20 mL solutions with different concentrations (0–30 mg/L) of petroleum colloids were added to each vial. The mixed solutions were shaken for 3 d at 25 °C. The vials were then centrifuged (3000 rpm, 30 min) to remove porous media from petroleum colloid suspension. The concentrations of petroleum colloids in the suspension were measured by infrared spectrophotometry method [31]. The concentrations of petroleum colloids

attached to sand or soil were calculated based on a mass balance approach. The attachment experiments were done in duplicate. The experimental isotherm data of petroleum colloids was correlated by the Linear model, which can be written as follows [35,36]:

$$q = K_d C_e \quad (1)$$

where q (mg/g) is the equilibrium attached concentration of petroleum colloids; C_e (mg/L) is the equilibrium aqueous concentration of petroleum colloids; K_d (L/g) is the distribution coefficients of the Linear model. The corresponding Linear isotherm parameters are listed in Table S3. It is noteworthy that the attachment data obtained by batch experiments were only used as the additional evidence to explain the response of transport behaviors of petroleum colloids to the changes in solution chemistry. Since the transport of colloids in porous media may be affected not only by thermodynamic factors but also by hydrodynamics. On one hand, some procedures used in batch experiment would expose additional attachment sites to petroleum colloids, however, these sites are not available in the column experiment (i.e., colloids could contact sufficiently with grains during the shaking procedures); on the other hand, the deposition of petroleum colloids could also be influenced by aquifer properties (e.g., the blocking effect; the distribution of chemical composition at the pore-scale; and the surface roughness of sand particles) during transport process [37–39].

2.5. Model simulation

To elucidate the mechanism controlling the transport of petroleum colloids, a two-site transport model that accounts for both attachment and straining was used to analyze the experimental breakthrough curves and retention profiles [40]. The two-site model divides the deposition sites into an attachment site and a straining site:

$$\frac{\partial C}{\partial t} + \frac{\rho}{\theta} \frac{\partial S_1}{\partial t} + \frac{\rho}{\theta} \frac{\partial S_2}{\partial t} = D \frac{\partial^2 C}{\partial x^2} - v \frac{\partial C}{\partial x} \quad (2)$$

$$\frac{\rho}{\theta} \frac{\partial S_1}{\partial t} = K_{att} \psi_1 C, \quad \psi_1 = \frac{S_{max} - S_1}{S_{max}} \quad (3)$$

Table 1
Summary of experimental conditions and selected properties of influent solution and porous media.

Column No.	porous media	Background solution	pH	ζ potential of petroleum colloids ^a (mV)	ζ potential of porous media ^b (mV)	Z_{ave} . petroleum colloids ^c (μ m)	d_p/d_c ^d
1	sand	10 mM NaCl	5.0	-23.3 ± 1.2	-19.5 ± 1.5	0.76 ± 0.05	0.003
2	sand	20 mM NaCl	5.0	-18.7 ± 0.3	-15.3 ± 1.7	0.85 ± 0.12	0.003
3	sand	30 mM NaCl	5.0	-13.2 ± 0.9	-11.7 ± 0.9	1.23 ± 0.09	0.003
4	sand	50 mM NaCl	5.0	-7.5 ± 1.9	-8.6 ± 0.7	1.56 ± 0.18	0.003
5	soil	10 mM NaCl	5.0	-23.3 ± 1.2	-22.7 ± 0.3	0.76 ± 0.05	0.005
6	soil	20 mM NaCl	5.0	-18.7 ± 0.3	-19.6 ± 1.2	0.85 ± 0.12	0.005
7	soil	30 mM NaCl	5.0	-13.2 ± 0.9	-15.2 ± 1.1	1.23 ± 0.09	0.005
8	soil	50 mM NaCl	5.0	-7.5 ± 1.9	-11.3 ± 0.8	1.56 ± 0.18	0.005
9	sand	0.1 mM CaCl ₂	5.0	-25.6 ± 0.8	-16.2 ± 0.8	0.81 ± 0.03	0.003
10	sand	0.5 mM CaCl ₂	5.0	-20.1 ± 1.5	-12.9 ± 1.3	0.99 ± 0.11	0.003
11	sand	1.0 mM CaCl ₂	5.0	-15.6 ± 0.7	-8.9 ± 2.1	1.18 ± 0.06	0.003
12	soil	0.1 mM CaCl ₂	5.0	-25.6 ± 0.8	-18.3 ± 1.5	0.81 ± 0.03	0.005
13	soil	0.5 mM CaCl ₂	5.0	-20.1 ± 1.5	-15.6 ± 0.5	0.99 ± 0.11	0.005
14	soil	1.0 mM CaCl ₂	5.0	-15.6 ± 0.7	-12.5 ± 0.7	1.18 ± 0.06	0.005
15	sand	30 mM NaCl	7.0	-16.5 ± 1.7	-14.2 ± 1.7	1.05 ± 0.02	0.003
16	sand	30 mM NaCl	9.0	-19.8 ± 0.6	-17.9 ± 1.3	0.92 ± 0.09	0.003
17	soil	30 mM NaCl	7.0	-16.5 ± 1.7	-18.7 ± 0.6	1.05 ± 0.02	0.005
18	soil	30 mM NaCl	9.0	-19.8 ± 0.6	-20.5 ± 1.0	0.92 ± 0.09	0.005
19	sand	30 mM NaCl + 10 mg/L SDS	5.0	-14.9 ± 1.1	-12.9 ± 0.5	0.82 ± 0.12	0.003
20	soil	30 mM NaCl + 10 mg/L SDS	5.0	-14.9 ± 1.1	-16.7 ± 1.7	0.82 ± 0.12	0.005

^a Zeta potential of petroleum colloids; values after ± sign represent standard deviation of five replicates.

^b Zeta potential of quartz sand; values after ± sign represent standard deviation of five replicates.

^c Hydrodynamic diameter of petroleum colloids based on DLS analysis; values after ± sign represent standard deviation of three replicates.

^d d_p/d_c represent ratio of Z_{ave} of petroleum colloids to average diameter of porous media.

$$\frac{\rho}{\theta} \frac{\partial S_2}{\partial t} = K_{str} \psi_2 C, \quad \psi_2 = \left(\frac{d_c + z}{d_c} \right)^{-\beta} \quad (4)$$

where ρ (g/cm^3) is the dry bulk density of the packed column; θ (-) is porosity of the packed column; D (m^2/d) is hydrodynamic dispersion coefficient; v (m/d) is the pore-water velocity; C (mg/L) is concentration of petroleum colloids in the aqueous phase; S_1 (mg/kg) and S_2 (mg/kg) are concentrations of petroleum colloids in the attachment site and the straining site, respectively; K_{att} (h^{-1}) and K_{str} (h^{-1}) are the attachment rate and straining rate, respectively; ψ_1 (-) and ψ_2 (-) represents the blocking factor and straining factor, respectively; S_{max} (mg/kg) is the maximum retention capacity of petroleum colloids on the attachment site; d_c (cm) is average diameter of the sand/soil grains; z (cm) is the down gradient distance from the porous medium inlet; and β (-) is a fitting parameter controlling the shape of nanoparticle spatial distribution. A value of 0.432 was assigned for β [40]. The BTCs and retention profiles of petroleum colloids were fitted with Eqs. (2)–(4) using the HYDRUS-1D software [41]. K_{att} , S_{max} , and K_{str} were used as the fitting parameters.

With the help of CXTFIT 2.1 code, the value of dispersion coefficient (D) was determined by fitting the breakthrough curves of the conservative tracer (KBr) (Fig. S4) [42]. Bromide concentrations were determined using an ICS-2100 ion chromatograph (Dionex Corporation, Sunnyvale, CA, USA). K_{att} (i.e., the attachment rate), S_{max} (as the maximum retention capacity of petroleum colloids in the attachment

site), and K_{str} (i.e., the straining rate) were used as the fitting parameters. The detailed equations can be found in Supplementary Material. Furthermore, to investigate the effect of various fitting parameters on model results, we conducted a sensitivity analysis. Critical parameters such as K_{att} , S_{max} , and K_{str} were selected to analyze the model behavior. The sensitivity trials illustrated that the change of three fitting parameters significantly affects modeling results (Fig. S5). Hence, the description of the colloid transport was improved significantly when all parameters were optimized. The fitting parameters are listed in Table S4. Under different test conditions, the transport of petroleum colloids can be well fitted ($r^2 > 0.96$). Also, the results suggest that this modeling approach effectively describes the observed spatial distribution of colloid for all conditions. Similarly, Bradford et al. reported that a conceptual model (which takes into account both attachment and straining) could accurately fit the breakthrough curves and retention profiles of colloids [40].

3. Results and discussion

3.1. Effect of ionic strength

Fig. 1 clearly shows that ionic strength (IS) could affect the transport and retention properties of petroleum colloids. The results showed that transport of petroleum colloids was inhibited with the increase of IS. Under conditions of low ionic strength (10 mM NaCl), the

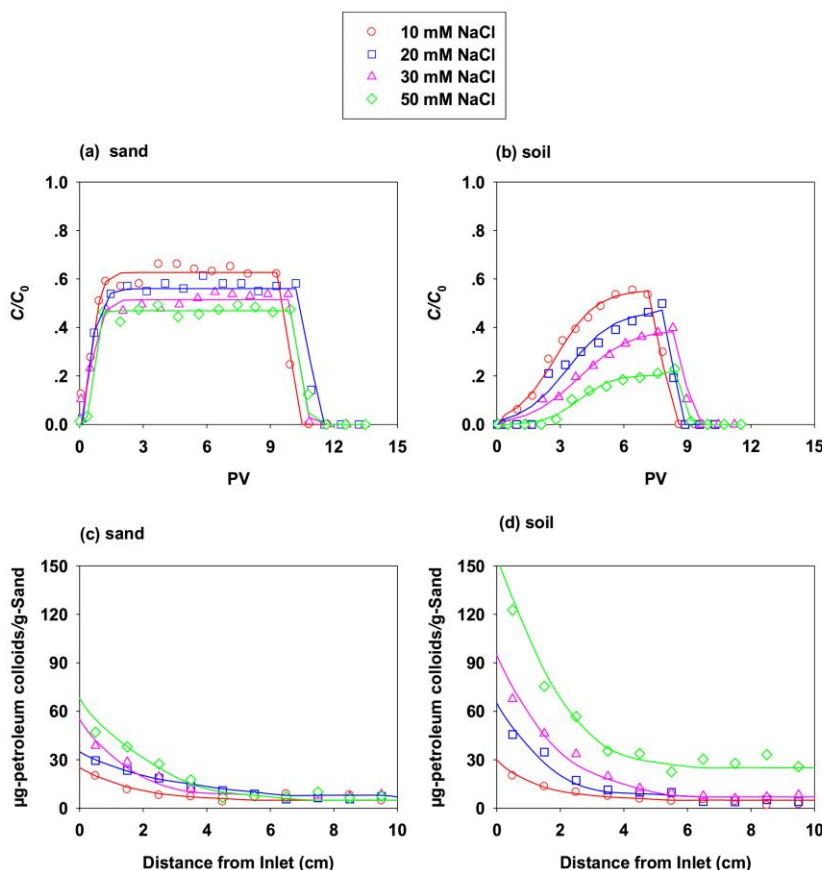


Fig. 1. Breakthrough curves (a and b) and retention profiles (c and d) of petroleum colloids (10 mg/L at pH 5.0) under different NaCl concentrations from sand columns (a and c, columns 1–4) and soil columns (b and d, columns 5–8). Solid lines (—) were plotted by fitting the BTCs and retention profiles with the two-site transport model.

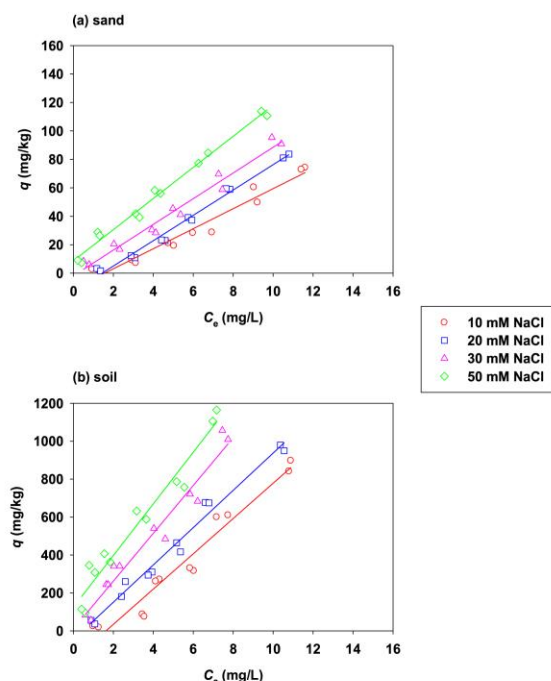


Fig. 2. Effects of ionic strength on attachment of petroleum colloids onto sand (a) and soil (b) at pH 5.0. The solid lines on the two panels are the Linear model fitting results.

breakthrough (as indicated by the C/C_0 value) reached 63% and 53% in sand and soil, respectively. When the IS was 50 mM NaCl, the values of C/C_0 were only 47% and 20% in sand and soil, respectively. The

observation indicated that the retention of petroleum colloids in the column increased with the increasing of IS. The phenomenon is interpreted with the mechanisms controlling the transport of negatively charged colloids. Under the test conditions, both petroleum colloids and porous media are negatively charged (Table 1). There are two main reasons to lead to the negative charge of these colloids. One is the presence of minority molecules adsorbed onto the surface, such as OH^- species from aqueous phase; the other one is, possibly, charged impurities from the oil (e.g., free fatty acids) [43–45]. Increasing Na^+ concentration compresses the thickness of the electrical double layer, then the double layer repulsion between colloids and grain surfaces would be reduced [21], which could be proved by the changes of ζ -potential (when IS increased from 10 to 50 mM NaCl, the ζ -potential value of petroleum colloids increased from -23.3 mV to -7.5 mV, Table 1). In addition, significant aggregation of petroleum colloids was observed with increasing Na^+ concentration [9,46,47]. For example, the particle sizes of petroleum colloids increased from $0.76 \mu\text{m}$ to $1.56 \mu\text{m}$ at 10 mM NaCl and 50 mM NaCl, respectively (Table 1). Tufenkji et al. indicated that straining plays an important role in colloid deposition especially when the ratio of diameters of particle to collector (d_p/d_c , where d_p and d_c are the median grain diameters of particle and the collector, respectively) is more than 0.002–0.003 [40,48,49]. As shown in Table 1, straining was likely an important deposition mechanism for petroleum colloids under the test conditions. Meanwhile, the obviously decreased particle sizes in effluents, in comparison to the respective sizes in influents, may also be indicative of straining (Fig. S6a). Meanwhile, deposition of colloids in zones of relative flow stagnation can be more significant at higher ionic strength [50]. Furthermore, the secondary energy minimum between colloids and porous media also increase with increasing IS [48]. Comparison of the retention profiles of colloids in the sand and soil revealed that more colloids were retained at the column inlet in the soil than in the sand. This is indicative of enhanced straining in the soil column [51]. Finally, as expected, the trends are in accordance with the batch experiment results (Fig. 2), i.e., the attachment affinities of petroleum colloids to sand/soil were increased with the increase of IS.

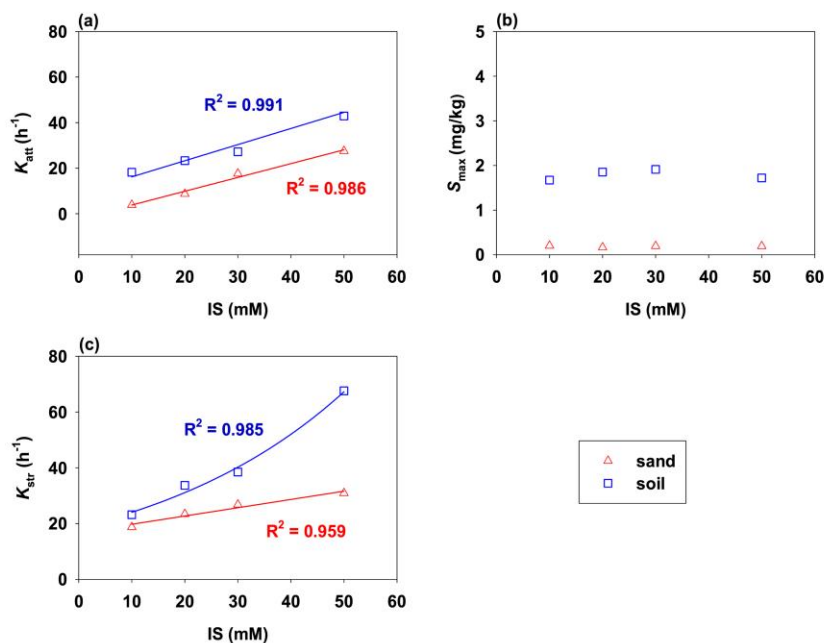


Fig. 3. Correlations between fitted parameters of two-site transport model (based on breakthrough data of columns 1–8) and ionic strength.

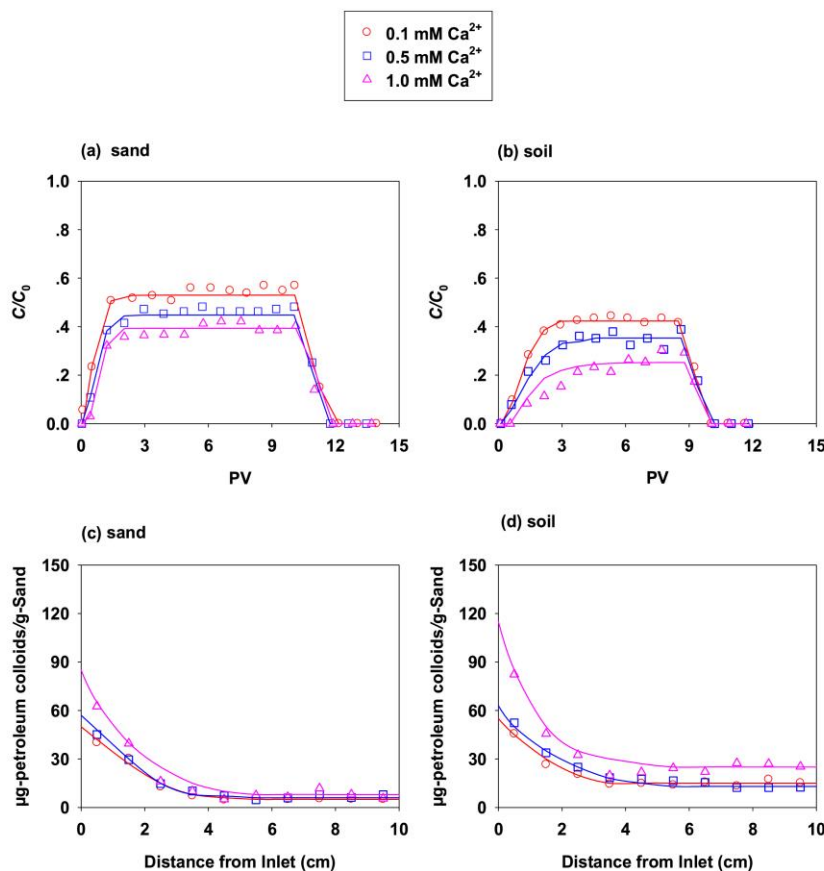


Fig. 4. Breakthrough curves (a and b) and retention profiles (c and d) of petroleum colloids (10 mg/L at pH 5.0) under different CaCl_2 concentrations from sand columns (a and c, columns 9–11) and soil columns (b and d, columns 12–14). Solid lines (—) were plotted by fitting the BTCs and retention profiles with the two-site transport model.

In addition, at the same ionic strength, petroleum colloids exhibited greater mobility in sand than in soil. For example, the breakthrough reached 53% and 37% in sand and soil at 30 mM NaCl, respectively. Compared with quartz sand, soil contained considerable amounts of impurities as sand, silt, metal oxides, and clay; and the impurities could serve as the favorable sites for the deposition of petroleum colloids [52]. That is, petroleum colloids would interact with soil particles by the way of directing aggregation or adsorption on the particle phase [53]. Also, soil usually has many unique characteristics, like a wider particle size distribution, more irregular grain shapes, and rougher surfaces, which could result in complex flow pathways and narrower pore throat in the soil columns. Consequently, the likelihood of petroleum colloid deposition by straining in soil is much greater than that in sand. Furthermore, this is evident by the sand/soil–water distribution coefficients (K_d) (the values are summarized in Table S3). For a given Na^+ concentration, the K_d for petroleum colloids attachment on soil was higher than that on sand.

Moreover, the BTCs of petroleum colloids were fitted by a two-site transport model. Fitted values of K_{att} , S_{max} , and K_{str} are plotted against ionic strength (see Fig. 3). The increases of K_{att} and K_{str} with IS are consistent with the mechanisms controlling the effects of IS on the transport of colloids. The increase in the K_{att} value was likely due to the reduction in the electrostatic repulsion between colloids and grain surfaces, and the increase in the K_{str} value might be attributable to the increase in particle size with increasing IS (Table 1). Furthermore, note

that the increase of ionic strength affects K_{att} and K_{str} more significantly for soil than for sand. The probable reason is the heterogeneous characteristics of soil. On one hand, the natural soil has more complex ingredients than quartz sand as mentioned above. On the other hand, the size of soil components varies within relatively wide range (e.g. clay and metal oxides). It has been found that soil components (such as clay, soil organic matter, and silt) played a significantly important role in retaining petroleum hydrocarbons [54]. Interestingly, Fig. 3c shows that linear increase in K_{att} values for sand induced by increasing ionic strength, however, K_{str} increases with ionic strength near exponentially for soil. This observation indicated that the straining effects played a more important role in relatively heterogeneous porous media (i.e., soils) [27].

3.2. Effects of divalent cations

The effects of Ca^{2+} (a model divalent cation) on the transport of petroleum colloids are shown in Fig. 4. Overall, transport of petroleum colloids in the porous media was inhibited with increasing the concentration of Ca^{2+} . For example, With the increase of Ca^{2+} concentration the maximum C/C_0 value of petroleum colloids decreased from 54% at 0.1 mM Ca^{2+} , to 45% and 39% at 0.5 and 1.0 mM Ca^{2+} in the sand columns, respectively (Fig. 4a); accordingly, the mass of petroleum colloids retained in column increased from 45.5% to 55.2% and to 62.0% (Fig. 4b and Table S2). The effect of Ca^{2+} exhibited the same

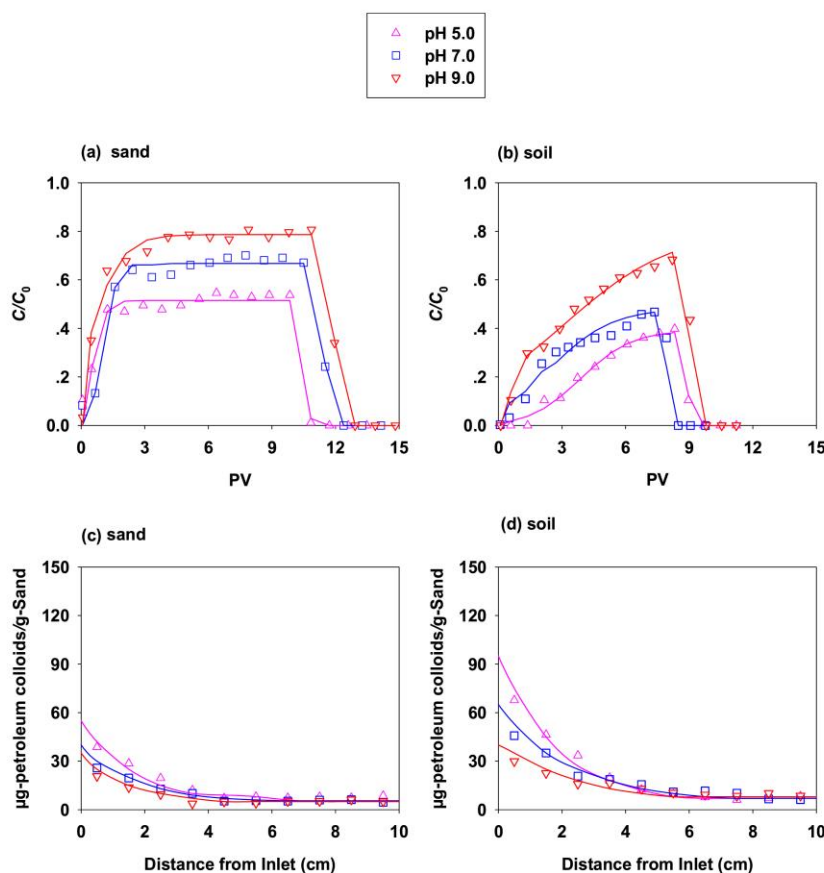


Fig. 5. Breakthrough curves (a and b) and retention profiles (c and d) of petroleum colloids (10 mg/L) under different pH from sand columns (a and c, columns 3, 15–16) and soil columns (b and d, columns 7, 17–18). Solid lines (—) were plotted by fitting the BTCs and retention profiles with the two-site transport model.

trend in the soil columns. Ca^{2+} likely to inhibit the transport of petroleum colloids via the following mechanisms. First, petroleum colloids and porous media became less negatively charged with increasing Ca^{2+} concentration (Table 1), resulting in decreasing the electrostatic repulsion between colloids and grains and enhancing attachment of colloids to the grain surfaces (see the attachment isotherms of petroleum colloids onto sand/soil at different Ca^{2+} concentrations, Figs. S7a and S7b). Second, Ca^{2+} could effectively enhance aggregation of petroleum colloids as indicated by the Z_{ave} values (Table 1), leading to more significant straining in with the increase of Ca^{2+} concentration. Also, when Ca^{2+} was the background cation considerable size fractionation occurred during transport process (Fig. S6b). Both corroborate the important contribution of straining. Fig. S8 clearly shows that K_{str} values increased substantially with increasing Ca^{2+} concentration. Third, cation bridging has been recognized as an important deposition mechanism for negatively charged colloids [55,56]. It is well known that abundance of organic matters (e.g., naphthenic acids, phenols) are naturally occurring compounds present in petroleum [57], these acids contains amount of oxygen functional groups such as carboxyl, hydroxyl, and phenol. In this case, petroleum colloids could bind to the sand/soil grains through Ca^{2+} bridging (i. e., Ca^{2+} could serve as a bridging agent between carboxylic and/or hydroxyl groups of petroleum and oxygen functional groups of porous media).

Note that petroleum colloids exhibited smaller mobility in sand columns than in soil columns at the same Ca^{2+} concentrations, and the

effect of Ca^{2+} exhibited more remarkable in the soil columns. For instance, all the C/C_0 values reached the maximum value within about 3 PV in sand columns at three different Ca^{2+} concentrations. However, for soil columns, the C/C_0 values reached the maximum value within about 3 PV, 4 PV, and 5 PV at 0.1 mM, 0.5 mM, and at 1.0 mM Ca^{2+} , respectively. The more significant transport-inhibition effects of Ca^{2+} in soil than in sand likely stemmed from the heterogeneous characteristics of soil as mentioned above. The soil can provide a lot of complexation sites for Ca^{2+} , such as clay minerals, metal oxides and soil organic matter (SOM) [27]. Thus, the bridging effect of Ca^{2+} can be more profound for soil than for sand.

3.3. Effects of pH

In general, over a pH range of 5.0–9.0, transport of petroleum colloids was enhanced with increasing pH under the experimental condition (i.e., the influent contained 30 mM NaCl) (Fig. 5). For example, the maximum C/C_0 of colloids only reached 53% in sand column at pH 5.0, but at pH 7.0 and 9.0, the maximum C/C_0 reached 68% and 78%, respectively. For soil column, the maximum C/C_0 values reached 38%, 45% and 66% at pH 5.0, 7.0 and 9.0, respectively. We propose that pH affected the transport of petroleum colloids mainly via the following mechanisms. On the one hand, particle sizes (Z_{ave}) were decreased with increasing pH (Table 1); consequently, reduction in particle size may weaken the straining effects. This is evidenced by the decrease of K_{str}

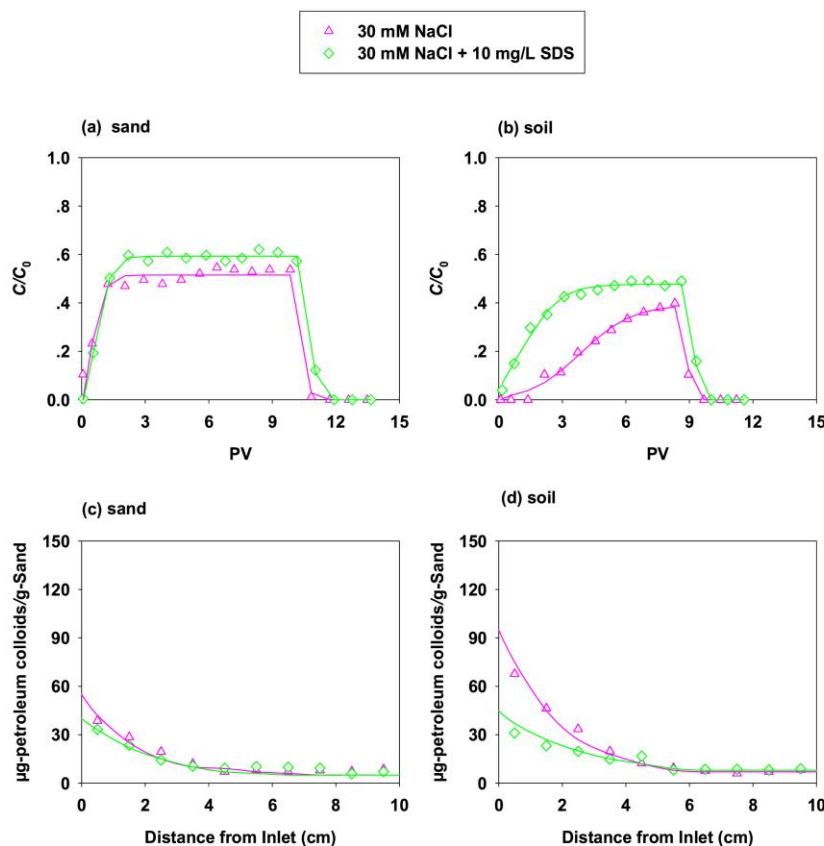


Fig. 6. Breakthrough curves (a and b) and retention profiles (c and d) of petroleum colloids (10 mg/L) with or without Sodium Dodecyl Sulfate (SDS) from sand columns (a and c, columns 3, 19) and soil columns (b and d, columns 7, 20). Solid lines (—) were plotted by fitting the BTCs and retention profiles with the two-site transport model.

values (Table S4 and Fig. S9b). On the other hand, pH affected the electrostatic interaction between collector and colloids. As mentioned above, petroleum is rich in oxygen functional groups. The overdose of H^+ or OH^- could alter the surface charge of the oil droplets [58,59]. Surface charges of petroleum colloids are more negatively charged due to the fact that some of the acidic groups can deprotonate at relatively high pH [60,61]. In addition, the zeta potential values prove that the surface charges of petroleum colloids and porous media are more negative with increasing pH (Fig. S10). Therefore, strong electrostatic repulsion effectively inhibited attachment of colloids to the grain surfaces (as evidenced by the attachment of petroleum colloids onto sand/soil in Figs. S7c and S7d). Furthermore, the effect of pH was relatively less remarkable on the transport of petroleum colloids in the soil columns compared with the transport of colloids in the sand columns. A possible explanation for this observation was that straining played a more important role in the retention of petroleum colloids in the soil columns. This is consistent with the fitted parameters. That is, the difference in the attachment rate (i.e., K_{att} values) between sand and soil became smaller with increasing pH; however, the fitted K_{str} values for soil are approximately two times greater than those of sand at the same pH (Fig. S9b).

3.4. Effects of surfactant

Surfactants are synthetically produced and can be used during various petroleum operations such as inhibition of emulsifiers,

asphaltene precipitation, drilling fluids, foaming agents, cleaners, etc [62]. Hence, the effects of surfactant on the transport of petroleum colloids were tested, using sodium dodecyl sulfate (SDS) as a model surfactant. The results showed that SDS could enhance the transport of petroleum colloids under the test condition (30 mM NaCl, pH 5.0) (Fig. 6). For instance, the maximum C/C_0 values increased from 53% and 38% (with SDS) to 60% and 48% (without SDS) in sand and soil columns, respectively. We propose that SDS probably enhance the transport of petroleum colloids via three major mechanisms. First, due to the amphiphilic nature of surfactants, the interaction between surfactants with both water (hydrophilic) and oil (lipophilic) works. It has been proposed that surfactant-facilitated dispersion or solubilization of oil leads to the formation of surfactant-coated oil droplets or partitioning of oil into the surfactant micelles [9,62–64]. The resulting dispersed oil droplets could significantly inhibit the aggregation of colloids (see Table 1), and enhance the transport of petroleum colloids. Second, a study conducted by Paria and Khilar (2004) reported that some processes, like hydrophobic bonding, ion exchange, ion pairing and adsorption by polarization of electrons or dispersion forces, could facilitate surfactants to be adsorbed onto solid matrices [65]. Consequently, SDS adsorbed on colloids and on the surfaces of soil/sand grains could enhance the steric hindrance between the colloids and porous media [66–69]. Third, when SDS is in the presence of solution (Table 1), petroleum colloids and porous media are more negatively charged. Thus, the electrostatic repulsion between colloids and soil/sand grains will increase.

Furthermore, the presence of SDS had a small effect on the transport of petroleum colloids in sand but a more significant effect on the transport in soil. This phenomenon is attributed to differences in the physicochemical properties of porous media. Compared with quartz sand, soil grains are more heterogeneous and much smaller; the pore distribution in the soil column consists not only of smaller pores, but these are also more tortuous [70]. Consequently, the decrease in particle size contributed to the enhancement of the colloids transport in soil columns was more significant.

4. Conclusions

The transport propensity of colloid in saturated porous media is the most fundamental basis for environmental scientists who are assessing the potential risks of petroleum colloid in aquifer systems. Findings of this study indicate that petroleum colloid is able to break through sand and soil materials. The solution chemistry conditions (i.e., ionic strength, divalent cations, pH, and surfactant) significantly affect the transport of petroleum colloids in saturated porous media. The observation indicated that more petroleum colloids were deposited in the column with increasing ionic strength and decreasing pH. This may be due to the aggregation of petroleum colloids and the reduction in electrostatic interactions between colloids and grain surfaces. Moreover, the effects of increasing ionic strength on the transport in soil were more significant than that in sand. This can probably be ascribed to higher heterogeneous of soil. Ca^{2+} could significantly inhibit the transport of petroleum colloids in porous media. This was attributed to the aggregation of colloids and cation bridging mechanism. Furthermore, SDS could considerably enhance the transport of petroleum colloids due to steric repulsion and reduction in particle sizes of petroleum colloids. Additionally, the trends of transport behaviors are in accordance with the batch experiment results. Finally, the transport properties of petroleum colloids can be fitted well by a two-site transport model. This study is expected to provide critical knowledge to evaluate the fate and transport of petroleum colloids in the subsurface environments. Moreover, it is unclear the relative contribution of different mechanisms to the retention of petroleum colloids due to the complex components of petroleum and the heterogeneous nature of soils. Further studies are needed to provide more direct microscopic evidence to find out the main mechanisms on colloid deposition under unfavorable attachment conditions.

Declaration of Competing Interest

The authors declare that they have no known competing financial interests or personal relationships that could have appeared to influence the work reported in this paper.

Acknowledgments

This project was supported by the National Natural Science Foundation of China (Grants 21707081), the Natural Science Foundation of Shandong Province (ZR2017BB083), the Project Management of Innovation and Entrepreneurship Training Program for Minsheng College Students (MSCXC2018023), Key R & D Plan of Shandong Province (2017GSF217004), the Forestry Science and Technology Innovation Project of Shandong province of China (LYCX03-2018-13) and Chinese Scholarship Council (201708420145).

Appendix A. Supplementary data

Supplementary material related to this article can be found, in the online version, at doi:<https://doi.org/10.1016/j.colsurfa.2019.124134>.

References

- [1] L. Liu, L. Wang, W. Song, L. Yang, L. Yin, S. Xia, H. Wang, P.J. Strong, Z. Song, Crude oil removal from aqueous solution using raw and carbonized *Xanthoceras sorbifolia* shells, *Environ. Sci. Pollut. Res.* 25 (2018) 29325–29334.
- [2] S. Park, K.S. Kim, D. Kang, H. Yoon, K. Sung, Effects of humic acid on heavy metal uptake by herbaceous plants in soils simultaneously contaminated by petroleum hydrocarbons, *Environ. Earth Sci.* 68 (2013) 2375–2384.
- [3] J. Zhang, X. Zheng, L. Chen, Y. Sun, Effect of residual oil saturation on hydrodynamic properties of porous media, *J. Hydrol.* 515 (2014) 281–291.
- [4] G. Wu, X. Zhu, H. Ji, D. Chen, Molecular modeling of interactions between heavy crude oil and the soil organic matter coated quartz surface, *Chemosphere* 119 (2015) 242–249.
- [5] E.W. North, E.E. Adams, A.E. Thessen, Z. Schlag, R. He, S.A. Socolofsky, S.M. Masutani, S.D. Peckham, The influence of droplet size and biodegradation on the transport of subsurface oil droplets during the Deepwater Horizon spill: a model sensitivity study, *Environ. Res. Lett.* 10 (2015) 024016.
- [6] P.J. Brandvik, O. Johansen, F. Leirvik, U. Farooq, P.S. Daling, Droplet breakup in subsurface oil releases—part 1: experimental study of droplet breakup and effectiveness of dispersant injection, *Mar. Pollut. Bull.* 73 (2013) 319–326.
- [7] M. Bettahar, J. Ducreux, G. Schafer, F.V. Dorpe, Surfactant enhanced in situ remediation of Inapl contaminated aquifers: large scale studies on a controlled experimental site, *Transp. Porous Med.* 37 (1999) 255–276.
- [8] T.B. Ryerson, R. Camilli, J.D. Kessler, E.B. Kujawinski, C.M. Reddy, D.L. Valentine, E. Atlas, D.R. Blake, J.D. Gouw, S. Meinardi, D.D. Parrish, J. Peischl, J.S. Seewald, C. Warneke, Chemical data quantify deepwater horizon hydrocarbon flow rate and environmental distribution, *Proc. Natl. Acad. Sci. U. S. A.* 109 (2012) 20246–20253.
- [9] Y. Gong, X. Zhao, Z. Cai, S.E. O'Reilly, X. Hao, D. Zhao, A review of oil, dispersed oil and sediment interactions in the aquatic environment: influence on the fate, transport and remediation of oil spills, *Mar. Pollut. Bull.* 79 (2014) 16–33.
- [10] S.M. Burkitbaev, K.V. Kotoyants, N.K. Nadirov, P.P. Poluektov, Water droplet coagulation during electrical dehydration of petroleum, *J. Eng. Thermophys.* (1987) 1137–1139.
- [11] M. Yang, Y.S. Yang, X. Du, Y. Cao, Y. Lei, Fate and transport of petroleum hydrocarbons in vadose zone: compound-specific natural attenuation, *Water Air Soil Pollut.* 224 (2013) 1439.
- [12] H. Liu, J. Wang, Y. Xie, D. Ma, X. Shi, Flow characteristics of heavy oil through porous media, *Energ. Source. Part A* 33 (2011) 347–359.
- [13] K.M. Bushnaf, S. Puricelli, S. Saponaro, D. Werner, Effect of biochar on the fate of volatile petroleum hydrocarbons in an aerobic sandy soil, *J. Contam. Hydrol.* 126 (2011) 208–215.
- [14] X. Zheng, H. Qiu, J. Jing, G. Liu, Numerical analysis of the transport and restoration schemes of aqueous oil in soils, *Environ. Geol.* 40 (2011) 750–754.
- [15] Y.J. Lin, P. He, M. Tavakkoli, N.T. Mathew, Y.Y. Fatt, J.C. Chai, A. Goharzadeh, F.M. Vargas, S.L. Biswal, Examining asphaltene solubility on deposition in model porous media, *Langmuir* 32 (2016) 8729–8734.
- [16] J. Sun, H. Zhang, M. Hu, X. Meng, S. Yuan, Molecular dynamics study on oil migration inside silica nanopore, *Chem. Phys. Lett.* 678 (2017) 186–191.
- [17] Q. Xue, Y. Tao, Z. Liu, S. Lu, X. Li, T. Wu, Y. Jin, X. Liu, Mechanism of oil molecules transportation in nano-sized shale channel: MD simulation, *RSC Adv.* 5 (2015) 25684–25692.
- [18] E.A. Taborada, C.A. Franco, S.H. Lopera, V. Alvarado, F.B. Cortés, Effect of nanoparticles/nanofluids on the rheology of heavy crude oil and its mobility on porous media at reservoir conditions, *Fuel* 184 (2016) 222–232.
- [19] H. Chen, S. Chen, X. Quan, Y. Zhao, Importance of environmental black carbon to dissolved petroleum hydrocarbons sorption on soil, *Soil Sediment Contam.* 18 (2009) 184–194.
- [20] H. Chen, S. Chen, X. Quan, Y. Zhao, H. Zhao, Solubility and sorption of petroleum hydrocarbons in water and cosolvent systems, *J. Environ. Sci.* 20 (2008) 1177–1182.
- [21] J.N. Ryan, M. Elimelech, Colloid mobilization and transport in groundwater, *Colloids Surf. A Physicochem. Eng. Asp.* 107 (1996) 1–56.
- [22] Y. Du, C. Shen, H. Zhang, Y. Huang, Effects of flow velocity and nonionic surfactant on colloid straining in saturated porous media under unfavorable conditions, *Transp. Porous Med.* 98 (2013) 193–208.
- [23] V.L. Morales, W. Zhang, B. Gao, L.W. Lion, J.J. Bisogni Jr., B.A. McDonough, T.S. Steenhuis, Impact of dissolved organic matter on colloid transport in the vadose zone: deterministic approximation of transport deposition coefficients from polymeric coating characteristics, *Water Res.* 45 (2011) 1691–1701.
- [24] X. Li, T.D. Scheibe, W.P. Johnson, Apparent decreases in colloid deposition rate coefficients with distance of transport under unfavorable deposition conditions: a general phenomenon, *Environ. Sci. Technol.* 38 (2004) 5616–5625.
- [25] K.E. Nelson, T.R. Ginn, Colloid filtration theory and the Happel sphere-in-cell model revisited with direct numerical simulation of colloids, *Langmuir* 21 (2005) 2173–2184.
- [26] G. Boccardo, R. Sethi, D.L. Marchisio, Fine and ultrafine particle deposition in packed-bed catalytic reactors, *Chem. Eng. Sci.* 198 (2019) 290–304.
- [27] L. Zhang, L. Hou, L. Wang, A.T. Kan, W. Chen, M.B. Tomson, Transport of fullerene nanoparticles ($n\text{C}_{60}$) in saturated sand and sandy soil: controlling factors and modeling, *Environ. Sci. Technol.* 46 (2012) 7230–7238.
- [28] N.T. Mattison, D.M. O'Carroll, R. Kerry Rowe, E.J. Petersen, Impact of porous media grain size on the transport of multi-walled carbon nanotubes, *Environ. Sci. Technol.* 45 (2011) 9765–9775.
- [29] J.E. Saiers, J.J. Lenhart, Ionic-strength effects on colloid transport and interfacial

- reactions in partially saturated porous media, *Water Resour. Res.* 39 (2003) 1256.
- [30] J. Fang, X. Shan, B. Wen, J. Lin, G. Owens, Stability of titania nanoparticles in soil suspensions and transport in saturated homogeneous soil columns, *Environ. Pollut.* 157 (2009) 1101–1109.
- [31] APHA; AWWA; WEF, *Standard Methods for the Examination of Water and Wastewater*, 20th ed., American Public Health Association, Washington, DC, 1998.
- [32] A.O. Adeniji, O.O. Okoh, A.I. Okoh, Analytical methods for the determination of the distribution of total petroleum hydrocarbons in the water and sediment of aquatic systems: a review, *J. Chem.* 2017 (2017) 1–13.
- [33] T. Strother, S. Lowry, B. Bravo, Measurement of Dispersed Oil in Water Using an Infrared Analysis Method, Application Note 52439 Termo Fisher Scientific Inc, 2013.
- [34] J. Li, J. Chen, T. Lu, Y. Wang, H. Zhang, Z. Shang, D. Li, Y. Zhou, Z. Qi, Effects of low-molecular weight organic acids on the transport of graphene oxide nanoparticles in saturated sand columns, *Sci. Total Environ.* 666 (2017) 94–102.
- [35] X. Xu, X. Li, Sorption and desorption of antibiotic tetracycline on marine sediments, *Chemosphere* 78 (2010) 430–436.
- [36] Y. Yin, X. Guo, C. Yang, L. Gao, Y. Hu, An efficient method for tylosin removal from an aqueous solution by goethite modified straw mass, *RSC Adv.* 6 (2016) 95425–95434.
- [37] Y. Liu, C. Liu, C. Zhang, X. Yang, J.M. Zachara, Pore and continuum scale study of the effect of subgrid transport heterogeneity on redox reaction rates, *Geochim. Cosmochim. Acta* 163 (2015) 140–155.
- [38] V.L. Morales, B. Gao, T.S. Steenhuis, Grain surface-roughness effects on colloidal retention in the vadose zone, *Vadose Zone J.* 8 (2009) 11–20.
- [39] P.R. Johnson, M. Elimelech, Dynamics of colloid deposition in porous media: blocking based on random sequential adsorption, *Langmuir* 11 (1995) 801–812.
- [40] S.A. Bradford, J. Simunek, M. Bettahar, M.T. van Genuchten, S.R. Yates, Modeling colloid attachment, straining, and exclusion in saturated porous media, *Environ. Sci. Technol.* 37 (2003) 2242–2250.
- [41] J. Simunek, M.T. van Genuchten, M. Sejna, The HYDRUS-1D Software Package for Simulating the One-Dimensional Movement of Water, Heat, and Multiple Solutes in Variably-Saturated Media, Ver 3.0, Department of Environmental Science, University of California Riverside, Riverside, CA, USA, 2005.
- [42] N. Toride, F.J. Leij, M.T. van Genuchten, The CXTFIT Code for Estimating Transport Parameters From Laboratory or Field Tracer Experiments, U.S. Salinity Laboratory, Riverside, CA, USA, 1999.
- [43] M.M. Sakuno, M. Shinya, S. Kawai, K. Taihei, Y. Matsumura, Adsorption and structural change of β -Lactoglobulin at the diacylglycerol-water interface, *Langmuir* 24 (2008) 11483–11488.
- [44] S. Mun, E.A. Decker, D.J. McClements, Influence of emulsifier type on in vitro digestibility of lipid droplets by pancreatic lipase, *Food Res. Int.* 40 (2007) 770–781.
- [45] A. Gomes, A.L.R. Costa, R.L. Cunha, Impact of oil type and WPI/Tween 80 ratio at the oil-water interface: adsorption, interfacial rheology and emulsion features, *Colloids Surf. B Biointerfaces* 164 (2018) 272–280.
- [46] S. Le Floch, J. Guyomarch, F.X. Merlin, P. Stoffyn-Egli, J. Dixon, K. Lee, The influence of salinity on oil-mineral aggregate formation, *Spill Sci. Technol. Bull.* 8 (2002) 65–71.
- [47] J.M. Younker, M.E. Walsh, Impact of salinity and dispersed oil on adsorption of dissolved aromatic hydrocarbons by activated carbon and organoclay, *J. Hazard. Mater.* 299 (2015) 562–569.
- [48] N.E. Tufenkji, M. Elimelech, Deviation from the classical colloid filtration theory in the presence of repulsive DLVO interactions, *Langmuir* 20 (2004) 10818–10828.
- [49] S.A. Bradford, S. Torkzaban, S.L. Walker, Coupling of physical and chemical mechanisms of colloid straining in saturated porous media, *Water Res.* 41 (2007) 3012–3024.
- [50] W.P. Johnson, X. Li, G. Yal, Colloid retention in porous media: mechanistic confirmation of wedging and retention in zones of flow stagnation, *Environ. Sci. Technol.* 41 (2007) 1279–1287.
- [51] S.A. Bradford, S.R. Yates, M. Bettahar, J. Simunek, Physical factors affecting the transport and fate of colloids in saturated porous media, *Water Resour. Res.* 38 (2002) 1327.
- [52] G. Cornelis, L. Pang, C. Doolette, J.K. Kirby, M.J. McLaughlin, Transport of silver nanoparticles in saturated columns of natural soils, *Sci. Total Environ.* 463–464 (2013) 120–130.
- [53] B. Chen, Y. Wang, D. Hu, Biosorption and biodegradation of polycyclic aromatic hydrocarbons in aqueous solutions by a consortium of white-rot fungi, *J. Hazard. Mater.* 179 (2010) 845–851.
- [54] K.G. Gillian Adama, David G. Morrisa, Harry Duncana Effect of alcohol addition on the movement of petroleum hydrocarbon fuels in soil, *Sci. Total Environ.* 286 (2002) 15–25.
- [55] M. Pham, E.A. Mintz, T.H. Nguyen, Deposition kinetics of bacteriophage MS₂ to natural organic matter: role of divalent cations, *J. Colloid Interface Sci.* 338 (2009) 1–9.
- [56] P. Yi, K.L. Chen, Influence of surface oxidation on the aggregation and deposition kinetics of multiwalled carbon nanotubes in monovalent and divalent electrolytes, *Langmuir* 27 (2011) 3588–3599.
- [57] A. Janfada, J.V. Headley, K.M. Peru, S.L. Barbour, A laboratory evaluation of the sorption of oil sands naphthenic acids on organic rich soils, *J. Environ. Sci. Heal. Part A* 41 (2006) 985–997.
- [58] J. Jin, H. Wang, Y. Jing, M. Liu, D. Wang, Y. Li, M. Bao, An efficient and environmental-friendly dispersant based on the synergy of amphiphilic surfactants for oil spill remediation, *Chemosphere* 215 (2019) 241–247.
- [59] H. Boleyde, N. Mirghaffari, O. Farhadian, Comparative study on adsorption of crude oil and spent engine oil from seawater and freshwater using algal biomass, *Environ. Sci. Pollut. R.* 25 (2018) 21024–21035.
- [60] E.H. Trond, J. Sjöblom, E.V. Jens, Oil/Water-Partitioning and interfacial behavior of naphthenic acids, *J. Disper. Sci. Technol.* 24 (2003) 789–801.
- [61] A.L. Nenningsland, B. Gao, S. Simon, J. Sjöblom, Comparative study of stabilizing agents for water-in-oil emulsions, *Energy Fuel* 25 (2011) 5746–5754.
- [62] A.A. Vallejo-Cardona, R. Cerón-Camacho, J.R. Karamath, R. Martínez-Palou, J. Aburto, A study of the effect of surfactants on the aggregation behavior of crude oil aqueous dispersions through Steady-State Fluorescence Spectrometry, *Appl. Spectrosc.* 71 (2017) 1519–1529.
- [63] A.M. Atta, H.A. Allohedan, G.A. El-Mahdy, Dewatering of petroleum crude oil emulsions using modified Schiff base polymeric surfactants, *J. Petrol. Sci. Eng.* 122 (2014) 719–728.
- [64] S.M. Hashmi, K.X. Zhong, A. Firoozabadi, Acid-base chemistry enables reversible colloid-to-solution transition of asphaltene in non-polar systems, *Soft Matter* 8 (2012) 8778.
- [65] S. Paria, K.C. Khilar, A review on experimental studies of surfactant adsorption at the hydrophilic solid-water interface, *Adv. Colloid Interf. Sci.* 110 (2004) 75–95.
- [66] C. Chen, M.J. Kadhum, M.C. Mercado, B. Shiao, J.H. Harwell, Surfactant-only stabilized dispersions of multiwalled carbon nanotubes in high-electrolyte-concentration brines, *Energy Fuel* 30 (2016) 8952–8961.
- [67] B.D. Ma, B.Y. Gao, L. Zhang, Q.T. Gong, Z.Q. Jin, L. Zhang, Influence of polymer on dynamic interfacial tensions of EOR surfactant solutions, *J. Appl. Polym. Sci.* 131 (2014) 40562.
- [68] K.E.J. Rocchio, J. Neilsen, G.D. Bothun, A solvent-free lecithin-tween 80 system for oil dispersion, *Colloids Surf. A Physicochem. Eng. Asp.* 533 (2017) 218–223.
- [69] P. Venkataraman, J. Tang, E. Frenkel, G.L. McPherson, J. He, S.R. Raghavan, V. Kolesnichenko, A. Bose, V.T. John, Attachment of a hydrophobically modified biopolymer at the oil-water interface in the treatment of oil spills, *ACS Appl. Mater. Inter.* 5 (2013) 3572–3580.
- [70] Z. Qi, L. Zhang, W. Chen, Transport of graphene oxide nanoparticles in saturated sandy soil, *Environ. Sci. Process. Impacts* 16 (2014) 2268–2277.

Supplementary Material Cover Sheet

Factors affecting the transport of petroleum colloids in saturated porous media

Ying Wang^{1,2,a}, Taotao Lu^{3,a}, Haojing Zhang², Yanxiang Li⁴, Yumeng Song²,

Jiuyan Chen², Xiaowen Fu¹, Zhichong Qi^{1,2,*} and Qiang zhang^{1,**}

¹ Ecology institute of the Shandong academy of sciences, Qilu University of Technology

(Shandong Academy of Sciences), Jinan 250353, China

² Henan Joint International Research Laboratory of Environmental Pollution Control

Materials, College of Chemistry and Chemical Engineering, Henan University, Kaifeng

475004, China

³ Department of Hydrology, University of Bayreuth, Bayreuth 95440, Germany

⁴ The Testing Center of Shandong Bureau of China Metallurgical Geology Bureau, Jinan

250014, China

^a Ying Wang and Taotao Lu contributed equally.

*Corresponding author: Zhichong Qi (qizhichong1984@163.com);

**Corresponding author: Qiang zhang (zhbuaiji@sina.com)

Manuscript prepared for *Colloids and Surfaces A: Physicochemical and Engineering*

Aspects

S1. Procedures used to remove impurities from petroleum

First, a small amount of original petroleum was dissolved in 100 mL of petroleum ether (boiling range, 30–60 °C), and then the supernatant was withdrawn to a beaker. Then, the solvent containing petroleum was drained through a funnel containing a filter paper and 10 g anhydrous sodium sulphate to remove moisture. Afterward, the solvent was poured into an evaporating dish and placed in an incubator to remove residual petroleum ether at 40 °C for 12 h. The final materials were used as petroleum standard samples in this study.

S2. Determination of petroleum colloid concentrations

The concentrations of petroleum colloids in the influent (C_0) and effluent (C) were determined by using a previously developed solvent exchange method.[1] Briefly, the collected sample was transferred to a 20-mL separatory funnel, followed by 1 mL H_2SO_4 (1:1) and 5 mL tetrachloromethane, respectively. Then the funnel was shaken vigorously for 3 min and stood for a few minutes. Organic layer was separated from the aqueous phase. Next, the aqueous phase was transferred into the original sample container. The rest was drained through a funnel containing a filter paper and 10 g anhydrous sodium sulphate to remove moisture before the concentration determination. The aqueous layer and some remaining emulsion were recombined in the separatory funnel and extracted followed previous method. The filtrate was made up to 50 ml with tetrachloromethane. Then the mixture was stirred with sufficient silica gel to remove fatty matter before the absorbance measurement from 3200 cm^{-1} to 2700 cm^{-1} by infrared spectrophotometry (Affinity-1, Shimadzu Scientific Instruments). The final reading was then compared with the absorbance of the petroleum standard samples as mentioned in S1. [2, 3]

S3. Procedures used to obtain the retention profiles of petroleum colloids in the column

To obtain the retention profiles of petroleum colloids in the column at the end of the transport experiments, the columns were dissected into 10 layers of 1-cm segments. First, 10 mL of tetrachloromethane was added to the vials, then agitating for 3 h on an oscillating shaker (KS 260 Basic, IKA). Afterward, the mixture was sonicated for 1 h. Then, the mixture was transferred to a centrifugation tube, and was centrifuged at 3000 rpm for 30 min. The tetrachloromethane supernatant was withdrawn to measure the concentration of petroleum colloids by infrared spectrophotometry method described above. The sand/soil segments were oven-dried at 90 °C overnight to obtain the dry weight of the porous media in each segment.

S4. Sensitivity analyses of various fitting parameter

To investigate the effect of various fitting parameters on model results, we conducted a sensitivity analysis. Critical parameters such as K_{att} , S_{max} , and K_{str} were selected to analyze the model behavior. Other parameters were left unchanged unless otherwise specified. The ranges of rate constants depend on the surface characteristics of colloids and/or porous medium. The results are showed in Fig S5.

Table S1. Summary of column properties.

Column No.	porous media	Column properties		
		Length (cm)	Bulk density (g/cm ³)	Porosity (-)
1	sand	10.0	1.55	0.42
2	sand	10.3	1.53	0.42
3	sand	10.2	1.51	0.41
4	sand	10.0	1.50	0.43
5	soil	10.1	1.42	0.47
6	soil	9.9	1.45	0.48
7	soil	10.0	1.39	0.49
8	soil	10.2	1.42	0.47
9	sand	10.1	1.56	0.41
10	sand	10.1	1.54	0.42
11	sand	10.0	1.53	0.40
12	soil	10.2	1.43	0.49
13	soil	10.1	1.40	0.49
14	soil	9.9	1.42	0.48
15	sand	10.0	1.53	0.42
16	sand	10.1	1.52	0.43
17	soil	10.2	1.39	0.48
18	soil	10.3	1.42	0.46
19	sand	10.0	1.51	0.43
20	soil	10.1	1.39	0.47

Table S2. Mass balance expressed as percentage of effluent mass, eluted mass during each flushing step, and mass recovered from column

Column No.	porous media	Background solution	pH	Effluent Mass (%)	Eluted mass (%)	Mass recovered from column (%)	Mass balance ^a (%)
1	sand	10 mM NaCl	5.0	58.2	2.2	30.6	91.0
2	sand	20 mM NaCl	5.0	53.8	0.7	41.2	95.7
3	sand	30 mM NaCl	5.0	48.3	0.1	42.2	90.6
4	sand	50 mM NaCl	5.0	42.8	1.0	52.1	95.8
5	soil	10 mM NaCl	5.0	52.0	4.5	42.4	98.9
6	soil	20 mM NaCl	5.0	35.4	1.4	60.8	97.7
7	soil	30 mM NaCl	5.0	26.3	1.0	71.5	98.8
8	soil	50 mM NaCl	5.0	8.8	0.1	88.2	97.2
9	sand	0.1 mM CaCl ₂	5.0	50.8	1.2	45.5	97.6
10	sand	0.5 mM CaCl ₂	5.0	42.1	2.0	55.2	99.3
11	sand	1.0 mM CaCl ₂	5.0	35.1	1.1	62.0	98.2
12	soil	0.1 mM CaCl ₂	5.0	34.9	2.0	55.7	92.7
13	soil	0.5 mM CaCl ₂	5.0	30.8	1.5	60.7	93.0
14	soil	1.0 mM CaCl ₂	5.0	14.1	1.1	75.4	90.6
15	sand	30 mM NaCl	7.0	59.2	1.9	36.7	97.8
16	sand	30 mM NaCl	9.0	71.6	2.8	24.1	98.5
17	soil	30 mM NaCl	7.0	29.3	2.6	62.5	94.3
18	soil	30 mM NaCl	9.0	46.3	4.0	42.3	92.7
19	sand	30 mM NaCl +10 mg/L SDS	5.0	53.9	1.0	43.1	98.0
20	soil	30 mM NaCl +10 mg/L SDS	5.0	39.6	1.1	53.0	93.8

^a Mass balance was calculated as: (effluent mass + eluted mass + mass recovered from column)/mass injected.

Table S3. List of petroleum colloids attachment isotherm parameters

No.	sorbent	Background solution	pH	K_d (L/Kg)	r^2
1	sand	10 mM NaCl	5.0	5.68	0.952
2	sand	20 mM NaCl	5.0	7.13	0.961
3	sand	30 mM NaCl	5.0	8.41	0.985
4	sand	50 mM NaCl	5.0	13.6	0.990
5	soil	10 mM NaCl	5.0	54.6	0.973
6	soil	20 mM NaCl	5.0	87.1	0.991
7	soil	30 mM NaCl	5.0	127.8	0.986
8	soil	50 mM NaCl	5.0	157.4	0.987
9	sand	0.1 mM CaCl ₂	5.0	9.29	0.968
10	sand	0.5 mM CaCl ₂	5.0	14.2	0.985
11	sand	1.0 mM CaCl ₂	5.0	19.4	0.969
12	soil	0.1 mM CaCl ₂	5.0	83.3	0.927
13	soil	0.5 mM CaCl ₂	5.0	93.2	0.918
14	soil	1.0 mM CaCl ₂	5.0	205.2	0.959
15	sand	30 mM NaCl	7.0	3.85	0.981
16	sand	30 mM NaCl	9.0	3.46	0.956
17	soil	30 mM NaCl	7.0	93.7	0.985
18	soil	30 mM NaCl	9.0	59.5	0.939
19	sand	30 mM NaCl +10 mg/L SDS	5.0	5.93	0.989
20	soil	30 mM NaCl +10 mg/L SDS	5.0	91.5	0.953

Table S4. Fitted parameters of two-site transport model from breakthrough results of column experiments

Column No.	porous media	Background solution	pH	Parameters of two-site transport model			
				K_{att} (h ⁻¹)	S_{max} (mg/kg)	K_{str} (h ⁻¹)	r^2
1	sand	10 mM NaCl	5.0	3.83	0.199	18.7	0.957
2	sand	20 mM NaCl	5.0	8.69	0.162	23.4	0.956
3	sand	30 mM NaCl	5.0	17.6	0.192	26.8	0.981
4	sand	50 mM NaCl	5.0	27.5	0.191	30.9	0.989
5	soil	10 mM NaCl	5.0	18.2	1.67	23.2	0.990
6	soil	20 mM NaCl	5.0	23.3	1.85	33.7	0.989
7	soil	30 mM NaCl	5.0	28.6	1.91	38.5	0.990
8	soil	50 mM NaCl	5.0	42.9	1.29	67.6	0.988
9	sand	0.1 mM CaCl ₂	5.0	8.06	0.183	25.7	0.968
10	sand	0.5 mM CaCl ₂	5.0	10.2	0.235	32.8	0.978
11	sand	1.0 mM CaCl ₂	5.0	17.3	0.269	38.5	0.979
12	soil	0.1 mM CaCl ₂	5.0	11.7	0.479	32.3	0.963
13	soil	0.5 mM CaCl ₂	5.0	13.6	0.468	43.1	0.988
14	soil	1.0 mM CaCl ₂	5.0	27.3	0.485	57.8	0.972
15	sand	30 mM NaCl	7.0	11.5	0.486	16.2	0.972
16	sand	30 mM NaCl	9.0	4.33	0.339	9.57	0.985
17	soil	30 mM NaCl	7.0	18.5	1.50	29.6	0.986
18	soil	30 mM NaCl	9.0	7.66	2.69	18.5	0.991
19	sand	30 mM NaCl +10 mg/L SDS	5.0	10.7	0.305	20.1	0.997
20	soil	30 mM NaCl +10 mg/L SDS	5.0	12.8	0.811	20.2	0.990

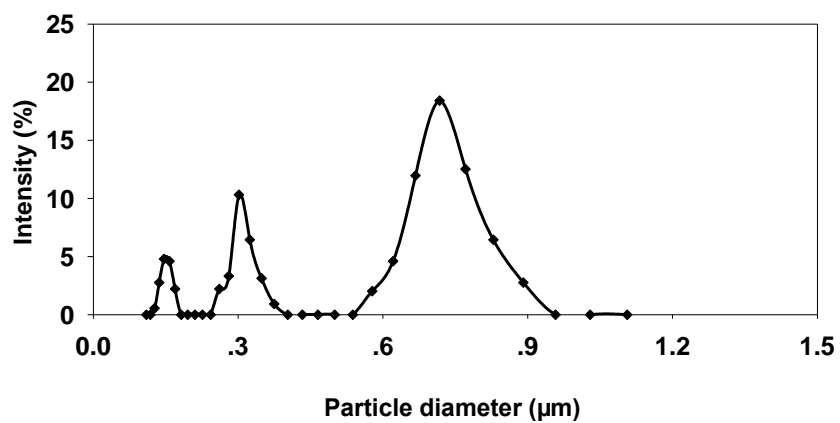


Fig. S1 Intensity-weighted particle size distribution of petroleum colloids in stock petroleum suspensions.

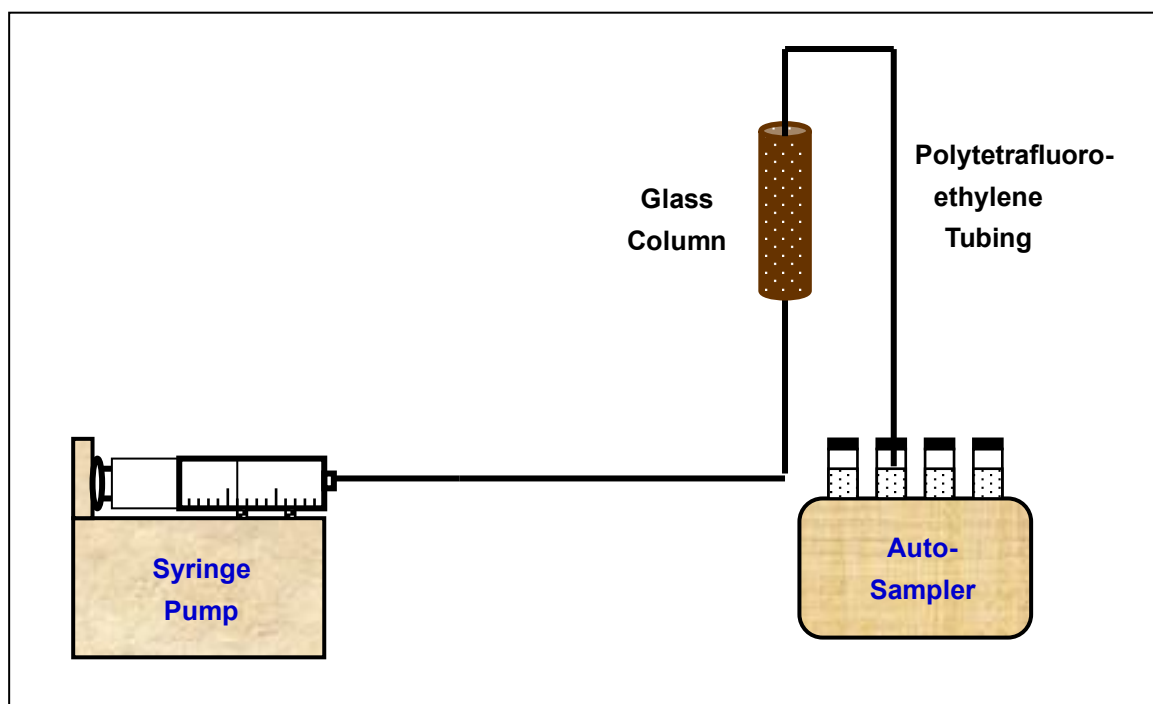


Fig. S2 Schematic illustration of experimental apparatus of column tests.

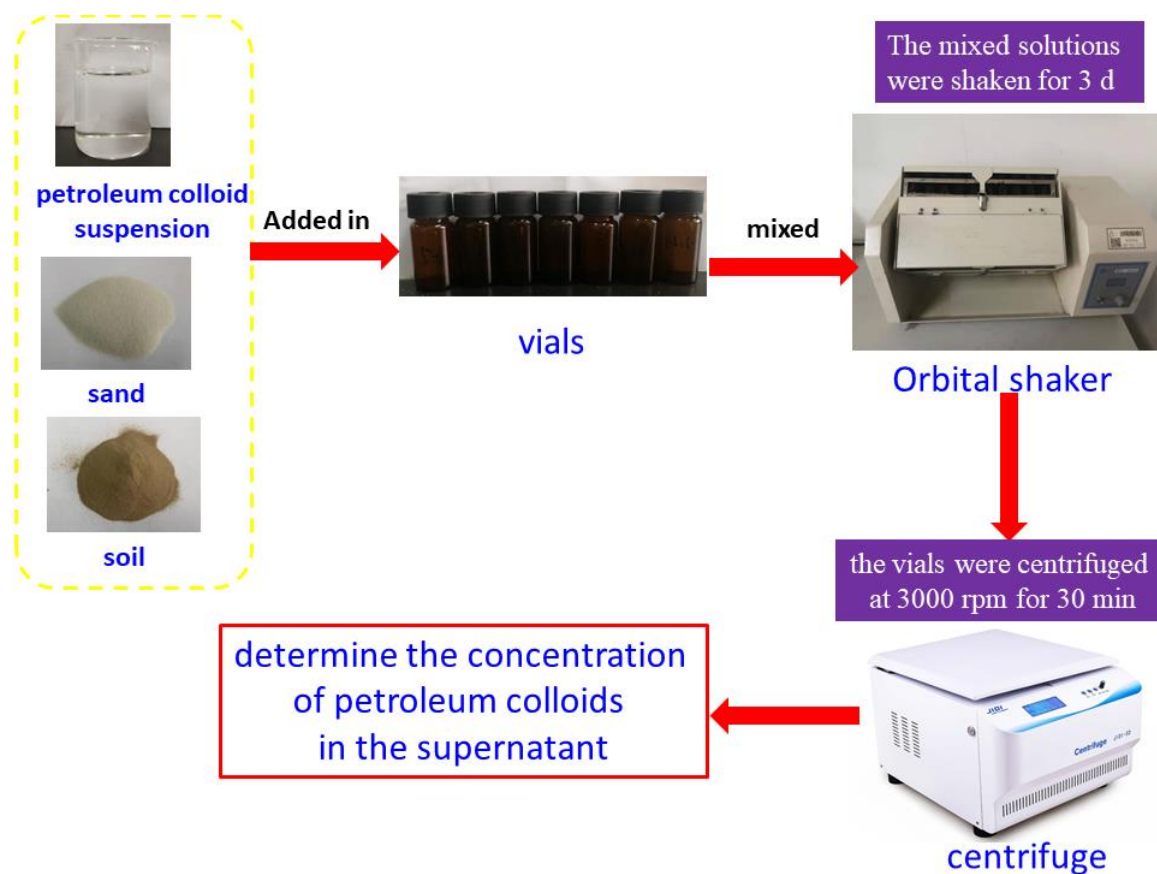


Fig. S3 Procedures used to obtain attachment isotherms of petroleum colloids to sand or soil.

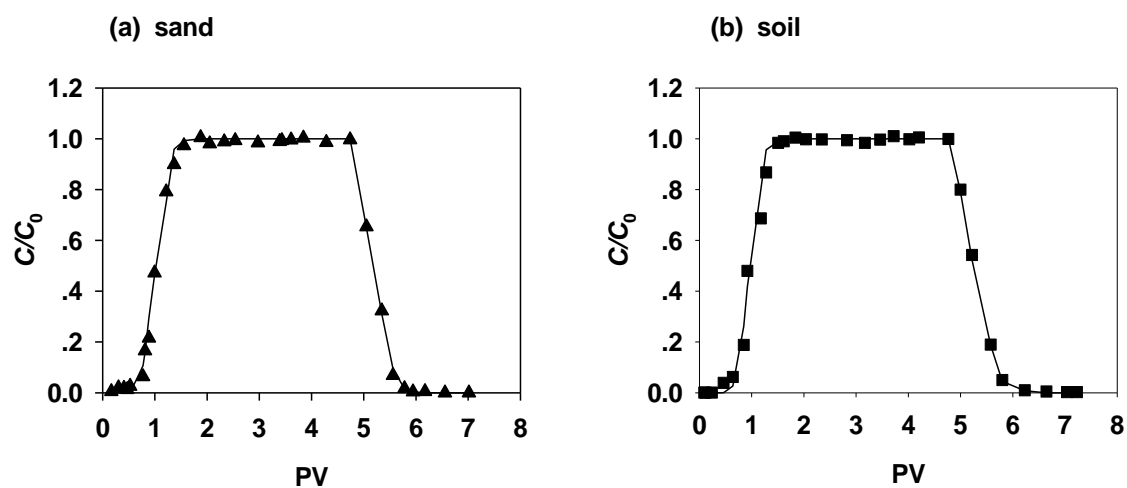


Fig. S4 Representative breakthrough curve of conservative tracer (Br^-): (a) sand; and (b) soil.

The line was plotted by fitting the breakthrough data with the one-dimensional steady-state advection–dispersion equation.

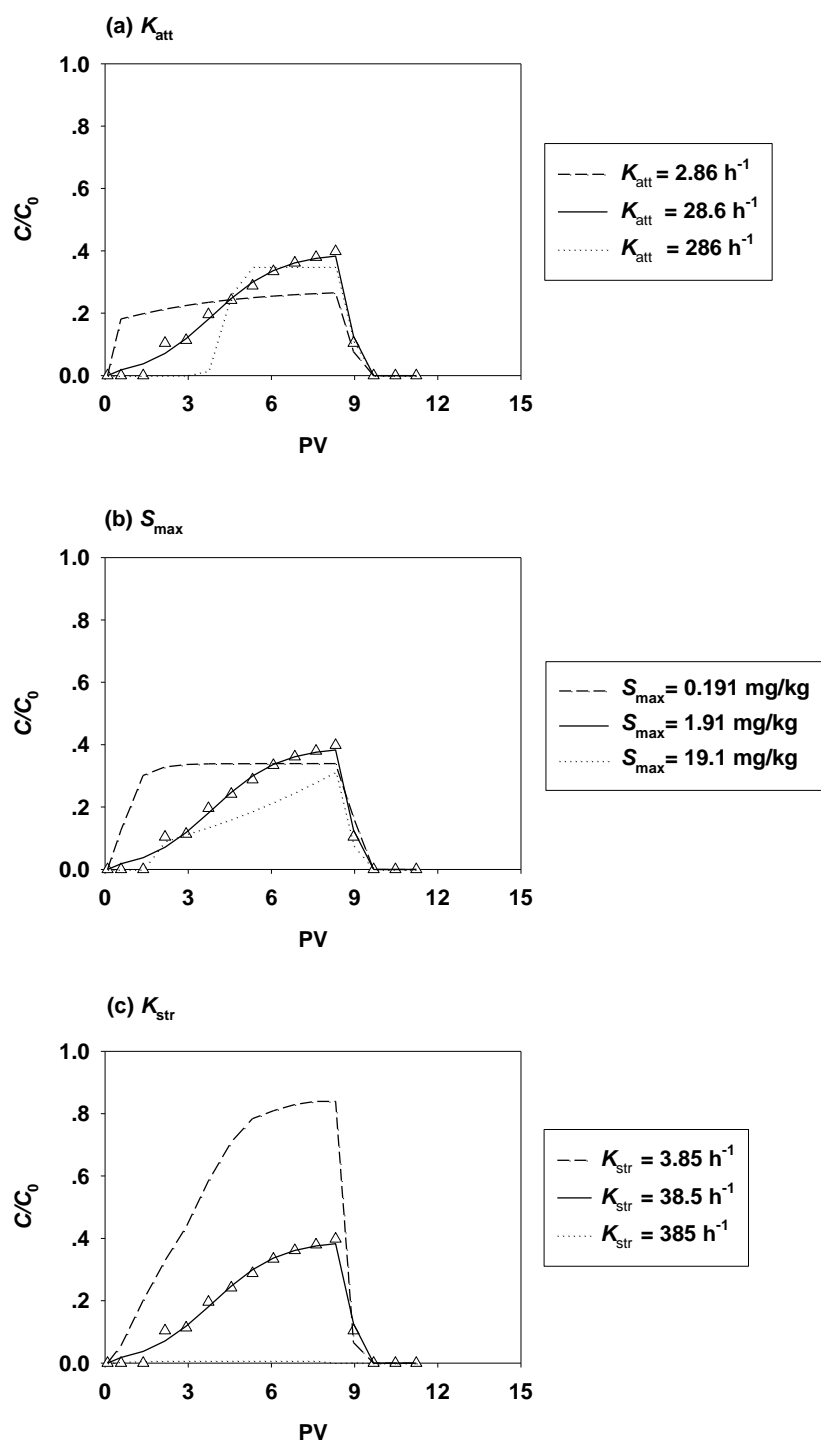


Fig. S5 Sensitivity analyses of various fitting parameter (Column 7): (a) K_{att} ; (b) S_{max} ; and (c)

K_{str} .

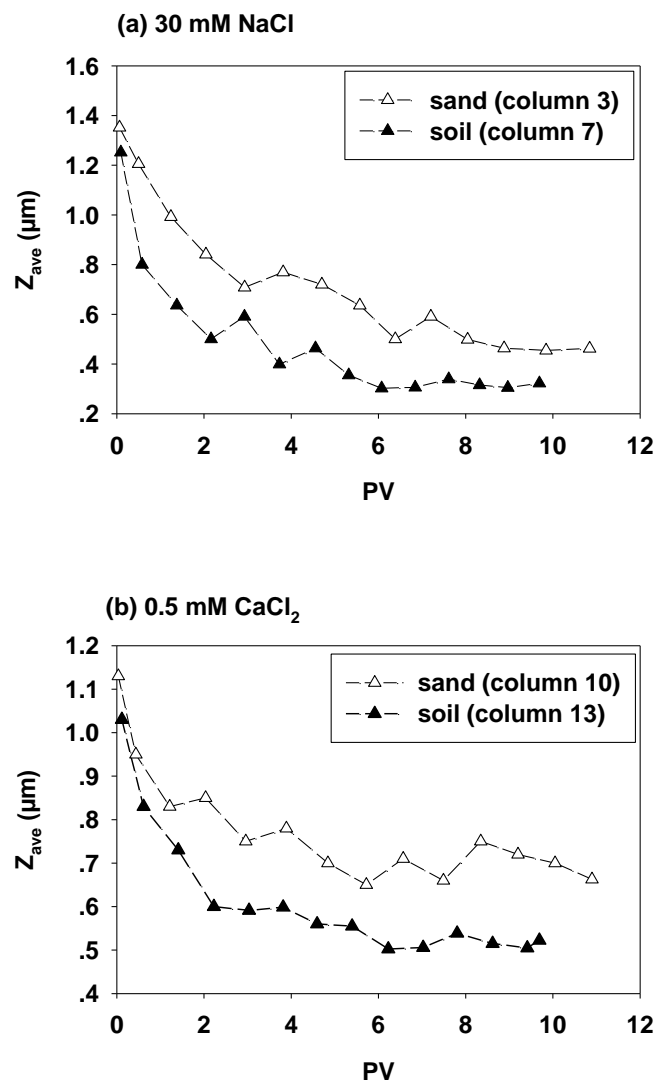


Fig. S6 Changes of petroleum colloid size in effluents of column experiments (Columns 3, 7, 10 and 13).

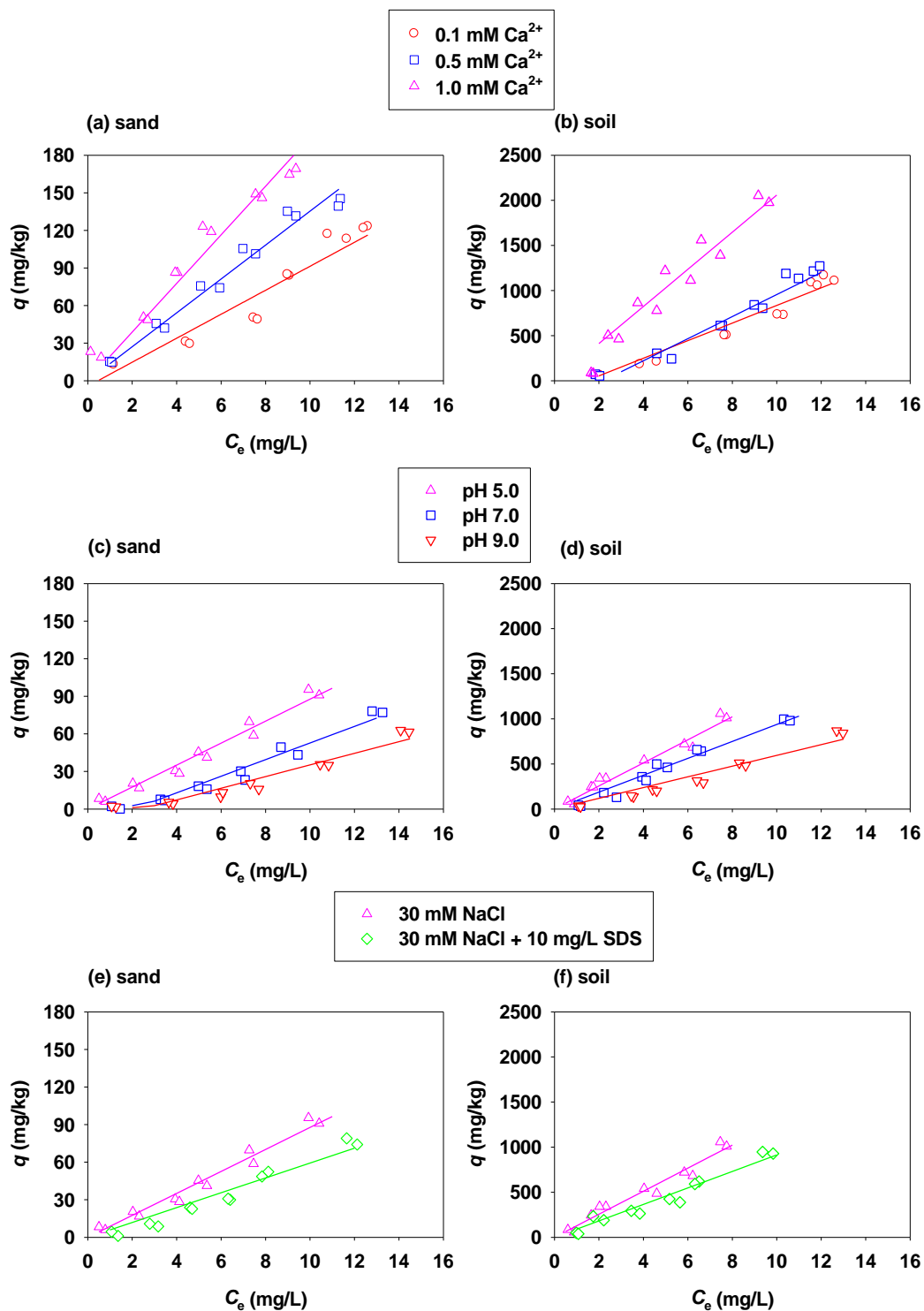


Fig. S7 The attachment of petroleum colloids onto sand (a, c and e) and soil (b, d and f) under different solution chemistry conditions. The solid lines on the two panels are the Linear model fitting results.

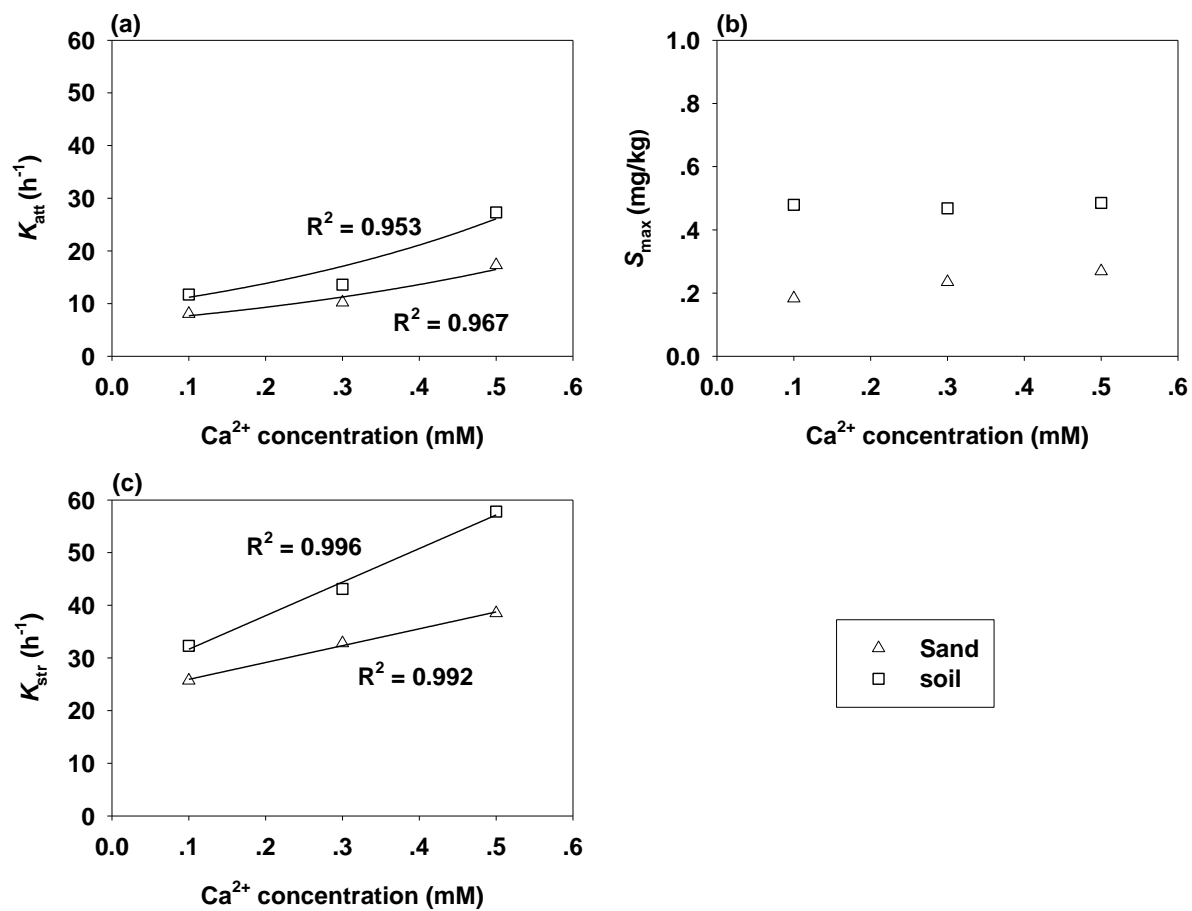


Fig. S8 Correlations between fitted parameters of two-site transport model (based on breakthrough data of columns 9–14) and Ca^{2+} concentrations.

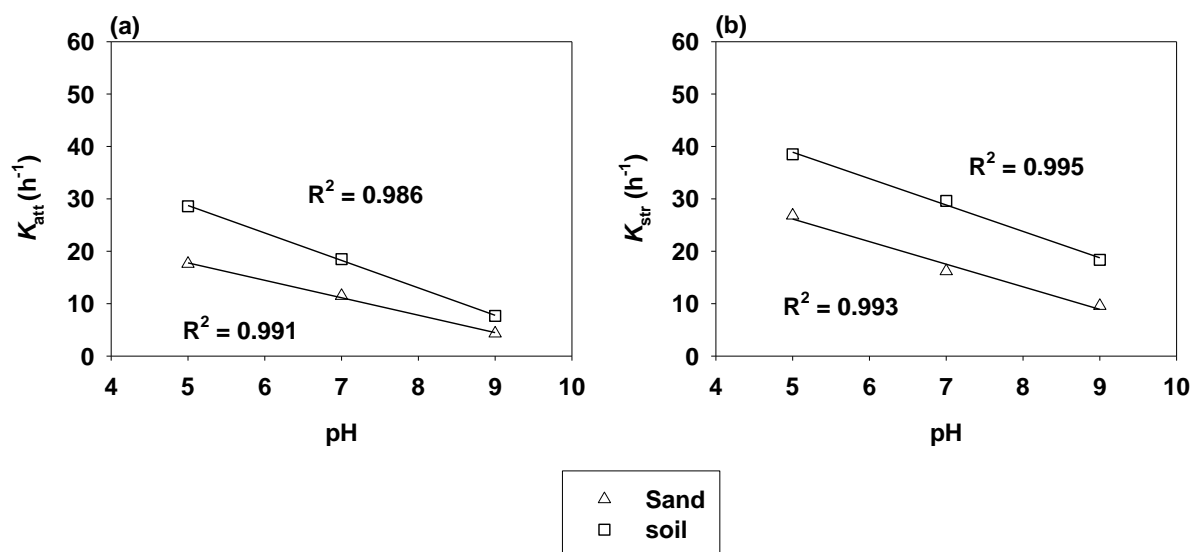


Fig. S9 Correlations between fitted parameters of two-site transport model (based on breakthrough data of columns 3, 7, 15–18) and pH.

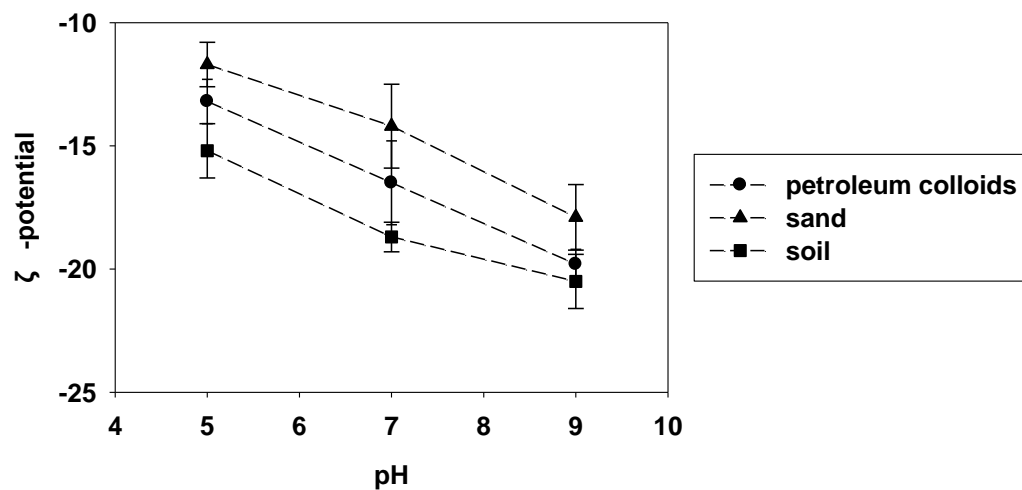


Fig. S10 Zeta potential of quartz sand, soil and petroleum colloids as affected by pH.

References:

- [1] APHA; AWWA; WEF, *Standard Methods for the Examination of Water and Wastewater*, 20th ed.; American Public Health Association: Washington, DC, 1998.
- [2] Agency for Toxic Substances and Disease Registry (ATSDR), Toxicological Profile for Total Petroleum Hydrocarbon, US Department of Health and Human Services, Public Health Service, Atlanta, Ga, USA, 1999.
- [3] EPA 821R00003, 2000. Analytical method guidance for EPA method 1664: a implementation and use, Downloadable at <http://www.epa.gov/waterscience/methods/method/oil/1664guide.pdf>

Study 3: Relevance of iron oxyhydroxide and pore water chemistry on the mobility of nanoplastic particles in water-saturated porous media environments

Taotao Lu, Benjamin S. Gilfedder, Hao Peng, Stefan Peiffer, Georg Papastavrou, Katharina Ottermann, Sven Frei

Published in *Water, Air, & Soil Pollution* (Vol. 232, 2021)



Relevance of Iron Oxyhydroxide and Pore Water Chemistry on the Mobility of Nanoplastic Particles in Water-Saturated Porous Media Environments

Taotao Lu · Benjamin S. Gilfedder · Hao Peng ·
Stefan Peiffer · Georg Papastavrou ·
Katharina Ottermann · Sven Frei

Received: 22 January 2021 / Accepted: 12 April 2021

© The Author(s), under exclusive licence to Springer Nature Switzerland AG 2021

Abstract The increasing use of plastic products and its inevitable decomposition after improper disposal has led to large numbers of nano- and microplastic in aqueous environments. There is currently a critical need to investigate the transport and retention mechanisms of nanoplastic particles in water-saturated porous media (e.g., aquifers or sediments) to better understand residence times and ecosystem exposure of these particles in aqueous environments. In this study, we performed a set of column experiments in order to investigate and understand the primary controls on the mobility of nanoplastics in a controlled laboratory environment. As part of the experiments, we used polystyrene nanoplastic particles (PS-NPs, 50 nm) in combination with iron oxyhydroxide-coated sand, which is known for its high

surface reactivity and often can be found in natural systems in environmentally relevant amounts. We also adjusted pore water chemistry (pH, ionic strength, cation species) to represent non-uniform geochemical conditions in nature and to understand how these conditions quantitatively affect the transport of nanoplastics. Mobility and retention of PS-NPs were assessed by analyzing breakthrough curves. For negatively charged iron oxyhydroxide coatings (at $\text{pH} > \text{pH}_{\text{pzc}}$), only little retention of PS-NPs could be observed. In contrast, positively charged iron oxyhydroxide coatings ($\text{pH} < \text{pH}_{\text{pzc}}$) provided favorable deposition sites for the negatively charged PS-NPs. DLVO theory was used to show that high pH and low ionic strength increased the energy barriers between PS-NPs and the porous media. In contrast, low pH and high ionic strength decreased the barriers and thus increased retention in the columns. Finally, bridging agents, such as Ca^{2+} and Ba^{2+} , resulted in the significant deposition of nanoplastics by forming bonds between O-containing functional groups on both the plastic and sediment surfaces. These findings indicate that the deposition and fate of nanoplastic particles are strongly affected by the water chemistry and soil components in subsurface environments.

T. Lu (✉) · B. S. Gilfedder · S. Peiffer · S. Frei
Department of Hydrology, Bayreuth Center of Ecology and
Environmental Research (BAYCEER), University of Bayreuth,
Universitätsstraße 30, 95440 Bayreuth, Germany
e-mail: Taotao.Lu@uni-bayreuth.de

B. S. Gilfedder
Limnological Research Station, Bayreuth Center of Ecology and
Environmental Research (BAYCEER), University of Bayreuth,
Universitätsstraße 30, 95440 Bayreuth, Germany

H. Peng
School of Environmental Studies, China University of
Geoscience, Wuhan 430074, China

G. Papastavrou · K. Ottermann
Physical Chemistry II, University of Bayreuth, Universitätsstraße
30, 95440 Bayreuth, Germany

Keywords Polystyrene nanoplastic · Transport · DLVO theory · Iron oxyhydroxide · coated sand

1 Introduction

Plastic polymers are essential for the maintenance of the current standard of living and are found in a large variety

of products such as cosmetics, electronic devices, packaging materials, and medical products (da Costa et al., 2016; Mattsson et al., 2018). In 2017, the production of plastics exceeded 8300 million metric tons with global production capacities still increasing (Geyer et al., 2017). Although there are significant benefits for society from polymers like polyethylene (PE), polystyrol (PS), and polypropylene (PP), incorrect disposal has resulted in at least 23 million metric tons of plastic waste that can be found in oceans (Derraik, 2002; Roos Lundström and Martensson, 2015; Wang et al., 2020), stream or lake systems (Frei et al., 2019; Klein et al., 2015), and groundwater (Hurley and Nizzetto, 2018; Möller et al., 2020; Rodríguez-Seijo and Pereira, 2019; Wanner, 2021). Natural degradation and fragmentation processes of polymers, including weathering (Silva et al., 2018), photo-oxidation (Yousif and Haddad, 2013), and biodegradation (Albertsson and Karlsson, 1994), degrade macroplastics (fragments > 5000 μm) into microplastics (MPs) (particles in between 100 nm and 5000 μm) and nanoplastics (NPs) (< 100 nm) (Arthur et al., 2008; Dawson et al., 2018; Gigault et al., 2018; Mattsson et al., 2018). To date, the detection of NPs in environmental samples is not possible (current detection limit is $\sim 1 \mu\text{m}$); recent studies have suggested that the abundances of plastic particles, in general, are increasing with decreasing particle size (Frei et al., 2019).

Compared with macroplastics, NP particles in the environment have several unique properties, such as a higher surface-to-volume ratio resulting in stronger interactions between NP particles and other substances in groundwater (e.g., humic acid). These substances will affect the NP-particle transport in aquifers (Koelmans et al., 2015). Further, plastic polymers are known to contain a multitude of chemical additives such as flame retardants or plasticizers that are often carcinogenic or hormone active, exhibiting high potential for leaching (Thaysen et al., 2018) and accumulation in higher trophic levels (Hahladakis et al., 2018). Compared to rivers and streams, NPs in streambed sediments face considerably longer exposure times to benthic organisms, increasing the chance of uptake; for example, an uptake of NPs by seawater organisms has been shown by Silva et al. (2020). However, reliable data concerning the mobility of NPs in interstitial pore spaces (e.g., in hyporheic systems or shallow aquifers) at the interface between surface water and groundwater is rare.

Studies that have investigated transport and retention of NPs in porous media (Bouchard et al., 2013; Franchi

and O'Melia, 2003; Mitzel et al., 2016; Quevedo and Tufenkji, 2012; Shani et al., 2008; Shen et al., 2008; Treumann et al., 2014; Tripathi et al., 2011; Tufenkji and Elimelech, 2005; Zhuang et al., 2005) mainly have focused on how the mobility of these particles is influenced by pore water chemistry. However, there is currently little systematic data on how NP mobility is affected by monovalent (e.g., Na^+ , K^+ , and Cs^+) vs. divalent cations (e.g., Mg^{2+} , Ca^{2+} , Ba^{2+}) (Elimelech and O'Melia, 1990; Quevedo and Tufenkji, 2012). In addition to pore water chemistry, the surface properties of the porous media are also an essential factor affecting the mobility of NPs (Wu et al., 2020). To date, the majority of experimental setups used clean glass beads or purified quartz sands as porous media materials, which are seldom found in nature (Franchi and O'Melia, 2003; Shen et al., 2008; Treumann et al., 2014; Tufenkji and Elimelech, 2005; Zhuang et al., 2005). There has only been a limited number of studies that have used sediments that more closely represent the real-world complexity of porous media systems. Wu et al. (2020) proposed that the transport of PS-NPs in different soils was positively correlated with the Fe/Al oxide contents. Thus, it is necessary to study the effects of iron oxide.

Iron oxides are one of the most ubiquitous and environmentally important constituents of natural soils (Ryan et al., 1999). They are usually positively charged under environmentally relevant pH conditions due to their relatively high point of zero charge (between 8.5 and 8.8) (pH_{pzc}) (Wang et al., 2012; Cornell & Schwertmann, 2003). This favors sorption reactions and is responsible for the retention of chemical substances in soils and sediments. Despite their high abundance in natural systems, to our knowledge, the influence of iron oxides on the mobility of MPs and NPs has not been investigated systematically in the literature. Some studies focused on the interactions between NPs with iron oxide colloids; they found that the NPs would be adsorbed to the iron oxide colloids by electrostatic effects (Oriekhova & Stoll, 2018; Li et al., 2019a). However, it is still uncertain how iron oxide-coated sand affects NP transport. Some information from the research about titanium dioxide nanoparticles may be transferable to NPs. Wang et al. (2017) reported that negatively charged graphene oxide deposited more easily on iron oxyhydroxide-coated sand due to charge heterogeneity. Han et al. (2014) also found that the retention of titanium dioxide nanoparticles was

determined by the strong attractive electrostatic force derived from the iron oxides. In addition to charge heterogeneity, iron oxide coatings may change the surface morphology of the porous media to retard the transport of nanoparticles. For example, Wang et al. (2017) suggested that the physical “straining” effect was enhanced due to the narrowing of the pore throat caused by iron oxide coatings.

This work aims to better understand the role of iron oxyhydroxide on PS-NP transport and retention in water-saturated porous media environments. Here, we are using column experiments as analogs for PS-NP transport in real systems such as aquifers or hyporheic sediments. In addition, the influence of pore water chemistry on NP transport in these systems also was investigated. The following research hypotheses were addressed:

- (1) Compared to pure quartz sand, the retention of NPs is considerably higher when iron oxyhydroxide-coated sand is used. The degree of retention depends mainly on the content of iron oxyhydroxide used in the column experiment.
- (2) The pH and ionic strength of the pore water affect the transport and retention of NPs by modifying the surface charge and interaction energy of both particles and porous media.
- (3) Divalent cation species in the pore water solution have a larger impact on the mobility of NPs compared to monovalent cations due to the bridging effect between O-groups on the surface of PS-NPs and the sediment.

2 Materials and Methods

2.1 Preparation and Characterization of Polystyrene Nanoplastic Suspension

Fluorescent polystyrene (PS) spheres (PolyScience Co.), modified with a layer of carboxylate group to improve water suspension, were used as model NPs as part of the column experiments. Because of the vinyl structure of PS, PS has low heat resistance and weathering resistance; thus, it is easier to form NPs in the environment (Wang et al., 2000). The PS particles have an average nominal size of 50 nm, and the particle density is 1.05 g cm^{-3} . The maximum excitation and emission wavelength of the fluorescent coating was

441 nm and 486 nm, respectively. The stock solution (25 g L^{-1}) was diluted by Milli-Q water to achieve a suspension with a concentration of 25 mg L^{-1} .

The pH (5–9) of the suspension was adjusted using HCl (0.1 M) and NaOH (0.1 M). 0.1 M NaCl was used to modify the ionic strength. Monovalent (0.1 M NaCl, KCl, and CsCl) and divalent cations (0.1 M MgCl_2 , CaCl_2 , and BaCl_2) were used to change cation species in the suspension. Electrophoretic mobility and hydrodynamic diameters of the PS-NPs were measured using a Malvern Zetasizer Nano ZS (Malvern Instruments Ltd, UK). The zeta potential of the PS-NPs was derived from electrophoretic mobility using the Smoluchowski equation (cf. Supplementary Material, eq. S1) considering the spherical shape of the PS-NPs. A summary of the composition of the different suspensions used as part of the column experiments can be found in Table 1.

2.2 Preparation of Iron Oxyhydroxide-Coated Sand

Quartz sand (Honeywell, Germany) with an average grain size of 0.22 mm was used in all column experiments. Prior to the iron oxyhydroxide coating process, the sand was thoroughly washed by soaking in 0.1 M HCl for 3 h and then in 5 wt.% H_2O_2 for 3 h. The sand was rinsed by Milli-Q ($18.2 \text{ M}\Omega$) water until the pH returned to that of Milli-Q water. The washed sand was dried at $105 \text{ }^\circ\text{C}$ for 24 h and stored for future use. The detailed procedure used for the iron oxyhydroxide coating is provided in Wang et al. (2012). Briefly, 250 g of washed quartz sand was placed into an evaporation dish, followed by separately adding 43.75 mL of 0.17 M $\text{Fe}(\text{NO}_3)_3$ and 45 mL of 0.52 M NaOH. After the mixture was stirred for 2 h, it was dried at $105 \text{ }^\circ\text{C}$ for 24 h. During this process, the mixture was stirred regularly in order to achieve a uniform coating on the sand surface. Finally, 1.0 mM HCl and 1.0 mM NaOH were used for rinsing the coated sand to remove weakly coated iron oxyhydroxide from the sand surface. Scanning electron microscopy (Jeol JSM-6510) was employed to characterize the surface morphology between the coated and uncoated sand (Fig. 1). The content of iron from the coating procedure was measured at 1.2 mg/g (Hanna, 2007).

2.3 Column Experiments

In total, 16 individual column experiments were conducted. These experiments were further sub-divided into

Table 1 Experimental protocols of column tests

Column no.	Column properties			Influent properties					
	Porous media	Fe content (%)	Porosity (–)	Background solution	pH	PS-NP conc. (mg/L)	ζ -potential (mV)	Z_{ave}^a	d_p/d_c^b
1	Sand + coated sand	15	0.411	1 mM NaCl	5.8	25.2	-28.4 ± 1.2	52.2 ± 0.9	0.0002
2	Sand + coated sand	30	0.415	1 mM NaCl	5.8	26.1	-28.4 ± 1.2	52.2 ± 0.9	0.0002
3	Sand + coated sand	45	0.416	1 mM NaCl	5.8	23.8	-28.4 ± 1.2	52.2 ± 0.9	0.0002
4	Sand + coated sand	15	0.422	1 mM NaCl	5	24.6	-24.6 ± 1.3	52.7 ± 0.5	0.0002
5	Sand + coated sand	15	0.422	1 mM NaCl	7	26.4	-32.7 ± 1.9	50.3 ± 1.6	0.0002
6	Sand + coated sand	15	0.422	1 mM NaCl	9	26.1	-42.6 ± 1.3	50.2 ± 0.8	0.0002
7	Sand + coated sand	15	0.423	3 mM NaCl	5.8	25.4	-28.3 ± 1.2	51.9 ± 1.6	0.0002
8	Sand + coated sand	15	0.427	5 mM NaCl	5.8	24.7	-27.4 ± 1.3	50.1 ± 2.9	0.0002
9	Sand + coated sand	15	0.419	0.1 mM CaCl ₂	5.8	25.9	-19.1 ± 1.5	54.9 ± 0.6	0.0003
10	Sand + coated sand	15	0.423	0.3 mM CaCl ₂	5.8	25.5	-18.5 ± 1.2	52.8 ± 0.4	0.0002
11	Sand + coated sand	15	0.420	0.5 mM CaCl ₂	5.8	24.9	-14.8 ± 1.9	54.5 ± 1.0	0.0002
12	Sand + coated sand	15	0.423	3 mM KCl	5.8	24.8	-24.7 ± 0.9	51.9 ± 1.7	0.0002
13	Sand + coated sand	15	0.424	3 mM CsCl	5.8	25.6	-22.6 ± 1.3	50.7 ± 0.7	0.0002
14	Sand + coated sand	15	0.426	0.3 mM MgCl ₂	5.8	26.0	-17.6 ± 2.3	52.8 ± 1.0	0.0002
15	Sand + coated sand	15	0.423	0.3 mM BaCl ₂	5.8	26.1	-12.5 ± 2.0	50.9 ± 0.5	0.0002
16	Sand	0	0.425	1 mM NaCl	5.8	27.0	-28.4 ± 1.2	52.2 ± 0.9	0.0002

Values after sign (\pm) represent the standard deviation of three replicates

^a Hydrodynamic diameter of PS-NPs based on DLS analysis

^b d_p/d_c represents the ratio of Z_{ave} of PS-NP aggregates to the average diameter of sand grains

four major groups (Table S1): (1) Different mass fractions of iron oxyhydroxide-coated sand (θ) were chosen ($\theta = 0, 0.15, 0.3,$ and 0.45 g coated sand/g total sand), while maintaining constant conditions for pH (5.8) and ionic strength (1 mM NaCl).

(2) The content of oxyhydroxide-coated sand ($\theta = 0.15$) and the ionic strength (1 mM NaCl) were held constant, while the pH was adjusted to 5, 7, and 9.

(3) The content of oxyhydroxide-coated sand ($\theta = 0.15$) and the pH (5.8) were kept constant, while the ionic strength was adjusted to 1, 3, and 5 mM by adding NaCl and to 0.1, 0.3, and 0.5 mM by adding CaCl₂.

(4) Monovalent cations (3 mM NaCl, KCl, and CsCl) and divalent cations (0.3 mM MgCl₂, CaCl₂, and BaCl₂) were used while the content of iron coating ($\theta = 0.15$) and pH (5.8) was kept constant.

All experiments were performed using a PS-NP suspension with a concentration of 25 mg/L.

Glass columns with a length of 10 cm and an inner diameter of 1.2 cm were used for all experiments. The sand was dry-packed into the columns with plastic screens on both ends to avoid sand loss. For each

column, there was approximately 12.6 g dry sand and the average length of the sand-filled section of the columns was around 7.1 cm. The schematic illustration of the experimental apparatus is shown in Fig. S1 as part of the Supplementary Material. Before the experiments, the column was saturated by slowly pumping Milli-Q water into the column in an upward direction using a peristaltic pump. The columns were then flushed (flow rate of 0.15 mL/min) with 200 mL PS-NP free-background electrolyte solution until equilibrium was achieved. In order to prevent homoaggregation of the PS-NPs, each influent PS-NP solution was sonicated for 30 min by an ultrasonic bath (Bandelin Sonorex, Rangendingen, Germany). Then, 50 mL PS-NP influent was pumped into the column from a 100-mL glass beaker at a constant flow rate of 0.2 mL/min (corresponding to a residence time of ~ 270 min), followed by 15 mL PS-NP free-background electrolyte solution to remove unabsorbed PS-NPs remaining in the column. At the outlet of the column, 4-mL glass vials were used to collect the effluent solution at 15-min intervals (around 0.9 pore volumes (PV) for each sample). In

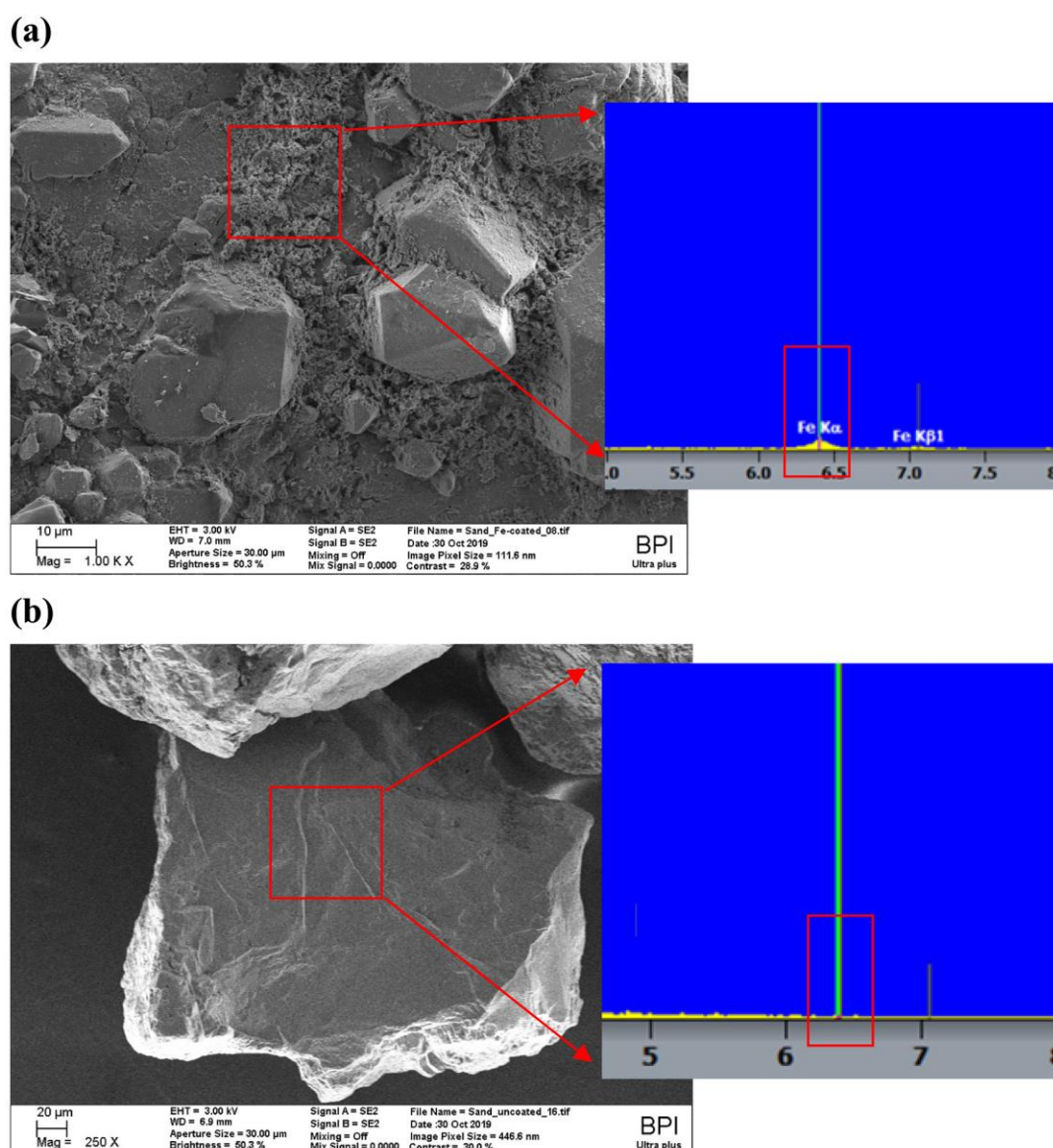


Fig. 1 The morphology and EDX analysis of **a** iron oxyhydroxide-coated sand and **b** pure quartz sand

total, 18 samples were collected for each column experiment. The fluorescent intensity of PS-NPs in each sample was measured using a fluorescence spectrometer (Perkin Elmer LS 55). The fluorescence intensity was linearly correlated to the PS-NP concentrations (the calibration curve is provided in Fig. S2). The measured concentrations of the effluent solution C were normalized to the influent solution C_0 .

The DLVO theory was used to calculate the interaction energy between PS-NPs and porous media (Huber et al., 2000; Nattich-Rak et al., 2012). Here, the detailed procedures in how the

DLVO theory was applied are provided in the Supplementary Material.

3 Results and Discussion

3.1 Effects of the Content of Iron Oxyhydroxide Coating on the Transport of PS-NPs

The retention of PS-NPs in the column increased with increasing iron oxyhydroxide content (Fig. 2). Minimum retention was observed for pure quartz sand,

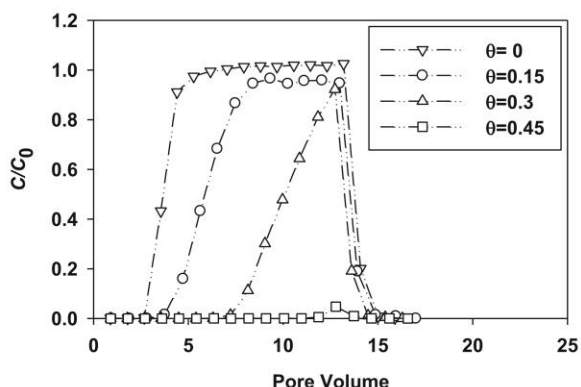


Fig. 2 Measured breakthrough curves (BTCs) of PS-NPs for different iron oxyhydroxide coating contents (θ) ranging from 0 to 0.45. All BTCs were obtained under identical conditions for pH = 5.8 and IS = 1 mM NaCl, respectively

where a breakthrough ($C/C_0 \sim 1$) was achieved within less than 5 pore volumes (PV). For an iron *oxyhydroxide* fraction of $\theta = 0.15$ (Fig. 2), $C/C_0 \sim 1$ was achieved after 7 PV. For the column experiments that used $\theta = 0.3$ and 0.45, the breakthrough concentration reached a maximum value of $C/C_0 = 0.9$ and 0.05, respectively, after approximately 13 PV.

The difference in observed BTCs could mainly be explained by the charge heterogeneity of the porous media. The point of zero charge (pH_{pzc}) of iron oxyhydroxides ranges between 8.5 and 8.8 (Cornell & Schwertmann, 2003). The pH for all iron oxyhydroxide column experiments in this study was 5.8 so that we can expect the iron oxyhydroxide coating to be positively charged. Since the PS-NPs were negatively charged (Table 1), the positively charged iron oxyhydroxides will electrostatically attract PS-NPs and provide favorable deposition sites on the surface of the coated sand grains. The increasing retention of PS-NPs observed for iron oxyhydroxide-coated sand ($\theta > 0$) can thus be explained by a higher availability of favorable deposition sites.

Scanning electron microscopy revealed a distinct difference in the morphology of the coated and uncoated sand (Fig. 1). Unlike the untreated sand, the iron oxyhydroxide-coated sand showed a rough surface (and thus a high surface area) providing many potential deposition sites for PS-NPs. Hence, in addition to attraction by favorable deposition sites, the increase in retention of PS-NPs with increasing θ could be also explained by more complex shaped pores of the iron oxyhydroxide-coated sand, resulting in smaller pore throats and an increased dead volume in the pore space (Wang et al., 2012).

3.2 Effects of pH on the Transport of PS-NPs

As shown in Fig. 3a, the pH of the suspension had a significant impact on the transport of PS-NPs in iron oxyhydroxide-coated sand ($\theta = 0.15$). Although the maximum C/C_0 values of three BTCs were close to 1, the numbers of required PVs were dependent on the pH value. At pH 5, it required around 10 PVs to reach $C/C_0 = 1$, but only 5 and 7 PVs were required at pH 7 and 9.

Such pH dependency in the retention of PS-NPs can be explained by the pH-dependent charge of the iron oxyhydroxide coating. The lower the pH, the larger the contribution of positive charges to the overall surface charge of the coating. For the case where the pH of the background solution was adjusted to 9, both the iron oxyhydroxide coatings on the sand surface and the PS-NPs were negatively charged. As a result, fewer PS-NP particles were attracted by iron oxyhydroxide, leading to increased mobility of PS-NPs at pH 9 compared to pH 5 and 7 where the iron oxyhydroxides were positively charged. Similar results were reported in Wang et al.

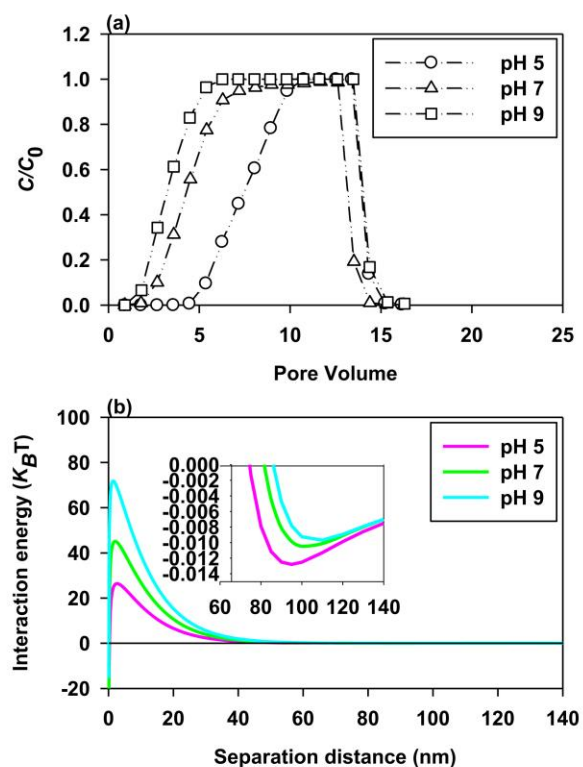


Fig. 3 Measured breakthrough curves (BTCs) of PS-NPs (a) and relative DLVO calculation results (b) at different pH ranging from 5 to 9; all BTCs were obtained under the conditions of 1 mM NaCl and a constant iron oxyhydroxide content of $\theta = 0.15$

(2012), where the absolute value of ζ -potential declined with the increasing pH resulting in less positively charged iron oxyhydroxides at higher pH values and less absorption of hydroxyapatite nanoparticles. All these aspects contribute to the apparent difference between BTCs at different pH.

DLVO theory is widely used to study the interaction energy between colloidal species and porous media (Li et al., 2019b; Lu et al., 2017). According to the interaction energy profiles calculated by DLVO theory using the dataset from Table 1 and Table S2 (see Fig. 3b), the maximum energy barriers (Φ_{\max}) were $71.8 K_B T$ at pH 9, $45.1 K_B T$ at pH 7, and $26.4 K_B T$ at pH 5. Further, the values of secondary minimum depth (Φ_{sec}) were $-0.013 K_B T$, $-0.0011 K_B T$, and $-0.009 K_B T$ at pH 5, 7, and 9, respectively. In summary, higher pH values will increase the maximum energy barrier and decrease the secondary minimum depth. The deeper Φ_{sec} is, the more likely it is that colloids will be deposited on the solid phase. In addition, when the Φ_{\max} is low, it means the colloid will likely overcome the energy barriers to deposit on the surface of the porous media. Consequently, this can explain why more PS-NPs are deposited on the sand at pH 5 compared to the higher pH values.

It further appears that physical straining, i.e., trapping of colloids in down-gradient pore throats, did not occur at the different pH values, as the PS-NPs did obviously not aggregate under the relevant conditions. In Table 1, the average values of the hydrodynamic diameter of PS-NPs were 52.7 nm at pH 5, 50.3 nm at pH 7, and 50.2 nm at pH 9, respectively. There was no significant difference between these values and the real PS-NP diameter (50 nm), which indicated an excellent dispersion of PS-NPs in the background solution. As a result, the ratio of d_p/d_c varied around 0.0002–0.0003 (d_p and d_c represent the average hydrodynamic diameter of PS-NP aggregates and the average diameter of sand grains, respectively), which was significantly below the critical value of $d_p/d_c = 0.002$ for which straining is reported to be relevant (Bradford et al., 2003).

3.3 Effects of Ionic Strength on the Transport of PS-NPs

As shown in Fig. 4a, for the monovalent electrolyte (NaCl), the mobility of PS-NPs in the columns decreased with increasing IS which is indicated by the different maximum ratios C/C_0 observed for the BTCs at different IS ($C/C_0 = 1, 0.6,$ and $0.3,$ respectively, when the IS increased from 1 to 5 mM). The

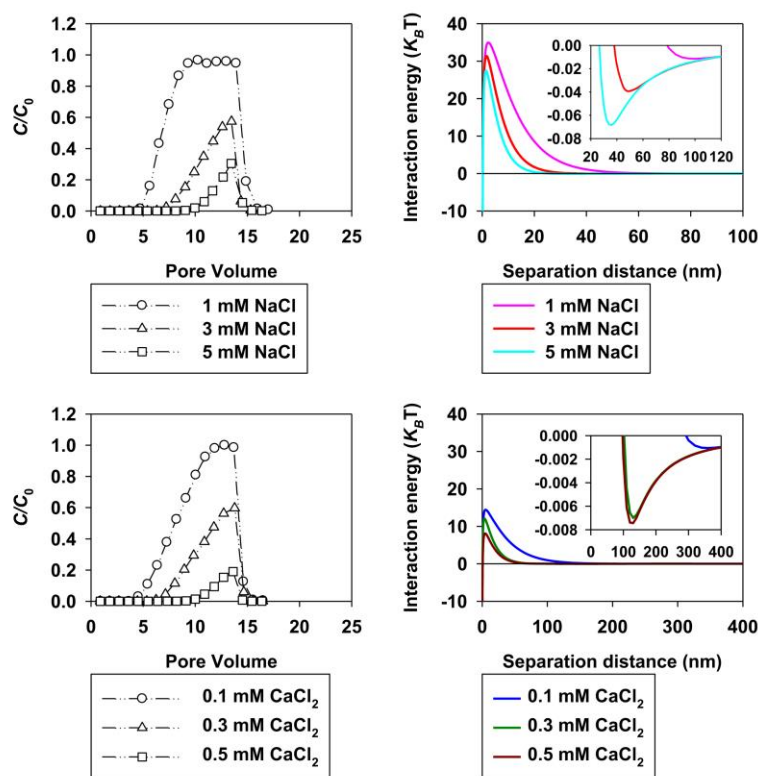
dependence of the BTCs on IS can be regarded as a blocking situation following changes in interaction energies (Quevedo and Tufenkji, 2012). At high IS (5 mM NaCl), the calculated maximum energy barrier (Φ_{\max}) and secondary minimum depth (Φ_{sec}) were lowest, which means that the PS-NPs easily can overcome the energy barrier and be subsequently deposited onto the surface of the quartz sand. Hence, PS-NP retention also increases with increasing ionic strength.

For a pH of 5.8, the iron oxyhydroxide coatings on the sand surface were positively charged for all IS experiments. With increasing IS (from 1 to 5 mM), the surface charge of PS-NPs became less negatively charged due to the compression of the electrical double layer (ζ -potential values of PS-NPs increased from -28.4 to -27.4 mV). The negatively charged PS-NPs would therefore deposit on the iron oxyhydroxide coatings. Interestingly, at higher IS, the ζ -potential values of PS-NPs decreased, which meant less PS-NPs would be attracted by the iron coatings; however, the PS-NP mobility still decreased at higher IS. Thus, the energy interactions (Φ_{\max} and Φ_{sec}) between PS-NPs and sand play a more important role in transport than iron oxyhydroxide coatings on sediment surfaces.

CaCl_2 was chosen as an example for a divalent electrolyte in the column experiments. In general, the characteristics of BTCs were similar to those observed for the monovalent electrolytes (Fig. 4c). At high IS (0.5 mM CaCl_2), the retention of PS-NPs was increased. Here, the maximum C/C_0 ratio only reached 0.2, which was lower than that at lower IS ($C/C_0 = 1$ and 0.6 at 0.1 mM and 0.3 mM CaCl_2 , respectively). The interaction energies between PS-NPs and the porous media (estimated by applying the DLVO theory) were also one of the main factors controlling the transport of PS-NPs in the IS experiments (Fig. 4d). At higher IS, both the maximum energy barrier as well as the secondary minimum were lower than those at lower IS, resulting in increased deposition of PS-NPs at high IS. Furthermore, the iron oxyhydroxide coatings still provided positively charged deposition sites for PS-NPs, as also observed in the experiments with NaCl solution.

Compared to the transport of PS-NPs in the monovalent NaCl solution, higher mobility of PS-NPs could only be achieved at the lowest CaCl_2 concentrations. Only at 0.1 mM CaCl_2 could a maximum $C/C_0 \sim 1$ be achieved, while for NaCl, $C/C_0 \sim 1$ still could be achieved for a much higher concentration of 1 mM. This discrepancy might be attributed to the bridging effect

Fig. 4 Measured breakthrough curves (BTCs) of PS-NPs (**a, c**) and relative DLVO calculation results (**b, d**) at different ionic strengths of monovalent and divalent cations (1–5 mM NaCl, 0.1–0.5 mM CaCl₂); all BTCs were obtained at pH 5.8 and a constant iron oxyhydroxide content of $\theta = 0.15$



caused by the calcium cation (Ca²⁺). Based on previous research performed by Chowdhury et al. (2014), the Ca²⁺ could work as a bridge between PS-NPs and quartz sand, resulting in higher deposition of PS-NPs onto the sand surface.

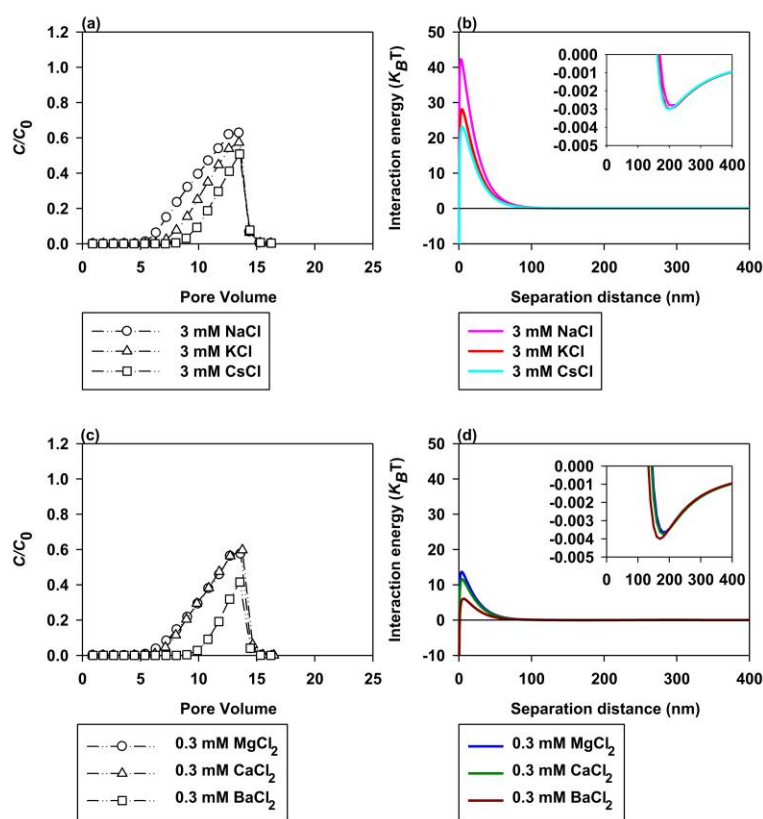
It is noted that there was no obvious PS-NP aggregation under the experimental conditions, which is in agreement with previous studies by Mitzel et al. (2016) and Quevedo and Tufenkji (2012). As shown in Table 1, the average hydrodynamic diameters of PS-NPs were around ~ 50 nm in both Na⁺ and Ca²⁺ solutions. Thus, the d_p/d_c values were well below the critical value for the straining effect (0.002). This suggested that physical straining could be neglected during transport of PS-NP.

3.4 Effects of Cation Species on the Transport of PS-NPs

Due to the differences in the mobility of PS-NPs caused by different valences of cations, we also studied the effects of different cation species on the transport of PS-NPs (Fig. 5). In general, the mobility of PS-NPs decreased according to the following sequence: Na⁺ > K⁺ > Cs⁺; Mg²⁺ ≥ Ca²⁺ > Ba²⁺.

Na⁺ had the least influence on the retention of PS-NPs, and the maximum C/C_0 was ~ 0.62. Cs⁺ exerted a significant effect on the retention of PS-NPs, and the maximum C/C_0 ratio was ~ 0.50 after 13 PV. The retention of PS-NPs for a K⁺ solution, with a maximum C/C_0 ratio of 0.57, was between that observed for Na⁺ and Cs⁺. An explanation for this phenomenon can be provided by applying the DLVO theory: In Fig. 5b, the height of the maximum energy barrier decreased in the order Na⁺ (42.3 $K_B T$) > K⁺ (28.1 $K_B T$) > Cs⁺ (23.2 $K_B T$). Consequently, for PS-NPs, it is hardest to overcome the maximum energy barrier to deposit on the sand surface when the background cation was Na⁺, followed by K⁺ and Cs⁺. The energy barriers calculated by DLVO theory could be used to explain this tendency. On the other hand, Xia et al. (2015) have shown that Cs⁺ worked as a bridging agent between graphene oxide nanoparticles and quartz sand, whereas Na⁺ and K⁺ did not seem to have such an effect. We, therefore, propose that deposition of PS-NPs on the coated sand surface in the presence of Cs⁺ was higher because Cs⁺ acts as a bridging agent between the carboxyl groups on the PS-NP surface and the coated quartz sand. In addition, the different hydrated radius of cations also affects

Fig. 5 Measured breakthrough curves (BTCs) of PS-NPs (a, c) and relative DLVO calculation results (b, d) of different cation species (monovalent (3 mM NaCl, KCl, and CsCl) and divalent cation (0.3 mM MgCl₂, CaCl₂, and BaCl₂)); all BTCs were obtained at a constant pH of 5.8 and a fixed iron oxyhydroxide content of $\theta = 0.15$



the deposition of PS-NPs on the sand surface to different extents due to the steric hindrance (accumulation of large hydrated Na⁺ ions hindering the interaction between PS-NPs and the grain surface) (Nightingale, 1959; Xia et al., 2017). In Table S3, the hydrated radius of three monovalent cations followed the order of Na⁺ > K⁺ > Cs⁺, which meant Cs⁺ had the weakest steric hindrance, followed by K⁺ and Na⁺.

The influences of divalent cations on the transport of PS-NPs are also shown in Fig. 5c. In general, the inhibition of the mobility of PS-NPs caused by divalent cations follows the following sequence: Ba²⁺ > Ca²⁺ ≥ Mg²⁺. Maximum C/C_0 ratios were ~ 0.60 for Ca²⁺ followed by Mg²⁺ with ~ 0.60 and Ba²⁺ with ~ 0.40. The energy profile of Ba²⁺ had the lowest maximum energy barrier (Φ_{max}) and the lowest secondary minimum depth (Φ_{sec}) (Fig. 5d). Thus, the PS-NPs in solution are more easily able to overcome the energy barriers to deposit on the sand surface. Interestingly, the energy profiles for Ca²⁺ and Mg²⁺ are nearly overlapping, which was in accordance with the shape of BTCs. Further, Ba²⁺ is a much stronger bridging agent than Ca²⁺ or Mg²⁺ as it tends to form inner-sphere complexes

with carboxyl groups on the PS-NP surfaces and oxygen groups on the sediment surface. In contrast, the other two ions tend to form outer-sphere complexes and thus are more weakly bound to the solid phase. Similar behavior also has been shown for graphene oxide used by Xia et al. (2015).

The physical straining effect again can be ruled out as a relevant blocking mechanism due to the stable dispersion of PS-NPs in both monovalent and divalent electrolyte solutions (no apparent aggregation was observed; Table 1).

4 Summary, Conclusions, and Implications

The main objective of this study was to investigate the mobility of NPs in water-saturated porous media under environmentally relevant conditions. Since iron oxides are abundant in many environmental compartments affected by plastic pollution (e.g., streams, hyporheic sediments, aquifers, or soils), a special emphasis was put on understanding how transport of PS-NPs is affected by iron oxides. Results from our column experiments

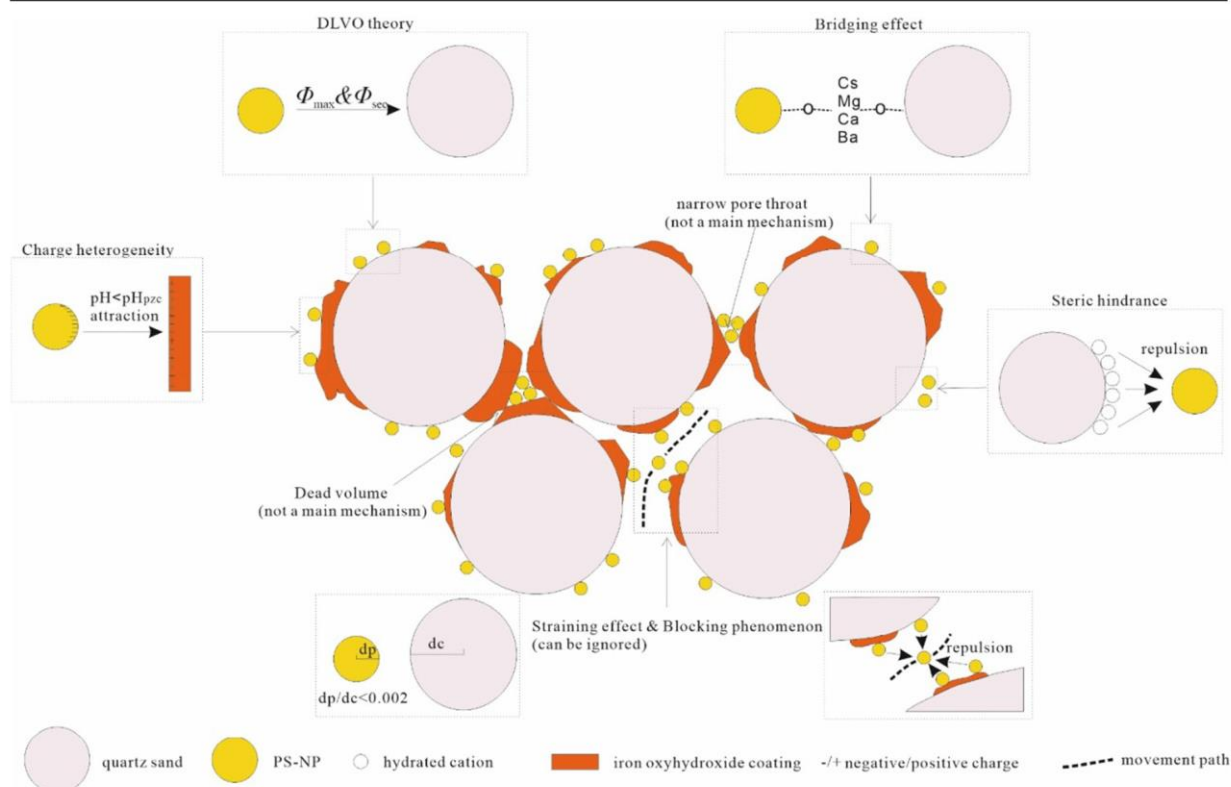


Fig. 6 The conceptual model shows the possible mechanisms that happened during the transport of PS-NPs in iron oxyhydroxide-coated sand

indicated that iron oxides with their high surface reactivity have a significant influence on the mobility of PS-NPs in the porous media. Surface charge heterogeneity of iron oxides provided favorable deposition sites for NPs leading to increased heteroaggregation behavior and lower particle mobility (Fig. 6). PS-NP particles behaved similarly to non-polymeric nanoparticles which also have been reported in the literature to have a strong tendency to aggregate with iron oxides (Han et al., 2014). Besides iron oxide contents, pore water chemistry also had an impact on the mobility of PS-NPs in porous media. Ionic strength and pH influence the ζ -potential of the polymer particles and the sand grains alike, either lowering (at low pH, high IS) or increasing (at high pH, low IS) the energy barrier for particle-grain interactions. This phenomenon successfully could be explained by the DLVO theory (Fig. 6). Finally, the type of cations in the pore water solution was also relevant for PS-NP mobility. Monovalent and divalent cations in the pore water affect the transport of PS-NPs in different ways. Cations like Cs^+ , Ca^{2+} , and Ba^{2+} act as bridging agents (Xia et al. 2017) building a connection

between the charged particle surface (O-containing functional groups) and the surface of the sand grains (Fig. 6). Physical straining, describing the blocking of pore throats by particles or aggregates (Fig. 6), only played a subordinate role as the PS particles were too small. However, the physical straining effect may be more relevant for larger NPs and especially MPs.

But how transferable are these results from controlled laboratory conditions to natural systems? Hyporheic sediments and shallow aquifers often represent regions of sharp transitions in (bio-)geochemical properties (pH, ionic strength, or redox potential) resulting in highly complex conditions of pore water chemistry (Boano et al., 2014). Iron oxides are stable under oxic conditions, but tend to be unstable and to be reduced to dissolved iron under anoxic conditions. Changes in redox conditions can also change the pH and ionic strength of pore waters as species are converted from one form to another (e.g., sulfate reduction produced alkalinity, increasing pH). Both anoxic and oxic areas can be found under natural conditions in hyporheic sediments or aquifers (Lewandowski & Nützmann,

2010). Based on our results, we believe that sediment layers with a high iron oxide content may be accumulation zones for MPs and NPs in the environment. However, it is still unclear if NPs and MPs are immobilized permanently or only temporarily under natural conditions. For streambed sediments, redox conditions can change very rapidly (e.g., due to surface water–level fluctuations, bioturbation, organic carbon input, or streambed erosion), turning oxic areas anoxic or vice versa (Krause et al., 2009). In theory, MPs and NPs even can create anoxic micro-sites in hyporheic sediments by blocking or reducing advective water flow that is supplying the pore space with oxygen from the streamflow (Fig. 6) (Briggs et al., 2015).

Re-mobilization of aggregated MPs and NPs can occur if redox conditions in the porous media change from oxic into anoxic where iron oxide minerals become unstable. Re-mobilized particles can re-enter the stream (under gaining conditions) or be transported into the shallow groundwater (under losing conditions) which can pose a threat to local drinking water supplies (Schaller et al., 1997). If the particle immobilization is permanent, sediment layers containing iron oxides may pose a high threat for the benthic organism as the very long exposure times increase the probability for uptake.

Supplementary Information The online version contains supplementary material available at <https://doi.org/10.1007/s11270-021-05125-z>.

Author Contribution Taotao Lu designed the research and performed the experiments; Hao Peng and Taotao Lu did data analysis and wrote the paper; Benjamin S. Gilfedder, Stefan Peiffer, and Sven Frei revised the manuscript and discussed the outcome of the experiments; Georg Papastavrou and Katharina Ottermann conducted the zeta potential measurement; all authors read and approved the final manuscript.

Funding This research was conducted in the context of CRC 1357 - funded by the German Research Foundation (DFG) under the project number 391977956 and the Chinese Scholarship Council (201708420145).

Data Availability The datasets used and analyzed during the current study are available from the corresponding author on reasonable request. **Supplementary Information** The online version contains supplementary material available at <https://doi.org/10.1007/s11270-021-05125-z>.

Disclosures

Ethics Approval and Consent to Participate Not applicable.

Consent for Publication Not applicable.

Conflict of Interest The authors declare no competing interests.

References

- Albertsson, A., & Karlsson, S. (1994). Chemistry and biochemistry of polymer biodegradation. In G. J. L. Griffin (Eds.), *Chemistry and Technology of Biodegradable Polymers* (pp. 7–17). Blackie Academic & Professional.
- Arthur, C., Baker, J., Bamford, H. (2008). International research workshop on the occurrence, effects, and fate of microplastic marine debris (pp. 9–11). *In: Conference Proceedings*.
- Boano, F., Harvey, J. W., Marion, A., Packman, A. I., Revelli, R., Ridolfi, L., & Wörman, A. (2014). Hyporheic flow and transport processes: mechanisms, models, and biogeochemical implications. *Reviews of Geophysics*, *52*, 603–679.
- Bouchard, D., Zhang, W., & Chang, X. (2013). A rapid screening technique for estimating nanoparticle transport in porous media. *Water Research*, *47*, 4086–4094.
- Bradford, S. A., Simunek, J., Bettahar, M., van Genuchten, M. T., & Yates, S. R. (2003). Modeling colloid attachment, straining, and exclusion in saturated porous media. *Environmental Science & Technology*, *37*, 2242–2250.
- Briggs, M. A., Day-Lewis, F. D., Zarnetske, J. P., & Harvey, J. W. (2015). A physical explanation for the development of redox microzones in hyporheic flow. *Geophysical Research Letters*, *42*, 4402–4410.
- Chowdhury, I., Duch, M. C., Mansukhani, N. D., Hersam, M. C., & Bouchard, D. (2014). Interactions of graphene oxide nanomaterials with natural organic matter and metal oxide surfaces. *Environmental Science & Technology*, *48*, 9382–9390.
- Cornell, R.M., & Schwertmann, U. (2003). *The iron oxides: structure, properties, reactions, occurrences and uses* (2nd ed.). Wiley-VCH.
- da Costa, J. P., Santos, P. S., Duarte, A. C., & Rocha-Santos, T. (2016). (Nano) plastics in the environment—sources, fates and effects. *Science of the Total Environment*, *566*, 15–26.
- Dawson, A. L., Kawaguchi, S., King, C. K., Townsend, K. A., King, R., Huston, W. M., & Nash, S. M. B. (2018). Turning microplastics into nanoplastics through digestive fragmentation by Antarctic krill. *Nature Communications*, *9*, 1001.
- Derraik, J. G. (2002). The pollution of the marine environment by plastic debris: a review. *Marine Pollution Bulletin*, *44*, 842–852.
- Elimelech, M., & O'Melia, C. R. (1990). Effect of particle size on collision efficiency in the deposition of Brownian particles with electrostatic energy barriers. *Langmuir*, *6*, 1153–1163.
- Franchi, A., & O'Melia, C. R. (2003). Effects of natural organic matter and solution chemistry on the deposition and

- reentrainment of colloids in porous media. *Environmental Science & Technology*, 37, 1122–1129.
- Frei, S., Piehl, S., Gilfedder, B., Löder, M., Krutzke, J., Wilhelm, L., & Laforsch, C. (2019). Occurrence of microplastics in the hyporheic zone of rivers. *Scientific Reports*, 9, 1–11.
- Geyer, R., Jambeck, J. R., & Law, K. L. (2017). Production, use, and fate of all plastics ever made. *Science Advances*, 3, e1700782.
- Gigault, J., ter Halle, A., Baudrimont, M., Pascal, P.-Y., Gauffre, F., Phi, T.-L., El Hadri, H., Grassl, B., & Reynaud, S. (2018). Current opinion: what is a nanoplastic? *Environmental Pollution*, 235, 1030–1040.
- Hahladakis, J. N., Velis, C. A., Weber, R., Iacovidou, E., & Purnell, P. (2018). An overview of chemical additives present in plastics: migration, release, fate and environmental impact during their use, disposal and recycling. *Journal of Hazardous Materials*, 344, 179–199.
- Han, P., Wang, X., Cai, L., Tong, M., & Kim, H. (2014). Transport and retention behaviors of titanium dioxide nanoparticles in iron oxide-coated quartz sand: effects of pH, ionic strength, and humic acid. *Colloids and Surfaces A: Physicochemical and Engineering Aspects*, 454, 119–127.
- Hanna, K. (2007). Adsorption of aromatic carboxylate compounds on the surface of synthesized iron oxide-coated sands. *Applied Geochemistry*, 22, 2045–2053.
- Huber, N., Baumann, T., & Niessner, R. (2000). Assessment of colloid filtration in natural porous media by filtration theory. *Environmental Science & Technology*, 34, 3774–3779.
- Hurley, R. R., & Nizzetto, L. (2018). Fate and occurrence of micro (nano) plastics in soils: knowledge gaps and possible risks. *Current Opinion in Environmental Science & Health*, 1, 6–11.
- Klein, S., Worch, E., & Knepper, T. P. (2015). Occurrence and spatial distribution of microplastics in river shore sediments of the Rhine-Main area in Germany. *Environmental Science & Technology*, 49, 6070–6076.
- Koelmans, A. A., Besseling, E., & Shim, W. J. (2015). Nanoplastics in the Aquatic Environment. Critical Review. In M. Bergmann, L. Gutow, & M. Klages (Eds.), *Marine Anthropogenic Litter* (pp. 325–340). Springer.
- Krause, S., Heathwaite, L., Binley, A., & Keenan, P. (2009). Nitrate concentration changes at the groundwater-surface water interface of a small Cumbrian river. *Hydrological Processes: An International Journal*, 23, 2195–2211.
- Lewandowski, J., & Nützmann, G. (2010). Nutrient retention and release in a floodplain's aquifer and in the hyporheic zone of a lowland river. *Ecological Engineering*, 36, 1156–1166.
- Li, M., He, L., Zhang, M., Liu, X., Tong, M., & Kim, H. (2019a). Cotransport and deposition of iron oxides with different-sized plastic particles in saturated quartz sand. *Environmental Science & Technology*, 53, 3547–3557.
- Li, J., Chen, J., Lu, T., Wang, Y., Zhang, H., Shang, Z., Li, D., Zhou, Y., & Qi, Z. (2019b). Effects of low-molecular weight organic acids on the transport of graphene oxide nanoparticles in saturated sand columns. *Science of the Total Environment*, 666, 94–102.
- Lu, T., Xia, T., Qi, Y., Zhang, C., & Chen, W. (2017). Effects of clay minerals on transport of graphene oxide in saturated porous media. *Environmental Toxicology and Chemistry*, 36, 655–660.
- Mattsson, K., Jovic, S., Doverbratt, I., & Hansson, L.-A. (2018). Nanoplastics in the aquatic environment. In Eddy Y. Zeng (Eds.), *Microplastic Contamination in Aquatic Environments* (pp. 379–399). Elsevier.
- Mitzel, M. R., Sand, S., Whalen, J. K., & Tufenkji, N. (2016). Hydrophobicity of biofilm coatings influences the transport dynamics of polystyrene nanoparticles in biofilm-coated sand. *Water Research*, 92, 113–120.
- Möller, J. N., Löder, M. G., & Laforsch, C. (2020). Finding microplastics in soils: a review of analytical methods. *Environmental Science & Technology*, 54, 2078–2090.
- Nattich-Rak, M., Adamczyk, Z., Sadowska, M., Morga, M., & Ócwieja, M. (2012). Hematite nanoparticle monolayers on mica: characterization by colloid deposition. *Colloids and Surfaces A: Physicochemical and Engineering Aspects*, 412, 72–81.
- Nightingale, J. E. (1959). Phenomenological theory of ion solvation. Effective radii of hydrated ions. *The Journal of Physical Chemistry*, 63, 1381–1387.
- Oriekhova, O., & Stoll, S. (2018). Heteroaggregation of nanoplastic particles in the presence of inorganic colloids and natural organic matter. *Environmental Science: Nano*, 5(3), 792–799.
- Quevedo, I. R., & Tufenkji, N. (2012). Mobility of functionalized quantum dots and a model polystyrene nanoparticle in saturated quartz sand and loamy sand. *Environmental Science & Technology*, 46, 4449–4457.
- Rodriguez-Seijo, A., & Pereira, R. (2019). Microplastics in Agricultural Soils. In Juan C. Sanchez-Hernandez (Eds.), *Bioremediation of Agricultural Soils* (pp. 45–60). CRC Press.
- Roos Lundström, F., & Martensson, A. (2015). The Journey of Plastic through Oceans: A study on quantifying micro plastic particles in ocean outside Costa Rican west coast. (Bachelor Thesis). School of Business, Engineering and Science, Halmstad University, Sweden.
- Ryan, J. N., Elimelech, M., Ard, R. A., Harvey, R. W., & Johnson, P. R. (1999). Bacteriophage PRD1 and silica colloid transport and recovery in an iron oxide-coated sand aquifer. *Environmental Science & Technology*, 33, 63–73.
- Schaller, T., Moor, H. C., & Wehrli, B. (1997). Sedimentary profiles of Fe, Mn, V, Cr, As and Mo as indicators of benthic redox conditions in Baldeggersee. *Aquatic Sciences*, 59, 345–361.
- Shani, C., Weisbrod, N., & Yakirevich, A. (2008). Colloid transport through saturated sand columns: influence of physical and chemical surface properties on deposition. *Colloids and Surfaces A: Physicochemical and Engineering Aspects*, 316, 142–150.
- Shen, C., Huang, Y., Li, B., & Jin, Y. (2008). Effects of solution chemistry on straining of colloids in porous media under unfavorable conditions. *Water Resources Research*, 44, W05419.
- Silva, A. B., Bastos, A. S., Justino, C. I., da Costa, J. P., Duarte, A. C., & Rocha-Santos, T. A. (2018). Microplastics in the environment: challenges in analytical chemistry—a review. *Analytica Chimica Acta*, 1017, 1–19.
- Silva, M. S., Oliveira, M., Valente, P., Figueira, E., Martins, M., & Pires, A. (2020). Behavior and biochemical responses of the polychaeta *Hediste diversicolor* to polystyrene nanoplastics. *Science of the Total Environment*, 707, 134434.

- Thaysen, C., Stevack, K., Ruffolo, R., Poirier, D., De Frond, H., DeVera, J., Sheng, G., & Rochman, C. M. (2018). Leachate from expanded polystyrene cups is toxic to aquatic invertebrates (*Ceriodaphnia dubia*). *Frontiers in Marine Science*, *5*, 71.
- Treumann, S., Torkzaban, S., Bradford, S. A., Visalakshan, R. M., & Page, D. (2014). An explanation for differences in the process of colloid adsorption in batch and column studies. *Journal of Contaminant Hydrology*, *164*, 219–229.
- Tripathi, S., Champagne, D., & Tufenkji, N. (2011). Transport behavior of selected nanoparticles with different surface coatings in granular porous media coated with *Pseudomonas aeruginosa* biofilm. *Environmental Science & Technology*, *46*, 6942–6949.
- Tufenkji, N., & Elimelech, M. (2005). Breakdown of colloid filtration theory: role of the secondary energy minimum and surface charge heterogeneities. *Langmuir*, *21*, 841–852.
- Wang, D., Bradford, S. A., Harvey, R. W., Gao, B., Cang, L., & Zhou, D. (2012). Humic acid facilitates the transport of ARS-labeled hydroxyapatite nanoparticles in iron oxyhydroxide-coated sand. *Environmental Science & Technology*, *46*, 2738–2745.
- Wang, M., Gao, B., Tang, D., Sun, H., Yin, X., & Yu, C. (2017). Effects of temperature on graphene oxide deposition and transport in saturated porous media. *Journal of Hazardous Materials*, *331*, 28–35.
- Wang, S., Chen, H., Zhou, X., Tian, Y., Lin, C., Wang, W., Zhou, K., Zhang, Y., & Lin, H. (2020). Microplastic abundance, distribution and composition in the mid-west Pacific Ocean. *Environmental Pollution*, *264*, 114125.
- Wang, X., Chen, L., & Yoshimura, N. (2000). Erosion by acid rain, accelerating the tracking of polystyrene insulating material. *Journal of Physics D: Applied Physics*, *33*, 1117.
- Wanner, P. (2021). Plastic in agricultural soils—a global risk for groundwater systems and drinking water supplies?—A review. *Chemosphere*, *264*, 128453.
- Wu, X., Lyu, X., Li, Z., Gao, B., Zeng, X., Wu, J., & Sun, Y. (2020). Transport of polystyrene nanoplastics in natural soils: effect of soil properties, ionic strength and cation type. *Science of the Total Environment*, *707*, 136065.
- Xia, T., Fortner, J. D., Zhu, D., Qi, Z., & Chen, W. (2015). Transport of sulfide-reduced graphene oxide in saturated quartz sand: cation-dependent retention mechanisms. *Environmental Science & Technology*, *49*, 11468–11475.
- Xia, T., Qi, Y., Liu, J., Qi, Z., Chen, W., & Wiesner, M. R. (2017). Cation-inhibited transport of graphene oxide nanomaterials in saturated porous media: the Hofmeister effects. *Environmental Science & Technology*, *51*, 828–837.
- Yousif, E., & Haddad, R. (2013). Photodegradation and photostabilization of polymers, especially polystyrene. *Springerplus*, *2*, 398.
- Zhuang, J., Qi, J., & Jin, Y. (2005). Retention and transport of amphiphilic colloids under unsaturated flow conditions: effect of particle size and surface property. *Environmental Science & Technology*, *39*, 7853–7859.

Publisher's Note Springer Nature remains neutral with regard to jurisdictional claims in published maps and institutional affiliations.

Supplementary Material Cover Sheet

Relevance of iron oxides and pore water chemistry on the mobility of nanoplastic particles in water saturated porous media environments

Taotao Lu ^{a*}, Benjamin S. Gilfedder ^{a,b}, Hao Peng ^c, Stefan Peiffer ^a, Georg Papastavrou ^d,
Katharina Ottermann ^d, Sven Frei ^a

^a Department of Hydrology, Bayreuth Center of Ecology and Environmental Research (BAYCEER), University of Bayreuth, Universitätsstraße 30, 95440, Bayreuth, Germany

^b Limnological Research Station, Bayreuth Center of Ecology and Environmental Research (BAYCEER), University of Bayreuth, Universitätsstraße 30, 95440, Bayreuth, Germany

^c School of Environmental Studies, China University of Geoscience, Wuhan, 430074, China

^d Physical Chemistry II, University of Bayreuth, Universitätsstraße 30, 95440, Bayreuth, Germany

*Corresponding author: Taotao Lu (Taotao.Lu@uni-bayreuth.de)

Manuscript prepared for *Water, Air, & Soil Pollution*

Calculation of interaction energy between particles and the pore walls using DLVO theory

The total interaction energy between particle and collector (V_{TOT}) can be defined as the sum of two interactions, the attractive van der Waals interaction (V_{VDW}) and the repulsive electrostatic double layer interaction (V_{EDL}) (Hogg et al., 1966):

$$V_{TOT} = V_{VDW} + V_{EDL} \quad (1)$$

We assumed that the contribution of the ferric oxide coating to the repulsive forces is neglectable in all experiments due to their generally positive or neutral surface charges at the experimental pH values. Therefore the interaction energy calculated for the porous medium considered only the quartz grains. This assumption may no longer hold at pH 9 and will be explicitly discussed later in the text.

The van der Waals interaction was calculated using the Hamaker approach and Gregory's formulation (Gregory, 1981):

$$V_{VDW}(h) = \frac{Ar_{NP}}{6h(1 + \frac{14h}{\lambda})} \quad (2)$$

Where A is the Hamaker constant for the system polystyrene-water-quartz sand (9.25×10^{-21} J, cf. Supplementary Material for its derivation); r_{NP} is the radius of PS-NPs (~ 50 nm, cf. Table 1); h is the separation distance between PS-NPs and quartz surface; λ is the characteristic wavelength ($\lambda = 100$ nm).

The electrical double layer interaction was calculated as (Elimelech et al., 1990; Hogg et al., 1966):

$$V_{EDL}(h) = \pi r_{NP} \epsilon_0 \epsilon_r \left\{ 2\varphi_1 \varphi_2 \ln \left[\frac{1 + \exp(-\kappa h)}{1 - \exp(-\kappa h)} \right] + (\varphi_1^2 + \varphi_2^2) \ln [1 - \exp(-2\kappa h)] \right\} \quad (3)$$

where ε_0 is the vacuum permittivity ($8.85 \times 10^{-12} \text{ C}^2/\text{Jm}$), ε_r is the relative dielectric permittivity of water (78.4), φ_1 denotes the measured zeta potential of the PS-NPs; φ_2 corresponds to the zeta potential of quartz sand. These values were obtained by Tufenkji's method (cf. Supplementary Material) (Tufenkji & Elimelech, 2004) and are listed in Table S2.

The Debye reciprocal length κ can be calculated as (Russel et al., 1989):

$$\kappa = \sqrt{\frac{2N_A e^2 I}{\varepsilon_0 \varepsilon_r K_B T}} \quad (4)$$

where N_A is the Avogadro number ($6.02 \times 10^{23} \text{ mol}^{-1}$), e is the electron charge ($-1.60 \times 10^{-19} \text{ C}$), I is the ionic strength of the background electrolyte, K_B is Boltzmann constant ($1.38 \times 10^{-23} \text{ J/K}$), and T is Kelvin temperature (298 K)

To obtain the zeta potential from electrostatic mobility

Based on the equation proposed by Henry (1948) as follows:

$$\mu = \frac{2\varepsilon_r\varepsilon_0\zeta}{3\eta} f(k\alpha) \quad (\text{S1})$$

Where μ is the electrostatic mobility, ζ is the zeta potential, η is the viscosity of electrolyte solution, ε_0 is the vacuum permittivity ($8.85 \times 10^{-12} \text{ C}^2/\text{Vm}$), ε_r is the relative permittivity (78.4), $f(k\alpha)$ is the Henry equation.

When $k\alpha$ is approaching 0, namely the ratio of particle radius to electric double layer thickness is much smaller than 1, this particle can be regarded as a point charge, and $f(k\alpha) = 1$ can be obtained, similar to Hückel equation (Hückel, 1924)

When $k\alpha$ is approaching ∞ , namely the ratio of particle radius to electric double layer thickness is much larger than 1, $f(k\alpha) = 1.5$ can be obtained, similar to Smoluchowski equation (Smoluchowski, 1921)

In this research, considering that the Smoluchowski equation is usually used to calculate zeta potentials of dispersed colloidal systems containing spherical particles, and the PS-NPs are spherical particles. As a result, $f(k\alpha)$ is 1.5

To obtain the Hamaker constant for polystyrene-water-quartz sand

The Hamaker constant for polystyrene-water-quartz sand (A) is calculated by equation S2:

$$A = (\sqrt{A_{11}} - \sqrt{A_{33}})(\sqrt{A_{22}} - \sqrt{A_{33}}) \quad (\text{S2})$$

Where A_{11} is the Hamaker constant of polystyrene (7.85×10^{-20} J) (Henry, 2004); A_{22} is the Hamaker constant of quartz sand (8.86×10^{-20} J) (Lu et al., 2017); A_{33} is the Hamaker constant of water (3.7×10^{-20} J) (Israelachvili, 1992)

To obtain the electrokinetic properties of quartz sand

10 g clean quartz sand was sonicated for 30 min in 50 mL DI water by an ultrasonic device (Bandelin Sonorex, Rangendingen, Germany). After sonication, the supernatant of samples was collected and adjusted based on different experimental conditions. After stirring for 30 min, the electrophoretic mobility of each sample was measured by a Malvern Zetasizer Nano ZS (Malvern Instruments Ltd, UK).

Table S1. Experiment settings

Groups	Iron oxyhydroxide-coated sand content	PS-NPs concentration	pH	Ionic strength	Cation species
Effects of different contents of iron coatings	0	25 mg/L	5.8	1 mM NaCl	-
	0.15	25 mg/L	5.8	1 mM NaCl	-
	0.3	25 mg/L	5.8	1 mM NaCl	-
	0.45	25 mg/L	5.8	1 mM NaCl	-
	0.15	25 mg/L	5.0	1 mM NaCl	-
Effects of pH	0.15	25 mg/L	7.0	1 mM NaCl	-
	0.15	25 mg/L	9.0	1 mM NaCl	-
	0.15	25 mg/L	5.8	1 mM NaCl	-
	0.15	25 mg/L	5.8	3 mM NaCl	-
Effects of IS	0.15	25 mg/L	5.8	5 mM NaCl	-
	0.15	25 mg/L	5.8	0.1 mM CaCl ₂	-
	0.15	25 mg/L	5.8	0.3 mM CaCl ₂	-
	0.15	25 mg/L	5.8	0.5 mM CaCl ₂	-
	0.15	25 mg/L	5.8	-	3 mM NaCl
Effects of cation species	0.15	25 mg/L	5.8	-	3 mM KCl
	0.15	25 mg/L	5.8	-	3 mM CsCl
	0.15	25 mg/L	5.8	-	0.3 mM MgCl ₂
	0.15	25 mg/L	5.8	-	0.3 mM CaCl ₂
	0.15	25 mg/L	5.8	-	0.3 mM BaCl ₂

Table S2. Calculated maximum energy barriers (Φ_{\max}), secondary energy minimum depth (Φ_{sec}), and the respective separation distances of particle–collector DLVO interaction energy profiles

Minerals	Background solution		ζ potential (mV)	Φ_{\max}		Φ_{sec}	
	IS	pH		height ($K_B T$)	distance (nm)	depth ($K_B T$)	distance (nm)
	1 mM NaCl	5.8	-48.1 ± 0.6	35.5	2.4	-0.012	100
	1 mM NaCl	5	-42.7 ± 1.2	26.4	2.7	-0.013	95
	1 mM NaCl	7	-53.6 ± 0.8	45.1	2.1	-0.011	100
	1 mM NaCl	9	-58.5 ± 0.9	71.8	1.5	-0.009	110
	3 mM NaCl	5.8	-46.9 ± 0.9	42.3	2.9	-0,003	220
	5 mM NaCl	5.8	-46.4 ± 0.5	31.1	1.5	-0.046	45
Quartz sand	0.1 mM CaCl ₂	5.8	-24.1 ±0.5	14.4	5.4	-0.001	340
	0.3 mM CaCl ₂	5.8	-24.8 ± 1.1	13,7	3,9	-0,004	180
	0.5 mM CaCl ₂	5.8	-22.8 ± 0.4	8.1	4.4	-0.007	130
	3 mM KCl	5.8	-44.6 ± 1.2	28,1	4,2	-0,003	200
	3 mM CsCl	5.8	-42.9 ± 0.7	23,2	4,6	-0,003	200
	0.3 mM MgCl ₂	5.8	-24.7 ± 0.5	11,6	4,4	-0,004	180
	0.3 mM BaCl ₂	5.8	-22.5 ± 0.9	6,0	6,5	-0,004	170

Table S3. The hydrated radii of monovalent and divalent cations

Cation species	Hydrated Radii (Å) (Nightingale, 1959)
Na ⁺	3.58
K ⁺	3.31
Cs ⁺	3.29
Mg ²⁺	4.28
Ca ²⁺	4.12
Ba ²⁺	4.04

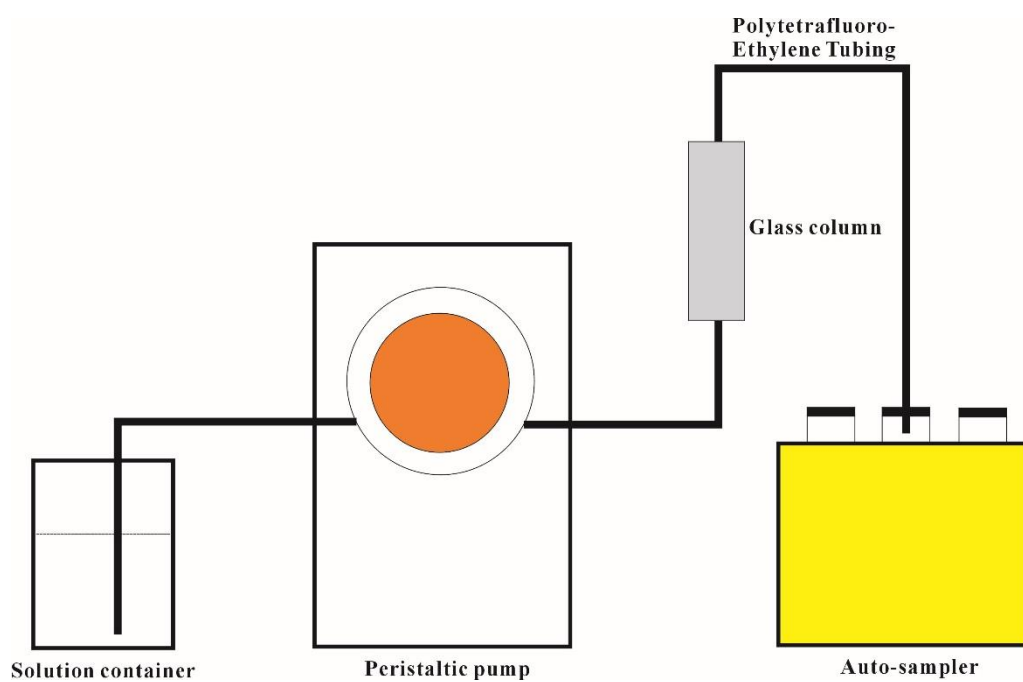


Fig. S1 Schematic illustration of experimental apparatus of column tests.

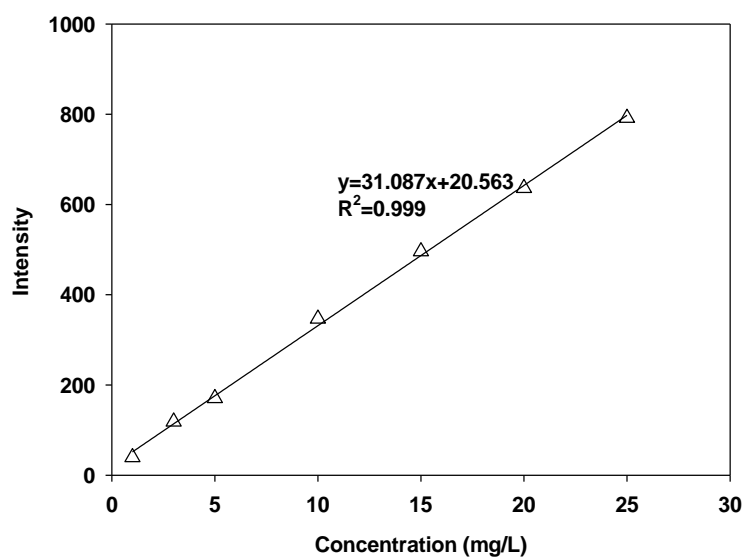


Fig. S2 Calibration curves as the intensity at the excitation wavelength of 441 nm and an emission wavelength of 486 nm versus concentration of PS-NPs in suspension.

References

- Elimelech, M., O'Melia, C.R. (1990). Effect of particle size on collision efficiency in the deposition of Brownian particles with electrostatic energy barriers. *Langmuir*, 6, 1153–1163.
- Gregory, J. (1981). Approximate expressions for retarded van der waals interaction. *Journal of Colloid and Interface Science*, 83,138–145.
- Henry, M. (2004). Nanocrystals from Solutions and Gels. In Encyclopedia of Nanoscience and Nanotechnology. *American Scientific Publishers*.
- Henry, D.C. (1948). The electrophoresis of suspended particles. IV. The surface conductivity effect. *Transactions of the Faraday Society*, 44, 1021–1026.
- Hogg, R., Healy, T.W., Fuerstenau, D.W. (1966). Mutual coagulation of colloidal dispersions. *Transactions of the Faraday Society*, 62, 1638.
- Hückel, E. (1924). Die kataphorese derkugel. *Physikalische Zeitschrift*, 25, 204–210.
- Israelachvili, J.N. (1992). Intermolecular and Surface Forces. *Academic Press: San Diego, CA*
- Lu, T., Xia, T., Qi, Y., Zhang, C., Chen, W. (2017). Effects of clay minerals on transport of graphene oxide in saturated porous media. *Environmental Toxicology and Chemistry*, 36, 655–660.
- Russel, W.B., Saville, D.A., Schowalter, W.R. (1989). Colloidal Dispersions. *Cambridge University Press, Cambridge*.
- Tufenkji, N., Elimelech, M. (2004). Deviation from the classical colloid filtration theory in the presence of repulsive DLVO interactions. *Langmuir*, 20(25), 10818–10828.
- Von Smoluchowski, M. (1921). In Greatz E (ed) Handbuch der Elektrizität und des Magnetismus. *Barth, Leipzig*

Study 4: Effects of clay minerals on the transport of nanoplastic particles in water-saturated porous media

Taotao Lu, Benjamin S. Gilfedder, Hao Peng, Geng Niu, Sven Frei

Under review in *Science of the Total Environment*

Under review

Effects of clay minerals on the transport of nanoplastic particles in water-saturated porous media

Taotao Lu ¹, Benjamin S. Gilfedder ^{1,2}, Hao Peng ³, Geng Niu ⁴, Sven Frei ¹

¹ Department of Hydrology, Bayreuth Center of Ecology and Environmental Research (BAYCEER), University of Bayreuth, Universitätsstraße 30, 95440, Bayreuth, Germany

² Limnological Research Station, Bayreuth Center of Ecology and Environmental Research (BAYCEER), University of Bayreuth, Universitätsstraße 30, 95440, Bayreuth, Germany

³ School of Environmental Studies, China University of Geoscience, Wuhan, 430074, China

⁴ Wuhan Zondy W&R Environmental Technology Co., Ltd, Wuhan 430078, China

Abstract

Clay minerals are important constituents of porous media. To date, only little is known about the transport and retention behavior of nanoplastics in such clay-containing sediments. In order to investigate the effects of clay minerals on the mobility of nanoplastic particles in saturated porous media, polystyrene nanoplastic particles (PS-NPs) at different pH and ionic strengths (IS) were pumped through columns packed with sand and clay minerals (kaolinite and illite). In general, the retention of PS-NPs resulting from the increasing clay contents was attributed to physical straining effects (the smaller pore throat and more complex flow pathways). In addition, the varying pH and IS altered the surface charges of both PS-NPs and porous media and thus affecting the interaction energy. For example, when the IS increased from 10 mM to 50 mM NaCl, the zeta potential of PS-NPs and porous media became less negative, and the maximum energy barrier and secondary minimum decreased. Thus, the maximum C/C_0 ratio decreased from ~51% to ~0% (pH 5.9, 3% kaolinite). Among the two clay minerals, kaolinite showed a stronger inhibitory effect on PS-NPs transport compared to illite. For instance, at the same condition (3% clay content, pH 5.9, 10 mM NaCl), the $(C/C_0)_{\max}$ of PS-NPs in kaolinite was ~51%, while that in illite was ~77%. The difference in transport inhibition was mainly attributed to amphoteric sites on the edges of kaolinite which served as favorable deposition sites at pH 5.9 ($\text{pH}_{\text{pzc-edge}}$ is ~2.5 for illite and ~6.5 for kaolinite). Results and conclusions from the study will provide some valuable insights to better understand the fate of NPs in the soil-aquifer system.

Keywords: Polystyrene nanoplastic; Transport; Clay minerals; Amphoteric edge sites

Introduction

Plastic polymers are widely used materials that can be found in many different products such as electronic devices, cosmetics, packaging materials, and medical products (da Costa et al., 2016). In 2017 plastic production was reported to surpass 8300 million metric tons (Geyer et al., 2017). Increasing production and usage of plastic products is associated with an increase in plastic pollution and improper release into the environment. Larger plastic fragments are affected by natural degradation and fragmentation processes such as abrasion, weathering, and UV/photo-oxidation (Silva et al., 2018; Yousif and Haddad, 2013), processes

43 that eventually produce nano-scale plastic particles (<100 nm, NPs) (Dawson et al., 2018;
44 Gigault et al., 2018). Distribution and transport mechanisms as well as hazardous effects of
45 NPs in the environment are only poorly understood and recently have become a major focus
46 for environmental research (Chae and An, 2017; Koelmans et al., 2015; Yu and Flury, 2021).

47 Transport characteristics of NPs in saturated porous media in the past have been
48 addressed by various experimental as well as modeling studies (Dong et al., 2020; Mitzel et
49 al., 2016; Quevedo and Tufenkji, 2012; Shaniv et al., 2021; Wu et al., 2020). Most of these
50 studies primarily focus on how NPs mobility was influenced by pore water chemistry (e.g.,
51 pH, ionic strength, and ionic species) using pure quartz sand as the porous media (Franchi and
52 O'Melia, 2003; Mitzel et al., 2016; Quevedo and Tufenkji, 2012). Pure quartz sand seldomly
53 can be found in natural subsurface environments such as soils, streambeds, lake sediments or
54 aquifers. In these systems, clay minerals, metal oxides, and soil organic matter are abundant
55 materials which are known to interact differently with NPs compared to pure quartz sand (Lu
56 et al., 2021; Wu et al., 2020). For example, Lu et al. (2021) observed that the presence of iron
57 oxides strongly reduces the mobility of NPs by electrostatic attraction processes. Wu et al.
58 (2020) proposed that the charge heterogeneity caused by iron oxides and clay minerals in
59 different soils exerted significant inhibition on NPs transport.

60 Clay minerals are typically characterized by permanent and variable charge components
61 (Schoonheydt and Johnston, 2006). The permanent charge is caused by the isomorphous
62 substitution in the lattice structure of sheet silicates (e.g., Al^{3+} for Si^{4+} in silicon-oxygen
63 tetrahedrons; Mg^{2+} and Fe^{2+} for Al^{3+} in aluminum-oxygen octahedra) of the clay minerals;
64 and variable charge results from broken edges of silicate minerals (Singh et al., 2014).
65 Variable charge components in clay minerals are more easily affected by the composition of
66 pore water chemistry (Van Alfen, 2014). The variable surface charge results in a large number
67 of potential amphoteric exchange sites under environmentally relevant conditions (pH values
68 between 4.5–9.0) (Marazuela and García-Fresnadillo, 2020; Mc Bride, 1989; Shivangi et al.,
69 2020), which in turn provide favorable deposition sites to negatively charged or positively
70 charged nanoparticles. Lu et al. (2017) found that at pH 5 the variable charges of kaolinite and
71 montmorillonite were positive, as the point of zero charge at edge sites was around pH~6.5,
72 leading to apparent inhibition of graphene oxide transport. Clay minerals have different
73 degrees of isomorphous substitution on the basal plane as well as different
74 protonation/deprotonation ability at the edge sites, which can result in the various surface
75 charges of clay minerals (Murray, 2000). The surface charge of 2:1 (one octahedral sheet to
76 two tetrahedral sheets) clay minerals (e.g., montmorillonite and illite) is dominated by
77 permanent negative charges, whereas that of 1:1 (one tetrahedral sheet to one octahedral
78 sheet) clay minerals (e.g., kaolinite) is mainly governed by variable charges (Bergaya and
79 Lagaly, 2013). Consequently, different clay minerals are likely to exert non-uniform
80 influences on NP transport in porous media. To date, only little is known about the effects of
81 clay minerals on the transport of NPs. In the study of Li et al. (2020), it was shown that PS-
82 NPs formed heteroaggregates with kaolinite colloids due to the surface chemical
83 heterogeneity of kaolinite, significantly affecting the mobility of NPs resulting from the
84 formation of clusters with kaolinite.

85 The main purpose of this study is to gain a more fundamental understanding on how the
86 transport of NPs is affected by the presence of clay minerals (kaolinite (1:1 type) and illite

87 (2:1 type)). The columns packed with a mixture of quartz sand and variable contents of clay
88 minerals were prepared for the experiment under the different pH and IS conditions.
89 Breakthrough curves of the NPs were obtained and evaluated to quantify NPs retention.
90 Derjaguin–Landau–Verwey–Overbeek (DLVO) theory was applied to estimate particle-porous
91 media interaction energies to understand the retention tendency of NPs under non-uniform pH
92 and IS. The following research hypotheses were formulated: 1) Due to the different types of
93 surface charges (permanent and variable charge components), the 1:1 and 2:1 clay minerals
94 affect the mobility of NPs to different degrees. As the variable charge is more easily
95 influenced by pore water chemistry, the effect of 1:1 clay mineral on the retention of NPs is
96 more significant. 2) The pH and IS of the pore water affect the transport and retention of NPs
97 by modifying the surface charge and interaction energies of both NPs and clay minerals. 3)
98 Physical straining exerts a significant impact on the mobility of NPs due to the small size of
99 clay minerals.

100

101 **Materials and methods**

102 *Materials*

103 Polystyrene nanoplastic particles (PS-NPs), modified with a layer of carboxylate groups
104 to improve their suspension performance (Huge Biotechnology Co., Ltd, China), were used as
105 model NPs. The PS-NPs were spheres with an average diameter of 100 nm and a density of
106 1.05 g cm^{-3} . The stock solution (100 g L^{-1}) was diluted by Milli-Q water to achieve the
107 suspension with a concentration of 15 mg L^{-1} .

108 Quartz sand with a mean diameter of 0.29 mm was obtained from Minerals Trading Co.,
109 Ltd (Huangshi, China). The sand was cleaned to remove metal oxides and organic impurities
110 before use (described in supplementary material). Kaolinite and illite were obtained from
111 Junhong New Materials Co., Ltd (Datong, China) and montmorillonite was purchased from
112 Macklin Biochemical Co., Ltd (Shanghai, China). The particle size distribution of the clay
113 minerals was measured using a particle size analyzer (Mastersizer-2000, Malvern Instruments
114 Ltd, UK); the size distributions can be found in Figure S1.

115

116 *Column experiments*

117 Detailed experimental protocols are provided as part of the supplementary material (see
118 Table S1). Column experiments were conducted using borosilicate glass columns (Shanghai
119 SuKe Industrial Co., Ltd.) with an inner diameter of 1.6 cm and a length of 20 cm, with
120 stainless-steel screens on both ends. The columns were operated vertically using syringe
121 pumps (TYD02, Lead Fluid Technology, Co., Ltd). Kaolinite and illite powders were mixed
122 with the quartz sand to achieve clay contents in the range of 1–5% (wt:wt) of the porous
123 media. The mixture was dry-packed into the columns to achieve a uniform distribution of clay
124 minerals. Each column contained approximately 21 g of porous media with an effective
125 length of $6.0 \pm 0.1 \text{ cm}$. The packed columns were saturated and equilibrated from bottom to
126 top by sequentially flushing with 50 mL Milli-Q water at a flow rate of 3.0 mL h^{-1} followed
127 by 100 mL background electrolyte solution. All influents were prepared immediately before
128 each column experiment. The pH was adjusted with 0.1 M HCl or 0.1 M NaOH, and the IS
129 was adjusted by 0.1 M NaCl. During the column experiments, the influent was pumped into
130 the column using a 100-mL glass syringe (Shanghai Bolige Industry & Trade Co.), followed

131 by a PS-NPs-free background electrolyte solution (until the effluent concentration of PS-NPs
132 was below the detection limit) at a flow rate of 10 mL h^{-1} . Column effluent samples were
133 collected by the automatic fraction collector (BSZ-40, Shanghai Qingpu Huxi Instrument
134 Factory) with glass vials at predetermined time intervals. A UV spectrophotometer (UV-8000,
135 Shanghai Metash Instruments Co., Ltd) was used to measure the absorbance of PS-NPs at 220
136 nm. The concentrations of PS-NPs were determined based on a pre-established calibration
137 curve (see Figure S2). All column experiments were repeated 2 times to ensure data
138 reliability.

139 Electrophoretic mobility (EPM) and hydrodynamic diameter (D_h) of PS-NPs in the
140 influents were measured with a Malvern Zetasizer Nano ZS (Malvern Instruments Ltd, UK).
141 Zeta potentials of the PS-NPs were derived from electrophoretic mobility using the
142 Smoluchowski equation considering the spherical shape of the PS-NPs; the values are
143 provided in the supplementary material (Table S2). The particle–collector interaction energy
144 profiles were calculated using the DLVO theory (detailed equations are provided in the
145 supplementary material). The calculated profiles are shown in Figures S3 and S4. The values
146 of the maximum energy barriers and secondary minimum depth are listed in Table 1.

147

148 **Results and discussion**

149 *Effects of clay minerals on the transport of PS-NPs*

150 When mixed with quartz sand, kaolinite and illite showed significant effects on the
151 transport of PS-NPs, where the extent of particle retention depended on the specific clay
152 mineral and the clay contents (Figure 1). For pure quartz sand (Column 1, Table S1), a
153 breakthrough of $\sim 90\%$ (i.e., C/C_0 is the ratio of effluent PS-NPs concentration, C , to influent
154 PS-NPs concentration, C_0) of the injected PS-NPs was reached after ~ 2 Pore volumes (PV),
155 indicating that only little PS-NPs were retained in the column. For this reference experiment,
156 the zeta potentials of PS-NPs and quartz sand were both negative (Table 2). Given the large
157 values for the secondary minimum (Φ_{sec}) and maximum energy barriers (Φ_{max}) (Table 1),
158 limited deposition of PS-NPs onto the surface of the quartz sand and, in turn, high mobility of
159 NPs was as expected. This observation is also consistent with findings from other literature
160 (Pradel et al., 2020). The presence of kaolinite minerals in the quartz sand resulted in
161 significantly increased retention of PS-NPs. For a kaolinite content of 1%, the gradient of the
162 breakthrough curve (Figure 1(a)) was much lower than the reference experiment with pure
163 quartz sand. Further, the observed maximum C/C_0 ratio ($(C/C_0)_{\text{max}}$) of the breakthrough curve
164 only reached $\sim 73\%$ after 7 PV. Even higher retentions of PS-NPs were observed for 3% and
165 5% kaolinite contents, and more PV were needed for PS-NPs breaking through the column
166 (Figure 1(a)). For the content of 5% kaolinite, no breakthrough of PS-NPs could be observed
167 at the outlet by the end of the experiment. The presence of illite also resulted in inhibited
168 transport of PS-NPs; however, the effects were less pronounced compared to kaolinite with
169 $(C/C_0)_{\text{max}} \sim 34\%$ at 5% illite content (Figure 1(b)).

170 To understand why there is a significant difference in inhibition of PS-NPs for the two
171 different clay minerals, the interaction energy profiles between PS-NPs and each of the clay
172 minerals were calculated and compared to the pure quartz sand (Figure 1(c)). For kaolinite,
173 the zeta potentials of kaolinite and quartz sand were -38.1 mV and -63.4 mV , respectively, and
174 the maximum energy barrier ($\Phi_{\text{min}} = 142 K_B T$) and the secondary minimum depth ($\Phi_{\text{sec}} = -0.10$

175 $K_B T$) indicated that the deposition tendency of PS-NPs onto the surface of the kaolinite
176 minerals is higher compared to pure quartz sand. As a result, the increase in kaolinite contents
177 is associated with higher retention of PS-NPs. Interestingly, for illite, the Φ_{\min} ($351 K_B T$) and
178 Φ_{sec} ($-0.09 K_B T$) were higher compared to those of quartz sand ($\Phi_{\min} = 318 K_B T$ and $\Phi_{\text{sec}} = -$
179 $0.10 K_B T$). The zeta potential of illite with -67.7 mV was more negative compared to those
180 estimated for quartz sand with -63.4 mV, indicating that the PS-NPs should deposit
181 preferentially onto the sand grains rather than the illite minerals. Given the interaction
182 energies and zeta potentials, a different mechanism is necessary to explain the observed
183 retention of PS-NPs in the experiments with illite minerals.

184 For 2:1 type clay mineral, such as illite, the permanent charge dominates the particle-
185 mineral interactions, while for 1:1 type minerals (kaolinite), the interaction is controlled by
186 the variable charge. The variable charge resulting from amphoteric sites, such as octahedral
187 Al–OH sites at broken edges and exposed hydroxyl-terminated planes of crystalline structures
188 (Keren and Sparks, 1995; Kriaa et al., 2009; Tombácz and Szekeres, 2006), depend on the pH
189 of the pore water solution due to the protonation/deprotonation of these functional groups
190 (Kim et al., 2012; Tombácz and Szekeres, 2006). The pH_{PZC} values of the edge sites for
191 kaolinite lie at ~ 6.5 (Tombácz and Szekeres, 2006) but only at ~ 2.5 for illite (Hussain et al.,
192 1996). Since the experiments were conducted at pH 5.9, it is reasonable to propose that a
193 significant fraction of the edge sites of kaolinite were positively charged (even though the net
194 charges of these clay minerals were still negative). These positively charged sites provide
195 favorable deposition sites for the negatively charged PS-NPs. For increasing kaolinite
196 contents, more positively charged edge sites were available, resulting in increased retention of
197 PS-NPs. In comparison, the edge sites of illite were negatively charged under pH 5.9.
198 Consequently, the observed retention of PS-NPs for experiments performed with illite
199 minerals cannot be explained by edge site interactions.

200 Another retention mechanism, associated with the presence of clay minerals, could be
201 the blockage or narrowing of pores inhibiting the mobility of PS-NPs in the porous media.
202 The average sizes of the clay minerals ($d(0.5) = 8.6 \mu\text{m}$ and $d(0.9) = 28.7 \mu\text{m}$ for kaolinite;
203 $d(0.5) = 4.5 \mu\text{m}$ and $d(0.9) = 13.9 \mu\text{m}$ for illite) were much smaller compared to quartz sand
204 ($d(0.5) = 292 \mu\text{m}$ and $d(0.9) = 451 \mu\text{m}$) (Figure S1). Thus, the clay minerals may alter the flow
205 pathways by creating narrower pore throats and dead-end pores (Lu et al., 2017; Qi et al.,
206 2014). This enhances the retention of PS-NPs through physical straining effects. In addition,
207 clay minerals under environmentally relevant conditions can contain metal and metal oxide
208 impurities due to different degrees of weathering (Bayat et al., 2015; Singer, 1984). It has
209 been reported that even small amounts of metal oxides can significantly affect the transport
210 behavior of negatively charged particles (Wu et al., 2020; Yang et al., 2011). However, due to
211 the high quality of the clay minerals used in this study, the retention of PS-NPs associated
212 with the presence of impurities played only a minor role, and physical straining effects for
213 illite were identified as the major mechanism to explain observed retention.

214

215 *pH-dependent transport-inhibition effects of different clay minerals*

216 For the two clay minerals, pH had a significant influence on the transport behavior of
217 PS-NPs (Figure 2). For kaolinite, significant retention was observed at pH 5.9; the $(C/C_0)_{\text{max}}$
218 was $\sim 51\%$ at ~ 8 PV. With the increase of pH, retention of PS-NPs gradually became lower,

219 and at pH 9.0, the $(C/C_0)_{\max}$ reached 80.4% after ~8 PV. Similarly, for illite, the strongest
220 retention of PS-NPs was found at pH 5.9 ($(C/C_0)_{\max} = 77\%$ at ~9 PV). Interestingly, at pH 7.0
221 and 9.0, the breakthrough curves of PS-NPs were almost identical, where $(C/C_0)_{\max}$ with
222 ~95% was achieved after only 2 PV.

223 For kaolinite, considering the $\text{pH}_{\text{PZC-edge}}$ value of kaolinite which lies around ~6.5
224 (Tombácz and Szekeres, 2006), the edge sites of kaolinite are positively charged at pH 5.9 but
225 negatively charged at pH 7.0 and 9.0. Consequently, retention of PS-NPs is significantly
226 diminished at $\text{pH} > 7.0$. Absolute values of the zeta potential for both PS-NPs and clay
227 minerals increased with increasing pH (Table 2). For example, zeta potentials for kaolinite
228 were -38.1 mV, -49.2 mV, -69.6 mV at pH 5.9, 7.0, and 9.0, respectively, indicating that
229 deposition of PS-NPs is becoming more difficult at higher pH. Results from the DLVO
230 calculation (Figure S3(a)) also support this conclusion. For illite, much weaker pH
231 dependencies were observed. Under all test conditions, the edge sites of illite were still
232 negatively charged due to the low $\text{pH}_{\text{pzc-edge}}$ of ~2.5. The permanent charge of illite seems to
233 be more critical for the transport of PS-NPs. At pH 5.9, the zeta potential of illite was -67.7
234 mV (Table 2), while the one of quartz sand was -63.4 mV. Thus, it seemed that the PS-NPs
235 more easily deposited onto the surface of quartz sand compared to illite, which also can be
236 seen by the energy interaction profiles shown in Figure S3(b, c). As a result, at pH 5.9, most
237 of the PS-NPs deposited onto the sand surface resulting in lower C/C_0 values. While at pH 7.0
238 and 9.0, the zeta potential values of illite were -75.2 mV and -75.4 mV, which were less
239 negative than those of quartz sand (-77.2 mV at pH 7.0; -88.8 mV at pH 9.0). Hence, PS-NPs
240 preferentially deposited onto illite rather than quartz sand. Due to the similar zeta potentials
241 and interaction energies (see Figure S3(b)), the breakthrough curves of PS-NPs in the
242 presence of illite essentially overlapped over a pH range of 7.0 and 9.0.

243 For all tested pH values, the magnitude of PS-NPs retention for kaolinite exceeded that
244 of illite. At low pH (5.9), the transport-inhibiting effects of the clay minerals were mainly
245 attributable to the existence of positively charged edge sites. Kaolinite contained positively
246 charged edge sites, while the edge sites of illite were negatively charged. To further illustrate
247 the importance of edge site charge effects, we performed a column experiment with 3%
248 montmorillonite at pH 5.9 (see Figure 3(a)). Although the zeta potential of montmorillonite
249 was more negative than that of kaolinite at pH 5.9 and the interaction energy between PS-NPs
250 and montmorillonite was higher compared to PS-NPs and kaolinite, the mobility of PS-NPs in
251 montmorillonite seemed to be similar to that observed for kaolinite (Figure 3(b)). Further, the
252 particle size distribution of montmorillonite was almost identical to kaolinite (Figure S1). We
253 propose that the edge sites charge of montmorillonite exerted a dominant influence on the
254 mobility of PS-NPs. The $\text{pH}_{\text{PZC-edge}}$ value of montmorillonite is ~6.5 (Tombacz and Szekeres,
255 2004), which is similar to that of kaolinite. At pH 5.9, the edge sites of montmorillonite are
256 positively charged causing similar retention of PS-NPs.

257 At pH 7.0, the $(C/C_0)_{\max}$ of PS-NPs was 72% in kaolinite and 95% in illite; the difference
258 between the $(C/C_0)_{\max}$ values was 23%. In comparison, the $(C/C_0)_{\max}$ was 80% in kaolinite and
259 96% in illite at pH 9.0; a difference of 16%. With increasing pH, the difference becomes
260 smaller. As the surface charges of 1:1 clay mineral are mainly composed of the variable
261 charge which depends on the pH, the zeta potential of kaolinite varies remarkably at different
262 pH values (-38.1 mV at pH 5.9; -49.2 mV at pH 7.0; -69.6 mV at pH 9.0). However, the

263 surface potentials of 2:1 clay mineral are mainly related to the permanent charge that is
264 insensitive to pH variations. Unlike kaolinite, the zeta potential of illite were relatively stable
265 (-67.7 mV at pH 5.9; -75.2 mV at pH 7.0; -75.4 mV at pH 9.0). Despite this, the surface
266 potential of illite was still more negative than that of kaolinite at the same pH, which led to
267 less inhibition of PS-NPs transport in illite.

268 *Ionic strength-dependent transport-inhibition effects of different clay minerals*

269 As shown in Figure 4, at a pH value of 5.9, IS played an important role in the transport
270 of PS-NPs in the columns. For kaolinite, the $(C/C_0)_{\max}$ decreased with increasing IS. At an IS
271 of 10 mM NaCl, the $(C/C_0)_{\max}$ was ~51% and by increasing the IS to 50 mM NaCl the
272 corresponding $(C/C_0)_{\max}$ dropped to ~0% (Figure 4(a)). A similar tendency also was found for
273 illite (Figure 4(b)). As the clay content and pH were kept constant, edge site charge effects
274 and physical straining can be ignored in the same clay mineral columns. Consequently, the
275 influence of IS on the surface charge of both PS-NPs and the porous media was the
276 controlling factor for the mobility of PS-NPs. The zeta potentials of PS-NPs were -78.9, -69.4,
277 and -61.7 mV at 10, 30, and 50 mM NaCl (Table 1) while the zeta potentials of kaolinite were
278 -38.1, -33.7 and -31.7 mV at 10, 30 and 50 mM NaCl, respectively. The surface charge of
279 both particles and porous media became less negative due to the compression of the double
280 layer with increasing IS. This mechanism could also be applied for illite. At higher IS, it is
281 more favorable for PS-NPs to deposit on the surface of the clay minerals and sand. This is
282 also supported by the DLVO theory in Figure S4.

283 For all tested IS, retention effects were generally higher for kaolinite compared to illite.
284 At pH 5.9, the $pH_{PZC-edge}$ value for kaolinite was ~6.5 and 2.5 for illite; thus the edge sites of
285 kaolinite were positively charged and those of illite were negative. The positively charged
286 edge sites of kaolinite provided favorable deposition sites for the negatively charged PS-NPs.
287 Furthermore, the zeta potentials of illite are more negative compared to kaolinite at the same
288 IS (Table 1). In addition, by comparing the PS-NPs-clay mineral interaction energy profile
289 (Figure S4), both Φ_{\max} and Φ_{\min} of PS-NPs-illite were higher compared to PS-NPs-kaolinite at
290 the same IS. Due to the similar size distribution of kaolinite and illite minerals, flow routes
291 (pore-throat and dead-volume) can be considered as identical (i.e., physical straining effects
292 can be ignored).

293 **Conclusion**

294 Clay minerals are important components of natural sediments. The findings here
295 demonstrated how significantly transport and retention of NPs are controlled by the specific
296 type and content of clay minerals, which are ubiquitous in natural subsurface environments.
297 Variable charge sites, preferentially located at the edge sites of clay minerals and controlled
298 by the pH of the pore water solution, provide favorable deposition sites for NPs. Apart from
299 NPs, clay minerals are also widely used as adsorbents for environmental contaminants due to
300 their unique charge properties. They can provide favorable deposition sites for various
301 pollutants such as heavy metals and graphene oxide via electrostatic interactions (Uddin,
302 2017). In addition, different clay minerals have different variable charges resulting in different
303 extents of deposition. With the exception of variable charges, the permanent surface charge of
304 clay minerals also depends on pore water chemistry (e.g., pH, IS), which affects the overall
305
306

307 particle–collector interaction energy. Natural sediments at the interface between the surface
308 and subsurface flow domain (e.g., shallow aquifers or streambed sediments) often represent
309 regions of sharp transitions in (bio-)geochemical and mineralogical properties (pH, IS, and
310 redox potential). As the surface charge of clay minerals is controlled by the pH and IS, a non-
311 stationary condition in pore water chemistry will also affect the retention efficiencies for NPs
312 of clay containing sediments. A sudden increase of the pH value or the solution IS, associated
313 with fluctuations of the local groundwater level, may lead to the situation where previously
314 adsorbed NPs are released into the pore water. Understanding the impact of such non-
315 stationary effects on the retention efficiencies of NPs in clay containing sediments is very
316 important to better assess the transport behavior of NPs under environmentally relevant
317 conditions and should be addressed in detail as part of future research.

318 The small size of clay minerals results in narrow and complex flow pathways and
319 contributes significantly to the physical straining in NPs transport; in particular, the porous
320 media in the natural environment consists of clay mineral mixtures. Therefore, more studies
321 are still needed to comprehensively understand how the complex interplay of porous media
322 heterogeneity (e.g., clay minerals, iron oxides, and mineral sediments), particle
323 physicochemical properties (e.g., surface charge), and solution chemistry (e.g., different ions
324 species and natural organic matter) will affect the transport of NPs.

325

326 **Supplemental Data**

327 All Supplemental Data may be found in the online version of this article.

328

329 **Acknowledgment**

330 This research was conducted in the context of CRC 1357 - funded by the German
331 Research Foundation (DFG) under project number 391977956 and the Chinese Scholarship
332 Council (201708420145).

333

334 **References**

335 Bayat, A.E., Junin, R., Mohsin, R., Hokmabadi, M., Shamshirband, S., 2015. Influence of clay
336 particles on Al₂O₃ and TiO₂ nanoparticles transport and retention through limestone
337 porous media: measurements and mechanisms. *J. Nanoparticle Res.* 17, 1–14.

338 Bergaya, F., Lagaly, G., 2013. General introduction: clays, clay minerals, and clay science, in:
339 Schoonheydt, R., Johnston, C.T., Bergaya, F. (Eds.), *Developments in Clay Science*,
340 Elsevier, pp.1–18.

341 Chae, Y., An, Y.J., 2017. Effects of micro-and nanoplastics on aquatic ecosystems: Current
342 research trends and perspectives. *Mar. Pollut. Bull.* 124, 624–632.

343 da Costa, J.P., Santos, P.S., Duarte, A.C., Rocha-Santos, T., 2016. (Nano) plastics in the
344 environment—sources, fates and effects. *Sci. Total Environ.* 566, 15–26.

345 Dawson, A.L., Kawaguchi, S., King, C.K., Townsend, K.A., King, R., Huston, W.M., Nash,
346 S.M.B., 2018. Turning microplastics into nanoplastics through digestive fragmentation
347 by Antarctic krill. *Nat. Commun.* 9, 1–8.

348 Dong, Z., Hou, Y., Han, W., Liu, M., Wang, J., Qiu, Y., 2020. Protein corona-mediated
349 transport of nanoplastics in seawater-saturated porous media. *Water Res.* 182, 115978.

350 Franchi, A., O'Melia, C.R., 2003. Effects of natural organic matter and solution chemistry on

- 351 the deposition and reentrainment of colloids in porous media. *Environ. Sci. Technol.* 37,
352 1122–1129.
- 353 Geyer, R., Jambeck, J.R., Law, K.L., 2017. Production, use, and fate of all plastics ever made.
354 *Sci. Adv.* 3, e1700782.
- 355 Gigault, J., Ter Halle, A., Baudrimont, M., Pascal, P.-Y., Gauffre, F., Phi, T.-L., El Hadri, H.,
356 Grassl, B., Reynaud, S., 2018. Current opinion: What is a nanoplastic? *Environ. Pollut.*
357 235, 1030–1034.
- 358 Hussain, S.A., Demirci, Ş., Özbayoğlu, G., 1996. Zeta potential measurements on three clays
359 from Turkey and effects of clays on coal flotation. *J. Colloid Interface Sci.* 184, 535–541.
- 360 Keren, R., Sparks, D., 1995. The role of edge surfaces in flocculation of 2: 1 clay minerals.
361 *Soil Sci. Soc. Am. J.* 59, 430–435.
- 362 Kim, H.-J., Phenrat, T., Tilton, R.D., Lowry, G.V., 2012. Effect of kaolinite, silica fines and
363 pH on transport of polymer-modified zero valent iron nano-particles in heterogeneous
364 porous media. *J. Colloid Interface Sci.* 370, 1–10.
- 365 Koelmans, A.A., Besseling, E., Shim, W.J., 2015. Nanoplastics in the aquatic environment.
366 Critical review, in: Bergmann, M., Gutow, L., Klages, M. (Eds.), *Marine anthropogenic*
367 *litter*, Springer, pp. 325–340.
- 368 Kriaa, A., Hamdi, N., Srasra, E., 2009. Proton adsorption and acid-base properties of Tunisian
369 illites in aqueous solution. *J. Struct. Chem.* 50, 273–287.
- 370 Li, M., He, L., Zhang, X., Rong, H., Tong, M., 2020. Different surface charged plastic
371 particles have different cotransport behaviors with kaolinite particles in porous media.
372 *Environ. Pollut.* 267, 115534.
- 373 Lu, T., Gilfedder, B.S., Peng, H., Peiffer, S., Papastavrou, G., Ottermann, K., Frei, S., 2021.
374 Relevance of Iron Oxyhydroxide and Pore Water Chemistry on the Mobility of
375 Nanoplastic Particles in Water-Saturated Porous Media Environments. *Water Air Soil*
376 *Pollut* 232, 1–13.
- 377 Lu, T., Xia, T., Qi, Y., Zhang, C., Chen, W., 2017. Effects of clay minerals on transport of
378 graphene oxide in saturated porous media. *Environ. Toxicol. Chem.* 36, 655–660.
- 379 Marazuela, M., García-Fresnadillo, D., 2020. An integrated photosensitizing/adsorbent
380 material for the removal of triclosan from water samples. *Sep. Purif. Technol.* 251,
381 117392.
- 382 Mc Bride, M., 1989. Surface chemistry of soil minerals, in: Dixon, B., Weed, S.B. (Eds.),
383 *Minerals in soil environments 1*, Soil Science Society of America, pp. 35–88.
- 384 Mitzel, M.R., Sand, S., Whalen, J.K., Tufenkji, N., 2016. Hydrophobicity of biofilm coatings
385 influences the transport dynamics of polystyrene nanoparticles in biofilm-coated sand.
386 *Water Res.* 92, 113–120.
- 387 Murray, H.H., 2000. Traditional and new applications for kaolin, smectite, and palygorskite: a
388 general overview. *Appl. Clay Sci.* 17, 207–221.
- 389 Pradel, A., El Hadri, H., Desmet, C., Ponti, J., Reynaud, S., Grassl, B., Gigault, J., 2020.
390 Deposition of environmentally relevant nanoplastic models in sand during transport
391 experiments. *Chemosphere* 255, 126912.
- 392 Qi, Z., Zhang, L., Chen, W., 2014. Transport of graphene oxide nanoparticles in saturated
393 sandy soil. *Environ. Sci. Process Impacts* 16, 2268–2277.
- 394 Quevedo, I.R., Tufenkji, N., 2012. Mobility of functionalized quantum dots and a model

- 395 polystyrene nanoparticle in saturated quartz sand and loamy sand. *Environ. Sci. Technol.*
396 46, 4449–4457.
- 397 Schoonheydt, R., Johnston, C., 2006. Surface and interface chemistry of clay minerals. *Dev.*
398 *Clay Sci.* 1, 87–113.
- 399 Shaniv, D., Dror, I., Berkowitz, B., 2021. Effects of particle size and surface chemistry on
400 plastic nanoparticle transport in saturated natural porous media. *Chemosphere* 262,
401 127854.
- 402 Shivangi, A.M., Sharma, A., Trakroo, M.D., Tewari, H., 2020. Macro benthic community
403 structure of artificially aerated Lake Naukuchiatal, India. *J. Entomol. Zool. Stud.* 8, 825–
404 830.
- 405 Silva, A.B., Bastos, A.S., Justino, C.I., da Costa, J.P., Duarte, A.C., Rocha-Santos, T.A., 2018.
406 Microplastics in the environment: Challenges in analytical chemistry-A review. *Anal.*
407 *Chim. Acta* 1017, 1–19.
- 408 Singer, A., 1984. The paleoclimatic interpretation of clay minerals in sediments—a review.
409 *Earth-Sci. Rev.* 21, 251–293.
- 410 Singh, B., Cattle, S., Field, D., 2014. Edaphic Soil Science, Introduction to, in: Neal K. Van
411 Alfen (Eds.), *Encyclopedia of Agriculture and Food Systems*, Elsevier, pp. 35–58.
- 412 Tombác, E., Szekeres, M., 2006. Surface charge heterogeneity of kaolinite in aqueous
413 suspension in comparison with montmorillonite. *Appl. Clay Sci.* 34, 105–124.
- 414 Tombacz, E., Szekeres, M., 2004. Colloidal behavior of aqueous montmorillonite
415 suspensions: the specific role of pH in the presence of indifferent electrolytes. *Appl. Clay*
416 *Sci.* 27, 75–94.
- 417 Uddin, M.K., 2017. A review on the adsorption of heavy metals by clay minerals, with special
418 focus on the past decade. *Chem. Eng. Sci.* 308, 438–462.
- 419 Van Alfen, N.K., 2014. *Encyclopedia of agriculture and food systems*. Elsevier.
- 420 Wu, X., Lyu, X., Li, Z., Gao, B., Zeng, X., Wu, J., Sun, Y., 2020. Transport of polystyrene
421 nanoplastics in natural soils: Effect of soil properties, ionic strength and cation type. *Sci.*
422 *Total Environ.* 707, 136065.
- 423 Yang, X., Flynn, R., Von Der Kammer, F., Hofmann, T., 2011. Influence of ionic strength and
424 pH on the limitation of latex microsphere deposition sites on iron-oxide coated sand by
425 humic acid. *Environ. Pollut.* 159, 1896–1904.
- 426 Yousif, E., Haddad, R., 2013. Photodegradation and photostabilization of polymers, especially
427 polystyrene. *Springerplus* 2, 1–32.
- 428 Yu, Y., Flury, M., 2021. Current understanding of subsurface transport of micro - and
429 nanoplastics in soil. *Vadose Zone J.*, e20108.

430 Table 1. Calculated maximum energy barriers (Φ_{\max}), secondary energy minimum depth
 431 (Φ_{sec}), and the respective separation distances of particle–collector DLVO interaction energy
 432 profiles

Minerals	Solution		Φ_{\max}		Φ_{sec}	
	pH	IS	height ($K_B T$)	distance (nm)	depth ($K_B T$)	distance (nm)
Quartz sand	5.9	10 mM NaCl	318	0.5	-0.10	32
	5.9	30 mM NaCl	257	0.5	-0.44	15
	5.9	50 mM NaCl	162	0.5	-0.75	10
	7.0	10 mM NaCl	469	0.4	-0.10	32
	9.0	10 mM NaCl	625	0.4	-0.10	30
Kaolinite	5.9	10 mM NaCl	142	1.1	-0.10	30
	5.9	30 mM NaCl	116	0.8	-0.42	14
	5.9	50 mM NaCl	84	0.7	-0.72	10
	7.0	10 mM NaCl	239	0.8	-0.09	30
	9.0	10 mM NaCl	461	0.5	-0.09	32
Illite	5.9	10 mM NaCl	351	0.5	-0.09	32
	5.9	30 mM NaCl	314	0.4	-0.36	16
	5.9	50 mM NaCl	210	0.4	-0.62	11
	7.0	10 mM NaCl	459	0.4	-0.09	32
	9.0	10 mM NaCl	516	0.4	-0.09	32
Montmorillonite	5.9	10 mM NaCl	273	0.6	-0.09	32

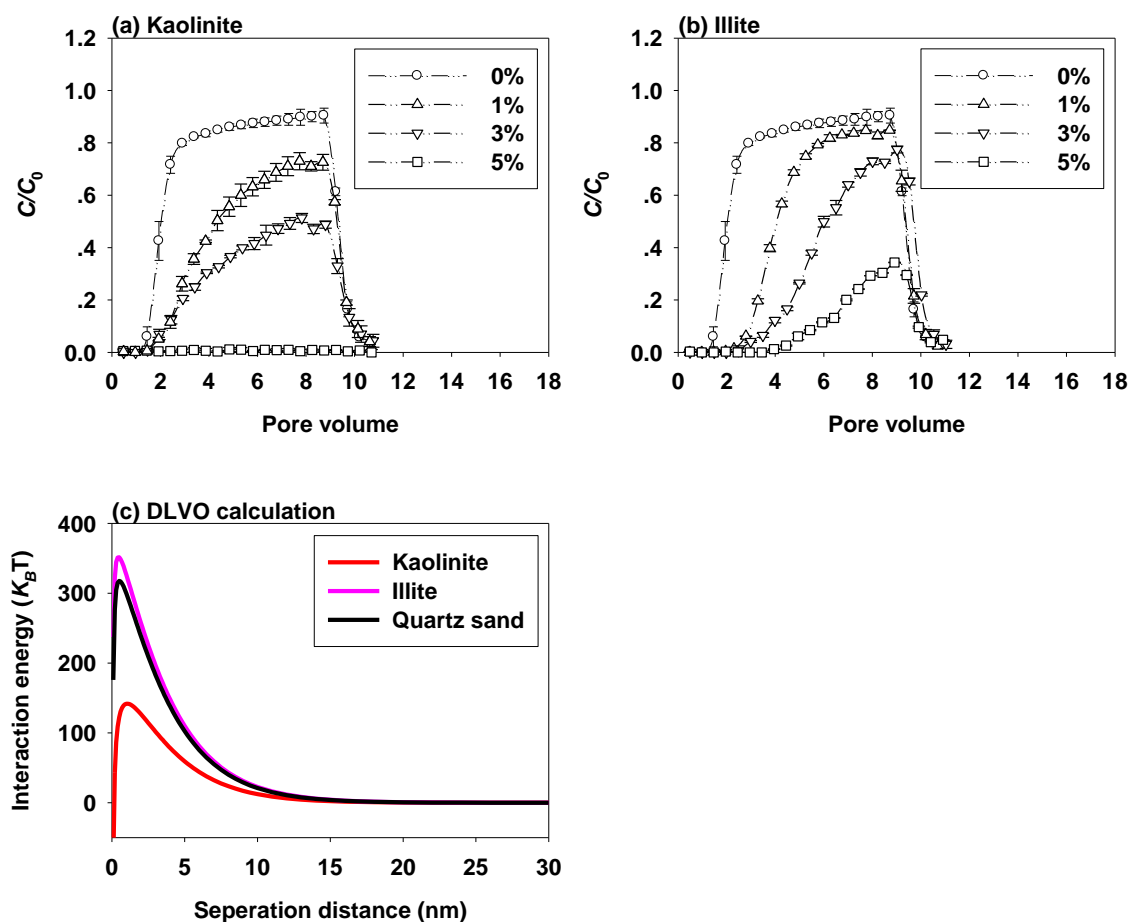
433

434 Table 2. Summary of ζ potential values of clay minerals and PS-NPs

Solution chemistry		ζ potential (mV)				
IS	pH	Kaolinite	Montmorillonite	Illite	Quartz sand	PS-NPs
10 mM NaCl	pH 5.9	-38.1± 1.6	-56.5± 2.1	-67.7± 1.5	-63.4± 1.3	-78.9± 1.3
10 mM NaCl	pH 7.0	-49.2± 3.7	--	-75.2± 1.3	-77.2± 1.6	-89.3± 0.6
10 mM NaCl	pH 9.0	-69.6± 1.0	--	-75.4± 0.4	-88.8± 3.6	-92.2± 2.2
30 mM NaCl	pH 5.9	-33.7± 0.9	--	-63.3± 0.8	-55.7± 2.6	-69.4± 5.0
50 mM NaCl	pH 5.9	-31.7± 0.1	--	-55.6± 0.8	-47.6± 0.1	-61.7± 2.0

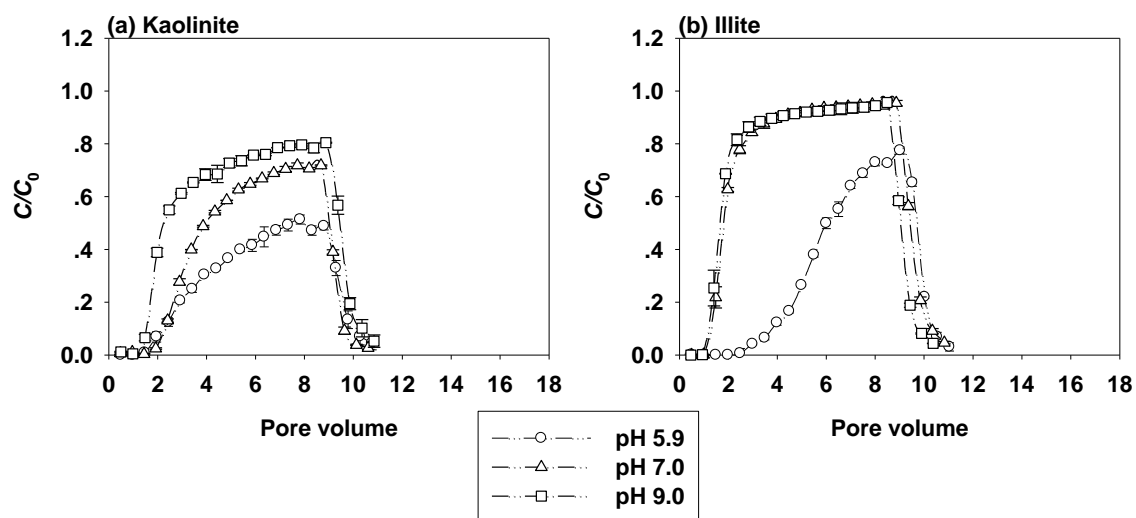
Note: values after \pm sign represent the standard deviation of triplicates. -- mean not applicable.

435

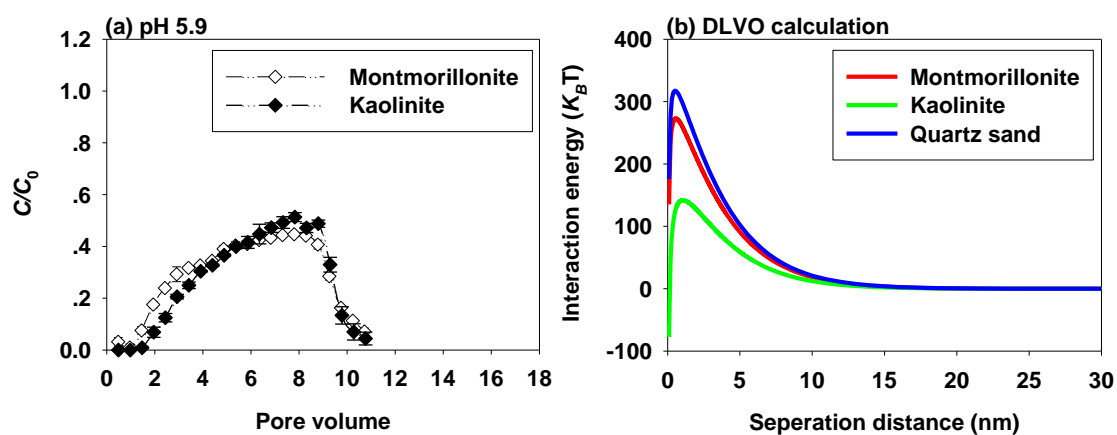


436

437 **Figure 1.** Effect of clay contents on the transport of PS-NPs in saturated porous media: (a)
438 kaolinite (Table S1 Columns 2–4); (b) illite (Table S1 Columns 5–7) and (c) Derjaguin-
439 Landau-Verwey-Overbeek (DLVO) particle–collector interaction profiles. All BTCs were
440 obtained under the conditions of 10 mM NaCl and pH 5.9.

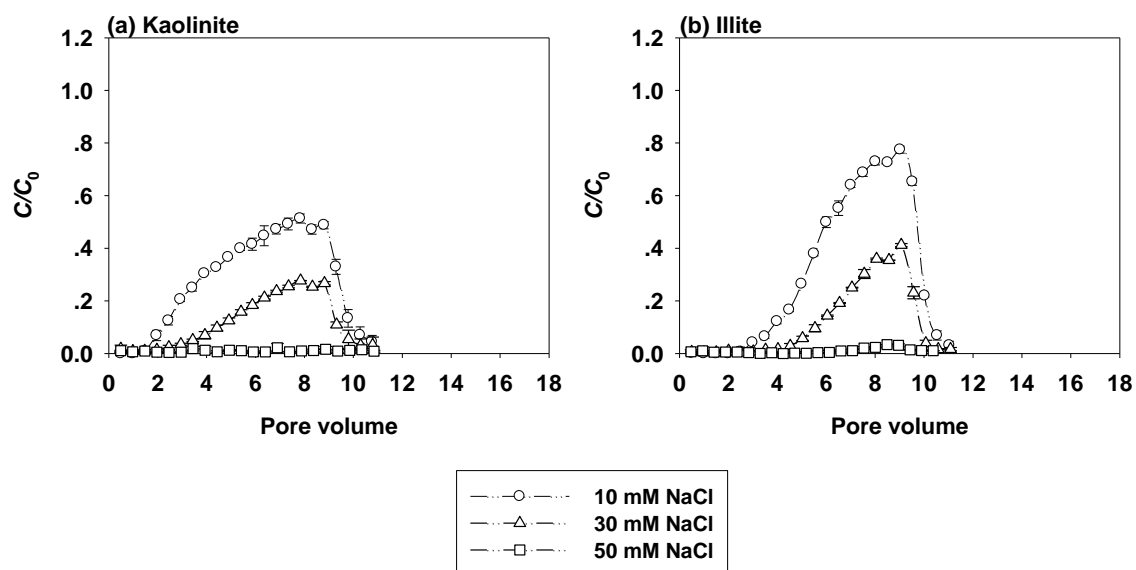


441
442 **Figure 2.** pH-dependent transport-inhibition effects of different types of clay minerals: (a)
443 kaolinite (Table S1 Columns 3, 8, and 9), and (b) illite (Table S1 Columns 6, 10, and 11); All
444 BTCs were obtained under the conditions of 10 mM NaCl and constant clay mineral content
445 (3%).



446

447 **Figure 3.** Effects of edge site charge on the PS-NPs transport: (a) breakthrough curves of PS-
448 NPs in columns packed with 3% montmorillonite or 3% kaolinite (Table S1 Columns 3 and
449 16); the experiments were conducted under pH 5.9 and 10 mM NaCl; (b) particle-collector
450 interaction profiles calculated by Derjaguin-Landau-Verwey-Overbeek (DLVO) theory.



451
452 **Figure 4.** Ionic strength-dependent transport-inhibition effects of different types of clay
453 minerals: (a) kaolinite (Table S1 Columns 3, 12, and 13), and (b) illite (Table S1 Columns 6,
454 14, and 15). All BTCs were obtained under the conditions of pH 5.9 and constant clay mineral
455 content (3%).

Supplementary Material Cover Sheet

**Effects of clay minerals on the transport of nanoplastic particles in water-saturated sand
columns**

Taotao Lu ¹, Benjamin S. Gilfedder ^{1,2}, Hao Peng ^{3*}, Geng Niu ⁴, Sven Frei ¹

¹ Department of Hydrology, Bayreuth Center of Ecology and Environmental Research
(BAYCEER), University of Bayreuth, Universitätsstraße 30, 95440, Bayreuth, Germany

² Limnological Research Station, Bayreuth Center of Ecology and Environmental Research
(BAYCEER), University of Bayreuth, Universitätsstraße 30, 95440, Bayreuth, Germany

³ School of Environmental Studies, China University of Geoscience, Wuhan, 430074, China

⁴ Wuhan Zondy W&R Environmental Technology Co., Ltd, Wuhan 430078, China

*Corresponding author: Hao Peng (penghao@cug.edu.cn)

Manuscript prepared for *Science of the Total Environment*

The procedures to clean quartz sand

The sand was thoroughly washed by soaking in 0.1 M HCl for 3 h and then in 5 wt.% H₂O₂ for 3 h. The sand was rinsed by Milli-Q (18.2 MΩ) water until the pH returned to that of Milli-Q water. The washed sand was dried at 105°C for 24 h and stored for future use.

Calculation of DLVO interaction energy

According to the Derjaguin–Landau–Verwey–Overbeek (DLVO) theory, the total interaction energy between particle and collector (V_{TOT}) can be defined as the sum of two interactions, the attractive van der Waals interaction (V_{VDW}) and the repulsive electrostatic double layer interaction (V_{EDL}) (Hogg et al., 1966):

$$V_{TOT} = V_{VDW} + V_{EDL} \quad (S1)$$

The van der Waals interaction is calculated using the Hamaker approach and Gregory's formulation (Gregory, 1981):

$$V_{VDW} = -\frac{Ar_{NP}}{6h\left(1 + \frac{14h}{\lambda}\right)} \quad (S2)$$

where A is the Hamaker constant for PS-NPs nanoparticles (9.25×10^{-21} J in quartz sand; 8.15×10^{-21} J for clay minerals) (Bayat et al., 2015), r_{NP} is the radius of PS-NPs nanoparticles, h is the separation distance between PS-NPs and quartz sand surface or between PS-NPs and clay mineral surface, and λ is the characteristic wavelength of PS-NPs ($\lambda = 100$ nm).

With the assumption of constant potential at the surface, the electrical double layer interaction can be calculated as (Elimelech and O'Melia, 1990):

$$V_{EDL} = \pi r_{NP} \varepsilon_0 \varepsilon_r \left\{ 2\phi_1 \phi_2 \ln \left[\frac{1 + \exp(-\kappa h)}{1 - \exp(-\kappa h)} \right] + (\phi_1^2 + \phi_2^2) \ln [1 - \exp(-2\kappa h)] \right\} \quad (S3)$$

where ε_0 is the vacuum permittivity (8.85×10^{-12} C²/Jm), ε_r is the relative dielectric permittivity of water (78.4), ϕ_1 denotes the measured zeta potential of the PS-NPs; ϕ_2 corresponds to the zeta potential of quartz sand and clay minerals. These values were obtained by Tufenkji's method (Tufenkji and Elimelech, 2004) and are listed in Table 2. κ is the Debye reciprocal length and can be calculated as (Russel et al., 1991):

$$\kappa = \sqrt{\frac{2N_A e^2 I}{\varepsilon_r \varepsilon_0 K_B T}} \quad (S4)$$

where N_A is the Avogadro number ($6.02 \times 10^{23} \text{ mol}^{-1}$), e is the electron charge ($-1.60 \times 10^{-19} \text{ C}$), I is the ionic strength of the background electrolyte, K_B is Boltzmann constant ($1.38 \times 10^{-23} \text{ J/K}$), and T is Kelvin temperature (298 K).

To obtain the Hamaker constant for polystyrene-water-quartz sand (clay minerals)

The Hamaker constant for polystyrene-water-quartz sand (A) is calculated by equation S2:

$$A = (\sqrt{A_{11}} - \sqrt{A_{33}})(\sqrt{A_{22}} - \sqrt{A_{33}}) \quad (\text{S2})$$

Where A_{11} is the Hamaker constant of polystyrene (7.85×10^{-20} J) (Henry, 2004); A_{22} is the Hamaker constant of quartz sand (8.86×10^{-20} J) and clay minerals (8.13×10^{-20} J) (Lu et al., 2017); A_{33} is the Hamaker constant of water (3.7×10^{-20} J) (Israelachvili, 2011)

Table S1. Experimental protocols of column tests

Column No.	Column properties		Influent properties		
	Porous media ^a	Porosity (-)	Background solution	pH	PS-NPs conc. (mg/L)
1	Quartz sand	0.47	10 mM NaCl	5.9	16.1
2	Quartz sand+1% kaolinite	0.47	10 mM NaCl	5.9	15.1
3	Quartz sand+3% kaolinite	0.46	10 mM NaCl	5.9	15.1
4	Quartz sand+5% kaolinite	0.45	10 mM NaCl	5.9	15.1
5	Quartz sand+1% illite	0.47	10 mM NaCl	5.9	15.4
6	Quartz sand+3% illite	0.46	10 mM NaCl	5.9	15.5
7	Quartz sand+5% illite	0.45	10 mM NaCl	5.9	15.1
8	Quartz sand+3% kaolinite	0.48	10 mM NaCl	7.0	16.0
9	Quartz sand+3% kaolinite	0.46	10 mM NaCl	9.0	15.2
10	Quartz sand+3% illite	0.47	10 mM NaCl	7.0	15.0
11	Quartz sand+3% illite	0.48	10 mM NaCl	9.0	15.0
12	Quartz sand+3% kaolinite	0.47	30 mM NaCl	5.9	15.7
13	Quartz sand+3% kaolinite	0.46	50 mM NaCl	5.9	14.5
14	Quartz sand+3% illite	0.46	30 mM NaCl	5.9	15.7
15	Quartz sand+3% illite	0.47	50 mM NaCl	5.9	15.0
16	Quartz sand+3% mont	0.45	10 mM NaCl	5.9	15.1

^a mont represents montmorillonite.

Table S2. Hydrodynamic diameter (D_h) and electrophoretic mobility of PS-NPs as affected by pH and IS

Solution chemistry	D_h^a (nm)	EPM ^b ($10^{-8} \text{ m}^2/\text{V}\cdot\text{s}$)
10 mM NaCl, pH 5.9	112.4	-6.19 ± 0.10
10 mM NaCl, pH 7.0	114.5	-7.00 ± 0.04
10 mM NaCl, pH 9.0	124.7	-7.23 ± 0.17
30 mM NaCl, pH 5.9	134.8	-5.44 ± 0.39
50 mM NaCl, pH 5.9	129.2	-4.84 ± 0.15

^a Hydrodynamic diameter of PS-NPs nanoparticles based on DLS analysis.

^b Values after \pm sign represent standard deviation of three replicates.

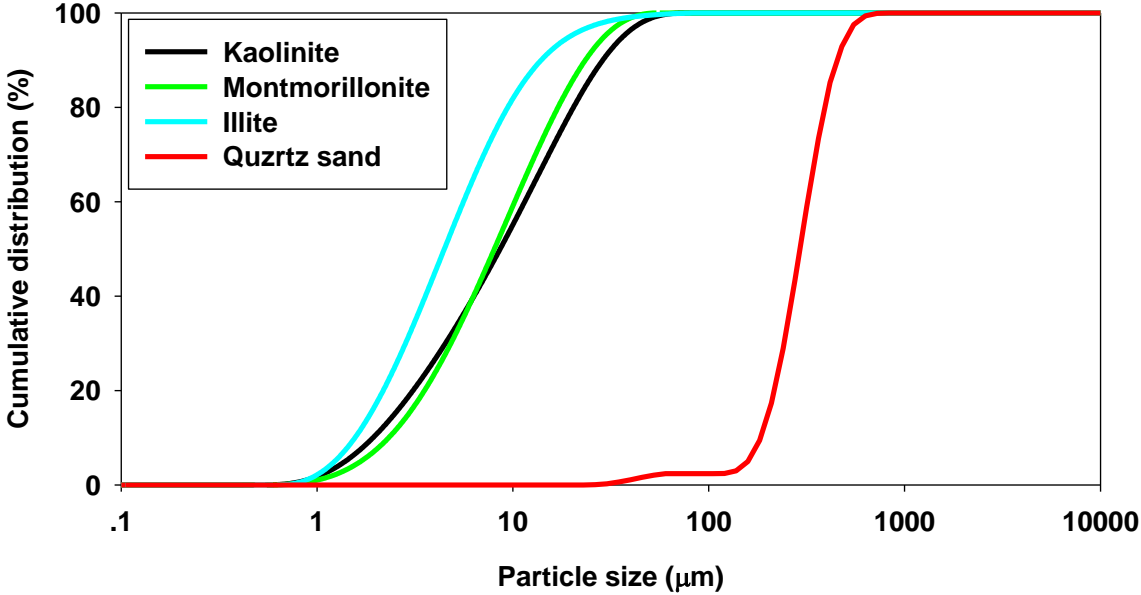


Figure S1. Particle size distributions of different clay minerals

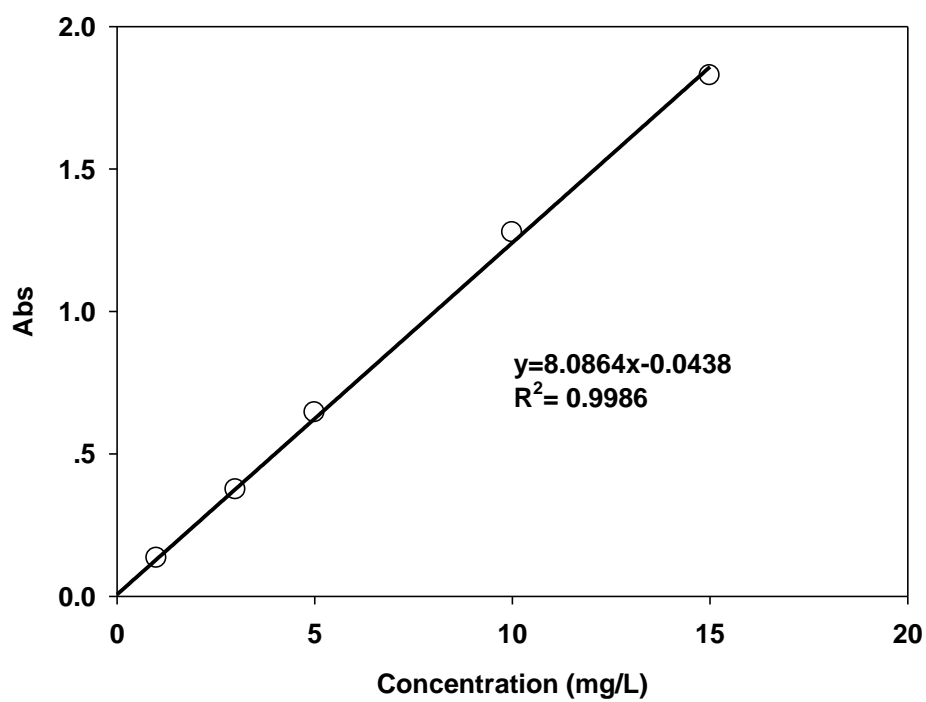


Figure S2. Calibration curves as absorbance at the wavelength of 220 nm versus PS-NPs concentration in suspension.

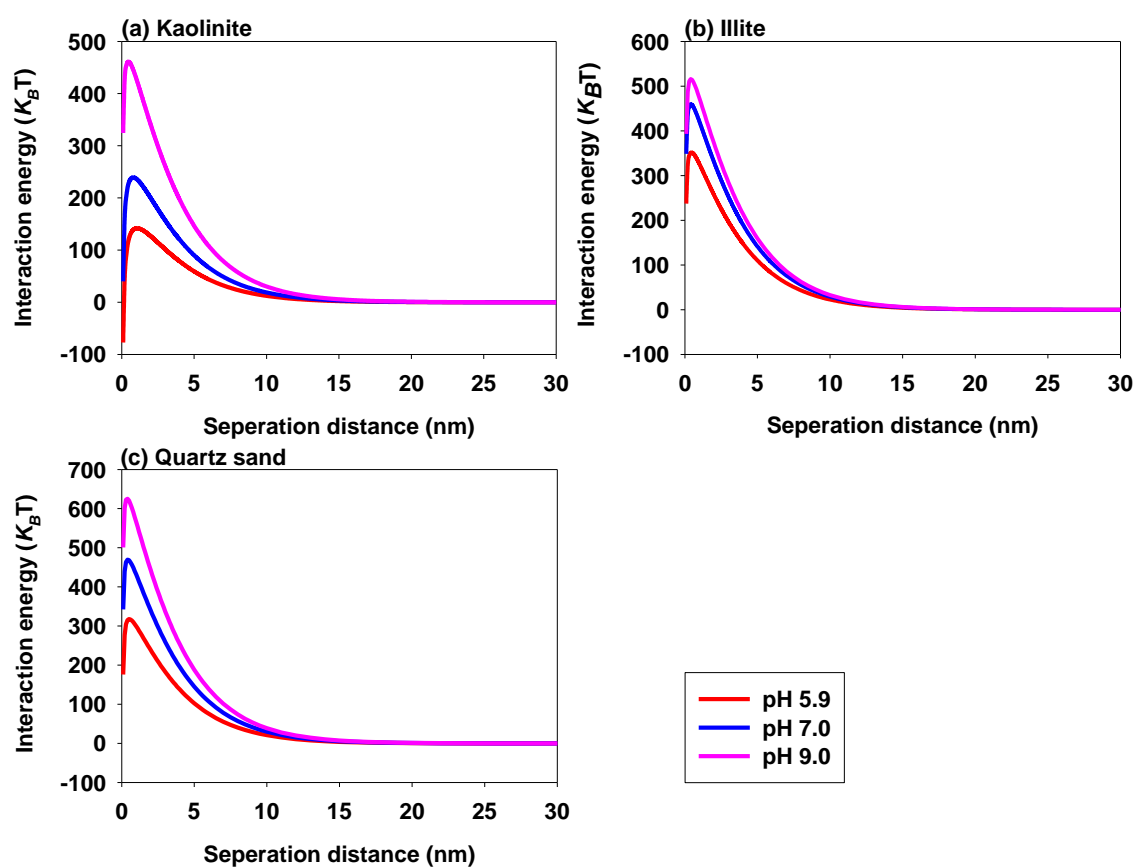


Figure S3. Comparison of particle–collector interaction energy profiles among different porous media at different pH: (a) kaolinite, (b) illite, and (c) quartz sand.

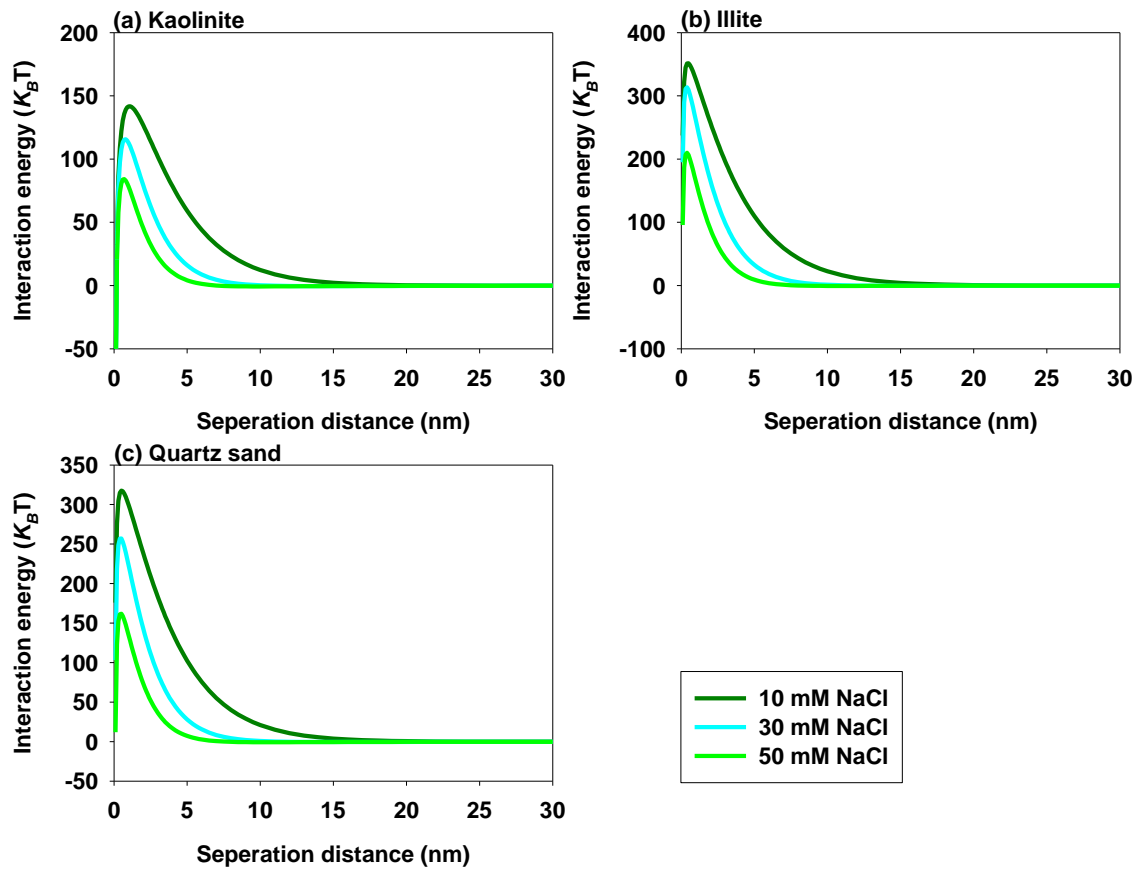


Figure S4. Comparison of particle–collector interaction energy profiles among different porous media at different IS: (a) kaolinite, (b) illite, and (c) quartz sand.

References

- Bayat, A.E., Junin, R., Mohsin, R., Hokmabadi, M., Shamshirband, S., 2015. Influence of clay particles on Al₂O₃ and TiO₂ nanoparticles transport and retention through limestone porous media: measurements and mechanisms. *J. Nanoparticle Res.* 17, 1–14.
- Elimelech, M., O'Melia, C.R., 1990. Effect of particle size on collision efficiency in the deposition of Brownian particles with electrostatic energy barriers. *Langmuir.* 6, 1153–1163.
- Gregory, J., 1981. Approximate expressions for retarded van der Waals interaction. *J. Colloid Interface Sci.* 83, 138–145.
- Henry, M. Nanocrystals from Solutions and Gels. *Encyclopedia of Nanoscience and Nanotechnology.* 6. American Scientific Publishers, 2004, pp. 555–586.
- Hogg, R., Healy, T.W., Fuerstenau, D.W., 1966. Mutual coagulation of colloidal dispersions. *Transactions of the Faraday Society.* 62, 1638–1651.
- Israelachvili, J.N., 2011. Intermolecular and surface forces. Academic press.
- Lu, T., Xia, T., Qi, Y., Zhang, C., Chen, W., 2017. Effects of clay minerals on transport of graphene oxide in saturated porous media. *Environ. Toxicol. Chem.* 36, 655–660.
- Russel, W.B., Russel, W., Saville, D.A., Schowalter, W.R., 1991. *Colloidal dispersions.* Cambridge university press.
- Tufenkji, N., Elimelech, M., 2004. Deviation from the classical colloid filtration theory in the presence of repulsive DLVO interactions. *Langmuir.* 20, 10818–10828.

(Eidesstattliche) Versicherungen und Erklärungen

(§ 9 Satz 2 Nr. 3 PromO BayNAT)

Hiermit versichere ich eidesstattlich, dass ich die Arbeit selbstständig verfasst und keine anderen als die von mir angegebenen Quellen und Hilfsmittel benutzt habe (vgl. Art. 64 Abs. 1 Satz 6 BayHSchG).

(§ 9 Satz 2 Nr. 3 PromO BayNAT)

Hiermit erkläre ich, dass ich die Dissertation nicht bereits zur Erlangung eines akademischen Grades eingereicht habe und dass ich nicht bereits diese oder eine gleichartige Doktorprüfung endgültig nicht bestanden habe.

(§ 9 Satz 2 Nr. 4 PromO BayNAT)

Hiermit erkläre ich, dass ich Hilfe von gewerblichen Promotionsberatern bzw. -vermittlern oder ähnlichen Dienstleistern weder bisher in Anspruch genommen habe noch künftig in Anspruch nehmen werde.

(§ 9 Satz 2 Nr. 7 PromO BayNAT)

Hiermit erkläre ich mein Einverständnis, dass die elektronische Fassung meiner Dissertation unter Wahrung meiner Urheberrechte und des Datenschutzes einer gesonderten Überprüfung unterzogen werden kann.

(§ 9 Satz 2 Nr. 8 PromO BayNAT)

Hiermit erkläre ich mein Einverständnis, dass bei Verdacht wissenschaftlichen Fehlverhaltens Ermittlungen durch universitätsinterne Organe der wissenschaftlichen Selbstkontrolle stattfinden können.

.....
Ort, Datum, Unterschrift